

**Synthesis and characterisation of carbon nanomaterials
using South African coal fly ash and their use in novel
nanocomposites**

Nomso Charmaine Hintsho (BSc Hons, MSc, UWC)

A thesis submitted in fulfilment of the requirements for the degree of
Doctor of philosophy,
Molecular Science Institute,
Department of Chemistry,
University of the Witwatersrand, Johannesburg
December 2015

Supervisor: Dr S Durbach
Co-supervisor: Dr P Franklyn
Dr A Shaikjee

Declaration

I declare that this Thesis, titled, '*Synthesis and characterisation of carbon nanomaterials using South African coal fly ash and their use in novel nanocomposites*' which I submit for the Degree of Doctor of Philosophy in the University of the Witwatersrand, Johannesburg, is my own, unaided work. It has not been submitted before for any degree or examination in any other institution.

Signed (Candidate)

On this _____ day of _____ December _____ 2015

Abstract

The synthesis and applications of carbon nanomaterials (CNMs) such as carbon nanofibres (CNFs), carbon nanotubes (CNTs) and carbon nanospheres (CNSs) have attracted a lot of attention due to their unique chemical and physical properties. For the synthesis of CNMs with desired morphology to occur, one needs to consider three components, namely, the catalyst, carbon source and source of power. However, the cost of the catalysts involved in making CNMs is one of the challenging factors. Due to properties such as high aspect ratio, CNM use as fillers in polymer nanocomposites has been on the forefront to improve the mechanical strength of polymer materials such as polyesters. Due to their hydrophobic nature, the interaction between the filler and matrix tends to be problematic.

In this study, we investigated the use of a waste material, coal fly ash as a catalyst for the synthesis of CNMs using the chemical vapour deposition method. The use of CO₂ and C₂H₂ as carbon sources, either independently or together, was also employed. A comparison of two different ashes was also investigated. Lastly, the use of these synthesized and acid treated CNMs as fillers was examined. The catalysts and synthesized CNMs were characterised using SEM, TEM, EDS, laser Raman spectroscopy, XRD, BET, TGA and Mössbauer spectroscopy. The mechanical properties were investigated by testing the tensile, flexural and impact properties.

The synthesis of CNMs using fly ash as a catalyst without pre-treatment or impregnating with other metals was achieved. Optimum yields and uniform morphology was obtained at 650 °C, at a flow rate of 100 ml/min using H₂ as a carrier gas and C₂H₂ as a carbon source. Mössbauer spectroscopy revealed that cementite (Fe₃C) was the compound responsible for CNF formation.

Further, CNMs were formed over fly ash as a catalyst, using CO₂ as a sole carbon source, an additive and a carbon source before reacting with C₂H₂. Duvha was

found to be a better fly ash catalyst compared to Grootvlei and an optimum loading was achieved at 0.25%. Treating the CNFs with HCl/HNO₃ resulted in the highest tensile, flexural and impact strengths.

This study has highlighted the use of two waste materials, as a catalyst and carbon source for CNM formation. These CNMs were shown to play a major role in the mechanical properties of polymers.

Dedication

This work is dedicated to my family

'All that I am, and all that I ever will be, it is because of U'

Thank You

:

Acknowledgements

I would like to thank the following:

- To God be the Glory, the most high and worthy to be praised. I thank you Father.
- My Supervisors, Dr P.J Franklyn, Dr S Durbach and Dr A. Shaikjee, for giving me this opportunity to work on this research project and for their guidance throughout this study.
- Eskom, the NRF and the DST/NRF Centre of Excellence in Strong Materials, the University of the Witwatersrand Postgraduate Merit Award and the Bradlow scholarship for their financial assistance.
- Prof D Naidoo and Dr H Masenda for Mössbauer analysis
- Prof J Muthu, for allowing me to do mechanical tests at his Composite lab, School of Metallurgical and Mechanical Engineering, Wits
- The XRD and MMU units at Wits for PXRD and TEM analyses
- My colleagues from the CATOMAT research group: Thank you guys for everything.
- Lastly and more importantly to my family (Nonkqubela Hintsho (mother), Busiswa Hintsho (sister), Zukile Mbita (husband) and Liyakhanya Mbita (son)).

Presentations and Publications

Published Papers:

- Hintsho, N.C; Shaikjee, A.; Masenda, H.; Naidoo, D.; Billing, D.; Franklyn, P.; Durbach, S. *Nanoscale Research Letters* 2014, 9, 1-11.
- N.C Hintsho; A. Shaikjee ;P.K Tripathi; P. Franklyn; S.D. Durbach, *RSC Advances* 2015, 5, 53776-53781
- Hintsho, N.; Shaikjee, A.; Tripathi P.K; Masenda, H.; Naidoo, D.; Franklyn, P.; Durbach, S. *Journal of Nanoscience and Nanotechnology*, 2016, ,16, 4672-4683

Conference Proceedings:

1. Poster Presentations

- Hintsho NC, A Shaikjee, P Franklyn and S Durbach, Direct synthesis of carbon nanofibres from fly ash as a catalyst, CoE workshop, 10th May 2013, Wits University
- Hintsho NC, A Shaikjee, P Franklyn and S Durbach, Effect of CO₂ on the synthesis of CNMs from fly ash, CATSA conference, 16-21th November 2014, St Georges Hotel.

2. Oral Presentations

- Hintsho NC, A Shaikjee, P Franklyn and S Durbach, Synthesis of carbon nanofibres from fly ash as a catalyst, NYRS conference, 9th September 2012, Wits University
- Hintsho NC, A Shaikjee, P Franklyn and S Durbach, Synthesis of carbon nanofibres from fly ash as a catalyst and their use as fillers to improve the strength of polyester composites, CoE workshop, 12th May 2015, Wits University

Table of Contents

Declaration	i
Abstract	ii
Dedication	iv
Acknowledgements	v
Presentations and Publications	vi
Table of Contents	vii
List of Figures	xiii
List of Tables.....	xix
Nomenclature	xx
List of Symbols and Abbreviations.....	xxi
1.0 Introduction.....	1
1.2 Problem Statement.....	3
1.3 Research Questions.....	3
1.4 Research Aims and Objectives	4
1.4.1 Broad Research Aims	4
1.4.2 Specific Aims:	4
2.1 Coal.....	10
2.1.1 Classification of coal	11
2.1.2 Mineralogy and chemistry of coal	11
2.2 Coal fly ash and its classification.....	12
2.2.1 Chemical composition and physical properties of coal fly ash.....	12
2.2.2 Disposal of fly ash	14
2.3 Uses of Fly Ash.....	14
2.3.1 Fly ash as filler in the polymer industry.....	16
2.3.2 Fly ash as filler in the construction industry	17
2.3.3 Fly ash as a soil additive	18
2.3.4 Fly ash in Environmental Protection.....	21
2.3.5 Fly Ash as a catalyst.....	21
2.4 Carbon nanomaterials (CNMs)	25
2.4.1 Carbon nanotubes and carbon nanofibres using fly ash as a catalyst	27
2.4.2 The effect CO ₂ as a carbon sources on the synthesis of CNMs	32

2.5 Methods used for the synthesis of carbon nanomaterials	33
2.5.1 Arc discharge	34
2.5.2 Laser ablation	34
2.5.3 Chemical Vapour Deposition.....	35
2.6 Other Methods used for the synthesis of carbon nanomaterials from fly ash .	36
2.6.1. Pyrolysis Method	36
2.6.2 Ball Milling	38
2.7 Mechanical Properties of Carbon nanotubes and Carbon nanofibres	39
2.8 Carbon nanomaterials/polymer nanocomposites	39
2.8.1 Preparation of carbon nanomaterial/polymer nanocomposites.....	40
2.8.2 Functionalisation of carbon nanomaterials	41
2.9 Application of carbon nanomaterials formed from fly ash as a catalyst.....	42
2.10. Conclusion	43
2.11 References	44
3.1 Introduction.....	55
3.2 Materials, Gases and Equipment used.....	55
3.2.1 Materials	55
3.3 Experimental Procedures	57
3.3.1 Synthesis of carbon nanomaterials via chemical vapour deposition (CVD)	57
3.3.2 Acid Treatment of synthesized Carbon Nanofibres (CNFs).....	58
3.3.2.1 Functionalisation of CNFs using KMnO_4	59
3.3.2.2 Functionalisation of CNFs using HCl/HNO_3	59
3.4 Characterization techniques and experimental details.....	59
3.4.1 Scanning electron microscope (SEM)	60
3.4.2 Transmission electron microscopy (TEM)	60
3.4.3 Brauner–Emmet-Teller (N_2 BET).....	61
3.4.4 Fourier transform infrared spectroscopy (FTIR)	61
3.4.5 Thermal gravimetric analysis (TGA).....	61
3.4.6 Laser Raman spectroscopy	62
3.4.7 X-ray diffraction (XRD)	62
3.4.8 X-ray fluorescence (XRF)	62
3.4.9 Mössbauer spectroscopy	63
3.5 The CNF polyester/ composite fabrication procedure.....	63
3.6 Mechanical Characterisation of CNFs-polyester composites.....	65

3.6.1 Testing procedure	65
3.6.1.1 Tensile testing	65
3.6.1.1 Tensile testing procedure	66
3.6.1.2 Flexural testing.....	67
3.6.1.2.1 Flexural testing procedure.....	68
3.6.1.3 Impact testing.....	69
3.6.1.3.1 Impact testing procedure.....	69
4.1 Introduction.....	71
4.2 Methods	72
4.2.1 Synthesis	72
4.2.2 Characterization.....	73
4.3 Results and Discussion	73
4.3.1 Morphological Studies.....	73
4.3.2 Laser Raman spectroscopy studies.....	76
4.3.3 Thermogravimetric studies	78
4.3.4 Particle Size and Surface area measurements.....	79
4.3.5 Composition, Mineral phase and oxidation state studies.....	82
4.4 Conclusions	87
4.5 References.....	89
5.1 Introduction.....	92
5.2 Experimental Section.....	93
5.2.1 Synthesis of CNMs using fly ash as a catalyst	93
5.2.2 Characterization.....	93
5.3 Results and Discussion	94
5.3.1 Carbon Yield.....	94
5.3.2 Morphological Studies.....	95
5.3.2.1 Synthesis of CNMs by reaction of fly ash and C ₂ H ₂ in N ₂ (C ₂ H ₂ _N ₂)....	95
5.3.2.2 Synthesis of CNMs by reaction of fly ash and C ₂ H ₂ in H ₂ (C ₂ H ₂ _H ₂)...97	97
5.3.2.3 Synthesis of CNMs by reaction of fly ash and C ₂ H ₂ using H ₂ as a pre-treatment and N ₂ as a carrier gas (H ₂ , C ₂ H ₂ _N ₂).....	99

5.3.2.4	Synthesis of CNMs by reaction of fly ash and C ₂ H ₂ using N ₂ as a pre-treatment and H ₂ as a carrier gas (N ₂ ,C ₂ H ₂ _H ₂).....	102
5.3.2.5	Synthesis of CNMs by reaction of fly ash and C ₂ H ₂ using H ₂ as a carrier gas at varying flow rates of (C ₂ H ₂ /N ₂).....	104
5.3.3.1	Laser Raman spectroscopy analyses (Graphicity Studies)	104
5.3.3.2	Raman spectroscopy analyses of CNMs formed by reaction of fly ash and C ₂ H ₂ in N ₂ and H ₂ respectively.....	105
5.3.3.3	Laser Raman spectroscopy analyses of CNMs formed by reaction of fly ash and C ₂ H ₂ using H ₂ as a pre-treatment and N ₂ as a carrier gas	106
5.3.3.4	Laser Raman spectroscopy analyses of CNMs formed by reaction of fly ash and C ₂ H ₂ using N ₂ as a pre-treatment and H ₂ as a carrier gas	106
5.3.5	Thermal stability analyses	107
5.3.5.1	Thermal stability of CNMs formed by reaction of fly ash and C ₂ H ₂ in N ₂ and H ₂ respectively	107
5.3.5.2	Thermal stability of CNMs formed by reaction of fly ash and C ₂ H ₂ using H ₂ as a pre-treatment and N ₂ as a carrier gas	109
5.3.5.3	Thermal stability of CNMs formed by reaction of fly ash and C ₂ H ₂ using N ₂ as a pre-treatment and H ₂ as a carrier gas	110
5.3.6	Composition, Mineral phase and oxidation state studies.....	111
5.3.6.1	Mineral phase identification analyses (PXRD).....	111
5.3.6.2	Mössbauer spectroscopy	111
5.4.	Conclusions	115
6.1	Introduction.....	119
6.2	Experimental.....	120
6.2.1	Synthesis of CNFs	120
6.2.2	Characterisation of CNFs	120
6.3	Results and Discussion	120
6.3.1	CO ₂ as a carbon source	121
6.3.2	CO ₂ as an additive to C ₂ H ₂	124
6.3.3	CO ₂ as a carbon source prior to C ₂ H ₂	127

6.4	Conclusions	130
6.5	References	131
7.1	Introduction.....	133
7.2.	Experimental.....	135
7.2.1	Materials	135
7.2.2	Synthesis of CNFs	135
7.2.3	Characterisation of CNFs	135
7.2.4	Fibre composite fabrication procedure	136
7.2.5	Mechanical Characterisation of CNFs.....	136
7.3	Results and discussion	136
7.3.1.	XRF analyses	136
7.3.2	Morphological and Product yield Studies	137
7.3.3.	Graphicity and Thermal stability studies	139
8.1	Introduction	146
8.2	Experimental.....	148
8.2.1	Materials	148
8.2.2	Synthesis of CNFs	148
8.2.3	Functionalisation of CNFs.....	148
8.2.4	Characterisation of CNFs	148
8.2.5	Fibre composite fabrication and testing procedure.....	149
8.3	Results and discussion	149
8.3.1	N ₂ Physisorption	149
8.3.2	Morphological Studies.....	150
8.3.3	Graphicity studies	151
8.3.4	Powder X-ray diffraction studies.....	152
8.3.5	Infrared Spectroscopy studies.....	153
8.3.6	Thermal stability	155
8.3.7	Evaluation of Tensile Strength	157
8.3.8	Evaluation of Flexural Toughness	158
8.3.9	Evaluation of Fracture Toughness	160
8.4	Conclusions	162
8.5	References.....	163
9.1	Introduction.....	165

9.2	Conclusions	166
9.2.1	Synthesis of CNFs from coal fly ash	166
9.2.2	Effect of gas environment, flow rate and temperature of CNM morphology	166
9.2.3	Effect of CO ₂ on the CVD synthesis of CNMs from coal fly ash	166
9.2.4	Comparison of two different ashes for CNM synthesis and testing their tensile strength	167
9.2.5	Effect of various treatments on CNFs and testing their tensile and impact tests	167
9.3	Recommendations.....	168
	Chapter 3: <i>Supplementary</i>	170
	Chapter 5: <i>Supplementary</i>	170
	Chapter 7: <i>Supplementary</i>	171
	Chapter 8: <i>Supplementary</i>	172

List of Figures

CHAPTER 2

Figure 2.1: Distribution of coal consumption worldwide in 2012 ³⁴	12
Figure 2.2: Various morphologies of coal fly ash ³⁴	13
Figure 2.3: Carbon nanostructures:(a) CNFs composed of stacked graphene cones;(b) herringbone type CNF and (c) Tubular type CNTs	26
Figure 2.4: Schematic diagram of CNT growth mechanism a) Root growth b) Tip growth	27
Figure 2.5: SEM images of CNMs by (a-b) Yasui, (c-d) Dunens and (e-f) Salah ³⁰	
Figure 2.6: SEM images of CNTs produced from Saudi Arabian fly ash	31
Figure 2.7: Schematic diagram of the chemical vapor deposition apparatus.....	36
Figure 2.8: TEM images of CNT, a) growth of aligned CNT ribbons, b) single ribbons, showing constant width; c) U-shaped and d) spiral shaped CNT ribbon structures ¹⁷⁸	37
Figure 2.9 (a-b): TEM images of fly ash samples ball milled for 60 hr ⁵³	39

CHAPTER 3

Figure 3.1: CVD set up for CNM synthesis using coal fly ash as a catalyst; acetylene as a carbon source and nitrogen as a carrier gas.	58
Figure 3.2: Plates of mould used for fabricating composite specimens	64
Figure 3.3: Mould used for fabricating composite specimens	64
Figure 3.4: Dog bone shape of polyester composite, using the dimensions of ASTM D638	66
Figure 3.5: Preferred dimensions for ASTM D790 test specimen.....	68
Figure 3.6: Impact testing requirements using ASTM D256 standard dimensions	69

CHAPTER 4

Figure 4.1: TEM images of : (a) as-received coal fly ash and CNFs synthesized at (b) 400 °C, (c) 500 °C, (d) 600 °C and (e-f) 700 °C.....	75
Figure 4.2: Proposed reaction scheme for CNF growth, using South African coal fly ash as a catalyst	76
Figure 4.3: Laser Raman spectroscopy spectra of as-received fly ash and products from fly ash exposed to acetylene at various temperatures and (b) I_D/I_G ratios of the carbon nanofibres formed in acetylene.....	77
Figure 4.4: The first order weight derivatives of as-received and acetylene treated coal fly ash at varying temperatures	79
Figure 4.5: Varying particle sizes of fly ash samples exposed to acetylene at different temperatures	80
Figure 4.6: (a) Particle size distribution of as-received fly ash, (b) Particle size distribution of acetylene treated fly ash at 500 °C.....	81
Figure 4.7: BET surface area of as received fly ash and CNFs formed by exposure of fly ash to acetylene to temperatures from 400 °C to 700 °C in H_2	81
Figure 4.8: EDS of CNFs formed at 700°C. Beryllium, carbon, aluminium, silica and iron were the elements identified after synthesis.....	82
Figure 4.9: XRD of as-received coal fly ash and CNFs synthesized at 700 °C....	83
Figure 4.10: Room temperature 57Mössbauer spectra for (a) as-received and (b) acetylene treated fly ash sample at 700°C.	86

CHAPTER 5

Figure 5.1: A plot of the percentage yield of CNMs grown from 450 °C–750 °C using N_2 or H_2 as carrier gases in the reaction of fly ash with C_2H_2	94
Figure 5.2: SEM micrographs of CNMs produced from $C_2H_2_N_2$ synthesized at (a) 450 °C, (b) 550 °C, (c) 650 °C and (d) 750 °C.	96
Figure 5.3: Fibre size distributions of CNMs produced from $C_2H_2_N_2$ synthesized at (a) 450 °C, (b) 550 °C, (c) 650 °C and (d) 750 °C.	97
Figure 5.4: SEM micrographs of CNFs produced from $C_2H_2_H_2$ synthesized at (a) 450 °C, (b) 550 °C, (c) 650 °C, and (d) 750 °C.	98

Figure 5.5: Fibre diameter size distributions of CNMs produced from $C_2H_2_H_2$ synthesized at (a) 450 °C, (b) 550 °C, (c) 650 °C and (d) 750 °C.....	99
Figure 5.6: TEM micrographs of CNFs produced from $H_2, C_2H_2_N_2$ CNFs synthesis at (a) 550 °C and (b) 650 °C.....	100
Figure 5.7: Fibre size distributions of CNMs produced from $N_2, C_2H_2_H_2$ synthesized at (a) 550 °C and (b) 650 °C.	101
Figure 5.8: A plot of the percentage yield of CNMs grown from 550 °C–650 °C using $H_2, C_2H_2_N_2$ or $N_2, C_2H_2_H_2$ as carrier gases in the reaction of fly ash with C_2H_2	102
Figure 5.9: TEM micrographs of CNFs produced from ($N_2, C_2H_2_H_2$) synthesized at (a) 550°C and (b) 650 °C.....	103
Figure 5.10: Fibre size distributions of CNMs produced from $N_2, C_2H_2_H_2$ synthesized at (a) 550 °C and (b) 650 °C.	103
Figure 5.11: Laser Raman spectroscopy spectra of CNFs synthesized at various temperatures in the presence of carrier gases under (a) N_2 and (b) H_2 , respectively.	105
Figure 5.12: Laser Raman spectroscopy spectra of CNFs synthesized from C_2H_2 when H_2 was used during pre-reaction and N_2 as a carrier gas at (a) 550°C and (b) 650°C.....	106
Figure 5.13: Laser Raman spectroscopy spectra of CNFs synthesized from C_2H_2 when N_2 was used during pre-reaction and H_2 as a carrier gas at: (a) 550°C and (b) 650 °C	107
Figure 5.14: Thermal stability of CNFs formed at varying temperatures (450-750 °C) in the presence of N_2 gas (a) percentage weight loss (b) weight derivative	108
Figure 5.15: Thermal stability of CNFs formed at varying temperatures (450-750°C) in the presence of H_2 gas (a) percentage weight loss (b) weight derivative	109
Figure 5.16: (a) Thermal stability and (b) derivative of CNFs synthesized materials at 550°C and 650°C temperatures using H_2 as a pre-reduction gas and N_2 as a carrier gas.....	110

Figure 5.17: (a) Thermal stability and (b) derivative of CNFs synthesized materials at 550 °C and 650 °C	110
Figure 5.18: PXRD patterns of C ₂ H ₂ treated sample in the presence of (a) C ₂ H ₂ _H ₂ , (b) C ₂ H ₂ _H ₂ , (c) H ₂ , C ₂ H ₂ _N ₂ and (d) N ₂ , C ₂ H ₂ _H ₂ , for samples synthesized at 650 °C	111
Figure 5.19: Room temperature Mössbauer parameters for: the acetylene treated sample in the presence of (a) C ₂ H ₂ _N ₂ , (b) C ₂ H ₂ _H ₂ , (c) H ₂ , C ₂ H ₂ _N ₂ , and (d) N ₂ , C ₂ H ₂ _H ₂ , for samples synthesized at 650 °C	112

CHAPTER 6

Figure 6.1: Synthesis of CNMs using CO ₂ as a sole carbon source, as an additive and as a carbon source prior to the reaction with C ₂ H ₂	121
Figure 6.2: TEM images of various amorphous carbon materials grown at 900 oC showing (a) Sheet-like material, (b) Sphere-like materials, (c) Carbon with metal particles and (d) Amorphous carbon with what appears to be unreacted fly ash.....	122
Figure 6.3: SEM images of (a) As-received fly ash, (b) Carbon materials grown at 900°C (c) Laser Raman spectroscopy of CNMs formed at 900°C	123
Figure 6.4:(a) Percentage yields of CNMs produced (b) Raman spectroscopy spectra of CNMs grown between 500-700°C and (c) I _D /I _G ratios of CNMs	124
Figure 6.5: (a) TGA profile, (b) Weight loss derivative, (c) Adsorption isotherms and (d) BET surface area and pore volumes of CNMs grown between 500-700°C.	125
Figure 6.6: TEM and SEM images of CNF/Ts formed (a-b) 500°C, (c-d) 600°C and (e-f) 700°C. The block gives the size of the scale bar.....	126
Figure 6.7: TEM and SEM images of CNF/Ts formed (a-b) 500°C, (c-d) 600°C and (e-f) 700°C.....	128
Figure 6.8:(a) Percentage yields of CNMs produced and (b) PXRD diffractograms of the raw fly ash and the CNMs that were formed from 500-700°C.....	129
Figure 6.9: (a) Thermal decomposition (b) Weight loss derivative, (c) laser Raman spectroscopy spectra and I _G /I _D ratio of CNF products from fly ash exposed to CO ₂ and then C ₂ H ₂ at 500-700°C.....	130

CHAPTER 7

Figure 7. 1: XRF analyses of Duvha and Grootvlei coal fly ash components	137
Figure 7. 2:Percentage yield of CNFs formed from coal fly ashes from Duvha and Grootvlei	138
Figure 7. 3: (a) SEM micrographs of CNFs produced from fly ash (a) Duvha fly ash (b) Grootvlei ash, (c) CNFs from Duvha ash and (d) CNFs from Grootvlei ash.....	139
Figure 7. 4: (a) Laser Raman spectroscopy spectra and (b) thermogravimetric analysis of spectra of CNFs produced from fly ash synthesized at 650°C ..	140
Figure 7. 5: (a) Tensile strength and (b) Young's Modulus of untreated and acid treated polyester composites	142
Figure 7.6: SEM images of fractured specimens (a) Neat polyester, (b) 0.125% CNFs, (c) 0.25% CNF and (d) 0.5% CNF loading	143

CHAPTER 8

Figure 8.1: (a) SEM micrographs of CNFs produced from fly ash and (b) Fibre diameter size distribution of CNFs at 650 °C respectively.....	150
Figure 8.2: a) SEM micrographs of CNFs produced from fly ash treated with (a) KMnO_4 and (b) HCl/HNO_3	151
Figure 8.3: Fibre size distributions of CNFs produced from fly ash synthesized at 650°C, treated with (a) KMnO_4 and (b) HCl/HNO_3	151
Figure 8.4:Laser Raman spectroscopy spectra of CNFs produced from fly ash, synthesized at 650 °C and treated with (a) KMnO_4 and HCl/HNO_3 (b) enlarged view of the CNFs treated with KMnO_4	152
Figure 8. 5:PXRD diffractograms of CNFs produced from fly ash synthesized at 650°C and treated with KMnO_4 and HCl/HNO_3 respectively	153
Figure 8. 6: (a) FTIR spectra of CNFs produced from fly ash synthesized at 650°C and treated with KMnO_4 and HCl/HNO_3	154

Figure 8.7:(a) Percentage Weight loss and (b) Weight derivative of CNFs produced from CNFs synthesized at 650 °C and treated with KMnO ₄ and HCl/HNO ₃	156
Figure 8.8: Stress vs strain graph of untreated and acid treated polyester composites	157
Figure 8.9: (a) Tensile strength and (b) Young’s Modulus of untreated and acid treated polyester composites	158
Figure 8. 10: Flexural stress vs strain graph of untreated and acid treated polyester composites	159
Figure8. 11: Flexural properties of untreated and acid treated polyester nanocomposites.....	160
Figure 8. 12: Fracture toughness of Modulus of untreated and acid treated polyester composites.....	161
Figure 8. 13: SEM micrographs of CNFs produced from fly ash (a) untreated and (b) HCl/HNO ₃	162

List of Tables

CHAPTER 2

Table2. 1: Minerals found in coal	11
Table2. 2: Fly ash as catalyst	23
Table 2.3: The use of CO ₂ as a carbon source for CNM synthesis	33

CHAPTER 3

Table3. 1: List of chemicals used in this study	56
Table3. 2: List of gases used in this study	56
Table3. 3:List of equipment used in this study	56

CHAPTER 4

Table4.1: The chemical composition of South African coal fly ash samples obtained by XRF.....	73
Table4. 2: Room temperature Mössbauer parameters for:(a) the as-received and (b) acetylene treated fly ash samples	87

CHAPTER 5

Table5. 1: Summary of the hyperfine parameters obtained from the fits to the data for all the samples	113
---	-----

CHAPTER 7

Table 7. 1: Mechanical properties of CNTs	134
---	-----

CHAPTER 8

Table8. 1: N ₂ Physisorption data of untreated and acid oxidized CNFs.....	149
Table8.2: FTIR spectroscopy band assignment table of CNFs produced from fly ash synthesized at 650°C and treated with KMnO ₄ and HCl/HNO ₃	155

Nomenclature

$\text{CO}_2\text{-C}_2\text{H}_2$:	CO_2 used as carbon source, then flushed out with hydrogen and then introducing C_2H_2
$\text{CO}_2/\text{C}_2\text{H}_2$:	CO_2 and C_2H_2 used as carbon sources in a reaction at the same time.
$\text{C}_2\text{H}_2\text{-H}_2$:	Hydrogen used as a carrier gas in the presence of acetylene as a carbon source
$\text{C}_2\text{H}_2\text{-N}_2$:	Nitrogen used as a carrier gas in the presence of acetylene as a carbon source
$\text{H}_2,\text{C}_2\text{H}_2\text{-N}_2$:	Hydrogen used as a pre- reductant in the presence of nitrogen as a carrier gas and acetylene as a carbon source
$\text{N}_2,\text{C}_2\text{H}_2\text{-H}_2$:	Nitrogen used as a pre- reaction gas in the presence of hydrogen as a carrier gas and acetylene as a carbon source

List of Symbols and Abbreviations

ASTM:	American Society for Testing and Materials
a.u:	Arbitrary unit
BET:	Brauner-Emmet Teller
Btu/lb:	British thermal unit/pound
C ₂ H ₂ :	Acetylene
ca:	Approximately
CNF(s):	Carbon nanofiber(s)
CNM(s):	Carbon nanomaterials
CNT(s):	Carbon nanotube(s)
CO ₂ :	Carbon dioxide
CNS(s):	Carbon nanosphere(s)
Cu:	Copper
Co:	Cobalt
CVD:	Chemical vapor deposition
EU:	European Union
EDS:	Energy dispersive spectrometer
FA:	Fly Ash
Fe:	Iron
Fe ₃ C:	Iron Carbide
Fe ₂ O ₃ :	Iron Oxide
FTIR:	Fourier transform infrared spectroscopy
g:	Gram(s)
h:	hour(s)
H ₂ :	Hydrogen
H ₂ O:	Water
H ₂ SO ₄ :	Sulfuric Acid
HCl:	Hydrochloric acid
HCNF:	Helical carbon nanofibres
ID:	Intensity of the D-band
IG:	Intensity of the G-band

JEOL:	Japan electron optics laboratory(s)
KMnO ₄ :	Potassium Permanganate
KV:	Kilovolts
min:	Minutes
mL:	Millilitres
mL/min:	Millilitres per minute
mm:	Millimetres
mol:	Moles
MWNT:	Multi walled carbon nanotubes
N ₂ :	Nitrogen
nm:	Nanometres
NPs:	Nanoparticles
ppm:	Parts per Million
PHR:	Parts per Hundred Rubbers
ScCO ₂ :	supercritical Carbon dioxide
SEM:	Scanning electron microscope
s:	Seconds
SrO:	Strontium oxide
SWNT:	Single walled carbon nanotubes
T:	Temperature
t:	Time
TEM:	Transmission electron microscope
TGA:	Thermogravimetric analysis
TPa:	Terapascal
TPR:	Temperature programmed reduction
UFS:	Ultimate Flexural Strength
US:	United States
VARTM:	Vacuum Assisted Resin Transfer Mould
wt.%:	Weight percentage
XRD:	X-Ray diffraction
XRF:	X-Ray Fluorescence

Chapter 1: Overview and Scope

1.0 Introduction

Fly ash, also known as pulverised ash, is one of the largest produced solid wastes in the world due to the global reliance on coal fired power plants for the generation of electricity¹. Fly ash mostly consists of silicon dioxide (SiO₂), aluminium oxide (Al₂O₃) and iron oxide (Fe₂O₃) minerals mixed with other elements such as calcium (Ca), magnesium (Mg), silica (Si), sodium (Na), aluminium (Al), iron (Fe), and potassium (K). In small amounts various trace elements such as cadmium (Cd), copper (Cu), arsenic (As), selenium (Se), zinc (Zn), molybdenum (Mo), manganese (Mn), lead (Pb), boron (B), chromium (Cr), cobalt (Co) and nickel (Ni) are also found.

At present less than 30% of the fly ash produced worldwide is currently being recycled. Countries that are on the forefront in terms of re-using fly ash include the EU (90%), China (67%), US (50%) and India (45%). Other nations such as South Africa (SA) are still struggling to find ways to reuse this material, with its usage levels at only 5% and this mostly in the construction industry.

The management and disposal of these large amounts of coal combustion by-products, such as fly ash, has led to many environmental problems². Major environmental concerns arise from the toxic metal content contained in these materials, albeit in small amounts. Dumping of the ash leads to the possibility of these toxic metals leaching out into the ground water, nearby surface water or by it being blown away, leading to air pollution³. There is also a long term financial burden associated with the maintenance of the land onto which it is dumped, which has led researchers to try find ways of using fly ash as a value added product⁴.

At present the fly ash has been used in a lot of applications such as in: construction, agriculture, environmental protection, depth separation, the ceramic

industry and in catalysis. In recent years, researchers have attempted to explore the use of coal fly ash as a catalyst for carbon nanomaterial (CNM) production. Factors such as the affordability of fly ash and its ready availability, have increased the interest of this waste material in the nanotechnology field^{5,6}. More importantly, it contains all the metals that are normally used as catalysts for CNM production such as Fe, Co and Ni.

In this study the Rosheville coal fly ash (a blended waste coal fly ash material) was used as a catalyst for CNM synthesis without any pre-treatment or the addition of other metals. Roscheville ash is a combination of different ashes that were manufactured at different power stations and were dumped off at Roscheville. Here, Mössbauer spectroscopy was used to identify which metal in the coal fly ash was responsible for CNM synthesis. After this, studies comparing nitrogen (N₂) and hydrogen (H₂) as carrier and pre-treatment gases were performed, by interchanging these gases in the reaction to obtain optimal yields of CNMs of uniform morphologies. In a follow up study, the use of a different carbon source (CO₂) which is a waste material as well, either as a sole source or as addition to the traditional carbon source (C₂H₂) was conducted. This was performed to see the effects that CO₂ would have on the yield and morphology of CNMs formed. A comparative study of two further waste coal fly ashes (i.e. Duvha and Grootvlei) was then conducted. These two ashes were chosen because of their vastly different textures and morphology to each other and Rosheville. Because of their excellent properties, these CNMs from ash were used as fillers to improve the tensile mechanical strength of polyesters. Different loadings were used and the one which gave the highest strength was used in the proceeding studies. To further improve the strength of these polymer materials, these CNMs were also treated with different oxidants and acids to assist with the interaction between filler and matrix.

Currently, CNMs are produced using a variety of techniques, such as laser ablation, arc-discharge and chemical vapour deposition (CVD). During laser ablation, a carbon target doped with catalyst particles is vaporised by a high-

powered laser and CNMs are formed. For the arc-discharge method, a large current is applied between two high purity graphite electrodes such as the anode and cathode which then leads to carbon vaporisation. In CVD, a hydrocarbon gas mixture (e.g. C_2H_2) is reacted over a supported metal catalyst resulting in CNMs being formed if proper parameters are maintained. All these techniques present their advantages and limitations, but the most promising and widely used method for CNM production to date has been the CVD technique. This is due to the method being straight forward, cheap and not requiring a lot of steps. The synthesis of CNMs using a CVD method was first reported in 1960⁷. However, interest in the field was only sparked after 1991, when Ijima reported the nanometre sized carbon nanotubes using the arc-discharge method⁸. Thereafter, CNMs such as carbon nanotubes (CNTs) and carbon nanofibres (CNFs) have received a lot of scientific and industrial attention, due to the unique properties they possess, including a high Young's modulus and tensile strength as well as good thermal and electrical conductivities⁹. These unique properties have led to CNMs being used in a lot of applications such as biomedical, electrical, automobile, aerospace and in catalysis to mention a few.

1.2 Problem Statement

A literature study of the CVD technique for CNM production has revealed that several factors still limit its commercial applicability^{7,10-16}. One of the major issues is the cost associated with the catalysts used in the CNM synthesis. CNMs are normally synthesized from expensive metal catalysts including transition metals such as Fe, Ni and Co. Fly ash contains them (Fe) in trace amounts (< 5%) as there is an abundant supply of fly ash, and hence the use of fly ash as a catalyst, offers an affordable alternative.

1.3 Research Questions

The following research questions were posed:

1. Can carbon nanomaterials (CNMs) be synthesized from South African coal fly ash without the addition of a catalyst or pre-treatment?
2. Is this method reproducible?

3. What are the optimum conditions to achieve reproducibility and high yield of these CNMs?
4. Can a waste product (i.e. CO₂) be used as a carbon source on its own or will its use as an additive or prereactant to acetylene give better yields, different types of morphology?
5. Can CNFs made from coal fly ash be used as a primary reinforcement in a polyester polymer? If so, will the mechanical strength of this composite be higher than the polyester by itself.

1.4 Research Aims and Objectives

1.4.1 Broad Research Aims

Studies that have demonstrated the use of fly ash as a catalyst or template in the synthesis of CNMs are limited^{5,6,17}. Fly ash has previously either been used directly as a support for other more active metallic catalyst particles^{5,17} or after extensive treatment⁶. At present, no research has been done using South African coal fly ash to make CNMs. The aim of this work is therefore to use South African coal fly ash as a catalyst to make CNMs via the CVD method.

This thesis reports a simple, direct route for the synthesis of carbon nanomaterials using coal fly ash as a catalyst. No pre-treatments or additions of expensive catalysts were used as the coal fly ash was used as received. This study also reports on the addition of functionalised CNFs into a polyester polymer to test their reinforcement capabilities.

1.4.2 Specific Aims:

The specific aims of this study have been to:

- i) Characterise as received fly ash using X-ray fluorescent spectroscopy (XRF), energy dispersive spectroscopy (EDS) and powder X-ray diffraction (PXRD).
- ii) Synthesize novel nanofibres from fly ash via CVD.
- iii) Understand the characteristics and chemical nature of the nanofibres by using powder X-ray diffraction (PXRD), energy dispersive spectroscopy

(EDS), Fourier transform infra-red spectroscopy (FTIR), nitrogen adsorption using Brauner-Emmett-Teller (N₂ BET) analysis, transmission electron microscopy (TEM), scanning electron microscopy (SEM), thermal gravimetric analysis (TGA) and Mössbauer spectroscopy.

- iv) Study the effect of the important operating variables, namely: flow rate, gases and temperature, for the synthesis of CNMs in order to obtain optimum reaction conditions.
- v) Compare the use of varying carbon sources such as carbon dioxide (CO₂) and acetylene (C₂H₂) for the synthesis of CNFs.
- vi) Test the mechanical properties, such as tensile strength of the polyester before and after mixing with CNF fillers.

1.5 Hypothesis

Based on studies that have been conducted using metallic catalysts with the same metals contained in fly ash¹⁸⁻²¹, the following hypothesis has been formulated:

Without any additional catalyst or pre-treatment, South African fly ash can act as a catalyst in the synthesis of carbon nanofibres.

1.6 Structure of the thesis

This thesis is organized into nine chapters, including this chapter, structured as follows:

Chapter 1: Overview and scope

This chapter gives an overview of the area under study, justification for the study and highlights the problems currently facing the synthesis of CNMs from fly ash as a catalyst.

Chapter 2: Literature review

Here a literature review on fly ash and CNMs is presented. This chapter reviews the different uses of fly ash and the effect of catalyst and carbon source on the synthesis of CNMs. Lastly the methods used to make these CNMs and their use in polymer composites is presented.

Chapter 3: Materials and methods

In this chapter the materials, methodology and characterization techniques used are presented.

Chapter 4: Direct synthesis of carbon nanofibres from waste coal fly ash and a study of the metals responsible for CNM production using EDS, Mössbauer and Powder X-ray diffraction

Results on the synthesis of CNMs using Rosheville fly ash as a catalyst are presented in this chapter. Here, the metals responsible for CNM synthesis were studied using EDS, Mössbauer and PXRD. This chapter has been published as: *Hintsho, N.; Shaikjee, A.; Masenda, H.; Naidoo, D.; Billing, D.; Franklyn, P.; Durbach, S. Nanoscale Research Letters 2014, 9, 1-11*

Chapter 5: Effect The effect of nitrogen and hydrogen gases on the CVD synthesis of carbon nanomaterials from acetylene, using South African coal fly ash as a catalyst.

In this chapter the effect nitrogen and hydrogen gases on the CVD synthesis of CNMs using acetylene as the carbon source, are presented. The chapter also provides the effects of using different temperatures and varying flow rates of these gases on the synthesis of CNMs.

Chapter 6: The effect of CO₂ on the synthesis of carbon materials via CVD using fly ash as a catalyst

Here, the use of CO₂ as a lone carbon source for CNM synthesis is presented. The effect of using CO₂ as an additive and a carbon source prior to reaction with C₂H₂ is also reported. This chapter has been published as: *N.C Hintsho; A. Shaikjee; P.K Triphati.; P. Franklyn; S.D. Durbach, RSC Advances 2015 5, 53776-53781.*

Chapter 7: A comparison of Duvha and Grootvlei fly ashes in their ability to synthesise CNFs

In this chapter a comparison of Duvha (very fine) and Grootvlei (very coarse) fly ash and their ability to form CNFs using acetylene as a carbon source and

hydrogen as a carrier gas at varying temperatures, is presented. Mechanical properties such as tensile strength are also presented.

Chapter 8: Synthesis and characterisation of a CNF/polyester composite

In this chapter the synthesis and characterisation of a novel CNF/polyester composite is reported. Special attention is given to the mechanical properties of this CNF reinforced polyester composite.

Chapter 9: General discussion and conclusions

In this final chapter the main findings of this entire study are summarized. In addition an outline of aspects that require further investigation based upon the results of this study are outlined.

1.3 References

1. S. Jala and D. Goyal, *Bioresource technology*, 2006, **97**, 1136-1147.
2. C. Rao, *Environmental pollution control engineering*, New Age International, 2007.
3. C. Sullivan, M. Tyrer, C. R. Cheeseman and N. J. Graham, *Science of the Total Environment*, 2010, **408**, 1770-1778.
4. M. Blanco-Carrasco, F. Hornung and N. Ortner, *Green Concrete Technologies*, 2010, 1-63
5. O. M. Dunens, K. J. MacKenzie and A. T. Harris, *Environmental science & technology*, 2009, **43**, 7889-7894.
6. N. Salah, S. S. Habib, Z. H. Khan, A. Memic and M. N. Nahas, *Digest Journal of Nanomaterials and Biostructures*, 2012, **7**, 1279-1288.
7. M. Sharon and M. Sharon, *Synthesis and Reactivity in Inorganic, Metal-Organic and Nano-Metal Chemistry*, 2006, **36**, 265-279.
8. S. Iijima, *Nature*, 1991, **354**, 56-58.
9. M. M. Shokrieh, A. Saeedi and M. Chitsazzadeh, *Journal of Nanostructure in Chemistry*, 2013, **3**, 1-5.
10. M. Sharon, P. Apte, S. Purandare and R. Zacharia, *Journal of Nanoscience and Nanotechnology*, 2005, **5**, 288-295.
11. R. Blackmon and A. Rinzler, *International assessment of research and development of carbon nanotube manufacturing and applications*, 2005, **4**, 7.
12. S. K. Chaudhuri and B. Sur, *Journal of Environmental Engineering*, 2000, **126**, 583-594.
13. Y. Li, J. Liu, Y. Wang and Z. L. Wang, *Chemistry of Materials*, 2001, **13**, 1008-1014.
14. Y. Li, D. Mann, M. Rolandi, W. Kim, A. Ural, S. Hung, A. Javey, J. Cao, D. Wang and E. Yenilmez, *Nano letters*, 2004, **4**, 317-321.
15. J.-F. Colomer, C. Stephan, S. Lefrant, G. Van Tendeloo, I. Willems, Z. Konya, A. Fonseca, C. Laurent and J. B. Nagy, *Chemical Physics Letters*, 2000, **317**, 83-89.

16. A. M. Cassell, J. A. Raymakers, J. Kong and H. Dai, *The Journal of Physical Chemistry B*, 1999, **103**, 6484-6492.
17. A. Yasui, Y. Kamiya, S. Sugiyama, S. Ono, H. Noda and Y. Ichikawa, *IEEJ Transactions on Electrical and Electronic Engineering*, 2009, **4**, 787-789.
18. T. Yamada, T. Namai, K. Hata, D. N. Futaba, K. Mizuno, J. Fan, M. Yudasaka, M. Yumura and S. Iijima, *Nature Nanotechnology*, 2006, **1**, 131-136.
19. M. C. Bahome, L. L. Jewell, D. Hildebrandt, D. Glasser and N. J. Coville, *Applied Catalysis A: General*, 2005, **287**, 60-67.
20. P. E. Nolan, A. H. Cutler and D. G. Lynch, *US Patent*, 1998.
21. G. Yamamoto, M. Omori, T. Hashida and H. Kimura, *Nanotechnology*, 2008, **19**, 315708.

Chapter 2: Literature Review

This chapter presents a review of literature associated with fly ash, carbon nanomaterials (CNMs) and carbon polymer nanocomposites. Firstly, this literature review will generally focus on fly ash, its disposal methods and its uses in different applications. Secondly, the use of fly ash as a catalyst for carbon nanomaterial (CNM) synthesis will be discussed and the methods used for their synthesis. Lastly, the use of CNMs such as carbon nanotubes/carbon nanofibres (CNT/Fs) in nanocomposites as fillers to improve the mechanical strength of polyesters will be discussed.

2.1 Coal

South Africa ranks highly amongst the countries that generate the most electricity from combustion of coal in power stations¹. Due to the increased demands of electricity, more than 100 million tons of coal are being used annually². South Africa is ranked as the fifth largest coal producer in the world and the third largest coal exporter, accounting for 12% of the international coal trade³⁻⁶. Several authors compared coal in terms of its export value⁷⁻¹². They clarified that the coal produced in South Africa is amongst the cheapest in terms of its mass and in terms of its energy content because of its low grade.

Coal is regarded as one of the primary energy sources in the world and has characteristics that are greatly dependent on the contents of moisture, ash, volatile matter, carbon, hydrogen, oxygen, sulphur, nitrogen, calorific value, coking parameters, ash composition and fusion characteristics due to its complex nature¹³⁻¹⁸. It is primarily formed from ancient plant material that accumulated in surface environments where the complete decay of organic matter was prevented^{19,20}. It is a hydrocarbon-rich, fossil-fuel resource and like other fossil fuels it has been formed over millions of years, hence it is classified as a non-renewable energy source²¹⁻²³.

2.1.1 Classification of coal

Coal is classified according to its heating value and its relative content of elemental carbon²⁴. There are three different forms of coal that exist, namely: anthracite, lignite and bituminous coals²⁵. Anthracite contains the highest proportion of pure carbon (about 86-98%) and heat value (13,500–15,600 Btu/lb) of all forms of coal. Bituminous coal has lower concentrations of pure carbon (46-86%) and lower heat values (8,300–15,600 Btu/lb). This form of coal is often subdivided on the basis of its heat value, being classified as low, medium, and high volatile bituminous and sub-bituminous. Lignite, the last form of coal, being the poorest of the true coals in terms of heat value (5,500-8,300 Btu/lb), is soft and contains (46-60%) pure carbon with low organic maturity²⁶.

2.1.2 Mineralogy and chemistry of coal

Carbonaceous material that results from the accumulation and decay of plant matter in a fresh water environment is the primary component of coal²⁷. Coal is a complex mixture of organic and inorganic constituents that contain intimately mixed solid, liquid, and gaseous phases²⁸. It contains environmentally detrimental minerals that were deposited along with the plant materials that were formed during calcification²⁹. The types of minerals that are mostly found in coal are depicted in Table 2.1.

Table 2.1: Minerals found in coal

Type of minerals found in coal	
Aluminosilicates	Sulphides
Calcites	Chlorides
Ankerite	Silicates
Dolomite	Pyrites
Siderite	Carbonates

The trace elements in coal are strongly associated with one or more of these minerals. It is also observed that the high ash (> 10 %) coal contains much more

quartz, whereas the carbonates are the dominant minerals in low ash (<10 wt %) coal²⁹⁻³¹.

2.2 Coal fly ash and its classification

The use of coal in combustion systems can give rise to operational and environmental problems, mainly due to the inorganic constituents present in coal^{32, 33}. As a result of coal combustion to generate electricity, more than 100 million tons of by-products, including the heterogeneous waste material known as coal fly ash are being generated annually, worldwide. Fly ash, also known as pulverised ash, is the largest produced industrial waste in the world due to the global reliance on coal fired power plants for the generation of electricity³⁴. According to Yao *et al.*, coal fired generation of electricity accounts for 30% of the world electricity supply². This is expected to increase to 46% by 2030³⁵. This is due to the fluctuating high prices for oil and natural gas, which makes the use of coal fired electricity generation economically attractive, especially in countries that are large coal producers (Fig. 2.1).

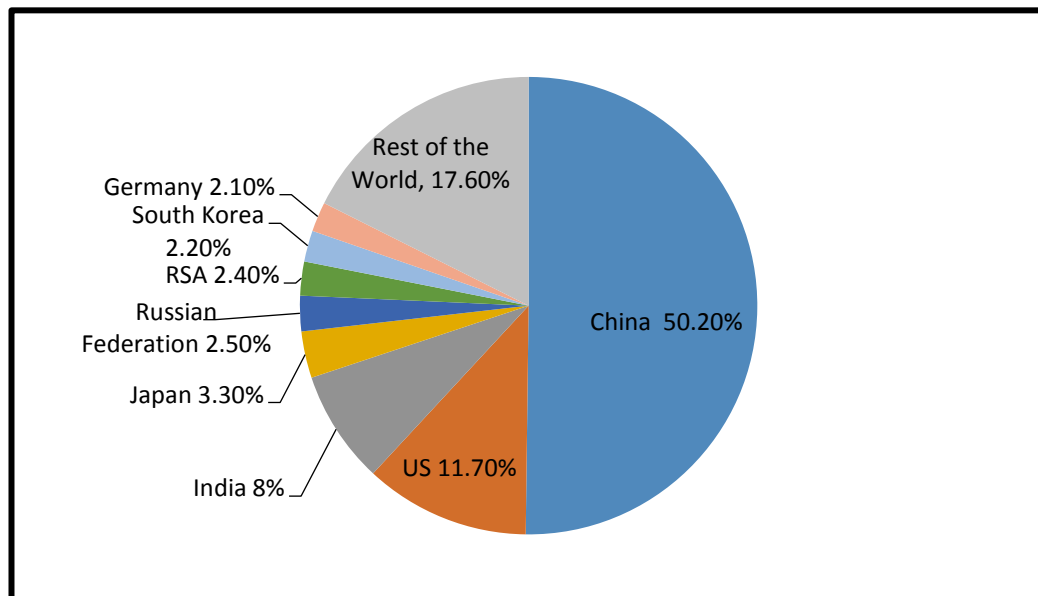


Figure 2.1: Distribution of coal consumption worldwide in 2012³⁴

2.2.1 Chemical composition and physical properties of coal fly ash

Coal fly ash is a grey powder (depending on the iron and un-burnt carbon content), that is light in texture and consists mostly of fine particles with an average size of < 20 μm . It is a heterogeneous material that is mostly amorphous,

depending on the coal type and combustion conditions. This material has a low to medium bulk density (0.54-0.86 g/cm³), surface area (300-500 m²/kg) and a pH range of 1.2-12.5, with most ashes showing alkalinity. Chemically, coal fly ash is composed of calcium (Ca), magnesium (Mg), silica (Si), sodium (Na), aluminium (Al), iron (Fe), and potassium (K) with various trace elements such as cadmium (Cd), copper (Cu), arsenic (As), selenium (Se), zinc (Zn), molybdenum (Mo), manganese (Mn), lead (Pb), boron (B), vanadium (V), chromium (Cr), cobalt (Co) and nickel (Ni)³⁵. Silicon dioxide (SiO₂), aluminium oxide (Al₂O₃) and iron oxide (Fe₂O₃) form the basis of the minerals that are present in coal fly ash³⁶.

Fly ash consists of particles that are spherical in shape that include solid spheres, cenospheres, irregular-shaped debris and porous un-burnt carbon (Fig. 2.2). There are mainly two types of ash, class F and C. Class F is highly pozzolanic, meaning that it reacts with excess lime generated in the hydration of Portland cement and contains less than 20% lime content. This type of ash is produced from anthracite, bituminous and sub-bituminous coals containing less than 7% CaO. Class C, normally originates from the sub-bituminous and lignite coals. It consists mainly of Ca, Al, and Si with a lower loss on ignition (LOI) than class F coal fly ash and contains more lime (5-30%)³⁷.

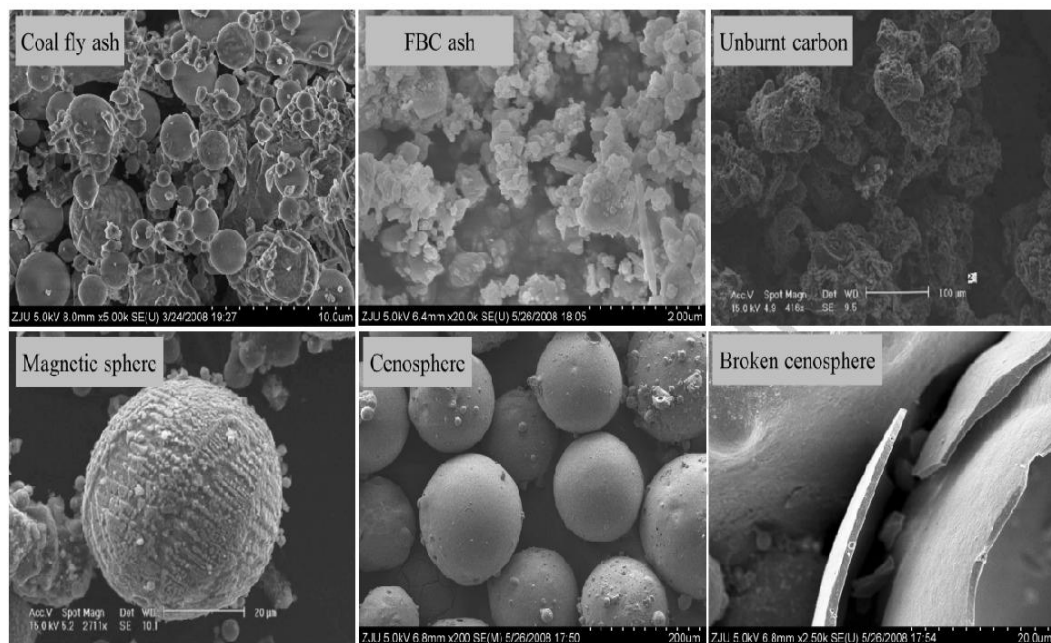


Figure 2.2: Various morphologies of coal fly ash³⁴

2.2.2 Disposal of fly ash

As a result of the increased demands for generating electricity, huge quantities of coal are being combusted, leading to high coal fly ash production and hence high disposal into ash dump sites³⁸. The management and disposal of large amounts of coal combustion by-products such as fly ash has led to a lot of environmental concerns^{2,39}. The major environmental concern arises due to some of the toxic metals contained in fly ash and dumping that might lead to leaching of the metals either into ground water or nearby surface water⁴. Some studies have reported that metal contaminants such as V, Cr, Ni, Cd and Pb have been shown to be hazards to the environment, even though they are found at low levels (ppm). Nyale *et al.* studied the leaching behaviour and geochemical partitioning of some trace elements in a 20 year old ash dump⁴⁰. Their results found that leaching of the trace elements occurred, thus leading to a threat to the air, surface and ground water, soil and crop produce. In another study by Neupane and Danahoe, batch and column leaching tests were conducted to evaluate the leachability of several elements⁴¹. Their findings showed that older unlined fly ash disposal sites could pose an environmental risk of contamination.

Two methods are currently used worldwide for disposing off fly ash, namely; dry disposal and wet disposal methods. During the dry disposal method, the ash is transported by truck from the site and then disposed of in any landfill⁴². In wet disposal, the ash gets transported as slurry through a pipe and disposed of in an ash pond. Wet disposal has been the method most commonly used because of the lower cost associated with it compared to the dry method. In recent years though, the former method has been under a scrutiny as more studies have revealed that due to the environmental reasons associated with the leaching of metals from ponds, wet disposal may not be so safe, hence the need to find a suitable utilization of the ash^{43,44}.

2.3 Uses of fly ash

In-order to find use for this material, understanding the physical, chemical and mineralogical properties of fly ash is of high importance, as these properties will

ultimately be the determining factor in its use. The specific properties depend mainly on the type of coal that was used, whether it was bituminous, lignite or sub-bituminous and also the combustion conditions. Research has shown the use of fly ash in various industries: construction, for the production of cement and concrete, catalysis for the synthesis of zeolites; as a filler in the polymer industry; as a soil additive in agriculture for composting; improving crop and growth yield, petroleum for use as catalysts; and water treatment for neutralization of acid mine drainage^{36,45-48}. Though the ash has been applied in various industries, its use is limited since more than 70% of the ash produced worldwide is still unattended to^{43,49,50}.

According to the Central Electricity Authority (CEA) in the 2013 financial year, about 160 million tons of ash was generated in China, which is the highest producer of ash, out of which 110.37 million tons was utilised. In 2013, South African electricity company, ESKOM, was reported to have produced about 25 million tons per annum of coal fly ash⁵¹. For that large amount of fly ash produced annually, only about 4.8% was used in the industries mentioned above, with the main uses being in the construction, agriculture and polymer industries. In the construction industry, the main benefit of coal fly ash was to reduce the amount of non-durable calcium hydroxide (lime), by converting it into calcium silicate hydrate (CSH), which is the strongest and most durable portion in concrete⁵².

In the polymer industry, which has grown vastly in the past 20 years, fly ash has been used as filler in an attempt to improve the strength of polymer materials⁵³.

Fillers can be defined as particles that can be added to plastics or composite materials either to lower the use of an expensive material or to improve the properties of the materials⁵⁴. At present, more than 53 million tons of different types of fillers are used every year. In the last decade, carbon nanomaterials have been shown to be the filler of choice due to their properties such as tensile strength, elastic modulus and electric and thermal conductivity⁵⁵⁻⁵⁷. Thus, with a

small addition of these, an improvement in the mechanical and electrical properties of various materials can be expected^{21,57,58}.

Recent reviews have presented the work done in terms of the uses of fly ash⁵⁹. Also other reviews have been conducted on fly ash utilisation, such as a soil additive^{1, 60-62}, glass ceramics⁶³, as a filler or substitute in concrete^{64,65}, catalyst for heterogeneous catalysis⁶⁶, adsorbents for mercury removal and waste water treatment^{67, 68} etc. However, as a recently growing field, the use of fly ash as a catalyst or catalyst support in the synthesis of carbon nanomaterial synthesis has not yet been explored or reviewed.

Other uses of this ash, such as in environmental protection, depth separation, and in the ceramic industry and as a valuable metal recovery element have also been explored²⁹. Recycling coal ash in these applications can assist in achieving significant economic and environmental benefits. At present, the re-use of fly ash is at an estimated 25% level with the leading regions or nations being the EU (90%), China (67%), US (50%) and India (45%). Other nations such as South Africa (SA) are still battling on how to reuse this material, with their usage levels at only 5%.

2.3.1 Fly ash as filler in the polymer industry

India, China, Australia and South Africa are the largest producers and users of coal^{69,70}. Researchers from across the globe have demonstrated the use of fly ash as a filler in the polymer, nanotechnology and construction industry⁷¹⁻⁷⁵. In one study, Hundiwale *et al.* investigated the use of different types of composites of varying percentages of Indian fly ash that were prepared using the two roll mill method⁷⁶. Tensile strength, modulus, hardness and density were some of the properties investigated. The study showed that the fly ash filled composites improved the mechanical strength of the rubber to a maximum compared to those filled with calcium carbonate.

In another study, Menon *et al.* used fly ash as a filler in the presence of cardanol prepolymers (PCP) and hexamethylene tetramine cure PCP⁴⁶. Their results showed a decrease in the amount of energy used for mixing and an increase in the tensile properties (tear strength and thermal stability). Though these results were positive, the majority of other investigations performed have found the improvement to be too marginal^{75,78,79}. In a different study, Chaowasakoo *et al.* found that the mechanical strength of polyisoprene rubber filled with fly ash was not improved when compared to the rubber filled with silica⁴⁹. Alkadasi *et al.* suggested that using silane coupling agents such as vinyl trichlorosilane in fly ash filled rubber could improve the mechanical properties and there was a 20% improvement in their tensile strength in their study⁵⁰. Additionally, Sombatsombop *et al.* studied the effects of untreated fly ash as filler in natural and styrene butadiene⁴⁴. They suggested that fly ash silica can be used in natural rubber at concentrations of less than 30 phr but could not be used in styrene butadiene due to deterioration of property.

Previous reports suggested that the decrease in the fly ash performance could be caused by the use of untreated fly ash, which leads to a reduction in filler-rubber interaction resulting in smooth surfaces^{82,83}. The induced crystallinity also played a role and Paul *et al.* overcame these difficulties by preparing nanostructured fly ash using mechanical activation⁵¹. Their results showed an increase in surface area, better surface activity and an amorphous material. They explained that the amorphous material would be beneficial for applications, such as a particulate nanofiller in polymer matrices, which could in principle lead to better compatibility with various polymer matrices^{57,74,84}.

2.3.2 Fly ash as filler in the construction industry

In the construction industry, fly ash has predominantly been used as a substitute, either as raw material or an additive. Fly ash has been shown to improve the long term durability properties of concrete by reducing the ingress of aggressive agents such as chloride ions⁸⁵. In general, the amount of ash added for concrete ranges from 15-35% and can go as much as 70% for concrete in construction like

pavement, walls and parking lots. McCarthy and Dhir investigated the use of low lime ash as a cement component where they found that up to 45% could be combined with Portland cement in-order to produce different kinds of concrete design strengths⁵⁹.

Joseph *et al.* evaluated the engineering properties of geopolymer concrete from alkali fly ash⁶⁰. Their results showed that the geopolymer concrete gave a higher value of modulus elasticity compared to ordinary cement concrete. This material was shown to be highly useful in geotechnical applications. Edil *et al.* studied the use of pozzolanic and compacted fly ash as a hydraulic barrier in landfills⁶¹. They found that pozzolanic fly ash did not crack due to the low shrinkage it possessed and compacted ash underwent a slight change. Therefore, pozzolanic ash was found to have better qualities.

From the above-mentioned studies, it has been shown that fly ash can be successfully used as filler in the construction industry. In other countries such as the US and EU, this industry can be affected by seasonal changes at times. The cement is mostly needed during the summer months when building conditions are at their peak, but the downside is that the ash is mostly produced during the winter months. This is due to coal generators that are restricted to double shifting in summer causing the loss on ignition (LOI) content of the ash to be increased, thus reducing the quality of the ash.

2.3.3 Fly ash as a soil additive

Research on the agricultural uses of fly ash has been on the forefront in the past few decades^{1,60,89-93}. This is due to the essential micronutrients that are contained in the ash. Fly ash contains macronutrients such as P, K, Ca, Mg and S and micronutrients such as Fe, Mn, Zn, Cu, Co, B and Mo, except organic carbon and nitrogen. This material has been shown to cause harm when it settles on leaves but when applied scientifically for agricultural purposes, it has proven to be beneficial⁸⁹. In agriculture, it has been used for improving soil properties, as a source of plant nutrients, as a pesticide, in composting and for improving crop and

growth yield. In an attempt to alter the soil texture, increase micro porosity and improve the water holding capacity. Basu *et al.* added this ash to improve the physical and chemical properties of soil and shifted the USDA textural class of the refuge from sandy loam to silt loam⁶⁷.

Chang *et al.* observed that among five soil types, Reyes silty clay showed an increase in the bulk density varying between 1.25 and 1.60 g⁶⁵. When testing the water holding capacity, Pandey *et al.* found that fly ash amendment increased the water holding capacity of sandy/loamy soils by 8%, which in turn led to an improvement in the hydraulic conductivity⁶⁴. In a similar study, Sakar and Rano revealed that the fly ash obtained from a thermal power plant working on stoker fired combustors had the highest water holding capacity, followed by one working on pulverised fuel combustor⁶⁸. This improvement in water holding capacity was of paramount importance for the growth of plants under rain fed agriculture.

Looking at other properties of fly ash, such as the soil pH, and depending on the source, fly ash can be acidic or alkaline. The hydroxide and carbonate salts found in the ash give it the ability to neutralize the acidity in soil. Fly ash has been shown to act as a limiting material to neutralise soil acidity and provide plant available nutrients⁹². Gupta *et al.* used an excessive quantity of un-weathered fly ash to alter the pH and increase the soil salinity⁶⁹.

In an effort to analyse the biological properties of soil, there has not been a lot of research that has been conducted in the field¹⁰¹. Several laboratory experiments have been conducted, where it has been shown that the un-weathered fly ash, particularly in a sandy soil, greatly inhibited the microbial respiratory enzymatic activity and soil N-cycling processes like nitrification and N-mineralisation¹⁰³. These inhibitions could have been caused by the excessive presence of soluble salts and trace elements found in the un-weathered ash or extremely alkaline (pH 11-12) ash⁹². Applying lignite fly ash also yielded negative results as there was a reduction in the growth of soil borne pathogenic microorganisms as reported by Karpagavalli *et al.* where the population of *Rhizobium* sp and P-solubilizing

bacteria were increased under the soil added with either farmyard manure or fly ash individually⁷⁰. Addition of Class F bituminous fly ash to soil produced positive results, as it improved the population of fungi, including *arbuscular mycorrhizal* fungi and gram negative bacteria as shown from the analysis of community of fatty acids.

Tiwari *et al.* isolated 11 bacterial strains from the rhizospheric zone of *Typhalatifolia* and inoculated them separately in the fly ash to investigate their ability to increase bioavailability of toxic metals⁷¹. They found that most of the bacterial strains either enhanced the mobility of Zn, Fe and Mn or immobilised the Cu and Cd. Though most of the fly ash applications have been covered in agriculture as an amendment, this waste material has also been used to solve soil shortage problems.

Fly ash was used as a source of plant nutrients. Chemically, fly ash contains elements such as Ca, Fe, Mg and K that are essential for plant growth but also other elements and metals that can be toxic to the plants. Basu *et al.* examined the principal chemical properties of artificial soil consisting of organic residue and inorganic fly ash⁶⁷. Their results showed that the artificial soil was suitable for agricultural use after irrigation and desalination.

Because fly ash lacks some nutrients, this deficiency has somehow limited the application of fly ash in agricultural use or as an additive. Therefore, several studies have been carried out to blend fly ash with potentially acid forming organic by-products such as sewage sludge, poultry and animal manure. Co-application of fly ash has been shown to have more advantages such as enhancing soil organic matters, decreased bioavailability of toxic metals and indirectly stimulating microbial activity. Amongst these amendments, the farm manure and sewage sludge have been found to be the most effective.

2.3.4 Fly ash in environmental protection

In an effort to increase the use of this material, it has also been used in the reduction of the environmental burden. Fly ash is mostly alkaline and mostly contains a large amount of un-burnt carbon with a negatively charged surface at high pH. Because of all these properties, it is expected to have a high adsorption capacity. The feasibility of using fly ash as a low cost adsorbent instead of using the commercial activated carbon or zeolites for various adsorption processes has been studied⁶⁷.

In the removal of organic pollutants, Gianoncelli *et al.* used dried activated sludge and fly ash to remove phenol⁷². They found that the maximum phenol loading capacity for each sorbent was 91.0 mg/g for dried activated sludges and 27.9 mg/g for fly ash at 100 mg/l initial phenol concentration. Kao also removed chlorophenol efficiently from waste water using a fly ash column⁷³. Matheswaran and Karumanithi investigated the removal of chrysoidine R from aqueous solution using fly ash as an adsorbent⁷⁴. Sing also showed the adsorption capacity of fly ash in the removal of metribuzin, metalochlor and atrazine from water⁷⁵. Increasing the fly ash content resulted in an increase in the amount of herbicides adsorbed. The maximum adsorption capacities were found to be 0.56, 1.0 and 3.33 mg/g respectively. Other organic pollutants such as chlorophenols, organic acids and polychlorinated biphenyls were also efficiently adsorbed by fly ash.

2.3.5 Fly ash as a catalyst

The use of metal and metal oxides as catalysts has been well documented¹⁰³⁻¹⁰⁶. In catalytic applications, coal fly ash has been investigated for its potential as a replacement to reduce consumption of materials that are expensive to produce¹⁰⁴⁻¹¹⁴.

In the past, fly ash had been used as a catalyst support in industries such as hydrogen production^{66,113}, water gas cleaning (SO_x and NO_x)¹¹⁴⁻¹¹⁶, methane oxidation, water treatment and petroleum hydrocracking¹¹⁷⁻¹²¹. Fly ash has also been used in the coal conversion processes for reactions in gas, liquid and solid

gas phase as a full catalyst^{66,122-125}. These studies include, the steam methane reforming and water gas shift reactions, gas phase oxidation, liquid phase hydrocarbon cracking and alkylation, aqueous oxidation, solid waste pyrolysis and solvent free reactions (Table 2.2)^{66,122-143}.

Though fly ash had been used for the above mentioned applications, of interest lately, has been its use as a catalyst for carbon nanomaterials synthesis^{5, 17, 128, 129}.

Table2. 2: Coal or Wood Fly ash as catalyst

Catalyst	Function	Application	References
Coal fly ash	Synthesis of novel zeolite NaX	Biodiesel production	103
Fe-impregnated ash	Synthesis of carbon nanomaterials	Carbon nanomaterial production	5
Japanese fly ash	Synthesis of carbon nanomaterials	Carbon nanomaterial production	17
Carbon rich fly ash	Synthesis of carbon nanomaterials	Carbon nanomaterial production	128
South African fly ash	Synthesis of carbon nanofibres	Carbon nanomaterial production	129
Coal ash	Catalytic activity of coal ash in gas phase reactions for syngas production	Steam methane reforming and water gas shift reaction	130
Coal fly ash	Catalytic oxidation of VOCs in the thermal process	Gas phase oxidation	131
Coal fly ash	Catalytic oxidation of VOCs in non-thermal process	Gas phase oxidation	132
Coal fly ash	Catalytic oxidation of odorous Sulphur compounds	Gas phase oxidation	133
Wood fly ash	Compare the activity of wood with coal fly ash in the catalytic oxidation of hydrogen sulfide and methanethiol	Catalytic ozonation	113
Wood fly ash	To destroy H ₂ S using the catalytic oxidation in air	Gas phase oxidation	134
Wood coal fly ash	Test wood fly ash as a catalyst for catalytic oxidation in aldehydes	Gas phase oxidation	113, 134, 135
Glass crystal microspheres separated from coal fly ash	Test the catalytic activity of three different types of microspheres separated from coal fly ash in oxidative conversion of methane	Gas phase oxidation	136
Coal fly ash	Synthesis of zeolite beta for commercial catalytic applications	Liquid phase hydrocarbon cracking and alkylation	137
Coal fly ash	Converting fly ash into a zeolite using the alkali fusion method and tested it for cracking of a heavy crude residue.	Liquid phase hydrocarbon cracking and alkylation	138
Coal fly ash (HZOP-31)	Alkylation of phenol with tert-Butyl alcohol over a catalyst synthesized from fly ash (HZOP-31)	Liquid phase hydrocarbon cracking and alkylation	139
Coal fly ash	Testing the fly ash samples for air oxidation of sodium sulfide	Aqueous oxidation	140

Coal fly ash	Investigated the application of fly ash as a heterogeneous fenton oxidation for reactive dye decomposition.	Aqueous oxidation	12
Coal fly ash	Removal of dye using fly ash as a catalyst	Aqueous oxidation	141
Coal fly ash	Pyrolysis of polypropylene using fly ash derived zeolite as catalysts	Solid waste pyrolysis	142
NaOH/Fly ash	Comparing the catalytic performance of FSA to commercial catalysts.	Solid waste pyrolysis	143
Fly ash supported CaO	Employing fly ash as a recyclable solid base	Knoeveld condensation reaction	144
Fly ash supported CaO	Synthesis of fly ash supported CaO for the transesterification of soybean oil and converting it to fuel grade	Transesterification	145
Activated fly ash	Synthesis of a solid acid catalyst for benzylolation reactions by loading zirconia on chemically activated fly ash	Benzylolation reactions	146
Coal fly ash	Investigation on the selective catalytic reduction of NO with NH ₃ using fly ash as a catalyst	Selective catalytic reduction	147

2.4 Carbon nanomaterials (CNMs)

Carbon nanomaterials can be defined as a group of different forms of carbon found in the nanometre range (1-100 nm). In the past 25 years, there has been extensive research in these materials since the landmark paper by Ijima in 1991. Prior to that, carbon was known to exist in two forms, diamond and graphite¹⁴³. From that work by Ijima, it was discovered that carbon with an sp^2 bonding can form other stable ordered graphitic structures such as CNTs, CNFs, graphene, amorphous carbon and CNSs to mention a few¹⁵⁰.

CNMs consisting of graphitic layers have been on the forefront due to their unique properties and potential use in varying applications. Amongst these CNMs, CNFs with a diameter range of 3-100 nm have attracted a lot of attention in the last two decades. This material was first discovered by mistake as an unwanted product during the catalytic conversion of carbon containing gases¹⁴⁸.

Carbon nanotubes (CNTs) and carbon nanofibres (CNFs) are cylindrical nanostructure materials, which are part of the carbon allotropes¹⁵⁰. CNTs/CNFs belong to the fullerene family, which is a group of materials that consist of 60 carbons¹⁵¹⁻¹⁵³. CNTs/CNFs possess interesting properties, such as their extraordinary electrical and high mechanical strength that make them useful in different applications such as polymer and other fields such as material science, functional and biomedical devices¹⁵⁴.

Thus far, the Chemical Vapour Deposition (CVD) method has been the most popular method used to manufacture carbon nanomaterials¹⁵⁵. This is due to the simplicity of the method, requiring low temperatures and more importantly, due to the suitability of the materials for use in industrial fluidized bed reactors. Generally, CNTs and CNFs can grow by diffusing carbon through a metal catalyst, thus resulting in a graphitic filament^{111,156}. Three types of filaments are formed based on the angle of graphene layers with respect to the filaments¹⁵⁷. They are either stacked, herringbone or nanotubular (Fig 2.3). If stacked or herringbone, they are called “nanofibres” (Fig 2.3a and b) and if they are

nanotubular in shape, they are called “nanotubes” (Fig 2.3c)^{157,158}. In alternative definitions, if the filaments are highly crystallized and have tubular structures approximately below 20 nm, they are nanotubes but if defective and have larger diameter filaments, they are nanofibres. According to Teo *et al.*, CNTs form when diameters of filaments are 50 nm or less¹³². This process occurs when the bond terminating species such as hydrogen in gaseous phase are not in abundance. This is due to the single graphene layers consisting of many dangling bonds that correspond to high energy states. Elimination of these species results in a high reduction of the total energy of a reduced number of carbon atoms, thus promoting the formation of tubular structures¹³².

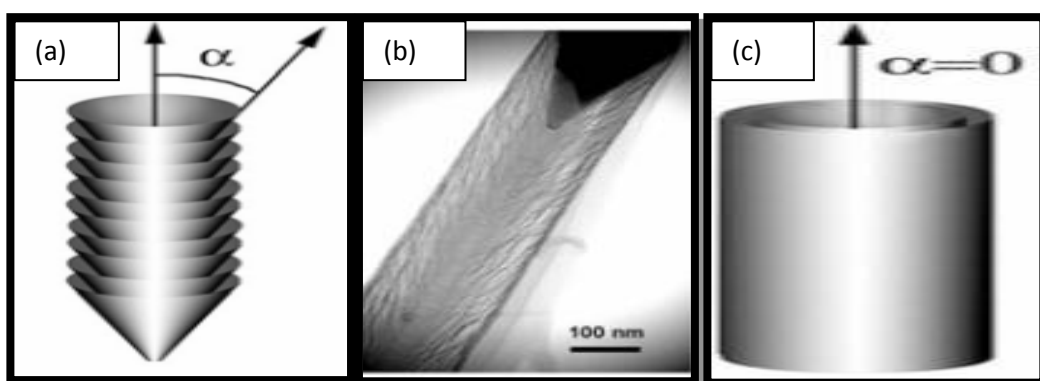


Figure 2.3: Carbon nanostructures:(a) CNFs composed of stacked graphene cones;(b) herringbone type CNF and (c) Tubular type CNTs⁸⁰

A study by Rodriguez *et al.* was one of the first to propose the mechanism of nanofibres growth⁸⁰. The study focused on the ability to create faceted catalyst particles by either controlling or tailoring the structure of nanofibres that are either herringbone or stacked⁸⁰. The study demonstrated under certain conditions that the catalyst particles went through surface faceted reconstruction to form different shapes of nanofibres. The study further showed that herringbone structures were formed when a catalyst particle was an alloy. It was shown that when Fe-Cu particles were used in a C_2H_2/H_2 gas mixture at 600 °C, stacked structures were formed from Fe-based catalyst in a Co- H_2 environment. Nolan and colleagues further stated that H_2 plays a huge role in nanofibre growth and the presence of H_2 can reduce the larger number of dangling bond at the edges of the stacked graphite

plates¹³⁵. H₂ also reduces the formation of undesirable carbon feedstock; this is due to the hydrogenation effect that H₂ has on the reactive carbon species in the gas phase²⁰. Even though transition metal particles can decompose the hydrocarbons from the carbon source gas, they require a support for the growth of nanotubes/nanofibres¹⁵⁷. Two growth models, namely tip growth and root growth are currently used to define the growth of these carbon nanomaterials^{161,162}. These growth patterns are based on the interaction between the catalyst and support. If there is a weak interaction between the two, tip growth is favoured, vice versa, if there are strong interactions, base growth occurs¹⁶³.

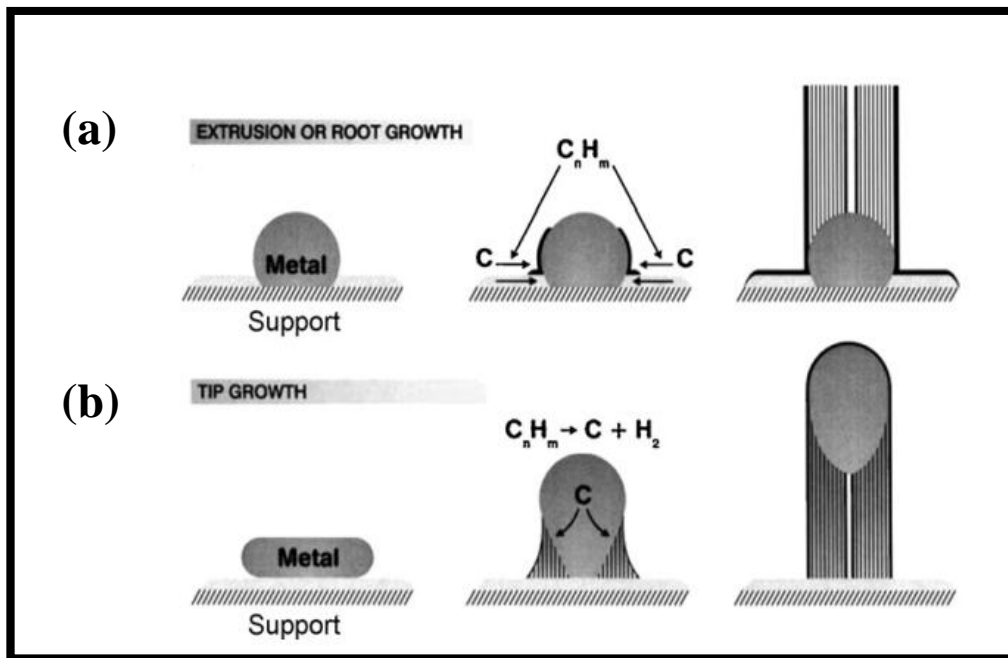


Figure 2.4: Schematic diagram of CNT growth mechanism a) Root growth b) Tip growth¹⁶³

2.4.1 Carbon nanotubes and carbon nanofibres using fly ash as a catalyst

Fly ash plays a major role during the formation of CNMs^{107,108}. These materials need to have the ability to decompose hydrocarbons and form CNMs, thus, emphasis has to be put on selecting the appropriate catalysts. Transition metals at present are seen as the most effective catalysts¹⁰⁹. This is due to their catalytic activity of decomposing volatile carbon compounds, ability of metastable carbide formation and diffusing carbons through and over metal particles¹¹⁰. Fe, Co and Ni are commonly used transition metals because the solubility of carbon in these

metals is finite¹¹¹. These metals are used due to them possessing unfilled “d” shells that give them the ability to interact with carbon and exhibit catalytic activity¹¹².

Reports on the effectiveness of fly ash as a catalyst or template in the synthesis of CNMs are limited^{5,6,17}. Six studies, thus far, have reported on the use of fly ash on its own as a catalyst for carbon nanomaterial production using the Fluidized Bed Chemical Vapour Deposition (FBCVD) method.

Yasui *et al.* synthesised CNTs (Fig 2.5a-b) using a Japanese fly ash in an electric tubular furnace as a catalyst⁵⁷. The aim was to produce tubes that could be used for the manufacturing of electronic devices and high frequency materials due to fly ash having properties such as low dielectric constant materials. Iron (5%) was added to the mixture with methane and ethanol used as carbon sources at high temperatures while helium and argon inert gases were used as carriers. CVD was used because it produces large amounts of CNTs and does not require a vacuum system¹⁶⁴. Their results showed a low production of CNTs that were of poor quality as a lot of amorphous carbon existed as manifested by the more intense D-peak than the G-peak under Raman spectroscopy⁵⁷. This therefore, leads to the realisation that in order for these CNTs to be used as electrical and optical absorbents, the processing during their production should be optimized.

Dunens *et al.* also showed that CNTs and CNFs (Fig 2.5c-d) could be produced using the Australian coal fly ash⁵⁵. However, multiple steps had to be followed and iron had to be impregnated on the Australian fly ash. This was done in order to produce a low cost catalyst of which after calcination, the resultant catalyst was formed. In their study, ethylene, which is expensive, was used as a carbon source to synthesize the materials at 650 °C. During that study, it was shown that natural iron in fly ash was inactive for CNT growth under selected reaction conditions. They postulated that the inactivity could be due to the heterogeneity of the iron location and composition of the received ash. Diamond *et al.* demonstrated through the use of various etching treatments that the location of the iron and its

morphology differs considerably between even fly ashes of the same sample¹⁴². That could be due to the non-homogeneous nature of the coal. Another possibility could be that iron appears in various forms; however, the required form for CNT growth is iron in reduced form, which can be achieved through the use of gases such as H₂. Therefore, it can be concluded that iron needs to be reduced or located on the surface or be in a form that is catalytically active for CNT growth. Due to the low bulk density, high strength and intrinsic stiffness, they suggested that the CNTs produced in that study had potential to be used in composite materials such as concrete and polymers⁵⁵.

In an effort to improve on the aforementioned studies, Salah *et al.* used carbon rich fly ash from Saudi Arabia as a catalyst for CNT production (Fig 2.5e-f)¹⁰⁴. Two pre-treated samples in air at 750 °C, to release unburned carbon, were synthesized using low pressure CVD⁶. Prior to synthesis, the fly ash was ultrasonically treated in order to produce an ultrafine powder. Acetylene was used as a carbon source while nitrogen was used as a carrier gas. The results showed iron as the most abundant element in sample 1 and nickel dominated sample 2. Iron also produced nanotubes and nanofibres with large diameters and lengths in a few micrometres. Their study showed that the approach taken could be used for large scale production of CNTs with different diameters at a lower price. Their study was rather an improvement to the studies conducted by Yasui *et al.* and Dunens *et al.* in terms of cost even though plenty of pre-steps needed to be taken to obtain their results^{55, 57}.

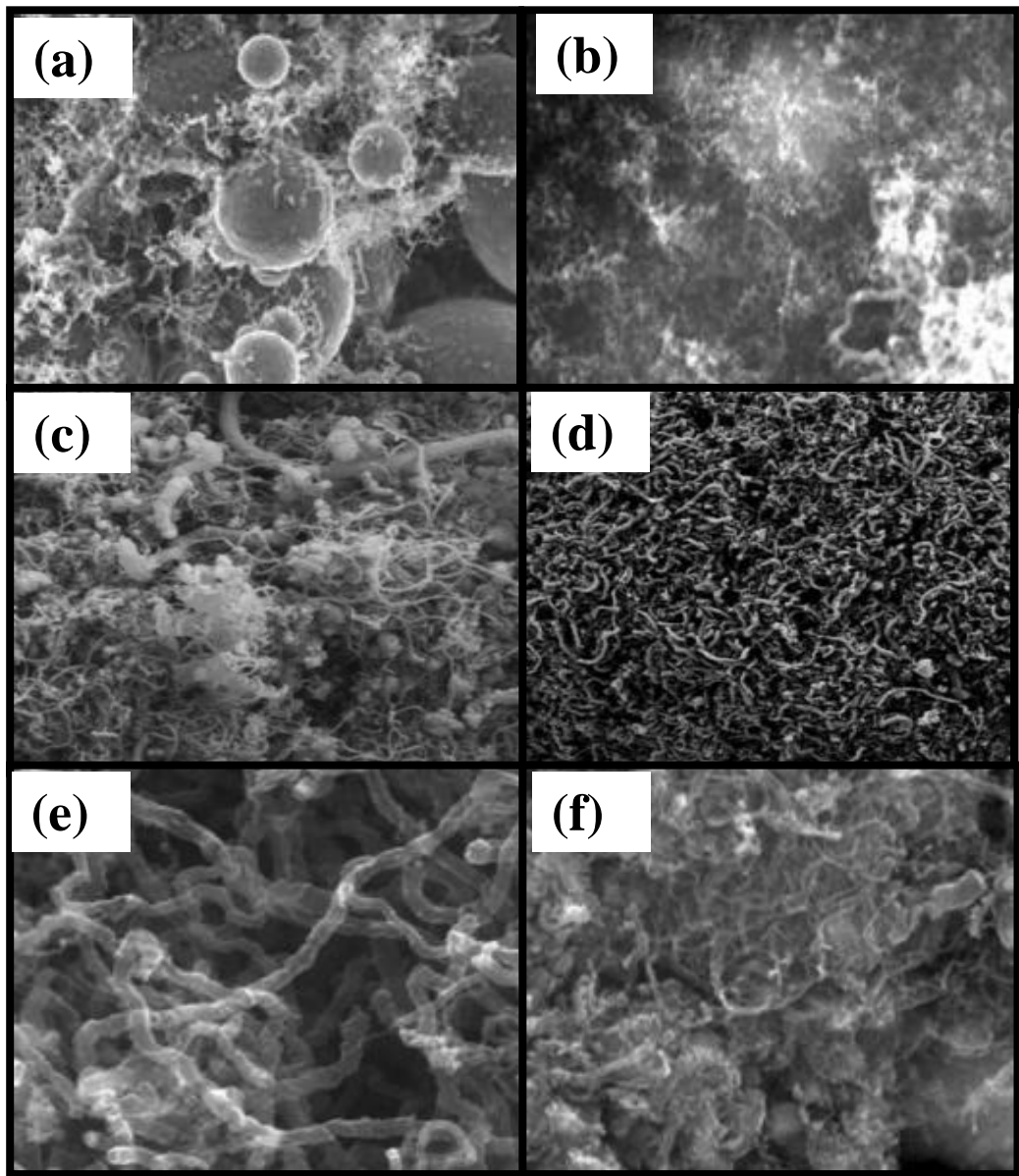


Figure 2.5: SEM images of CNMs by (a-b) Yasui¹⁴², (c-d) Dunens⁵⁵ and (e-f) Salah¹⁰⁴

In a recent study by Salah *et al.* several parameters were investigated, such as flow rate, gas pressure, temperature and growth time¹²⁸. The produced CNTs were characterised using TEM, micro Raman spectroscopy and XPS. Consistent results were found in-terms of uniformity, conversion and lengths produced under optimized values. The optimum temperature for producing these CNMs was 650 °C and the CNT diameters were found to be in the range of 20-40 nm. Raman spectroscopy showed the traditional D and G bands with an intensity ratio of 1.4.

Under XPS both sp² and sp³ type of bonding was observed. Two bands at 288.2 and 290.5 eV were also identified they could be assigned to carboxylic groups and π - π type bonds.

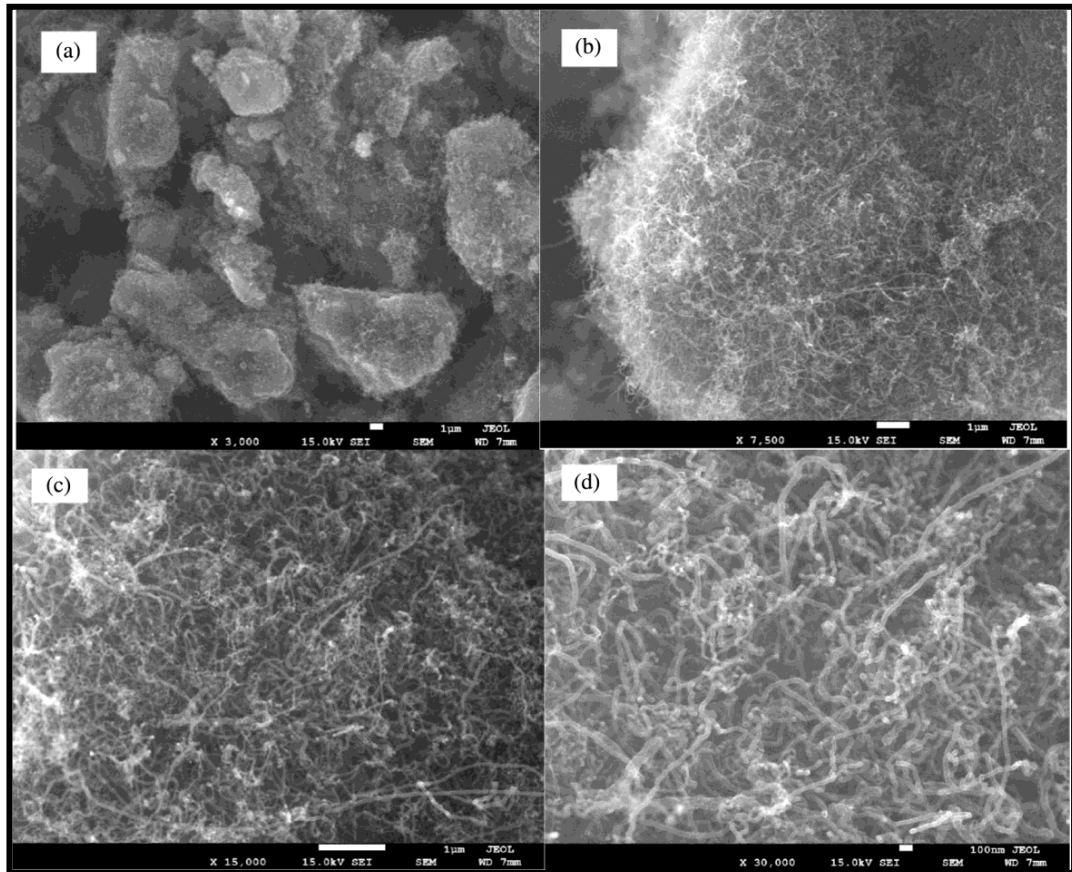


Figure 2.6: SEM images of CNTs produced from Saudi Arabian fly ash¹²⁸

These studies have been conducted using a waste materials as a catalyst in an effort to reduce the cost associated with manufacturing CNMs. It is well known that for the synthesis of CNMs to occur, factors such as energy source, catalyst and carbon sources are needed. The most commonly used carbon sources are hydrocarbons in particular acetylene and methane. Though these are widely used they have some drawbacks and require high temperatures for CNM synthesis. In recent times, researchers have attempted the use of oxygen containing species such as carbon dioxide as a carbon source for CNM synthesis (Table 2.3). This is due to the material also being a waste material”

2.4.2 The effect CO₂ as a carbon sources on the synthesis of CNMs

Several research groups have optimised the synthesis of these CNMs targeting different carbon sources, including carbon dioxide. Motiei *et al.* synthesized CNTs from scCO₂ using magnesium at temperatures above 1000 °C¹⁴³. In their study, CO₂ was reacted with metallic Mg in an autoclave for 3 hr. From this reaction, MgO, CNTs and fullerenes were formed. From this study, other studies followed.

Lou *et al.* reacted metallic lithium with CO₂ at temperatures > 550 °C¹⁴⁴. From that study, XRD patterns showed that well crystallized graphite was formed. Laser Raman spectroscopy also confirmed the D and G bands with the I_D/I_G ratio being greater than 1. A follow up study by Lou and others in 2005 using scCO₂ and alkali metals was conducted to form CNTs ranging from 600-750 °C¹⁴⁵. CNTs of different morphologies were formed such as helical, rope-like and porous etc.

In a study by Zhang *et al.*, Y junction CNTs were formed using sodium borohydride (NaBH₄) at 700 °C¹⁴⁷. The Y junction morphologies could have been caused by the presence of hydrogen as the reductant. From these studies it was clear that the catalyst used, temperatures, reductant and pressures used play a major role in the type of CNTs to be formed. For example, the use of supercritical carbon dioxide (scCO₂) required excessively high pressures. For the CNTs to have formed using manganese, temperatures as high as 1000 °C were needed. To combat these challenges, recent studies have shown that an addition of an O₂ species to the traditional carbon source such as C₂H₂ and CH₄ can assist in improving the yield of these CNMs. As shown in the table below (Table 2.3), product yields formed from these sources were very low; the amount of energy required for these CNMs to occur was very high as temperatures at times would get to 1000 °C.

In an effort to assist with the challenges with the use of this CO₂ as a sole carbon source, Magrez *et al.*, suggested using CO₂ in an equimolar ratio with C₂H₂ for the

synthesis of CNTs¹⁷⁷. This investigation was inspired by a study where CNTs were grown from using CaCO₃ support that produced CO₂ by thermal decomposition. For their studies though, MgO was used as a catalyst support instead. This choice in catalyst support was based on the fact that MgO could not form a carbonate at temperatures above 300 °C. From their study, increased yields and high quality CNTs were obtained at a maximum temperature of 680 °C, beyond this temperature amorphous carbon was observed. Another interesting fact to note from their study was that, normally 750 °C is required to form CNTs using MgO as a support but with the equimolar ratio, CNTs were formed from as low as 400 °C. They suggested that this could be due to oxidative dehydrogenation of acetylene with CO₂, which has been extensively used in the olefin industry for the manufacturing of unsaturated hydrocarbons.

Table 2.3: The use of CO₂ as a carbon source for CNM synthesis

Reductant	Yield (%)	Temp (°C)	Product	Refs
Manganese		1000	CNTs	¹⁴²
Lithium	90	550	CNTs, graphite and amorphous carbon	¹⁴³
Sodium Borohydrite	4.2	700	Y - Junction CNTs, Graphite	¹⁴⁴
Argon	50	790-810	CNTs	¹⁴⁶

2.5 Methods used for the synthesis of carbon nanomaterials

Several methods have been used in the formation of carbon nanomaterials in sizeable quantities. These include the pyrolysis of hydrocarbons using metal catalysts and carbon monoxide disproportionates on a metal catalyst. The three most commonly used techniques though, include, arc discharge, laser ablation, and CVD. Of these methods, CVD has been at the fore-front.

2.5.1 Arc discharge

An arc discharge can be defined as an electrical breakdown of a gas that produces an ongoing plasma discharge that comes from a current through non conductive environments such as air⁶⁵. This method is characterised by having a lower voltage than CVD and mostly depends on thermionic emission of electrons supporting the arc. For CNT synthesis, a current is made to pass through two graphite electrodes which are placed end to end in an inert gas filled environment such as helium, argon or nitrogen. Thereafter, a high potential difference of 20 kV and current ranging from 20 to 100 A is applied causing a high temperature discharge at ca. 4000 °C. The heat then causes sublimation of carbon on the positive electrode which in turn deposits on the negative end of the electrode resulting in the formation of CNTs. This method produces highly crystalline CNTs, but has a poor efficiency as the product contains more than 60% impurities. The quality of the CNTs mostly depends on the lowering of the current, meaning that the lower the current, the better the quality of CNFs. High energy amounts of energy consumed to make these CNTs also limits this technique for large scale CNT production⁴².

2.5.2 Laser ablation

This method was developed by Smalley and co-workers in 1995 at Rice University⁶⁸. At present, the arc discharge and the laser ablation method are the most commonly techniques for the synthesis of high quality CNTs. In this method, the carbon source is doped with small amounts of metallic catalysts (Co and Ni) that are then vaporised with the help of a pulsed laser beam in the presence of an inert gas at very high temperatures and constant pressure of 500 Torr. As the laser beam impregnates the target material, vaporisation and condensation also occurs at comparatively lower temperatures. However, these methods have a lot of limitations. The most notable one is the fact that high temperatures > 3000 °C are required to form CNTs, thus making this process not feasible for large scale synthesis.

2.5.3 Chemical Vapour Deposition

Chemical Vapour Deposition (CVD) can be defined as a gas phase deposition method that takes place in a vacuum chamber and involves the deposition of solid materials directly via vapour transformation. In the absence of chemical reactions, this method is known as physical vapour deposition. This is a simple and economical technique that is used for synthesis of carbon nanomaterials. Because of its versatility, a number of carbon sources in any state or form can be used.

This method, developed by Endo *et al.* consistently shows potential and is one of the well-researched methods for the deposition of catalysts onto supports¹⁴⁹. It is preferred because it is fast, efficient, and produces deposits that have shown high quality¹⁴⁹. Secondly, due to engineering and fundamental aspects, it can be applied in large scale applications. For the formation of a carbon nanomaterial during CVD, a catalyst, carbon source and heat are needed for a process that normally takes place in a horizontal tube furnace (Figure 2.7). This type of reactor normally consists of a furnace, quartz tube, a boat consisting of a catalyst, an inlet and an outlet gas connector. During CVD, transition metal particles act as a seed/nucleation site for carbon nanomaterial formation¹⁷⁴. These metals are used to catalyze the formation of carbon nanomaterials, thus playing a role in the structure and quality of materials produced⁴².

During this process, a growth temperature is set, a carrier gas such as argon (Ar), H₂ and N₂ are flushed through the quartz tube so as to form an inert atmosphere and reduce the catalyst particles during heating. It is worth stating that H₂ is mostly considered as a reactive gas rather than a carrier gas. This is due to hydrogen having the ability to create a reducing environment for the catalytic metal, thus, preventing poisoning of the catalytic surface by carbon deposition, which reduces undesirable carbon deposits formation¹⁵⁷⁻¹⁶⁶. After the ramping stage, a carbon source is introduced during the reaction phase, thereafter, the reaction is allowed to cool down and the sample is collected. Even though CVD has been the method of choice, as mentioned earlier, the pyrolysis method has also been used for CNT ribbon formation¹⁷².

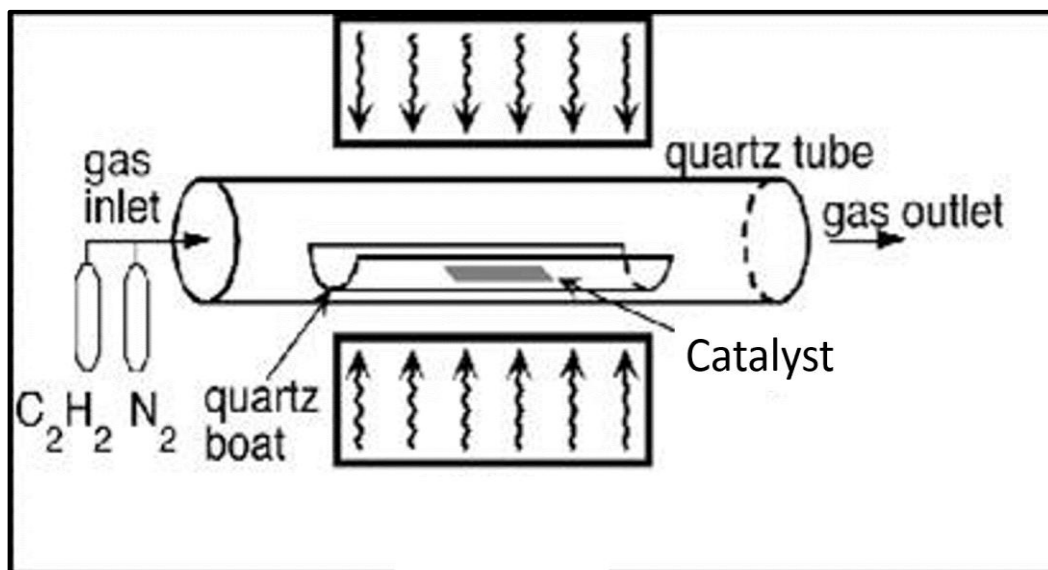


Figure 2.7: Schematic diagram of the chemical vapor deposition apparatus
149

2.6 Other methods used for the synthesis of carbon nanomaterials from fly ash

2.6.1. Pyrolysis method

Pyrolysis is one of the most common methods used in the chemical industry. It can be defined as an irreversible thermo chemical decomposition method of organic materials at elevated temperatures in the absence of O_2 . It involves the change of the chemical composition and physical phase. It is one of the processes involved in charring wood starting at $200\text{ }^\circ\text{C}$ - $300\text{ }^\circ\text{C}$.

During pyrolysis, samples are run at an isothermal condition in a horizontal quartz tube furnace under an inert gas. The hot zone of the furnace gets heated to a certain temperature and controlled using a thermocouple. The diagram of the set up has been shown in previous studies¹⁷². The weighed amount of the sample is kept in an alumina crucible, and then placed in a graphite feeder. Thereafter, the sample is inserted in the cold zone with an inert gas either in N_2 or Ar flowing under a specific flow rate and for short periods of time (30 s, 1 min, 2 min). It is placed back in a hot zone for a longer period (10, 20, 30 min). Then, after pyrolysis, the sample is removed back from the hot zone and placed in the cold

zone for 30 s using a graphite feeder. The resultant products are then stored in a small sample bottle used for calculation and analysis.

In one study, the pyrolysis method was used using a composite polyvinyl acetate (PVA) and Fly Ash (FA), where FA was a catalyst for the self-assembled CNT along geometrical CNT structures¹⁷². The aim was to make CNT ribbons/ropes grown on the surface of FA that would have potential to be used for fabrication of high strength composite materials. The results under SEM showed knotted, twisted ribbons while TEM also showed the formation of U- and spiral shaped CNT ribbons with sizes ranging from 8-80 nm in width (Fig. 2.8a-d). Good graphitisation with I_G/I_D ratio = 1.61 from Raman spectroscopy was also identified. This was a much bigger improvement from an I_G/I_D ratio of 1.17 obtained when fly ash iron impregnated iron nitrate was used, with gaseous mixtures such as ethylene, hydrogen and nitrogen⁵⁵. The study showed the produced CNTs had potential to be used as filler materials for the fabrication of composites with metals and polymer.

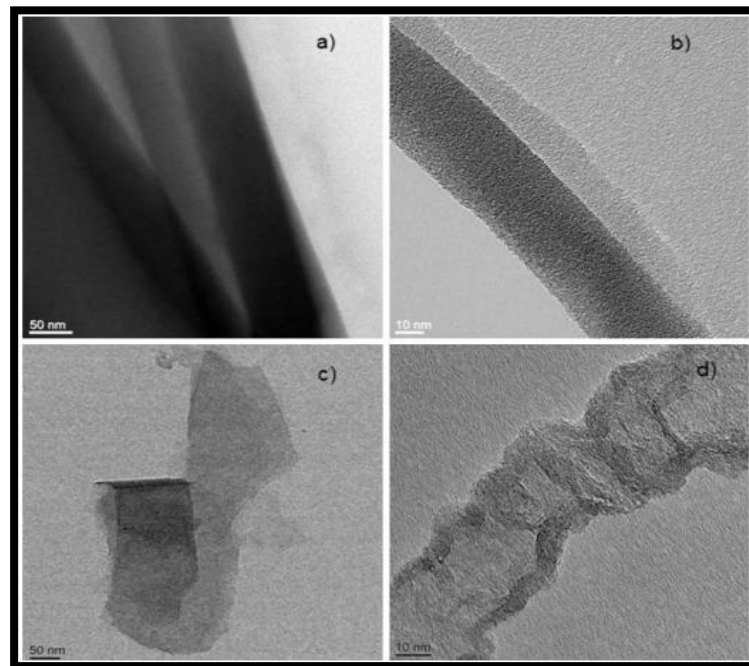


Figure 2.8: TEM images of CNT, a) growth of aligned CNT ribbons, b) single ribbons, showing constant width; c) U-shaped and d) spiral shaped CNT ribbon structures¹⁷²

2.6.2 Ball milling

Though CVD has been the most widely used method for the formation of carbon nanomaterials, other leading fly ash countries such as India, have been focusing on converting the micro-sized ash to nanomaterial ash that can be used in polymer composites^{39,53,180}. Ball milling has been the technique of interest due to its simplicity, relatively inexpensive production, its applicability to any class of materials and its ease to be scaled up to large quantities.

Ball milling is a mechanical treatment method where powder particles are subjected to a severe plastic deformation caused by ongoing compressive loads coming from the impacts between the balls and the ash¹⁵⁷. This process physically results in an altered fly ash from a smooth, glassy inert ash to a rough and more reactive ash. Chemically, the ash becomes amorphous with crystalline sizes at the nanometre level from micro-sized ash. The roughness could be caused by the exposure of the inner crystalline core which may have eroded during ball milling.

Indian ash has been used to convert microstructured materials to nanomaterials (Fig 2.9a-b) using high energy ball milling. India is one of the leading producers of ash and currently generates about 112 million tons annually⁵³. They are faced with a problem due to the shortage of space required to accommodate large volumes of its generation thus it has become a national will as it is an international priority to try and find new applications for this waste raw material. India has invested millions of dollars in polymer research as an initiative in trying to create nanostructured fly ash materials to be used as fillers in improving the strength of rubbers. Some groups used class F fly ash that was subjected to high energy ball milling for 60 hr and converted the ash to nanostructured materials⁸³. This is ash that is pozzolanic in nature that contains less than 20% lime (CaO) content. The results found that the average particle size was reduced while surface area and total surface free energy were increased. The surface texture change in morphology was depicted as can be observed in (Fig. 2.9a-b) from glassy to amorphous and the crystalline size was reduced dramatically.

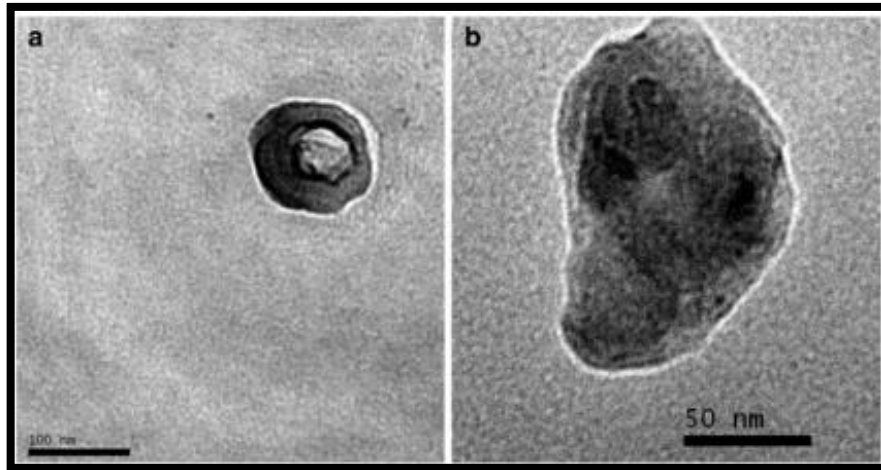


Figure 2.9 (a-b): TEM images of fly ash samples ball milled for 60 hr ⁵³

2.7 Mechanical properties of carbon nanotubes and carbon nanofibres

As mentioned before, CNT/Fs have unique electrical, mechanical and thermal properties but due to their small size it has been difficult to measure their mechanical properties by direct measurements⁵⁸. Experimental techniques such as SEM, TEM, AFM, laser Raman spectroscopy and theoretical models have been used to describe the mechanical properties of CNTs. Coleman *et al.* used laser Raman spectroscopy spectroscopy to measure the elastic moduli of CNTs and this was found to be 2.8-3.6 TPa⁷⁶. In their study, Mitall *et al.* reported a mechanical strength of 1.8 TPa for CNTs and reported that because of this high modulus, high stiffness coupled with a low density, these CNTs could be used to improve the mechanical strength of composites⁷⁴. Other researchers have also reported on these great properties⁷⁵. To fully use the mechanical properties of these CNT/Fs, CNM/polymer composites have been formulated, and because there is wide range of applications these nanocomposites can be used in almost every field. In this study we plan to use them in polymer composites as well.

2.8 Carbon nanomaterials/polymer nanocomposites

A polymer nanocomposites can be described as a combination of a polymer matrix and a filler that has at least one dimension in a nanometre range¹⁷². Carbonaceous nanofillers such as CNTs have been shown to play a very promising role due to their high aspect ratio, tensile strength and mechanical

strength¹⁷³. For the polymer nanocomposites to achieve their ultimate mechanical strength, certain parameters such as CNT/F structure, alignment of the filler into the matrix, dispersion technique of the CNT and the interaction between the nanofiller and polymer matrix need to be optimised¹⁷⁴. From the parameters listed above, the dispersion and the strong interaction between CNT and matrix have been the most challenging to overcome in the performance of CNT/polymer nanocomposites.

To overcome the dispersion challenge, several methods have been proposed in literature. These include solution mixing, melt processing and in-situ polymerisation.

2.8.1 Preparation of carbon nanomaterial/polymer nanocomposites

To optimise the properties of polymer nanocomposites, it is imperative to disperse the carbon nanomaterials in the polymer matrix efficiently in order to overcome some of these agglomeration challenges, hence the methods mentioned above have been preferred as they offer a lot of commercial viability.

Of these methods, solution mixing has been the most favoured because of its simplicity. During this method, the filler (CNT/F) and the polymer are mixed with a suitable solvent, which is then evaporated in a controlled condition after forming nanocomposite films on the surface of the substrate. In a study where CNFs were added to increase the fracture toughness of epoxy composites, 0.5 and 1% loading were enough to secure a 66% and 78% increment, respectively. Preparing the thermal-plastic polyurethane composites by melt mixing, the tensile strength of these nanocomposites was increased by 49% using a 4% loading. A further addition of these CNFs into the matrix, led to a dramatic reduction in the mechanical strength of these nanocomposites. This decrease could have been caused by increase in the voids or other defected sites coming from the CNF bundles. These normally lead to stress concentrations under dynamic loading thus, leading to failure at low strain values. Though this method is popular, Kang *et al.* used ultrasonic agitation for the dispersion of acid treated Multi-Walled Carbon

Nanotubes (MWCNT) into the polystyrene matrix⁷⁸. Using this method, it was observed that compatibility issues of the functional group and polymer matrix arose.

To overcome this problem, another method of surfactant addition was used. Beside those challenges, the restrictive factor of the solution mixing process is the solubility of the polymers into a solvent. To reduce these issues, melt processing was used, which is a method more suitable for thermosetting plastics polymers such as polyesters, polystyrene etc. This method is based on melting the polymer to form a viscous liquid and then blending it with the filler. This method even though it is more suitable for a wider range of polymers, can be less proficient than even solution mixing, especially if the thermoplastic is highly viscous. This high viscosity might lead to difficulty in achieving a homogeneous distribution of carbon nanomaterial in the polymer matrix.

To deal with the polymers that cannot be processed using melt mixing or solution processing, in situ polymerisation is used. This method is used for polymers that are insoluble and thermally unstable. Several investigations have been conducted using MWCNT/polyurethane^{165,166}, MWCNT/polypyrrole¹⁶⁷, MWCNT/nylon¹⁶⁸⁻¹⁷⁰ and some studies on epoxy based nanocomposites^{173,171}.

2.8.2 Functionalisation of carbon nanomaterials

As it was pointed out before, because of the strong van de Waals forces, the interaction between the filler and matrix needs to be enhanced as these carbon nanomaterials have a hydrophobic nature. It is of utmost importance to change the state of these carbon nanomaterials so as to achieve the ultimate mechanical strength. To enhance the strength of these polymer nanocomposites, several methods of functionalising of these CNMs have been conducted, and these include covalent and non-covalent functionalization.

Covalent functionalization is the most popular of the two. This method is based on the covalent linkage between carbon and other functional groups.

Functionalization occurs when the sp^2 hybridisation bonding changes to sp^3 . In this process, strong acids and other oxidising agents such as HCl ¹⁶², HNO_3 ¹⁶³, H_2SO_4 ¹⁶⁴, $KMnO_4$ ^{165,166} and H_2O_2 ¹⁶⁷ have been used to oxidise these carbon nanomaterials and insert functional groups such as carboxyl, ketone, alcohol, *etc.* on the surface. After the attachment of these groups, the nature of the carbon nanomaterials changes from hydrophobic to hydrophilic, thus leading to a strong interaction between the filler and polymer matrix. Kim *et al.* investigated the effect of acid and NH_2 treated MWCNTs on to epoxy resins³⁷. They found the tensile strength to have been greatly improved by 69% and 73% respectively, as compared to the untreated MWCNTs which recorded strength of 61%. Seyhan also tested the mechanical behaviour and fracture toughness of a hybrid polyester nanocomposite by using NH_2 treated different forms of CNTs through a 3 roll milling method. The results showed that all the amine functionalised CNTs performed better than the untreated CNTs¹⁶⁸.

2.9 Application of carbon nanomaterials formed from fly ash as a catalyst.

Up to date, no industrial scale application has been realised. The amorphous, alumina silicate nature of the fly ash makes it a possible raw material for many industrial applications. The iron identified in the ash, has been identified as the catalyst responsible for CNM formation, either found as FeO , Fe_2O_3 or Fe_3O_4 . Fly ash, thus far, has been used as an alternative to replace activated carbon or zeolite for water pollution treatment. This normally depends on the origin and chemical treatments used.

In recent years, some of the emerging fields such as biomedical, aerospace and catalysis have been using fly ash material for carbon nanomaterial production. Thus far, six studies have reported the production of carbon nanomaterials using fly ash as a catalyst via the CVD method^{55,57}. Yasui *et al.* formed CNTs of low quality using Japanese ash¹⁷. On the other hand, Dunens *et al.* synthesized MWCNTs and CNFs of high standard using the iron impregnated Australian fly ash⁵⁵. Salah *et al.* managed to form large, well dispersed, low cost CNTs using carbon rich Saudi Arabian fly ash¹⁰⁴. None of these studies though, have reported

on the application of the CNMs formed. Dunens *et al.* suggested that the CNTs and CNFs formed from the Australian ash could be used in polymer composites⁵⁵.

In the formation of other nanomaterials from ash by ball milling, most of the studies suggested that the formed nanostructures could be used as reinforcing fillers in polymer matrices^{53,169}. Though small advances have been made, there is still a lot of unused ash and several hindrances have to be overcome in order to use large amounts of fly ash in different industries. These are normally the technical, economical and legal barriers. The technical and economic barriers are mostly caused by fly ash production, specification and standards that are set, for this material to be used in several applications. Other economic factors could be the high cost associated with the transportation of low unit value ash and competition from locally available natural materials.

2.10. Conclusion

This review has shown the use of fly ash as a filler, a soil additive and a catalyst. In the catalysis field, the use of this material is moving more towards the importance of this material for CNM production. However, more research still needs to be conducted in the field where fly ash can be used solely as a catalyst without the use of a pre-treatment or impregnation to produce CNMs of high quality. As the previous studies have shown, to obtain the desired results, the process can be tedious and expensive hence optimisation studies studying the temperature, varying flow rates and carrier gases should be carried out. In addition to the catalyst, the carbon source also plays a huge role in-terms of cost and the quality of the CNMs produced. Furthermore, these materials need to be tested in different applications, so as to compare their performance with CNMs produced from pure catalysts. Several authors though strongly suggested their use as fillers in the polymer industry to be used as reinforcements. As had been pointed out in the previous sections for this application, CNMs generally need to be treated using various acids at moderate concentrations in order to remove impurities and assist with the interaction of the filler and polymer matrix.

2.11 References

1. S. Jala and D. Goyal, *Bioresource Technology*, 2006, **97**, 1136-1147.
2. Z. Yao, X. Ji, P. Sarker, J. Tang, L. Ge, M. Xia and Y. Xi, *Earth-Science Reviews*, 2015, **141**, 105-121.
3. A. Sarkar, R. Rano, G. Udaybhanu and A. Basu, *Fuel Processing Technology*, 2006, **87**, 259-277.
4. G. Madzivire, University of the Western Cape, *Thesis*, 2009.
5. P. Sun and H.-C. Wu, *Cement and Concrete Composites*, 2008, **30**, 29-36.
6. C. Rao, *Environmental pollution control engineering*, New Age International, 2007.
7. J. B. Rao, P. Narayanaswami and K. S. Prasad, *International Journal of Engineering, Science and Technology*, 2010, **2**, 284-299.
8. M. Blanco-Carrasco, F. Hornung and N. Ortner, *Green Concrete Technologies*, 2010, 1-63.
9. S. M. Nyale, C. P. Eze, R. O. Akinyeye, W. M. Gitari, S. A. Akinyemi, O. O. Fatoba and L. F. Petrik, *Journal of Environmental Science and Health, Part A*, 2014, **49**, 233-242.
10. G. Neupane and R. J. Donahoe, *Fuel*, 2013, **104**, 758-770.
11. K. N. Kumar and S. Goel, *Resources, Conservation and Recycling*, 2009, **53**, 166-174.
12. R. Haynes, *Journal of Environmental Management*, 2009, **90**, 43-53.
13. D. Fytili and A. Zabaniotou, *Renewable and Sustainable Energy Reviews*, 2008, **12**, 116-140.
14. S. Potgieter-Vermaak, J. Potgieter, R. Kruger, Z. Spolnik and R. van Grieken, *Fuel*, 2005, **84**, 2295-2300.
15. M. Ahmaruzzaman, *Advances in Colloid and Interface science*, 2011, **166**, 36-59.
16. A. S. Meawad, D. Y. Bojinova and Y. G. Pelovski, *Waste Management*, 2010, **30**, 2548-2559.
17. C. Klauber, M. Gräfe and G. Power, *Hydrometallurgy*, 2011, **108**, 11-32.

18. B. Ugheoke, O. Mamat and B. Ariwahjoedi, *Defect and Diffusion Forum*, 2010, **307**, 53-62.
19. E. Mumcu, *Weathering Effects on the Hydraulic Conductivity of Fly Ash Stabilized Soil Used in Levee and Embankment Construction*, ProQuest, 2008.
20. J. W. Riekert and S. F. Koch, *Journal of Energy in Southern. Africa*, 2012, **23**,4-11.
21. S. Anantharaman, Arizona State University, 2008.
22. K. K. Chawla, *Composite materials: science and engineering*, Springer, 2012.
23. S. Thomas and P. Visakh, *Handbook of Engineering and Specialty Thermoplastics, Nylons*, Wiley-Scrivener, 2011.
24. Z. Roslaniec, G. Broza and K. Schulte, *Composite Interfaces*, 2003, **10**, 95-102.
25. J. Sandler, M. Shaffer, T. Prasse, W. Bauhofer, K. Schulte and A. Windle, *Polymer*, 1999, **40**, 5967-5971.
26. G. Yamamoto, M. Omori, T. Hashida and H. Kimura, *Nanotechnology*, 2008, **19**, 315708.
27. E. T. Thostenson, Z. Ren and T.-W. Chou, *Composites science and technology*, 2001, **61**, 1899-1912.
28. M. Ahmaruzzaman, *Progress in Energy and Combustion Science*, 2010, **36**, 327-363.
29. D. Adriano, A. Page, A. Elseewi, A. Chang and I. Straughan, *Journal of Environmental Quality*, 1980, **9**, 333-344.
30. L. Ram and R. Mastro, *Earth-Science Reviews*, 2014, **128**, 52-74.
31. L. C. Ram and R. E. Mastro, *Journal of environmental management*, 2010, **91**, 603-617.
32. R. D. Rawlings, J. Wu and A. Boccaccini, *Journal of materials science*, 2006, **41**, 733-761.
33. E. Berry and V. M. Malhotra, *International Concrete Portal*, 1980, **2**, 59-72.
34. M. Thomas, *Building Research Establishment*, 1996.

35. S. Wang, *Environmental science & technology*, 2008, **42**, 7055-7063.
36. S. Babel and T. A. Kurniawan, *Journal of Hazardous Materials*, 2003, **97**, 219-243.
37. W. W. Ngah and M. Hanafiah, *Bioresource Technology*, 2008, **99**, 3935-3948.
38. H. Nugteren and R. Kruger, *Combustion residues: current, novel and renewable applications*, 2008, 315.
39. R. K. Sinha, G. Bharambe, J. Nair and S. Herat, *Progress in waste management research*, 2008, 11.
40. R. A. Kruger, M. Hovy and D. Wardle, *International Ash Utilisation Symposium*, 1999, 72.
41. K. Pal, S. K. Pal, C. K. Das and J. K. Kim, *Materials & Design*, 2011.
42. S. Robinson, T. H. Ferrigno and R. F. Grossman, *Handbook of Vinyl Formulating*, 2008, 151-171.
43. L. Bokobza and M. Kolodziej, *Polymer international*, 2006, **55**, 1090-1098.
44. N. Sombatsompop, S. Thongsang, T. Markpin and E. Wimolmala, *Journal of applied polymer science*, 2004, **93**, 2119-2130.
45. D. Hundiwale, U. Kapadi, M. Desai and S. Bidkar, *Journal of Applied polymer science*, 2002, **85**, 995-1001.
46. A. Menon, T. Sonia and J. Sudha, *Journal of applied polymer science*, 2006, **102**, 4801-4808.
47. B. Felekoğlu, K. Tosun, B. Baradan, A. Altun and B. Uyulgan, *Cement and concrete research*, 2006, **36**, 1719-1726.
48. T. Matsunaga, J. Kim, S. Hardcastle and P. Rohatgi, *Materials Science and Engineering: A*, 2002, **325**, 333-343.
49. T. Chaowasakoo and N. Sombatsompop, *Composites science and technology*, 2007, **67**, 2282-2291.
50. N. A. N. Alkadasi, D. Hundiwale and U. Kapadi, *Journal of applied polymer science*, 2004, **91**, 1322-1328.
51. K. T. Paul, S. Satpathy, I. Manna, K. Chakraborty and G. Nando, *Nanoscale Research Letters*, 2007, **2**, 397-404.

52. S. Thongsang and N. Sombatsompop, *Polymer Composites*, 2006, **27**, 30-40.
53. K. T. Paul, S. Pabi, K. Chakraborty and G. Nando, *Polymer Composites*, 2009, **30**, 1647-1656.
54. M. Moniruzzaman and K. I. Winey, *Macromolecules*, 2006, **39**, 5194-5205.
55. O. M. Dunens, K. J. MacKenzie and A. T. Harris, *Environmental science & technology*, 2009, **43**, 7889-7894.
56. N. Salah, S. S. Habib, Z. H. Khan, A. Memic and M. N. Nahas, *Digest journal of nanomaterials and biostructures*, 2012, **7**, 1279-1288.
57. A. Yasui, Y. Kamiya, S. Sugiyama, S. Ono, H. Noda and Y. Ichikawa, *IEEE Transactions on Electrical and Electronic Engineering*, 2009, **4**, 787-789.
58. P. Sarker and L. McKenzie, *Concrete Solutions*, 2009.
59. M. McCarthy and R. Dhir, *Fuel*, 2005, **84**, 1423-1432.
60. B. Joseph and G. Mathew, *Scientia Iranica*, 2012, **19**, 1188-1194.
61. T. B. Edil, L. K. Sandstrom and P. Berthouex, *Journal of Geotechnical Engineering*, 1992, **118**, 1410-1430.
62. M. Ghodrati, J. Sims and B. Vasilas, *Water, Air, and Soil Pollution*, 1995, **81**, 349-361.
63. J. Sims, B. Vasilas and M. Ghodrati, *Water, Air, and Soil Pollution*, 1995, **81**, 363-372.
64. V. C. Pandey and N. Singh, *Agriculture, ecosystems & environment*, 2010, **136**, 16-27.
65. A. Chang, L. J. Lund, A. L. Page and J. Warneke, *Journal of Environmental Quality*, 1977, **6**, 267-270.
66. B. Mitra, S. Karmakar, D. Swain and B. Ghosh, *Fuel*, 2005, **84**, 1447-1451.
67. M. Basu, M. Pande, P. Bhadoria and S. Mahapatra, *Progress in Natural Science*, 2009, **19**, 1173-1186.
68. A. Sarkar and R. Rano, *Energy Sources, Part A*, 2007, **29**, 471-482.

69. D. K. Gupta, U. N. Rai, R. D. Tripathi and M. Inouhe, *Journal of Plant Research*, 2002, **115**, 401-409.
70. S. Karpagavalli and R. Ramabadrán, *Souvenir*.1997,**6**, 11-16.
71. S. Tiwari, B. Kumari and S. Singh, *Bioresource Technology*, 2008, **99**, 1305-1310.
72. A. Gianoncelli, A. Zacco, R. P. Struis, L. Borgese, L. E. Depero and E. Bontempi, in *Pollutant Diseases, Remediation and Recycling*, Springer, 2013, pp. 103-213.
73. P.-C. Kao, J.-H. Tzeng and T.-L. Huang, *Journal of hazardous materials*, 2000, **76**, 237-249.
74. M. Matheswaran and T. Karunanithi, *Journal of hazardous materials*, 2007, **145**, 154-161.
75. N. Singh, *Journal of hazardous materials*, 2009, **168**, 233-237.
76. O. Babajide, N. Musyoka, L. Petrik and F. Ameer, *Catalysis Today*, 2012, **190**, 54-60.
77. W. Oelerich, T. Klassen and R. Bormann, *Journal of Alloys and Compounds*, 2001, **315**, 237-242.
78. M. Haruta, *Cattech*, 2002, **6**, 102-115.
79. D. W. McKee, *Carbon*, 1970, **8**, 623-635.
80. F. Rodriguez-Reinoso, *Carbon*, 1998, **36**, 159-175.
81. I. Dikic, *FEBS letters*, 2002, **529**, 110-115.
82. F. Teng, J.-M. Ting, S. P. Sharma and K.-H. Liao, *Nanotechnology*, 2008, **19**, 095607.
83. I. Gonzalez, J. C. De Jesus, E. Cañizales, B. Delgado and C. Urbina, *The Journal of Physical Chemistry C*, 2012, **116**, 21577-21587.
84. A.-C. Dupuis, *Progress in Materials Science*, 2005, **50**, 929-961.
85. M. Bouroushian, *Electrochemistry of metal chalcogenides*, Springer, 2010.
86. J. R. Kastner, K. Das, Q. Buquoi and N. D. Melear, *Environmental science & technology*, 2003, **37**, 2568-2574.
87. S. Wang and H. Wu, *Journal of Hazardous Materials*, 2006, **136**, 482-501.
88. K. Iida, T. Takashina and S. Honjo, *Journal*, 2003.
89. L. Baxter, *Fuel*, 2005, **84**, 1295-1302.

90. T. Berntsson, L. Persson Elmeroth, J. Algehed, E. Hektor, P.-Å. Franck, A. Åsblad, F. Johnsson, A. Lyngfelt, B. Gevert and T. Richards, , *Chalmers University of Technology*, 2008.
91. K. Verfondern, *Nuclear energy for hydrogen production*, Forschungszentrum Jülich, 2007.
92. J.T. Sims, B.L. Vasilas, M.Ghodrati, *Water, Air and Soil Pollution*,1995, **81**, 363-372.
93. G. Ordorica-Garcia, M. Nikoo, M. Carbo and I. Bolea, *Journal of Canadian Petroleum Technology*, 2012, **51**, 362-375.
94. P. Gosselin, S. E. Hrudey, M. Naeth, A. Plourde, R. Therrien, G. Van Der Kraak and Z. Xu, *Royal Society of Canada*, 2010, **8**, 4257–4258.
95. M. S. Milligan and E. R. Altwicker, *Environmental science & technology*, 1995, **30**, 225-229.
96. K. C. Galbreath and C. J. Zygarlicke, *Environmental science & technology*, 1996, **30**, 2421-2426.
97. D. N. Bangala, N. Abatzoglou, J.-P. Martin and E. Chornet, *Industrial & Engineering Chemistry Research*, 1997, **36**, 4184-4192.
98. P. McKendry, *Bioresource Technology*, 2002, **83**, 55-63.
99. M. Balakrishnan, V. Batra, J. Hargreaves and I. Pulford, *Green Chemistry*, 2011, **13**, 16-24.
100. R. Rinaldi and F. Schüth, *Energy & Environmental Science*, 2009, **2**, 610-626.
101. R. H. Baughman, A. A. Zakhidov and W. A. de Heer, *Science*, 2002, **297**, 787-792.
102. A. Rahman, I. Ali, S. M. Al Zahrani and R. H. Eleithy, *Nano*, 2011, **6**, 185-203.
103. H.-S. P. Wong and D. Akinwande, *Carbon nanotube and graphene device physics*, Cambridge University Press, 2011.
104. N. Salah, S. S. Habib, Z. H. Khan, A. Memic and M. N. Nahas, *Digest Journal of Nanomaterials and Biostructures*, 2012, **7**, 1279-1288.
105. N. Hintsho, A. Shaikjee, H. Masenda, D. Naidoo, D. Billing, P. Franklyn and S. Durbach, *Nanoscale Research Letters*, 2014, **9**, 1-11.

106. W. Chen, F. Sheu and R. Savage, *Fuel Processing Technology*, 1987, **16**, 279-288.
107. D. Van der Vaart, E. Marchand and A. Bagely-Pride, *Critical reviews in environmental science and technology*, 1994, **24**, 203-236.
108. J. Van Durme, J. Dewulf, C. Leys and H. Van Langenhove, *Applied Catalysis B: Environmental*, 2008, **78**, 324-333.
109. J. R. Kastner, K. Das and N. D. Melear, *Journal of Hazardous Materials*, 2002, **95**, 81-90.
110. J. R. Kastner, R. Ganagavaram, P. Kolar, A. Teja and C. Xu, *Environmental science & technology*, 2007, **42**, 556-562.
111. J. R. Kastner, Q. Buquoi, R. Ganagavaram and K. Das, *Environmental science & technology*, 2005, **39**, 1835-1842.
112. E. Fomenko, E. Kondratenko, A. Salanov, O. Bajukov, A. Talyshev, N. Maksimov, V. Nizov and A. Anshits, *Catalysis today*, 1998, **42**, 267-272.
113. M. W. Kasture, V. V. Bokade and P. N. Joshi, *Journal of the American Ceramic Society*, 2005, **88**, 3260-3263.
114. P. Kumar, Y. Oumi, T. Sano and K. Yamana, *Journal of Ceramic Society of Japan*, 2001, **109**, 968-973.
115. A. de Klerk and R. J. Nel, *Industrial & Engineering Chemistry Research*, 2007, **46**, 7066-7072.
116. D. Mallik and S. K. Chaudhuri, *Water Research*, 1999, **33**, 585-590.
117. S. K. Chaudhuri and B. Sur, *Journal of environmental engineering*, 2000, **126**, 583-594.
118. D. Chatterjee, B. Ruj and A. Mahata, *Catalysis Communications*, 2001, **2**, 113-117.
119. S.-S. Kim, J.-H. Kim and S.-H. Chung, *Journal of Industrial and Engineering Chemistry*, 2003, **9**, 287-293.
120. J.-G. Na, B.-H. Jeong, S. H. Chung and S.-S. Kim, *Journal of Material Cycles and Waste Management*, 2006, **8**, 126-132.
121. D. Jain, C. Khatri and A. Rani, *Fuel Processing Technology*, 2010, **91**, 1015-1021.

122. R. Chakraborty, S. Bepari and A. Banerjee, *Chemical Engineering Journal*, 2010, **165**, 798-805.
123. C. Khatri, M. K. Mishra and A. Rani, *Fuel Processing Technology*, 2010, **91**, 1288-1295.
124. E. Saputra, S. Muhammad, H. Sun, H. M. Ang, M. O. Tadé and S. Wang, *Catalysis today*, 2012, **190**, 68-72.
125. W. D. Zhang, B. Xu and L. C. Jiang, *J. Mater. Chem.*, 2010, **20**, 6383-6391.
126. A. Mostofizadeh, Y. Li, B. Song and Y. Huang, *Journal of Nanomaterials*, 2011, **2011**, 16.
127. D. S. Su and G. Centi, *Journal of Energy Chemistry*, 2013, **22**, 151-173.
128. S. Mohan, R. Ghandimathi, *Journal of Hazardous Materials*, 2009, **169**, 351-359
129. B. S. Harrison and A. Atala, *Biomaterials*, 2007, **28**, 344-353.
130. A. Jorio, G. Dresselhaus and M. S. Dresselhaus, *Springer Verlag*, 2008.
131. M. Lin, J. P. Y. Tan, C. Boothroyd, K. P. Loh, E. S. Tok and Y.-L. Foo, *Nano letters*, 2007, **7**, 2234-2238.
132. K. B. Teo, C. Singh, M. Chhowalla and W. I. Milne, *Encyclopedia of nanoscience and nanotechnology*, 2003, **10**.
133. A. V. Melechko, V. I. Merkulov, T. E. McKnight, M. Guillorn, K. L. Klein, D. H. Lowndes and M. L. Simpson, *Journal of Applied Physics*, 2005, **97**, 041301-041301-041339.
134. N. M. Rodriguez, A. Chambers and R. T. K. Baker, *Langmuir*, 1995, **11**, 3862-3866.
135. P. E. Nolan, D. C. Lynch and A. H. Cutler, *The Journal of Physical Chemistry B*, 1998, **102**, 4165-4175.
136. P. E. Nolan, A. H. Cutler and D. G. Lynch, *Journal*, 1998, **12**, 6-13.
137. M. Cantoro, S. Hofmann, S. Pisana, V. Scardaci, A. Parvez, C. Ducati, A. C. Ferrari, A. M. Blackburn, K.-Y. Wang and J. Robertson, *Nano letters*, 2006, **6**, 1107-1112.
138. E. C. Neyts, Y. Shibuta, A. C. van Duin and A. Bogaerts, *ACS nano*, 2010, **4**, 6665-6672.

139. Y. Wang, M. J. Kim, H. Shan, C. Kittrell, H. Fan, L. M. Ericson, W.-F. Hwang, S. Arepalli, R. H. Hauge and R. E. Smalley, *Nano letters*, 2005, **5**, 997-1002.
140. F. Danafar, A. Fakhru'l-Razi, M. A. M. Salleh and D. R. A. Biak, *Chemical Engineering Journal*, 2009, **155**, 37-48.
141. A. Rinzler, J. Liu, H. Dai, P. Nikolaev, C. Huffman, F. Rodriguez-Macias, P. Boul, A. H. Lu, D. Heymann and D. Colbert, *Applied Physics A: Materials Science & Processing*, 1998, **67**, 29-37.
142. S. Diamond, *Cement and concrete research*, 1986, **16**, 569-579.
143. M. Motiei, Y. Rosenfeld Hacoheh, J. Calderon-Moreno and A. Gedanken, *Journal of the American Chemical Society*, 2001, **123**, 8624-8625.
144. Z. Lou, Q. Chen, W. Wang and Y. Zhang, *Carbon*, 2003, **41**, 3063-3067.
145. Z. Lou, C. Chen, H. Huang and D. Zhao, *Diamond and related materials*, 2006, **15**, 1540-1543.
146. X.-j. Xu and S.-m. Huang, *Materials Letters*, 2007, **61**, 4235-4237.
147. J. Zhang, H. Zou, Q. Qing, Y. Yang, Q. Li, Z. Liu, X. Guo and Z. Du, *The Journal of Physical Chemistry B*, 2003, **107**, 3712-3718.
148. N. Hintsho, A. Shaikjee, P. K. Tripathi, P. Franklyn and S. Durbach, *RSC Advances*, 2015, **5**, 53776-53781.
149. M. Endo, T. Hayashi, Y. A. Kim, M. Terrones and M. S. Dresselhaus, *Mathematical, Physical and Engineering Sciences*, 2004, **362**, 2223-2238.
150. X. P. Shen, A. H. Yuan, F. Wang, J. M. Hong and Z. Xu, *Solid state communications*, 2005, **133**, 19-22.
151. Y. Lin, L. Liang and J. Liu, *Journal*, 2006.
152. R. Navarro, M. Pena and J. Fierro, *Chemical Reviews*, 2007, **107**, 3952-3991.
153. C. H. Bartholomew, *Applied Catalysis A: General*, 2001, **212**, 17-60.
154. D. C. Nath and V. Sahajwalla, *Journal of hazardous materials*, 2011, **192**, 691-697.
155. Y. Wen and Z. Shen, *Carbon*, 2001, **39**, 2369-2374.
156. A. G. Patil and S. Anandhan, *International Journal of Energy Engineering*.

157. R. A. Varin, T. Czujko and Z. S. Wronski, *Nanomaterials for solid state hydrogen storage*, Springer, 2009.
158. D. Paul and L. Robeson, *Polymer*, 2008, **49**, 3187-3204.
159. P.-C. Ma, N. A. Siddiqui, G. Marom and J.-K. Kim, *Composites Part A: Applied Science and Manufacturing*, 2010, **41**, 1345-1367.
160. G. Mittal, V. Dhand, K. Y. Rhee, S.-J. Park and W. R. Lee, *Journal of Industrial and Engineering Chemistry*, 2015, **21**, 11-25.
161. A. S. Hoang, *Advances in Natural Sciences: Nanoscience and Nanotechnology*, 2011, **2**, 025007.
162. I. Navarro-Baena, M. P. Arrieta, A. Mujica-Garcia, V. Sessini, D. Lopez, J. M. Kenny and L. Peponi, *Reactions and Mechanisms in Thermal Analysis of Advanced Materials*, 2015, 165-189.
163. S. Begum, A. Kausar, H. Ullah and M. Siddiq, *Polymer-Plastics Technology and Engineering*, 2015.
164. H. Mahfuz, A. Adnan, V. K. Rangari, M. M. Hasan, S. Jeelani, W. J. Wright and S. J. DeTeresa, *Applied Physics Letters*, 2006, **88**, 083119.
165. X. Wang, P. D. Bradford, W. Liu, H. Zhao, Y. Inoue, J.-P. Maria, Q. Li, F.-G. Yuan and Y. Zhu, *Composites Science and Technology*, 2011, **71**, 1677-1683.
166. P. R. Mantena, A. Al-Ostaz and A. H. Cheng, *Composites Science and Technology*, 2009, **69**, 772-779.
167. M. Ayatollahi, S. Shadlou, M. Shokrieh and M. Chitsazzadeh, *Polymer Testing*, 2011, **30**, 548-556.
168. A. Osorio, I. Silveira, V. Bueno and C. Bergmann, *Applied Surface Science*, 2008, **255**, 2485-2489.
169. W. Xia, C. Jin, S. Kundu and M. Muhler, *Carbon*, 2009, **47**, 919-922.
170. M. Kaempgen, C. K. Chan, J. Ma, Y. Cui and G. Gruner, *Nano letters*, 2009, **9**, 1872-1876.
171. V. Datsyuk, M. Kalyva, K. Papagelis, J. Parthenios, D. Tasis, A. Siokou, I. Kallitsis and C. Galiotis, *Carbon*, 2008, **46**, 833-840.
172. N. Zhang, J. Xie and V. K. Varadan, *Smart materials and structures*, 2002, **11**, 962.

173. Y. Peng and H. Liu, *Industrial & engineering chemistry research*, 2006, **45**, 6483-6488.
174. K.-S. Kim, K.-Y. Rhee, K.-H. Lee, J.-H. Byun and S.-J. Park, *Journal of Industrial and Engineering Chemistry*, 2010, **16**, 572-576.
175. A. T. Seyhan, M. Tanoglu and K. Schulte, *Materials Science and Engineering: A*, 2009, **523**, 85-92.
176. A. G. Patil and S. Anandhan, *International Journal of Energy*, 2012, **2**, 57-62.
177. A. Magrez, J. W. Seo, V. L. Kuznetsov and L. Forró, *Angewandte Chemie., International Edition.*, 2007, **119**, 445–448.

Chapter 3: Materials and Methods

3.1 Introduction

This chapter sets out information on the materials and a detailed methodology describing the instruments used for the characterization of materials that were synthesized, the chemical solutions and equipment used in this study. This chapter is divided into various sections and the lists of chemicals (Table 3.1), gases (Table 3.2) and equipment (Table 3.3) used in this study will be presented. The synthesis of carbon nanomaterials (CNMs) using the chemical vapour deposition (CVD) method is also detailed (Section 3.3.1). Acid functionalisation and treatment methods that were used on these CNMs are explained (Section 3.3.2). The techniques and methods used to characterise these CNMs are also described (Section 3.4). Lastly the use of these CNMs as fillers in an attempt to improve the strength of a polyester polymer will be described. Here the synthesis of this composite by vacuum assisted resin transfer moulding (VARTM) and the mechanical tests (tensile, flexural and impact) are fully described.

3.2 Materials, Gases and Equipment used

3.2.1 Materials

The chemicals, gases and equipment that were used in this study are presented in Tables 3.1 and 3.3 respectively. All the gases used in this study were supplied by AFROX (African Oxygen Limited) and were accompanied by a certificate of analysis.

Table3. 1: List of chemicals used in this study

Chemical Name	Specification (%)	Supplier
Ethanol	99.5	Sigma Aldrich, RSA
Hydrochloric Acid (HCl)	55	Sigma Aldrich, RSA
Potassium Permanganate (KMnO₄)	99	Sigma Aldrich, RSA
Nitric Acid (HNO₃)	98	Sigma Aldrich, RSA
Sulphuric Acid (H₂SO₄)	98	Sigma Aldrich, RSA
Polyester GP Lam 410	52-65	AMT resin
Butanox-M50 Catalyst	2%	AMT Resin

Table3. 2: List of gases used in this study

Chemical Name	Specification (%)	Supplier
Acetylene	99.9	Afrox, RSA
Hydrogen	99	Afrox, RSA
Nitrogen	99.99	Afrox, RSA
CO₂	99	Afrox, RSA

Table3. 3:List of equipment used in this study

Equipment	Supplier
Magnetic Stirrer Plate	<i>Kimix</i> Chemicals & Laboratory Suppliers, RSA
Porcelain Dishes	<i>Kimix</i> Chemicals & Laboratory Suppliers, RSA
Magnetic Bar	<i>Kimix</i> Chemicals & Laboratory Suppliers, RSA
Oven	Scientific, Series 2000, RSA
Muffle Furnace	Gallenkamp, USA
Pure Lab UHQ de- ionizer	ELGA, USA
Horizontal Tube Furnace (for CVD)	Home built
Mould	Home built

3.3 Experimental Procedures

3.3.1 Synthesis of carbon nanomaterials via chemical vapour deposition (CVD)

Untreated waste coal fly ash was obtained from the Electricity Supply Commission (ESKOM) Research and Innovation Centre (Rosheville, South Africa) and was used without any treatment or modification. Carbon deposition was achieved using CVD of acetylene (C_2H_2) over the untreated fly ash. In a standard reaction: fly ash was used as a catalyst, while either C_2H_2 and or CO_2 served as carbon sources, while H_2 and/or N_2 were used as carrier or pre-reaction gases.

In a typical synthesis experiment, 500 mg of as-received fly ash was uniformly spread in a small quartz boat and placed in a quartz tube, in the centre of a horizontal tube furnace to ensure controlled heating. A gas mixture of C_2H_2 , H_2 or N_2 was introduced into the quartz reaction tube through the gas inlet and exhausted through the gas outlet. Gas mixtures of three types (C_2H_2/N_2 , C_2H_2/H_2 and $C_2H_2/H_2/N_2$) with a total flow rate of 100 ml/min were studied. In addition, temperatures ranging from 450 °C to 750 °C in 100 °C intervals were studied, with these gas mixtures. The fly ash was first heated at 10 °C/min in H_2 , N_2 or a mixture of both gases for periods between 45 to 75 min to reach a desired temperature. Acetylene gas was then introduced into the reaction zone for a period of 45 min. Thereafter, the flow of C_2H_2 was terminated and the reactor was cooled under H_2 and/or N_2 to ambient temperature. A typical CVD synthesis set up is shown Fig. 3.1.

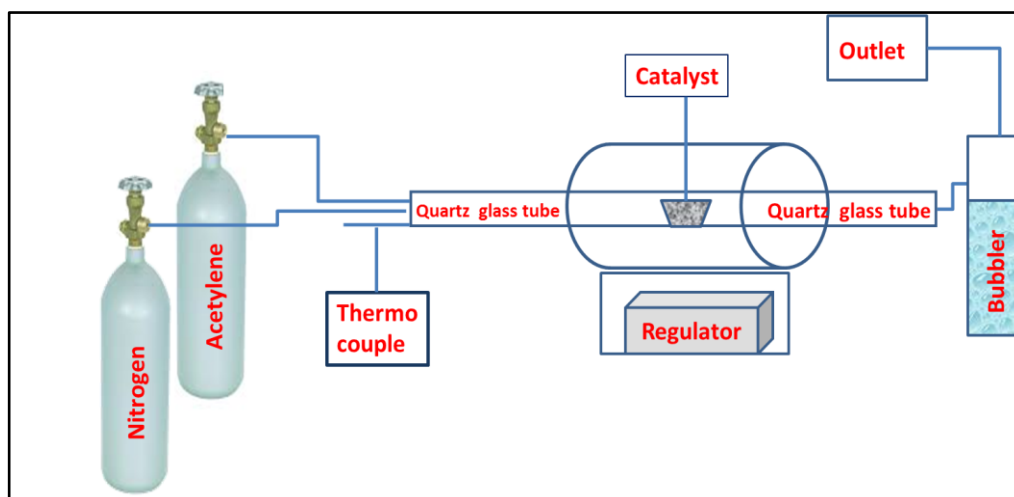


Figure 3.1: CVD set up for CNM synthesis using coal fly ash as a catalyst; acetylene as a carbon source and nitrogen as a carrier gas.

Upon obtaining the carbon nanomaterials formed, the percentage yield was calculated using the formula below:

$$\% \text{ Yield} = \frac{\text{gP}-\text{gC}}{\text{gC}} \times 100$$

Where:

% Yield= Percentage Yield

gP = Total mass of product

gC = Total mass of catalyst

3.3.2 Acid treatment of synthesized carbon nanofibres (CNFs)

Pre-treatment of CNFs with an acid or an oxidising agent was performed prior to mixing the CNFs with the polyester resin. The CNFs were acid-treated using a previously optimised method by Park *et al.* to observe whether acid washing would improve the adhesion between the CNFs and the polyester polymer¹. Acid treatment is primarily to add functional groups on the surface of the CNTs/CNFs to cause chemical attachment to the polymer and to enhance dispersion in the polymer matrix¹. The aim of pre-treating the CNFs in this study, was to reduce metal impurities from these materials and to generate functional groups such as carbonyl, carboxyl and oxygen containing groups on their surfaces. These functional groups have been reported to induce a change in the chemical make-up of the outer layer of such materials, helping them to change from a hydrophobic nature to a hydrophilic one². This in turn was expected to promote more uniform

dispersion of these CNFs in the polyester polymer. CNFs synthesized from Duvha fly ash were either treated with HCl/HNO₃ mixture and or KMnO₄ solution as follows:

3.3.2.1 Functionalisation of CNFs using KMnO₄

Aliquots of 500ml of a 1M solution of KMnO₄ was prepared by dissolving 7.9016 g of KMnO₄ in distilled water. The solution was stirred using a magnetic stirrer until the KMnO₄ had dissolved. 4g of CNFs was added to 200 ml of the KMnO₄ solution. The mixture was stirred for 4 hr at 40 °C. The CNFs were washed with distilled water to remove the residual KMnO₄. The CNFs were then dried overnight in the oven at 90 °C.

3.3.2.2 Functionalisation of CNFs using HCl/HNO₃

Approximately 4 g of CNFs were added to 300 ml mixture of 98% wt % hydrochloric acid and 38.0 wt % of nitric acid (volume ratio of 3:1). Thereafter, the mixture was refluxed for 2 hr at 90 °C. The CNFs were then washed with distilled water until the rinse solution reached pH 6-7. The acid treated CNFs were then dried overnight in an oven at 90 °C.

3.4 Characterization techniques and experimental details

Various techniques, such as, scanning electron microscopy (SEM), Energy Dispersive Spectroscopy (EDS), Brauner-Emmett-Teller N₂ adsorption (N₂BET), thermal gravimetric analysis (TGA), transmission electron microscopy (TEM), laser Raman spectroscopy, X-ray fluorescence (XRF), X-ray diffraction (XRD) and Mössbauer spectroscopy, were used to characterize the synthesized CNMs. A summary of the techniques used and the information they provide is given in Table 3.4 below. The aim of these characterization methods was to study the physical and chemical properties of the synthesized materials.

Table 3.4 Characterization techniques used during CNM synthesis

Techniques	Function
Brauner-Emmet-Teller (N₂BET)	Surface area, pore diameter and pore size distribution
Fourier transform infrared spectroscopy (FTIR)	Identification of functional peaks present
Transmission electron microscopy (TEM)	Crystallinity and particle size
Scanning electron microscopy (SEM) & Energy dispersive spectroscopy (EDS)	Surface morphology and elemental composition
Laser Raman spectroscopy	Crystallinity
Thermal gravimetric analysis (TGA)	Thermal stability
X-Ray diffraction (XRD)	Crystallinity, particle size and phase analysis
X-Ray fluorescence (XRF)	Elemental analysis of minor and major elements
Mössbauer spectroscopy	Chemical and structural information of iron in fly ash

3.4.1 Scanning electron microscope (SEM)

Scanning electron microscopy (SEM) micrographs were obtained using a FE-SEM ZEISS SIGMA microscope (Zeiss, UK). Carbon tape was placed on top of a specimen holder and a small, representative amount of fine powder was dusted on the tape. The specimen was then introduced into the SEM. This SEM was coupled with an EDS detector using GENESIS software for qualitative elemental analysis.

3.4.2 Transmission electron microscopy (TEM)

The surface morphology of the CNMs that were synthesised was further characterized using TEM (Tecnai, G2 F20 X-Twin MAT, Hillsboro, USA). A small amount (1-4 mg) of the powder samples of CNMs were diluted in 10 ml of

ethanol followed by sonication for 5 min. Specimens were transferred onto the holey carbon film double layer 400 mesh copper grids (i.e. the sample holder) and allowed to dry at room temperature. The specimens were then characterized by TEM.

3.4.3 Brauner–Emmet-Teller (N₂BET)

Surface areas, pore volumes and pore size distributions of the CNM samples were determined by means of the Bruner–Emmett-Teller (N₂ BET) technique using a Micrometrics Tri-Star instrument (Micrometrics Instrument Co., Norcross, GA, USA). Approximately 200 mg of the catalyst powder was weighed and degassed in micrometrics Tri star 3000 by flowing Helium (He) at 90 °C for 1 hr, and then held at 350 °C for 16 hrs. As the temperature increased, water vapour was desorbed from the surface and pores of the sample. The sample was then cooled down and weighed again. The TriStar machine used physical adsorption and capillary condensation of N₂ to obtain information about the surface area and porosity of each solid material.

3.4.4 Fourier transform infrared spectroscopy (FTIR)

A Bruker Tensor 27 Fourier transform infrared spectrometer (Bruker AXS, Karlsruhe, Germany) was used for the qualitative analysis of the functional groups that were present on the CNMs formed. The instrument was first cleaned and set up according to the manufacturer's instructions to obtain a background spectrum before the analysis. Approximately 15 mg of the catalyst powder was placed on the attenuated total reflectance (ATR) sample holder of a Bruker Tensor 27 Fourier transform infrared spectrometer. The sample were analysed in the range of 380-4000 cm⁻¹ and the then baselines were corrected and the spectra were smoothened. Spectra were the obtained depending on the characteristics of each sample.

3.4.5 Thermal gravimetric analysis (TGA)

To obtain the thermal stability of the carbon nanomaterial, thermal gravimetric analysis (TGA) was performed on a Perkin Elmer TGA 4000 Thermo-gravimetric

analyser (TGA; PerkinElmer, Waltham, MA, USA). Approximately 10 mg of the catalyst powder was weighed and inserted into the sample pan. The sample was heated from 35 °C to 900 °C at a rate of 10 °C/min under air (50 ml/min). The mass of all samples was kept constant (*ca.* 10 mg) in order to reduce the effects of variability in measurements.

3.4.6 Laser Raman spectroscopy

The structural features of the synthesized CNMs were investigated using laser Raman spectroscopy (Jobin–Yvon T64000 Raman spectrometer (Horiba Scientific, UK)). The spot size on the sample was ~1.5 µm in diameter and the excitation wavelength was 514.5 nm from an Ar ion laser. A grating with 600 grooves/mm was used to disperse the spectrum onto a charge coupled detector (CCD).

3.4.7 X-ray diffraction (XRD)

X-ray diffraction (XRD) experiments were performed on a D2 Advance diffractometer from Bruker AXS, (Bruker AXS, Karlsruhe, Germany). Approximately 100 mg of CNFs was ground to a homogeneous powder. The catalyst powder was placed into a sample holder using a spatula to make the surface even and introduced into the X-ray diffractometer. The phase identification was performed by searching and matching obtained diffraction patterns with the powder diffraction file data base with the help of EVA software.

3.4.8 X-ray fluorescence (XRF)

XRF analysis was performed on a PanAnalytical PW2404 wavelength dispersive spectrometer (PanAnalytical, Almelo, Netherlands). Approximately 5 g of fly ash was mixed thoroughly with 2% polyvinly glue, Mowiol binder. The mixture was then compressed under 10 MPa pressure in order to form a pellet for the analysis. The pellet was then exposed to $K_{\alpha} = 24.9$ and $K_{\beta} = 22$. X-rays were generated from a rhodium tube and the data was integrated and analysed.

3.4.9 Mössbauer spectroscopy

Mössbauer spectra were recorded using an acetone gas-filled resonance detector equipped with ^{57}Fe enriched stainless steel foils mounted on a conventional velocity drive system outside the implantation chamber. The detector was mounted 90° to the beam direction and 60° relative to the crystal surface normal. The velocity and isomer shift values are calibrated relative to $\alpha\text{-Fe}$ at room temperature.

3.5 The CNF polyester/ composite fabrication procedure

CNF/polyester composites were manufactured using the Vacuum Resin Transfer Moulding (VRTM) method. The fibre composite (FCs) specimens were fabricated using different fibre mass fractions of 0.125-0.5 % for all the different treated CNFs. The corresponding resin content was determined using the ISO-1268-2 standard:

$$M_2 = M_1 (100 - M_1 - W_g / W_g) K$$

where

M_1 = mass of fibre in grams

M_2 = mass of resin required in grams

W_g = fibre content as a percentage of the total mass

K = constant representing 10% of excess resin lost through spills.

Before proceeding with the fabrication process, the steel mould was cleaned using acetone and then dried using a dry cloth. As part of the priming procedure, a thin film of MR8 release agent was applied to the mould surface. Fig. 3.2 shows a schematic of the 3 piece VRTM mould used for specimen fabrication. The mould consists of two male plates (MP) with gasket grooves and a female plate (FP).

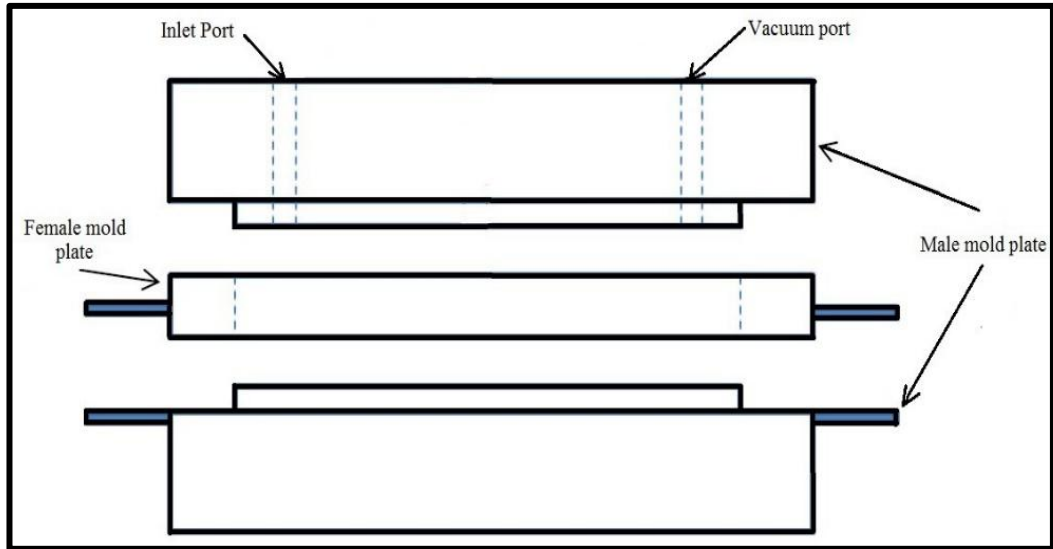


Figure 3.2: Plates of mould used for fabricating composite specimens

Once the cleaned mould was dried, the bottom male mould plate was placed on the mould stand. The female mould plate was pressed upon the bottom male plate and then the required fibre mat was placed inside the mould before being closed with the top male mould. The gasket grooves on the mould plates ensured a stable vacuum during manufacturing. A small pipe was used as resin trapper. The entire assembly was clamped to arrest any leakages and was also checked for leakage by connecting it to the vacuum pump.

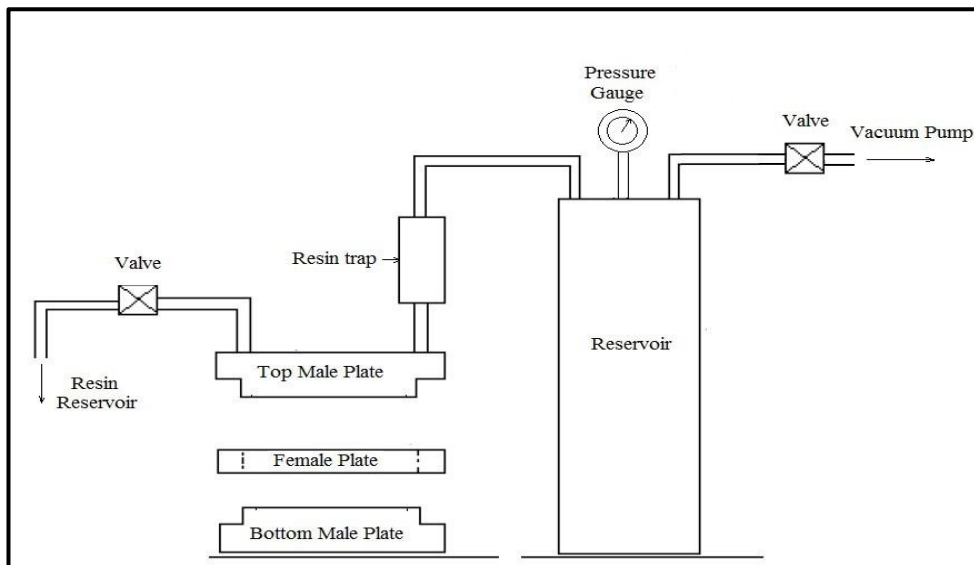


Figure 3.3: Mould used for fabricating composite specimens ¹

After setting up the VRTM, 300 ml of NCS polyester resin was mixed with 0.75 g of the Mekk catalyst as per the process manual and kept ready at the inlet port. The resin feed valve was then slowly opened. As the resin filled the mould, the vacuum pressure was maintained at a constant value of 18 kPa. The feed line was kept open until the resin exited the mould. Once the mould was filled, both the feed line and the vacuum line valve was closed and the resin was allowed to cure. A similar procedure was followed for manufacturing the CNF treated composites, except that the polymer matrix was mixed with three different weight fractions (i.e. 0.125 wt. %, 0.25 wt. % and 0.5 wt. %) of functionalized CNFs.

3.6 Mechanical characterisation of CNF-polyester composites

3.6.1 Testing procedure

In order to determine the mechanical properties of the CNF-polyester nanocomposites, a series of mechanical tests were carried out which included tensile testing, flexural testing and impact testing. Composites in general are tested using the standards developed by the American Society for Testing and Materials (ASTM) and the International Organization for Standardization (ISO) so that comparable results can be obtained by different researchers performing similar experiments elsewhere in the world. Therefore, all the testing done in this experimental research was performed in accordance with either the ASTM or ISO standards for each particular test. A summary of each testing procedure used is presented in the following Sections.

3.6.1.1 Tensile testing

The standard guidelines that pertain to the tensile testing of plastic composite materials are given in ASTM D638 which specifies that a tensile composite specimen should be cut into the dog-bone dimensions shown in Fig. 3.4. This particular shape of the dog-bone specimen guarantees that failure will occur at the region of minimum cross section, called the gauge length, which allows for repeatability and accuracy in the tensile testing of all composite materials.

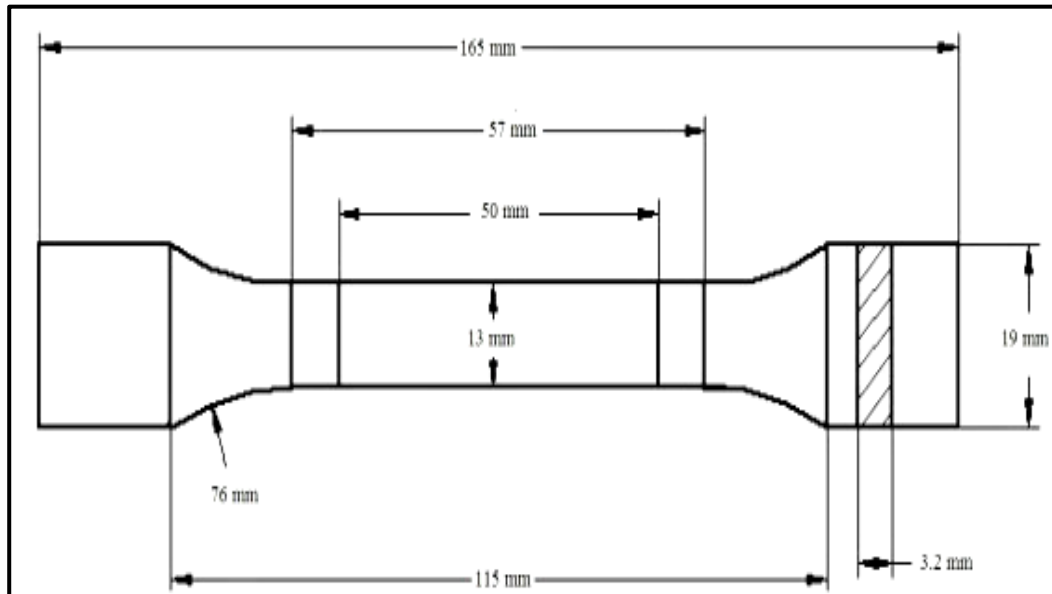


Figure 3.4: Dog bone shape of polyester composite, using the dimensions of ASTM D638¹

3.6.1.1 Tensile testing procedure

A load cell of 50 kN was used to conduct the tensile testing. Prior to testing, the thickness and width of the specimens were measured using a Vinear Calipers. Thereafter, the test specimen were placed into the jaws of the machine grips and tightened so that the specimen were held firmly enough in the jaws not to slip during testing. Then the extension indicator was attached onto the gauge length of the test specimen. The machine was then set to the desired testing speed and testing began. The data recorded during the testing procedure for each specimen was used to calculate the tensile properties of the material. This was done through averaging the sum of all the individual specimens per test batch of 5 samples and through using the following calculations.

$$A=W \times T \quad \text{(Equation 1)}$$

where:

A = Cross Sectional area of the gauge test Section [mm]

W = Width of the gauge test Section [mm]

T = Thickness of the gauge test Section [mm]

After obtaining the maximum tensile force at the point of failure, as well as the measured average cross-sectional area of the specimen, these were then used to calculate the ultimate tensile strength of the specimen which is given by Equation 2 below as:

$$\sigma_{\text{uts}} = F_{\text{max}}/A \quad \text{(Equation 2)}$$

where:

σ_{uts} = Ultimate tensile strength of specimen [MPa]

F_{max} = Maximum load during test [N]

Using the data recorded by the extensometer, the tensile strain of the specimen was then calculated using Equation 3 as:

$$\epsilon = \Delta l / l \quad \text{(Equation 3)}$$

where:

ϵ = Tensile strain

Δl = Extensometer displacement [mm]

l = Extensometer gauge length [mm]

Using the tensile stresses and strains calculated by equations 2 and 3 respectively; the Young's Modulus also known as modulus of strain, was then calculated using Equation 4 as:

$$E = \Delta \sigma / \Delta \epsilon \quad \text{(Equation 4)}$$

where:

E = Tensile modulus of elasticity of the specimen [GPa]

$\Delta \sigma$ = Difference in stress between two data points lying on the linear portion of the data set [MPa]

$\Delta \epsilon$ = Difference in strain between two data points lying on the linear portion of the data set [mm/mm]

3.6.1.2 Flexural testing

The standard guidelines that pertain to the flexural testing of plastic composite materials are given in ASTM D790 which makes use of the 'three-point bending' method which induces the bending loads in the test specimen until the specimen

fractures. The preferred dimensions for the test specimen according to the standards are given below in Fig. 3.5:

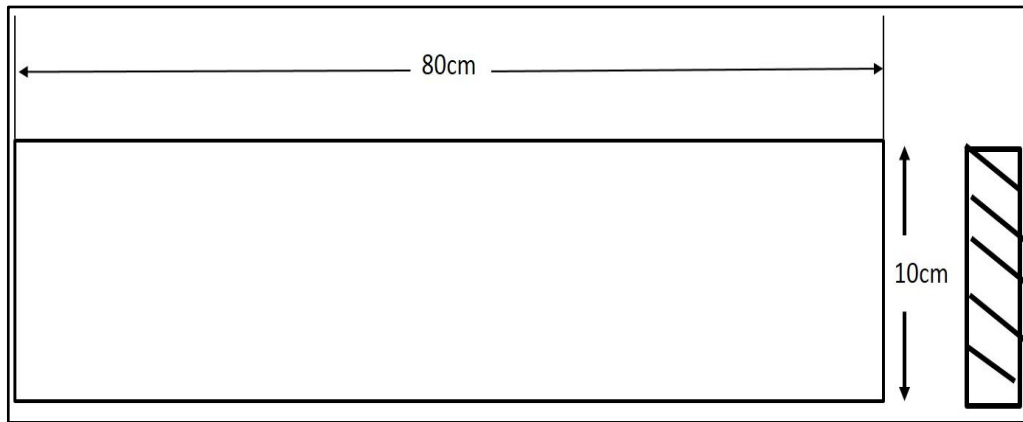


Figure 3.5: Preferred dimensions for ASTM D790 test specimen

3.6.1.2.1 Flexural testing procedure

The flexural testing was performed using the same Lloyd testing machine of 50 kN load cell using a 3 point flexural testing attachment as per ISO 178 standard. The built in encoder was used to acquire the required data. The distance between the specimen supports was 50 mm. The test specimens were cut along the longitudinal direction only. The Flexural test specimens were fabricated with the thickness span ratio of 1:16 and the tests were conducted at the cross head speed of 1 mm/min. The same number of specimens used in the tensile testing, five, was used for flexural testing. The flexural properties were obtained by averaging specimen properties using the same method as that used for the tensile properties. Using the averaged values of the three widths and thicknesses measured from the specimen as well as the load applied and the distance between the supports, the flexural stress in the specimen was calculated using Equation 5 below.

$$\sigma_f = \frac{3F_{\max}L}{2bh^2} \quad \text{(Equation 5)}$$

where:

σ_f = Specimen flexural stress [MPa]

F_{\max} = Load applied [N]

L = Length between supports [mm]

b = Width of specimen measured at its centre [mm]

h = Thickness of specimen measured at its centre [mm]

After obtaining the data recorded by the extensometer, the flexural strain of the specimen was then calculated using Equation 6 as:

$$\epsilon_f = 6hD/L^2 \quad \text{(Equation 6)}$$

Where:

ϵ_f = Flexural strain of specimen [mm/mm]

D = Vertical deflection of the specimen at the point of load application [mm]

L- Length

3.6.1.3 Impact testing

Impact testing generally known as the measure of toughness for plastic composites was determined using ASTM D 256. The toughness of the material was determined by the amount of energy absorbed by the specimen upon impact. This test requires that at least 5 specimens be tested and be averaged out in order for the results to be reliable.

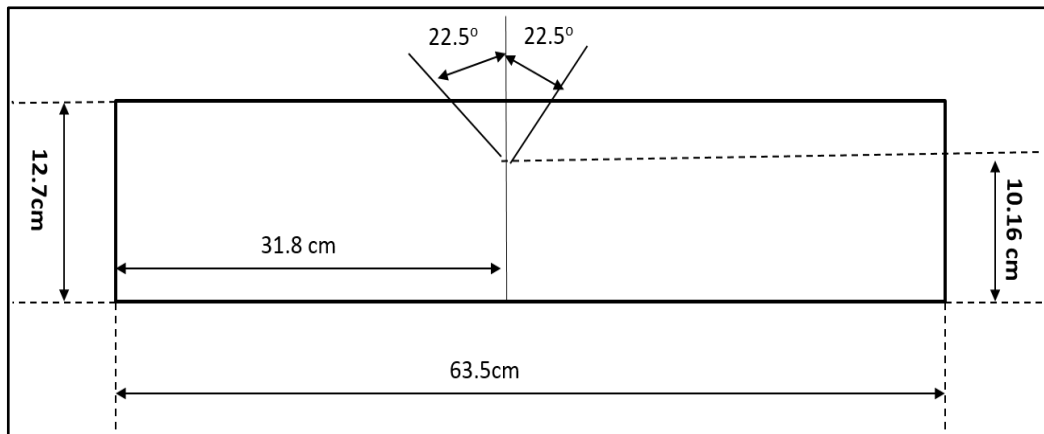


Figure 3.6: Impact testing requirements using ASTM D256 standard dimensions

3.6.1.3.1 Impact testing procedure

The Izod impact testing method was used to determine the impact strength of the fabricated composite specimens. An Avery pendulum impact testing machine with static dial arm, which can manually be moved was positioned prior to testing, at 4.2 J mark. This type of testing was conducted by clamping the test specimen in a vertical position and breaking it in two through a single swing of the pendulum arm of the test rig. In order to break the specimen, the pendulum arm had to lose a certain amount of energy in fracturing the test specimen. By recording the initial

height of the pendulum and the height which the pendulum reaches after impact, the energy absorbed by the specimen was then found.

The impact toughness is expressed as the energy lost per unit cross-sectional area. This was calculated using equation 7.

$$\mathbf{K} = \Delta e_I / A_I \quad \text{(Equation 7)}$$

where:

K = Impact toughness [J/mm^2]

Δe_I = Energy lost by pendulum due to impact [J]

A_I = Cross-Sectional area of impact specimen [mm^2]

References

1. H. J. Park, M. Park, J. Y. Chang and H. Lee, *Nanotechnology*, 2008, **19**, 335702.
2. E. G. Rakov, *Russian Chemical Reviews*, 2000, **69**, 35-39.

Chapter 4: Direct synthesis of carbon nanofibres from South African coal fly ash

4.1 Introduction

The synthesis of carbon nanomaterials (CNMs) has received tremendous interest in the last two decades¹⁻⁴. These endeavours are driven by the need to exploit the unique chemical and physical properties associated with CNMs (e.g. strength), as well as the desire to develop synthetic strategies that are cost effective and non-destructive to the environment⁶⁻⁸. The synthesis of well-structured CNMs is known to require three main components: a source of energy, a source of carbon and a template or catalyst¹¹. Recent publications have shown that efforts have focused on using lower energy sources (low temperature synthesis), natural or recyclable carbon reactants and appropriate templates¹²⁻¹⁵.

One of the main challenges in the chemical industry has been the development of low cost, recyclable and effective substrates (catalysts) upon which well-structured CNMs can grow¹⁶⁻¹⁸. This has prompted interest in several industrial by-products that contain components that are known to actively decompose carbon reagents into CNMs¹⁹⁻²². Of interest has been the study of the effect of coal fly ash as a catalyst for carbon nanomaterial growth. Currently, only a fraction of this material is utilized effectively, with the remainder proving to be environmentally hazardous due to the presence of several toxic elements like mercury, lead, etc.²³⁻²⁵. It has been shown that fly ash can produce CNMs, when used as a catalyst or support provided that the reaction conditions are correct^{26-27,36}. This is due mainly to the transition metal content found in certain fly ashes. Yasui *et al.* reported the first study, using Japanese fly ash, where Fe was added to the ash to enhance its activity¹⁷. Although CNTs were produced, these were of a very low yield and poor quality. Thereafter, Dunens *et al.* produced CNTs and CNFs from Australian coal fly ash using the CVD method⁵. However, because iron (was low in their fly ash < 2.5%), they had to impregnate it onto their substrate and with an expensive carbon source used (ethylene), this led to the cost

of CNT and CNF synthesis being high.. In trying to improve the above methods, Salah *et al.* used carbon rich Saudi Arabian fly ash to make CNTs⁶. In this method, pre-treatment of the ash was also conducted to remove unburnt fly ash in order to use the ash as a catalyst.

Reports on the effectiveness of fly ash as a catalyst or template in the synthesis of CNFs are limited^{5,6,17}. Moreover, fly ash is considered as either a support for other more active metallic catalyst particles or is used after extensive synthetic treatment^{5, 6,17}. On the other hand, no work has been done using a South African coal fly ash to make carbon nanofibres.

This chapter reports a simple, direct route for the synthesis of CNFs from South African coal fly ash and acetylene at varying temperatures. Here no pre-treatments or additions of expensive catalysts were required, as the fly ash was used as it was received.

4.2 Methods

4.2.1 Synthesis

Waste South African coal fly ash was obtained from ESKOM in Rosheville, South Africa and was used without any chemical pre-treatments or thermal modifications (Table4.1). Carbon deposition was achieved by the CVD of acetylene over the waste coal fly ash. In these reactions the coal fly ash was the catalyst, acetylene the carbon source and hydrogen the carrier gas. The procedure followed in each synthesis run is described in Section 3.3.1, in these reactions the flow rate was kept at 100 ml/min to temperatures between 400 °C and 700 °C in 100 °C increments. The resultant carbonaceous material was then harvested for characterization.

4.2.2 Characterization

The synthesized CNFs samples were characterized using scanning electron microscopy (SEM), thermogravimetric analysis (TGA) and laser Raman spectroscopy. For each characterisation, procedures described in Section 3.4.1, 3.4.5 and 3.4.6 respectively were followed. Nanofibre diameter distributions were measured using Image J⁵. To identify the metals responsible for CNF formation, their amounts and understand the crystallinity of the samples, Mössbauer spectroscopy, X-ray fluorescence (XRF) and x-ray diffraction (XRD) was employed respectively, using procedures followed in Sections 3.4.9, 3.4.7 and 3.4.8. To obtain the surface area of the materials, Brunner-Emmet Teller (BET) method was employed as described in Sections 3.4.3.

Table 4.1: The chemical composition of South African coal fly ash samples obtained by XRF

Fly ash component	Weight (%)
SiO ₂	55.03
Al ₂ O ₃	27.76
Fe ₂ O ₃	0.62
FeO	4.99
MnO	0.08
CaO	5
MgO	1.43
Na ₂ O	0.14
K ₂ O	0.9

4.3 Results and Discussion

4.3.1 Morphological Studies

The sizes, shapes and morphologies of the as-received and acetylene treated fly ash were investigated using TEM. The results can be observed in Fig. 4.1a-f. The as-received fly ash materials (Fig. 4.1a) appeared to be spherically shaped. Spherically shaped fly ash agglomerating like these have often been observed with inorganic salts and may be caused by inter-particulate fusion during the

cooling of the fly ash⁴¹. In Fig. 4.1b-e, it was observed that the glassy, smooth shaped fly ash particles began to be coated with regularly and irregularly shaped CNFs when subjected to acetylene. In Fig. 4.1(c-d), it was noted that the types of CNMs that were formed varied from large CNFs to smaller CNTs. While the exact growth mechanism of CNFs formed from fly ash as a catalyst is not yet fully known, it does appear from Fig. 4.1(e-f) that tip growth cannot be discounted (as seen by the red coloured circles). This type of growth has typically occurred when either iron (Fe) or cobalt (Co) were used as catalysts for CNM formation. While it is known from previous studies that at least 2.5% iron is required as a catalyst for CNF formation when using fly ash, the XRF data (Table 4.1) obtained for the South African coal fly revealed that at least 5.6% of iron (in the forms of Fe₂O₃ and FeO) was present. Based upon this information and observations made from this research, the reaction scheme shown below has been proposed (Figure 4.2).

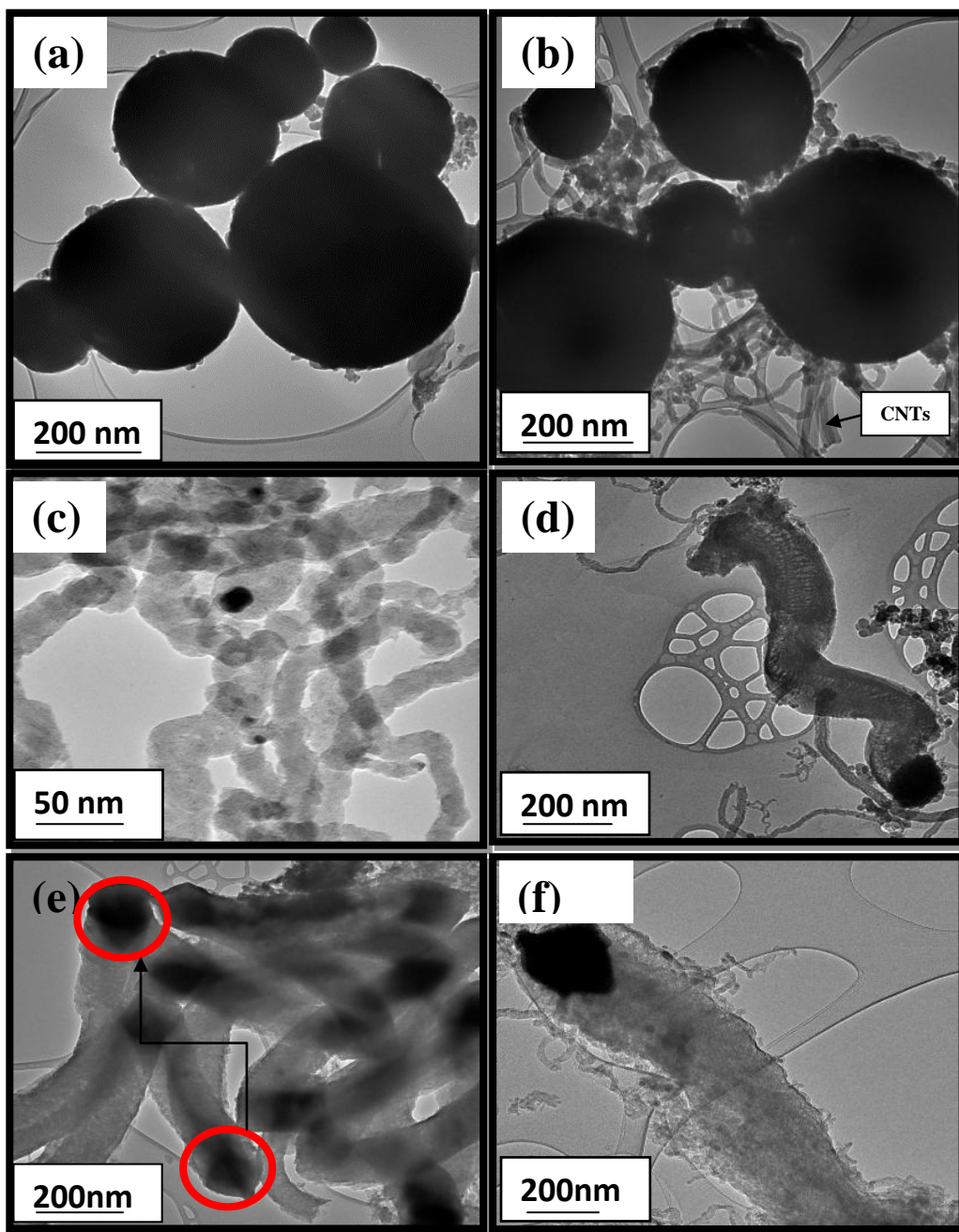


Figure 4.1: TEM images of (a) as-received coal fly ash and CNTs synthesized at (b) 400 °C, (c) 500 °C, (d) 600 °C and (e-f) 700 °C

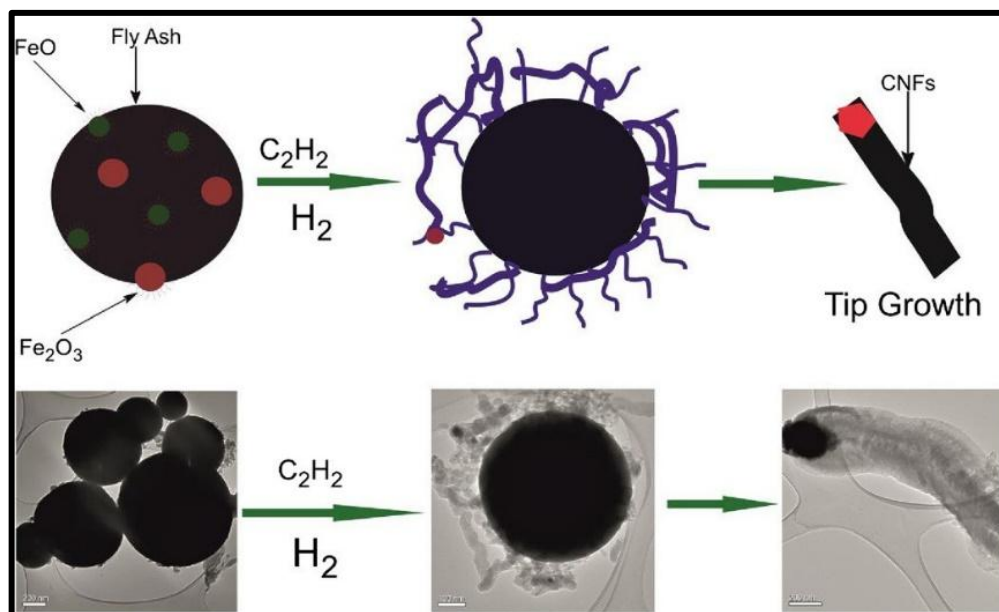


Figure 4.2: Proposed reaction scheme for CNF growth, using South African coal fly ash as a catalyst

For this type of growth to occur it is known that there is normally a weak interaction between the catalyst and support⁴². During this process the carbon reagent decomposes on the metal particle under specific reaction conditions. The carbon deposited on the metal then either dissolves/re-precipitates to form either CNT/Fs or carbon migrates over the metal particle to form a tube or a fibre⁴². If the catalyst particles are large then multi-walled carbon nanotubes (MWCNTs) and CNFs can be formed⁴².

4.3.2 Laser Raman spectroscopy studies

To determine the graphitic nature of the carbonaceous products, laser Raman spectroscopy was conducted. Fig. 4.3 shows the laser Raman spectroscopy spectra that were used to determine the structural formation of CNFs produced by the exposure of coal fly ash to acetylene. As expected, the spectrum of as-received fly ash did not show any peaks, but in the fly ash exposed to acetylene, peaks at 1350 cm^{-1} and 1590 cm^{-1} were observed. The intensity ratio of these peaks, known as the D-band (due to disordered carbon features) and G-band (due to the ordered graphitic carbon features) respectively, represents the degree of graphitization of carbon in the reaction products⁵. A low intensity ratio (I_D/I_G) indicates a greater

degree of wall graphitization, leading to a superior quality of CNFs and/or CNTs. The intensity ratios of the D and G bands (I_D/I_G) are depicted in Fig. 4.3b. The I_D/I_G ratio was found to be low at 400 °C indicating that the products contained more graphitic carbon than non-graphitic (non-crystalline) carbon. However, when the reaction temperature was increased to 500 °C, the I_D/I_G ratio was observed to have increased (to the highest value observed in these studies). The results of the derivative TGA analyses (Fig. 4.4) of the carbonaceous products formed at 500 °C revealed the presence of two combustion peaks i.e. two separate CNM products. While the exact reason for the formation of two types of CNMs at this temperature is not fully known, it is believed that this observation most likely accounts for the anomalous increase in the I_D/I_G ratio. Thereafter when the reaction temperature was increased to 600 °C and 700 °C, the I_D/I_G ratio decreased. This indicated the degree of disordered carbon that was formed decreased as the temperature was increased. These results showed that the CNFs produced at 700 °C had the highest quantity of graphitic carbon and were similar to those reported in previous studies where Fe supported catalysts were used²⁵.

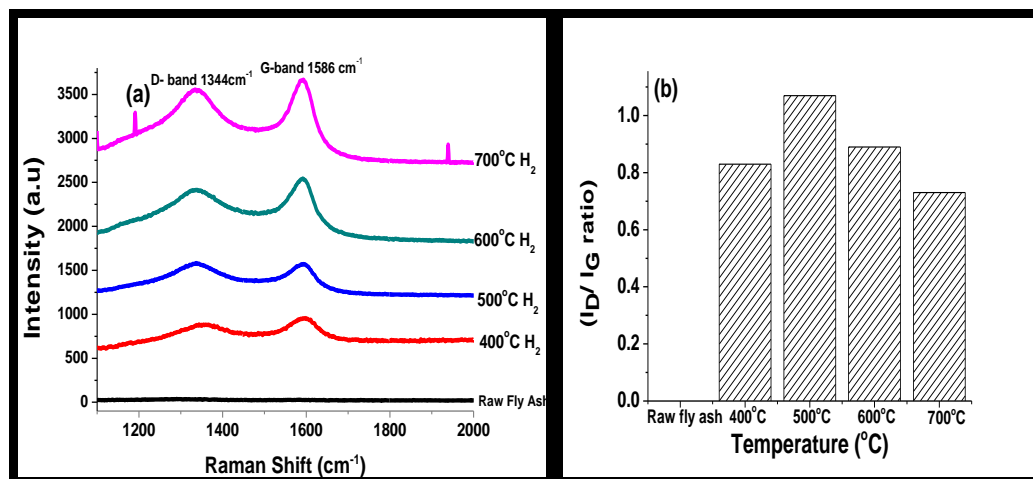


Figure 4.3: Laser Raman spectroscopy spectra of as-received fly ash and products from fly ash exposed to acetylene at various temperatures and (b) I_D/I_G ratios of the carbon nanofibres formed in acetylene.

4.3.3 Thermogravimetric studies

Thermogravimetric analyses were carried out to investigate the thermal degradation behaviour of as-received and acetylene treated fly ash. It has been reported that the graphitic nature of carbon nanomaterials are directly proportional to their thermal stability⁴³. Hence, the first order weight derivatives of the data so obtained, typically gives an indication of the type of carbon present (Fig. 4.4). Typically highly crystalline nanofibres have been found to be resistant to oxidation when compared to other forms carbon⁴⁴. Additionally the diameters and amount of defects in such materials has also been known to influence their oxidation temperatures⁵. From the TGA thermograms, it was observed that all of the CNMs produced had final oxidation temperatures that were greater than 550 °C. However, as previously stated, different forms of carbon were formed when the reaction temperature was 500 °C. These may have arisen due to the poor carbonization of acetylene and hence the formation of a higher degree of non-graphitic carbonaceous materials, as confirmed by the laser Raman spectroscopy results (Fig. 4.3a). However, CNFs synthesised at 700 °C had the highest oxidation temperature (c.a. 690 °C). These results concurred with the laser Raman spectroscopy data, where CNFs formed at 700 °C displayed the lowest I_D/I_G ratio i.e. were the most graphitic.

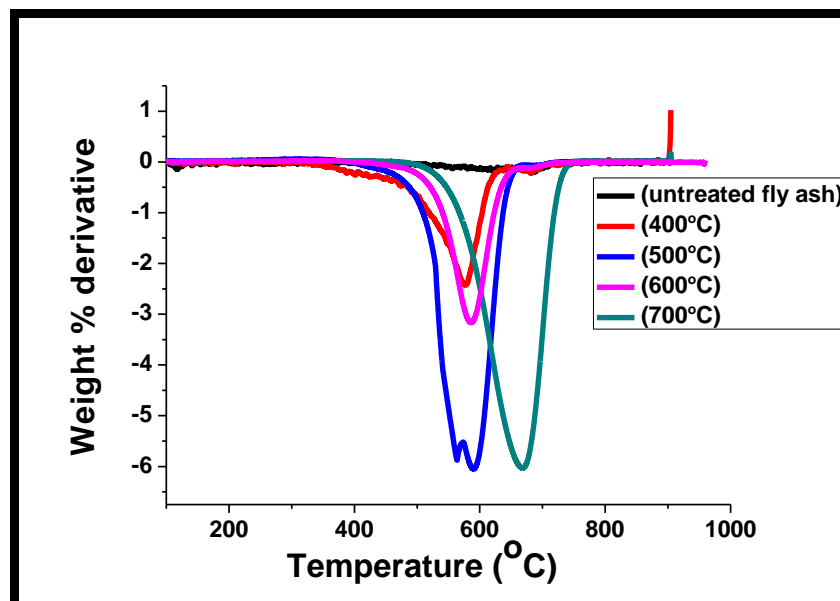


Figure 4.4: The first order weight derivatives of as-received and acetylene treated coal fly ash at varying temperatures

4.3.4 Particle size and surface area measurements

The particle sizes and surface areas of the as-received and acetylene treated coal fly ash reacted at temperatures between 400 °C to 700 °C are depicted in Fig. 4.5 to 4.7. As-received coal fly ash, when analysed in water had a particle size of 160 µm. After exposure to acetylene at 700 °C, this size was reduced to 130 µm. A small reduction in the particle size was anticipated, as the fly ash particles were entrained in the CNFs and hence this reduced their agglomeration. Likewise although the CNFs are known to be hydrophobic and not easily dispersed in water the entrained fly ash most probably enhanced their solubility³⁶. Both of these materials were then introduced into a dolapix polymer solution. Dolapix solution is known to have the ability to disperse such materials evenly, reducing cluster formation and agglomeration⁴⁶. However, in the dolapix solution, the particle size for the as-received coal fly ash increased to 180 µm. Here it appeared that cluster formation was even higher than before, suggesting that the as-received coal fly ash was less soluble in the polymer solution than in water. This could have been caused by the weak Van der Waals forces of attraction present between the inorganic fly ash particles. However, for all fly ash samples exposed to acetylene at temperatures between 400 °C to 700 °C, there was a huge reduction in the particle sizes. Those exposed to acetylene at 500 °C recorded the lowest particle

size i.e. 220 nm. For this reason a particle size distribution, based on the TEM images, was also conducted on these CNFs.

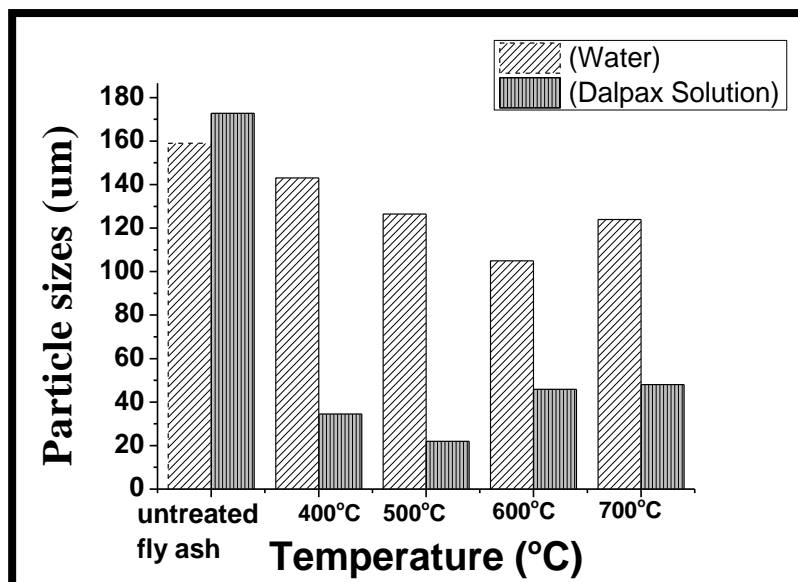


Figure 4.5: Varying particle sizes of fly ash samples exposed to acetylene at different temperatures

In Fig. 4.6, the materials found in the TEM images of as-received and acetylene treated fly ash samples at 500 °C were measured using image J⁴⁰. As can be seen, there was a huge reduction in the particle sizes measured by TEM, as compared to when the materials were measured using the particle size analyzer (Fig. 4.6). It was noted though that one of the drawbacks of using the particle size analyzer was that it did not allow particles to be individually measured. This explains the reduction in size when the data (Fig. 4.6) was compared to TEM analyses, as particles were individually measured. In the latter case, the average size was found to be 57 nm and 28 nm for as-received fly ash and CNFs from acetylene treated coal fly ash respectively. To confirm these findings, BET was used to study their surface areas (Fig. 4.7). The results showed that the CNFs produced at 500 °C displayed the highest surface area (59 m²g⁻¹). Studies have shown that the lower the particle size, the higher the surface area¹².

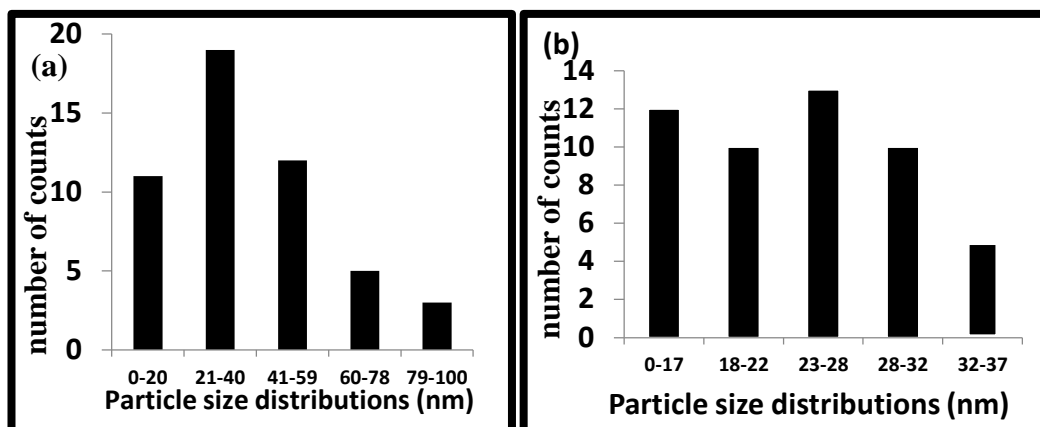


Figure 4.6: (a) Particle size distribution of as-received fly ash, (b) Particle size distribution of acetylene treated fly ash at 500 °C.

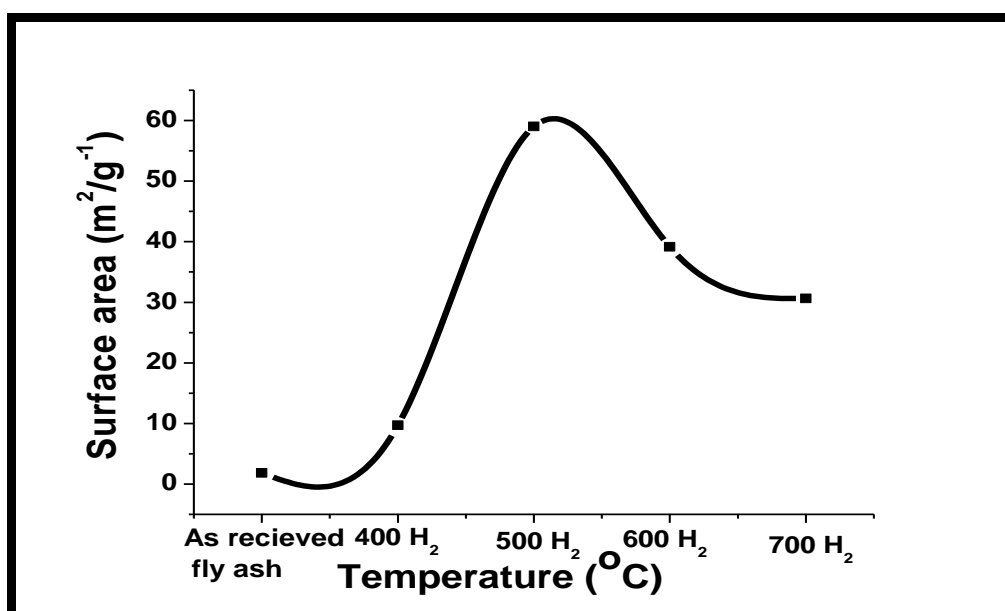


Figure 4.7: BET surface area of as received fly ash and CNFs formed by exposure of fly ash to acetylene to temperatures from 400 °C to 700 °C in H₂.

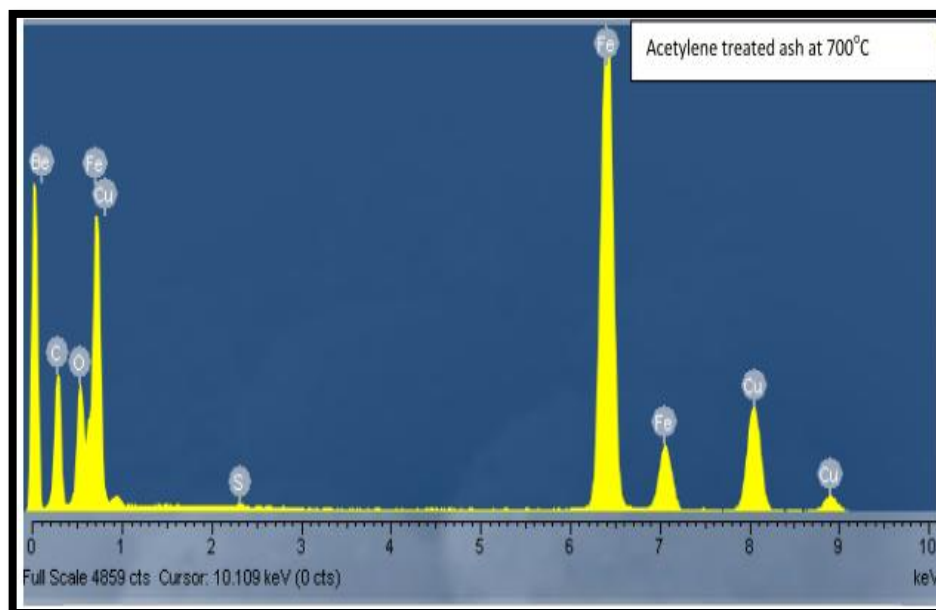


Figure 4.8: EDS of CNFs formed at 700°C. Beryllium, carbon, aluminium, silica and iron were the elements identified after synthesis

4.3.5 Composition, Mineral phase and oxidation state studies

To confirm the elements responsible for CNF formation, EDS, XRD and Mössbauer spectroscopy were employed. The catalyst suspected to be responsible for CNF formation was iron. The presence of this element is displayed in Fig. 4.8, XRD and Mössbauer spectroscopy were used in an attempt to clarify its connection with CNF formation. As-received and acetylene treated fly ash samples that were analysed by XRD Fig. 4.9, displayed changes in their XRD patterns suggesting that exposure to heat, acetylene and hydrogen induced significant phase changes to the ash.

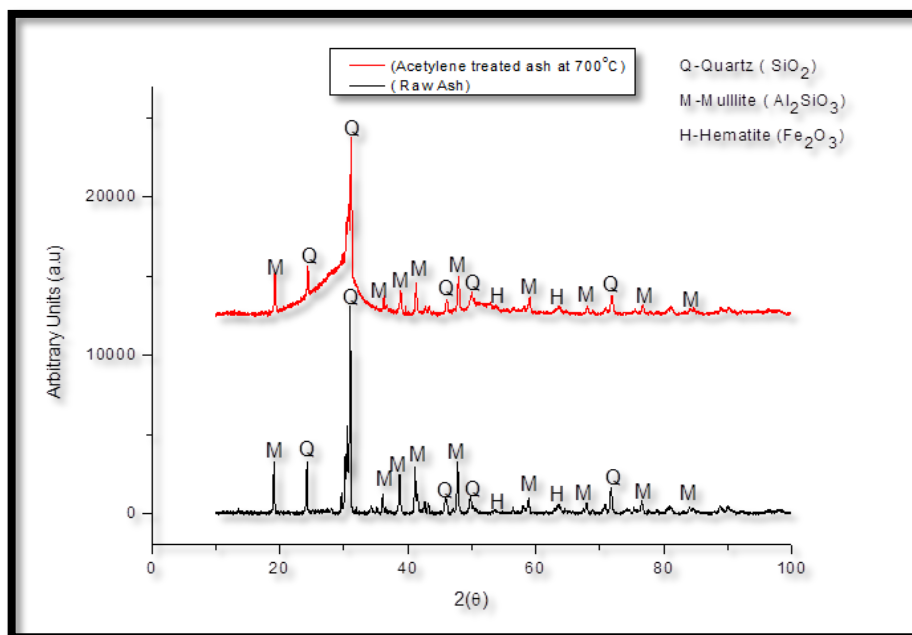


Figure 4.9: XRD of as-received coal fly ash and CNFs synthesized at 700°C

The major phases in the as-received fly ash were quartz (SiO_2), hematite ($\alpha\text{-Fe}_2\text{O}_3$) and mullite ($3\text{Al}_2\text{O}_3 \cdot 2\text{SiO}_2$). After exposure to acetylene it was noted that peak shifting and broadening had occurred, as was most evident in quartz at 30.5° (2θ) (Table 4.2). This may have been caused by amorphous glassy phases, found in the as-received fly ash, which when exposed to acetylene and hydrogen became more crystalline³⁵.

Table 4.2: XRD phases that had peak shifting and broadening

Phases	As-received ash	Acetylene treated ash
Mullite	34.5°	34.0°
Quartz	30.5°	29°

The iron content with the presence of silicates also became more apparent after CNF formation. However, the new phase of iron could not be identified with XRD, which is a bulk technique. Previous studies have shown that when iron is in low quantities and high dispersions, certain phases cannot be identified using XRD³⁶. Likewise it has been shown that in such cases the exact phase identification by XRD is difficult for iron as it tends to form a large variety of carbides⁴⁷. In one study cementite (Fe_3C), which could not be identified by XRD, was observed by Mössbauer spectroscopy during the formation of CNTs over iron catalysts from acetylene decomposition⁴⁷. Hence ^{57}Fe Mössbauer spectroscopy,

which is able to identify all forms of iron, was employed in this study. In order to obtain the chemical and structural information of iron containing materials, three main hyperfine parameters, namely the isomer shift, quadrupole splitting and magnetic splitting needed to be investigated.

Fig. 4.10a and b shows the fitted spectra obtained for the as-received fly ash sample and after being exposed to acetylene. The spectra are characterized by broadened six-line patterns and the central region is dominated by a distribution of quadrupole split doublets. The magnetic feature for the as-received fly ash sample (not subjected to acetylene) was fitted with three sextets (SX1_U, SX2_U and SX3_U), while the spectrum for the acetylene treated sample was analyzed with one sextet (SX1_T). For each spectrum, two doublets were required in the central region to give good fits. Table 4.3 gives a summary of the hyperfine parameters obtained from the fits to the data for both the as-received and acetylene treated samples. Isomer shifts and velocities were given relative to the centre of the spectrum of alpha-Fe at room temperature (RT). For the as-received fly ash sample, the hyperfine parameters extracted for SX1_U and SX3_U are: $B_{\text{hf}} = 49.0$ T, $\Delta = 0.40$ mm/s; $\Delta E_{\text{Q}} = -0.02$ mm/s and $B_{\text{hf}} = 44.2$ T, $\Delta = 0.59$ mm/s; $\Delta E_{\text{Q}} = -0.01$ mm/s. These values corresponds to Fe^{3+} ions on tetrahedral A-sites, and $\text{Fe}^{2.5+}$ -like average signals from octahedral B-sites, respectively and are identified as magnetite (Fe_3O_4). The SX2_U spectral component with hyperfine parameters of $B_{\text{hf}} = 51.6$ T, $\Delta = 0.45$ mm/s; $\Delta E_{\text{Q}} = -0.13$ mm/s is attributed to hematite (Fe_2O_3). The latter iron oxide was also detected by XRD. For the as-received sample, the hyperfine parameters determined for D1_U and D2_U are $\Delta = 0.45$ mm/s; $\Delta E_{\text{Q}} = 0.95$ mm/s and $\Delta = 0.79$ mm/s; $\Delta E_{\text{Q}} = 2.33$ mm/s characteristic of ferric and ferrous ions, respectively. The quadrupole split doublets are attributed to silicates.

After exposure to acetylene, only one sextet, SX1_T with a reduced magnetic field was observed in the spectrum with hyperfine parameters of $B_{\text{hf}} = 20.5$ T, $\Delta = 0.29$ mm/s; $\Delta E_{\text{Q}} = -0.003$ mm/s which has been identified as nanocrystalline iron carbide (Fe_3C). The hyperfine parameters of $\Delta = 0.43$ mm/s; $\Delta E_{\text{Q}} = 0.41$ mm/s

and $\Delta = 1.02$ mm/s; $\Delta E_Q = 2.15$ mm/s obtained for D1_T and D2_T, respectively are very similar to those obtained for the as-received sample except for the quadrupole splitting of D1_T which is lower indicating some structural relaxation. For the as-received fly ash sample, the total population of the oxides is 66% with the remaining fraction of 34% attributed to silicates. After exposure to acetylene, a decrease in the area fraction of 17% was observed for the oxides with a corresponding increase in the silicates. The abundance of the Fe^{2+} state before treatment was ~11% but showed an increase of ~19% after acetylene treatment due to the reduced magnetic field.

These results indicate a reduction in the oxidation state of iron (with decreasing oxide content), as a new phase of iron (Fe_3C) and silica emerged. This suggestion is in agreement with He *et al.* who have studied Mössbauer spectra of CNT formed from acetylene reacted over iron supported zeolite catalysts and who have found that the +3 oxidation state of iron was reduced to +2 by H_2 , which they concluded was the active phase for their synthesis⁴⁸. Dunens *et al.* found that iron also appeared in different forms in their ash and that H_2 could not reduce these, presumably because of their location in the fly ash particles⁵. Hence in their study, unlike in this present work, Dunens *et al.* were required to further impregnate their ash with iron in order for CNT/CNF growth to occur³⁶. In a similar manner Diamond *et al.* using acid etching techniques demonstrated that the location of the iron and its morphology greatly differed for every fly ash particle within the sample⁴⁹. This they suggested was caused by the inhomogeneous nature of coal.

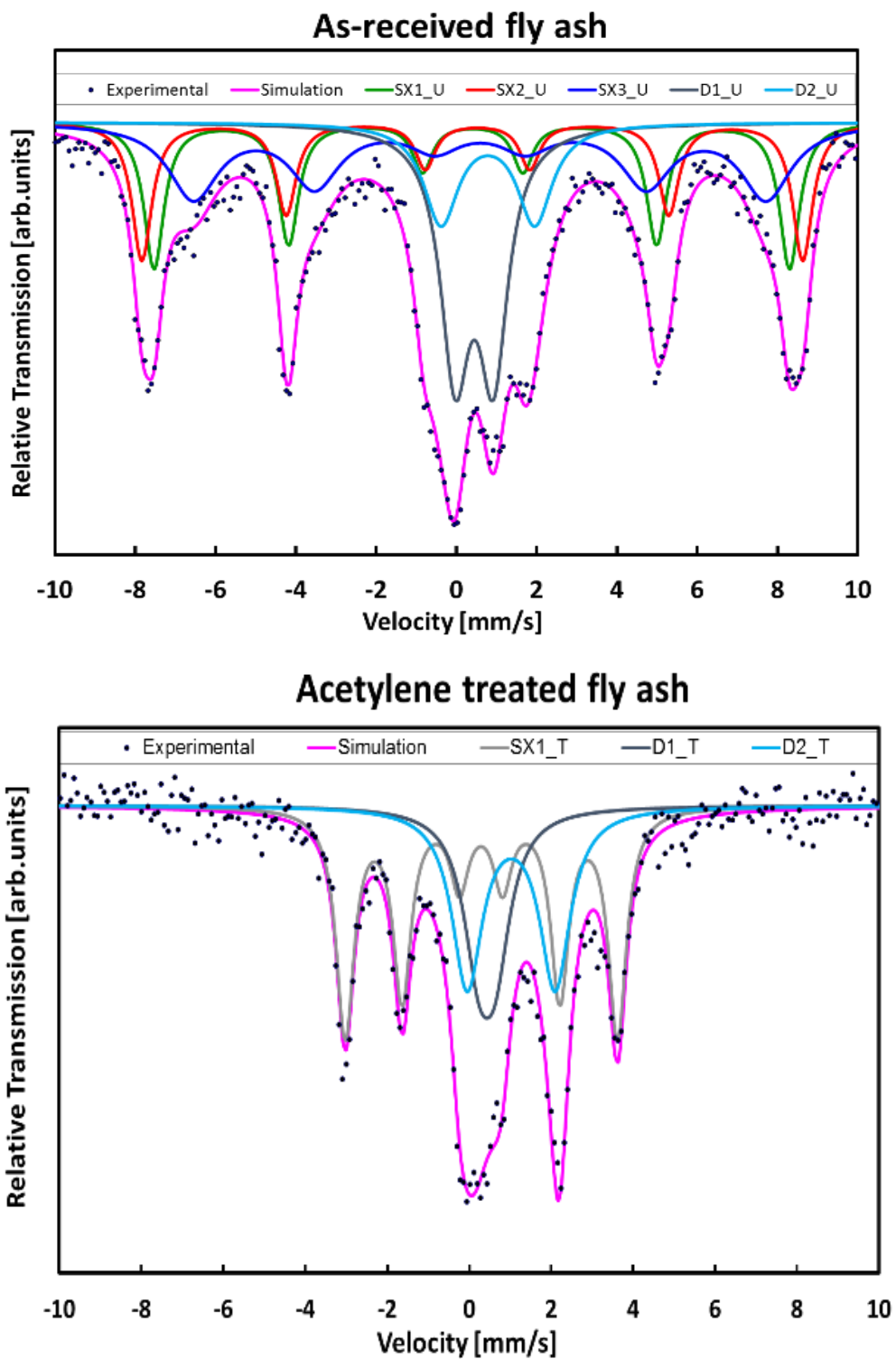


Figure 4.10: Room temperature ^{57}Fe Mössbauer spectra for (a) as-received and (b) acetylene treated fly ash sample at 700°C .

The magnetic feature for the as-received sample was fitted with three sextets (SX1_U, SX2_U and SX3_U) and the spectrum for the acetylene treated sample was analyzed with one sextet (SX1_T) whilst the non-magnetic spectral components for both samples were fitted with two quadrupole split doublets.

Table 4. 3: Room temperature Mössbauer parameters for:(a) the as-received and (b) acetylene treated fly ash samples

(a) As received	Sx1_u	Sx2_u	Sx3_u	D1_u	D2_u
$B_{\text{hf}} \text{ (t)}$	49.0	51.6	44.2	-	-
$\Delta \text{ (mm.s}^{-1}\text{)}$	0.40	0.45	0.59	0.45	0.79
$\Delta e_{\text{q}} \text{ (mm.s}^{-1}\text{)}$	-0.02	0.13	-0.01	0.95	2.33
Area (%)	21	18	27	23	11

(b) Treated	Sx1_t	D1_t	D2_t
$B_{\text{hf}} \text{ (t)}$	20.5	-	-
$\Delta \text{ (mm.s}^{-1}\text{)}$	0.29	0.43	1.02
$\Delta e_{\text{q}} \text{ (mm.s}^{-1}\text{)}$	-0.003	0.41	2.15
Area (%)	49	21	30

4.4 Conclusions

CNFs (and a small amount of CNTs) were successfully produced by directly using an as-received South African coal fly ash. The smooth, glassy and inert surfaces of the South African coal fly ash were converted to irregularly-shaped CNFs in the presence of acetylene and hydrogen at temperatures as low as 400 °C. Laser Raman spectroscopy confirmed the formation of CNFs. TGA showed there were different forms of carbon present. EDS, XRD and Mössbauer spectroscopy confirmed that iron, most likely in the form of iron carbide was directly associated with the formation of CNFs. Therefore this study has demonstrated the successful synthesis of carbon nanostructured materials from waste South African coal fly ash without chemical pre-treatments (such as the impregnation of other metals) or thermal modifications. Since carbon nanofibres may in the future be beneficial for applications such as particulate nanofillers in polymer matrices, this intervention

could result in a reduction in environmental pollution. There will also be relief of a financial burden involved in the disposal cost of this and related coal fly ash around the world.

4.5 References

1. R. J. White, R. Luque, V.L. Budarin, J. H. Clark, D. J. Macquarrie, *Chemical Society Reviews*, 2009, **38**,481-494.
2. P. J. Harris, *Cambridge University Press*; 2009,**2**, 6-13.
3. S. Bhaviripudi, E. Mile, S. A. Steiner, A.T. Zare , J.Kong, *Journal of the American Chemical Society*, 2007, **129**,1516-1517.
4. M. Cantoro , S. Hofmann, S. Pisana, V. Scardaci, A. Parvez, C. Ducati, A. C. Ferrari, A. M.Blackburn, K. Y. Wang, J. Robertson, *Nano letters*, 2006, **6**,1107-1112.
5. E. Couteau, K. Hernadi, J. W. Seo, L. Thien-Nga , C. Mikó, R.Gaal, L. Forro, *Chemical Physics Letters*, 2003, **378**, 9-17.
6. E.T. Thostenson, Z. Ren, T.W. Chou, *Composites science and technology*, 2001, **61**,1899-1912.
7. J. Wang, *Electroanalysis*, 2005, **17**,7-14.
8. O. Breuer, U. Sundararaj, *Polymer Composites* 2004, **25**,630-645.
9. J. B. Callis, D.L. Illman, B. R. Kowalski, *Analytical Chemistry*, 1987, **59**,624-637.
10. P. REUBEN, *Collection Forum*, 2006, **3**, 33-41.
11. C. M. Seah, S. P. Chai, A.R. Mohamed, *Carbon*, 2011, **49**, 4613-4635
12. K.T. Paul, S. Satpathy, I. Manna, K. Chakraborty , G. Nando, *Nanoscale Research Letters*, 2007, **2**, 397-404.
13. S. Wang, *Environmental Science & Technology*, 2008, **42**, 7055-7063.
14. A, Shaikjee, N. J. Coville, *Carbon*, 2012, **10**: 3376
15. P. Usubharatana, D. McMartin , A. Veawab A, P. Tontiwachwuthikul, *Industrial & engineering chemistry research*, 2006, **45**, 2558-2568.
16. V. Thavasi , G. Singh G, S. Ramakrishna, *Energy & Environmental Science*, 2008, **1**,205-221.
17. F. Zaera, *The Journal of Physical Chemistry Letters*, 2010, **1**, 621-627.
18. K.J. MacKenzie , O. M. Dunens , A.T. Harris, *Industrial & Engineering Chemistry Research*, 2010, **49**,5323-5338.
19. A.P. Moravsky, R.O. Loutfy, *EP Patent* 1,328,472; 2010.

20. K. Byrappa, *Journal of the Ceramic Society of Japan*, 2009, **117**, 236-244.
21. J. Li, J. Z. Zhang, *Carboxylic coordination Chemistry Reviews*, 2009, **253**, 3015-3041.
22. J. Baxter, Z. Bian , G. Chen , D. Danielson , M.S. Dresselhaus , A. G. Fedorov , T.S. Fisher, C.W.Jones , E. Maginn , U. Kortshagen , *Energy & Environmental Science*, 2009, **2**,559-588.
23. A. J. Minchener , *Fuel*, 2005, **84**, 2222-2235.
24. G. Ferraiolo, M. Zilli, A. Converti, :*Journal of Chemical Technology and Biotechnology*, 1990, **47**, 281-305.
25. U.C. Gupta, S. C. Gupta, *Communications in Soil Science & Plant Analysis*, 1998, **29**, 1491-1522.
26. R. B. Finkelman, H.E. Belkin, J.A. Centeno, *Geotimes*, 2006, **51**,24.
27. N. Salah, S. S. Habib, Z. H. Khan, A. Memic, M. N. Nahas , *Digest Journal of Nanomaterials and Biostructures*, 2012, **7**, 1279-1288.
28. A. Yasui , Y. Kamiya , S. Sugiyama , S. Ono , H. Noda , Y. Ichikawa, . *IEEJ Transactions on Electrical and Electronic Engineering*, 2009, **4**,787-789.
29. D.C. Nath, V. Sahajwalla. *Journal of Hazardous Materials*, 2011, **192**, 691-697.
30. Y. Li , D. Li, G. Wang, *Catalysis today*, 2011, **162**,1-48.
31. A. Huczko, *Applied Physics A*, 2000, **70**, 365-376.
32. M. Terrones, W. K. Hsu, H. W. Kroto, D.R. Walton, *Fullerenes and related structures*,Springer; 1999, 189-234
33. M. H. Rummeli, F. Schäffel, A. Bachmatiuk, M. Sparing, B. Rellinghaus , *ACS nano*, 2010, **4**,1146-1152.
34. C. Lai, Q. Guo, X. F. Wu, D.H. Reneker , H. Hou, *Nanotechnology*, 2008, **19**, 195303.
35. Y. Bing, H. Liu, L. Zhang, D. Ghosh, J. Zhang,*Chemical Society Reviews*, 2010, **39**, 2184-2202.
36. O. M. Dunens, K. J. MacKenzie, A. T. Harris, *Environmental science & technology*, 2009, **43**,7889-7894.

37. Z. Yu, D. Chen, B. Tøtdal, A. Holmen, *Materials Chemistry and Physics*, 2005, **92**, 71-81.
 38. A. V. Melechko, V.I. Merkulov, T.E. McKnight, M. Guillorn, K. L. Klein, D. H. Lowndes, M. L. Simpson, *Journal of Applied Physics*, 2005, **97**, 041301-041339.
 39. D. L. Plata, E. R. Meshot, C.M. Reddy, A. J. Hart, P.M. Gschwend., *ACS nano*, 2010, **4**, 7185-7192.
 40. W. S. Rasband, ImageJ, US National Institutes of Health, Bethesda, Maryland, USA, 1997.
 41. V. Fenelonov, M. Mel'gunov, V. Parmon, *Powder and Particle Journal*, 2010, 189-207.
 42. N. J. Coville, S. D. Mhlanga, E. N. Nxumalo, A. Shaikjee, *South African Journal of Chemistry*, 2011, **107**, 01-15.
 43. P. V. Shanahan , L. Xu , C. Liang , M. Waje , S. Dai , Y. Yan , . *Journal of Power Sources*, 2008, **185**, 423-427.
 44. J.H. Lehman, M. Terrones, E. Mansfield, K. E. Hurst, Meunier V: *Carbon*, 2011, **8**, 2581-2602
 45. F. Teng, J. M. Ting, S. P. Sharma, K.H. Liao, *Nanotechnology*, 2008, **19**, 595-607.
 46. J. F. Bartolome, A.H. De Aza, A. Martin, J.Y. Pastor, J. Llorca, R. Torrecillas, G. Bruno, *Journal of the American Ceramic Society*, 2007, **90**, 3177-3184.
 47. M. Pérez-Cabero, J. Taboada, A. Guerrero-Ruiz, A. Overweg, Rodríguez-Ramos I, *Physical Chemistry Chemical Physics*, 2006, **8**, 1230-1235.
 48. N. He, Y. Kuang, Q. Dai, Y. Miao, A. Zhang, X. Wang, K. Song , Z. Lu , C. Yuan, *Materials Science*, 1999, **8**, 151-157
 49. S. Diamond, *Cement and Concrete Research*, 1984, **4**, 455-462.
-

Chapter 5: Effect of nitrogen and hydrogen on the synthesis of carbon nanomaterials from coal waste fly ash as a catalyst

5.1 Introduction

The recyclability of coal fly ash, which is a waste by-product in coal-powered electricity generating plants, is essential for the alleviation of this environmental pollutant. Strict rules and rising costs associated with the disposal of coal fly ash have therefore led researchers to seek alternate ways of recycling this waste material.

Coal fly ash is comprised of small solid particles called precipitators; small hollow particles called cenospheres and thin walled hollow spheres called plerospheres¹. At present 800 million tons of coal based fly ash are produced annually worldwide, with only 15% being recycled². Currently, from the miniscule percentage that is recycled, the main uses of this waste coal fly ash are: mine fill and mine site remediation³. Other applications that have been successfully investigated include use in: agriculture and soil management, adsorbents for heavy metals and waste stabilization⁴⁻⁶. Fly ash has also been shown to be a suitable catalyst support for hydrogen production, as a catalyst for steam methane reforming and gas phase oxidation of volatile organic compounds^{7,32-33}. However, none of these previously mentioned applications are currently in commercial use. So far only six studies (including two of our own) have been reported, where fly ash has been used as a catalyst for carbon nanomaterial synthesis^{1,9-11,17}

Since a limited number of studies have been conducted using fly ash as a catalyst, one of the aims of this present study was to establish whether the morphology, yield and quality of CNMs so-formed could be improved by reaction of acetylene

with fly ash in either nitrogen, hydrogen or both of these gases during the syntheses. In so doing it was hoped that for the first time in such a system, with the aid of Mössbauer spectroscopy, the roles that these two gases played in the synthesis of CNMs could be clarified, while the active component in the fly ash catalyst under these conditions could be identified.

5.2 Experimental Section

5.2.1 Synthesis of CNMs using fly ash as a catalyst

The synthesis of CNMs was achieved via CVD through the use of waste coal fly ash from Roscheville. In these reactions, fly ash was used as a catalyst while C_2H_2 served as a carbon source; nitrogen (N_2) and/or hydrogen (H_2) were used as carrier or reduction/pre-reaction gases to create optimal reaction environments.

In a typical synthesis experiment, the procedure followed was described in Section 3.3.1. For these studies, gas mixtures of three types (C_2H_2/N_2 , C_2H_2/H_2 and $C_2H_2/H_2/N_2$) with a total flow rate of 25-100 ml/min were studied. A flow rate of 100 ml/min was used for reactions where nitrogen or hydrogen were used as carrier gases without any pre-treatments at a 1:1 C/H ratio.. Temperatures ranging from 450 °C to 750 °C in 100 °C intervals were studied with these gas mixtures.

5.2.2 Characterization

The synthesized CNFs samples were characterized using scanning electron microscopy (SEM), thermogravimetric analysis (TGA), laser Raman spectroscopy and X-ray diffraction (XRD). For each characterisation, procedures described in Section 3.4.1, 3.4.5 and 3.4.6 respectively were followed. Brunner-Emmet Teller (BET) were employed as described in Sections 3.4.4. X-ray diffraction and Mössbauer spectroscopy measurements were carried out as described in section 3.4.7 and 3.4.9 respectively. Mössbauer Measurements were performed at room temperature on the acetylene-treated fly ash samples synthesized at 650 °C.

5.3 Results and Discussion

5.3.1 Carbon yield

In these studies the product yields were determined from the amount of carbon deposited relative to the amount of acetylene passed over the catalyst. The yield of CNFs when either N₂ or H₂ were used as carrier gases in C₂H₂, i.e. C₂H₂-N₂ or C₂H₂-H₂ respectively, are shown in Fig.5.1.

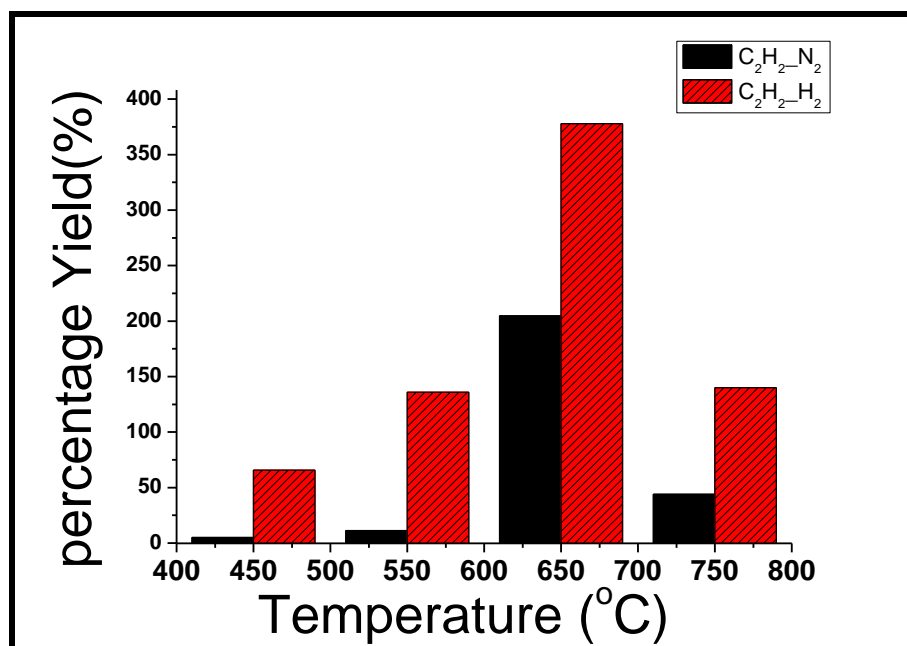


Figure 5.1: A plot of the percentage yield of CNMs grown at 450°C–750°C using N₂ or H₂ as carrier gases in the reaction of fly ash with C₂H₂.

As shown in Fig. 5.1, CNFs were formed across all temperatures when either N₂ or H₂ was used as carrier gases. However, minimal yields were obtained at 450°C where no reaction appeared to have occurred. As might have been expected, carbonaceous deposits increased as the temperatures increased, with maximal formation of CNFs at 650 °C. However, beyond 650 °C, it appeared that non-catalytic pathways occurred as the yield of CNFs decreased. From both these conditions, it was clear that reactions with H₂ produced a higher yield of CNFs as compared to those with N₂. Pattison *et al.* suggested that the slow growth rate of CNTs in the presence of N₂ gas as compared to H₂, may have been due to the saturation of their growing edges with N₂²⁰. Since a decrease in the growth rate

was observed in this present study, this suggests that N_2 may have had the same effect in the formation of CNFs over fly ash. Similarly to these present results for CNFs, higher yields of CNTs have been observed where H_2 was used as a carrier gas²¹. In that study it was reported that the role of H_2 decreased the contact time between the C_2H_2 and the catalyst in order to reduce the formation of amorphous carbon. Likewise Kuwana *et al.* have suggested that in such reactions H_2 also played a role in the pyrolysis of C_2H_2 ²². As before, these same effects may have given rise to the observed increase in yield of CNFs from acetylene over fly ash in H_2 . H_2 is believed to be involved in three stages: Firstly in the pre-treatment stage, H_2 is mainly used to reduce the oxidised catalyst particles. Then during the reaction, H_2 has the effect of reducing the decomposition of the carbon source. Lastly H_2 has been shown to prevent excess carbon decomposition at the surface of the catalyst²³.

5.3.2 Morphological Studies

5.3.2.1 Synthesis of CNMs by reaction of fly ash and C_2H_2 in N_2 ($C_2H_2_N_2$)

Fig. 5.2 shows TEM micrographs of CNFs formed at various temperatures (450-750 °C) under N_2 as a carrier gas in the absence of H_2 . The quality of the CNFs formed varied as the reaction temperature was increased. CNFs formed from 450-650 °C were light and spongy in texture, while those materials formed at 750 °C were coarser.

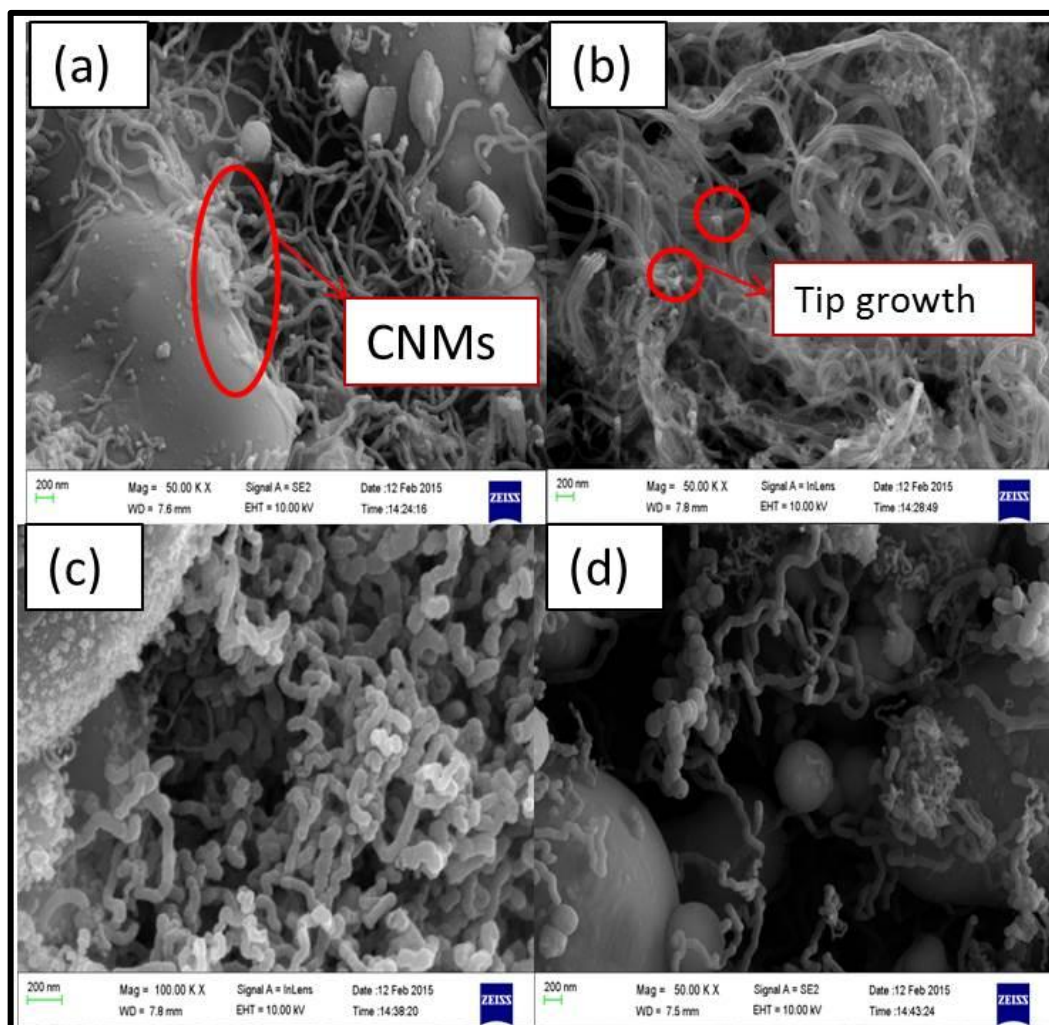


Figure 5.2: SEM micrographs of CNMs produced from C_2H_2/N_2 synthesized at (a) 450 °C, (b) 550 °C, (c) 650 °C and (d) 750 °C.

At 450 °C, a small amount of CNFs were formed in association with the spherically shaped fly ash (Fig. 5.2a). Increasing the temperature to 550 °C resulted in a thick mixture of CNFs together with amorphous carbon. These CNFs were observed to have formed by tip growth as metal catalyst particles were found to be located at the tips of these fibres (see encircled areas in the insert of (Fig. 5.2b). At 650 °C CNFs of uniform size were observed (Fig. 5.2c). On the other hand, at 750 °C fewer uniform sized CNFs were found mixed together with a large quantity of amorphous carbon.

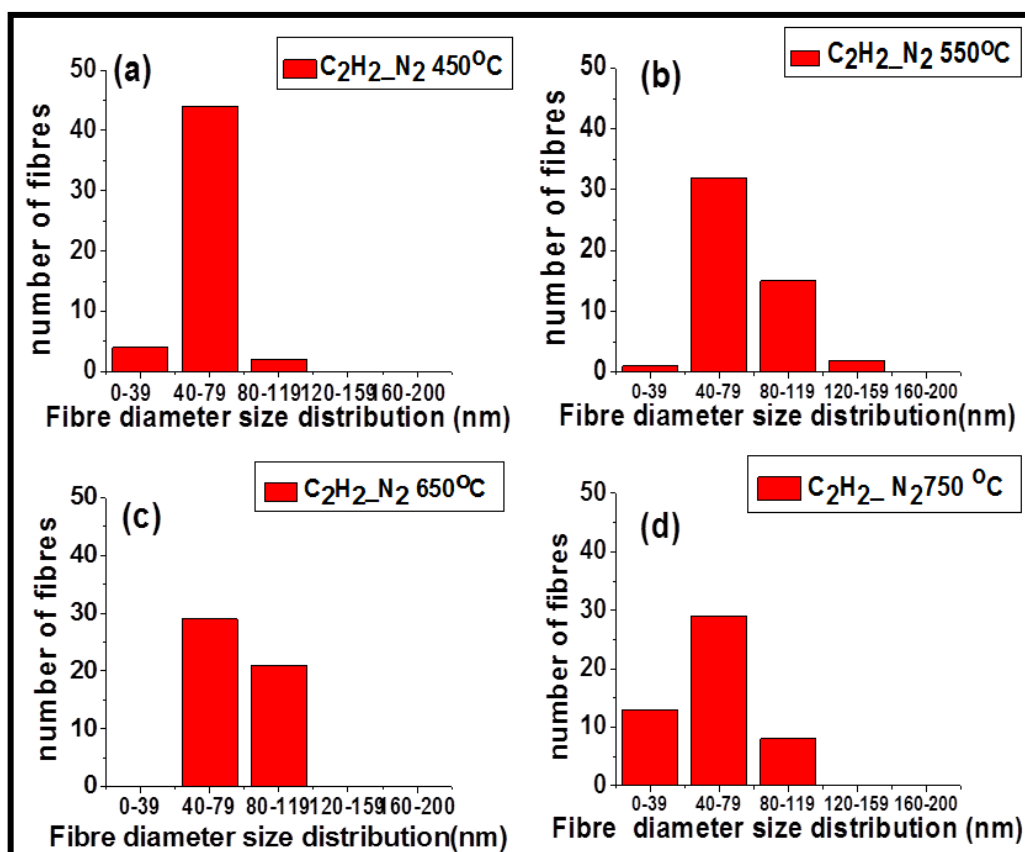


Figure 5.3: Fibre size distributions of CNMs produced from $C_2H_2-N_2$ synthesized at (a) 450 °C, (b) 550 °C, (c) 650 °C and (d) 750 °C.

5.3.2.2 Synthesis of CNMs by reaction of fly ash and C_2H_2 in H_2 ($C_2H_2-H_2$)

When H_2 was used as a carrier gas instead of N_2 a clear difference in yield and morphology was observed. At 450 °C the CNFs which formed around the large spherical fly ash particles had no metal nanoparticles at their tips, but rather revealed that base growth had occurred (see encircled areas in the insert of (Fig. 5.4a). At 550 °C CNFs predominantly of the same diameter size were formed (Fig. 5.3b). By contrast at 650 °C, CNFs with different diameters were formed (Fig. 5.3c). Hence mixtures of CNFs with smaller and larger diameters were observed. However, at 750 °C CNMs of a variety of morphologies (e.g. spiralled CNFs, CNFs with small and large diameters as well as CNTs) were observed (Fig. 5.3d). Shaikjee and Coville have previously postulated that at higher temperatures like in this case the composition of the gas phase intermediates and radical species which originated from C_2H_2 and H_2 , inevitably gave rise to unique building blocks that produced different types of CNFs and CNTs²⁴. This postulation may

rationalise the presence of the various morphologies of CNMs that were observed in this study at 750 °C when C₂H₂ was reacted over fly ash in H₂. This is also shown with the fibre size distributions, where CNFs from N₂ (Fig. 5.3c) had a narrow fibre size distribution as compared to CNFs reacted from H₂ (Fig. 5.5c).

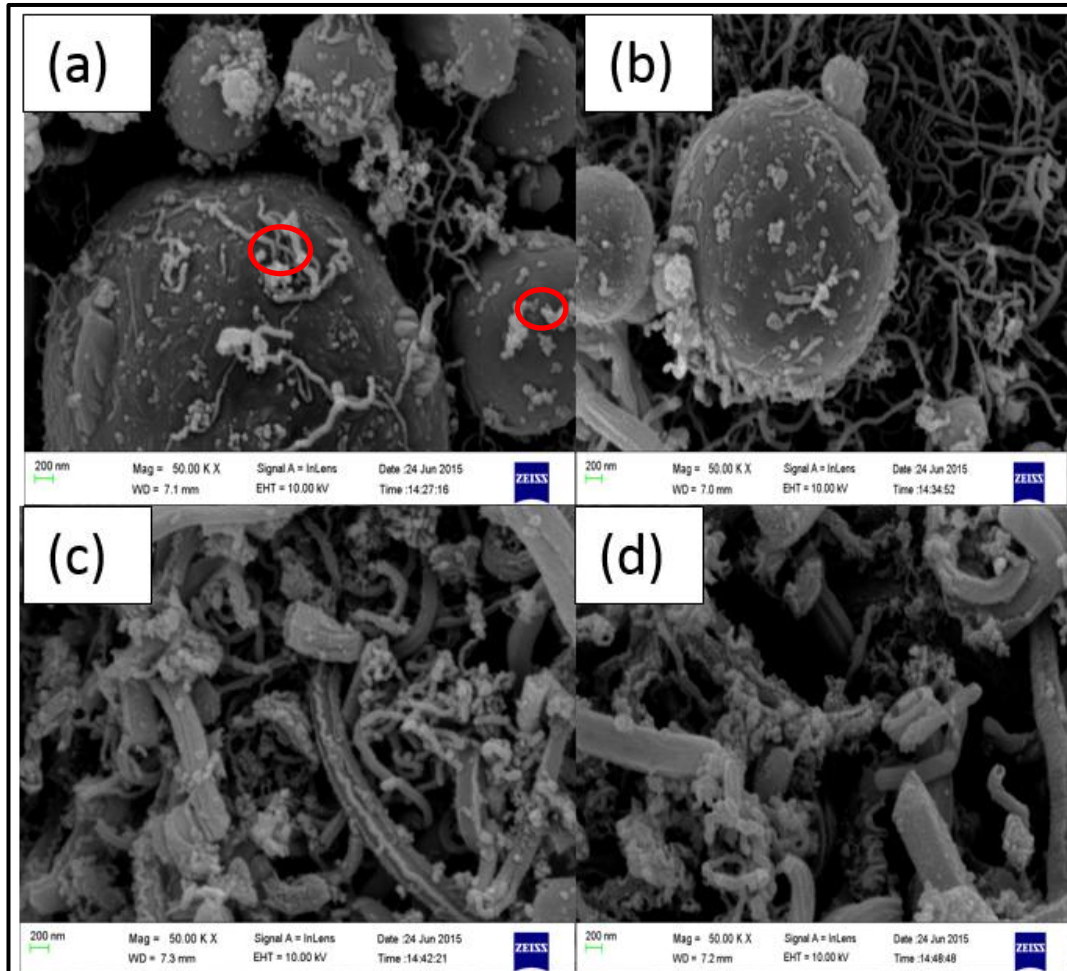


Figure 5.4: SEM micrographs of CNFs produced from C₂H₂/H₂ synthesized at (a) 450 °C, (b) 550 °C, (c) 650 °C, and (d) 750 °C.

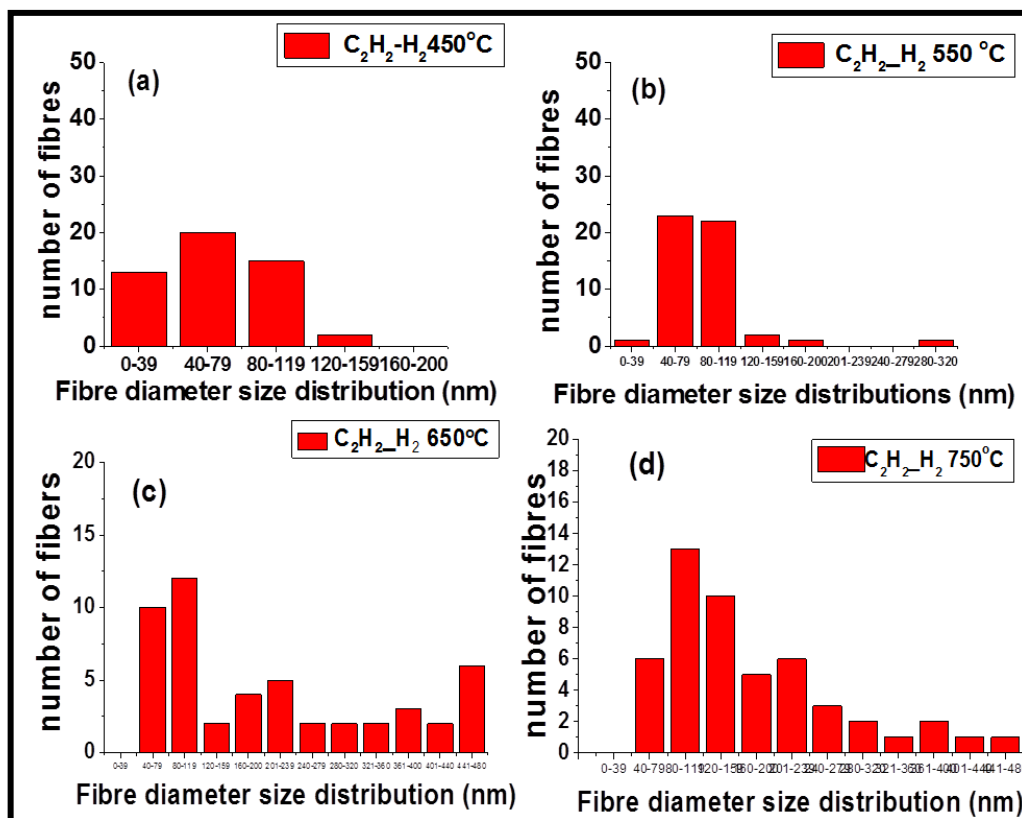


Figure 5.5: Fibre diameter size distributions of CNMs produced from $C_2H_2-H_2$ synthesized at (a) 450 °C, (b) 550 °C, (c) 650 °C and (d) 750 °C.

A comparison on the effect of the two carrier gases revealed that the optimum temperature for CNF formation for both gases was 650 °C. While H_2 appeared to be a better carrier gas to achieve a greater yield of CNFs at 650 °C, these fibres were more uniform in diameter in N_2 than in H_2 at the same temperature. In both cases the yields of CNFs decreased when reaction temperatures exceeded 650 °C.

5.3.2.3 Synthesis of CNMs by reaction of fly ash and C_2H_2 using H_2 as a pre-treatment gas and N_2 as a carrier gas ($H_2, C_2H_2-N_2$)

Although using H_2 as a carrier gas showed a higher yield of CNFs as compared to N_2 in this study, previous work by Shaikjee *et al.* showed that the best gas phase conditions which produced higher yields and more uniform CNFs were obtained when a combination of H_2 and N_2 were used²³. In their work they postulated that H_2 reduced the metal catalysts and created favourable CNM growth conditions. Furthermore they showed that H_2 produced higher yields when diluted with N_2 . In

a similar study carried out by Jung *et al.* utilizing pure metal catalysts, H_2 was used as a reduction gas and N_2 as carrier gas during the growth of CNTs/CNFs²⁵. Here it was shown that the use of H_2 during the pre-treatment of the catalyst was a time dependent process, which resulted in the alteration of the surface morphologies of a Co-Si catalyst. In their study, they showed that if pre-treatment with H_2 was prolonged then the nanoparticle, which formed during the reaction, agglomerated. They postulated that this led to a reduction in surface free energy and a corresponding reduction in the yield of CNTs/CNFs.

In an attempt to examine whether the order in which N_2 and H_2 were introduced into the reaction would have a similar effect or indeed would affect the morphology, yield and quality of CNMs formed, studies were then conducted at 550 °C and 650 °C where both gases had been shown to be effective in CNM synthesis. Here H_2 was used as a pre-treatment gas followed by the reaction of C_2H_2 over fly ash in N_2 .

When H_2 was passed over the fly ash prior to its reaction with C_2H_2 in N_2 , it was noted that, long defined CNFs (Fig. 5.6a), with an average diameter of 90 nm (Fig. 5.7a), had been formed at 550 °C. As observed previously in N_2 , these CNFs showed signs of tip growth.

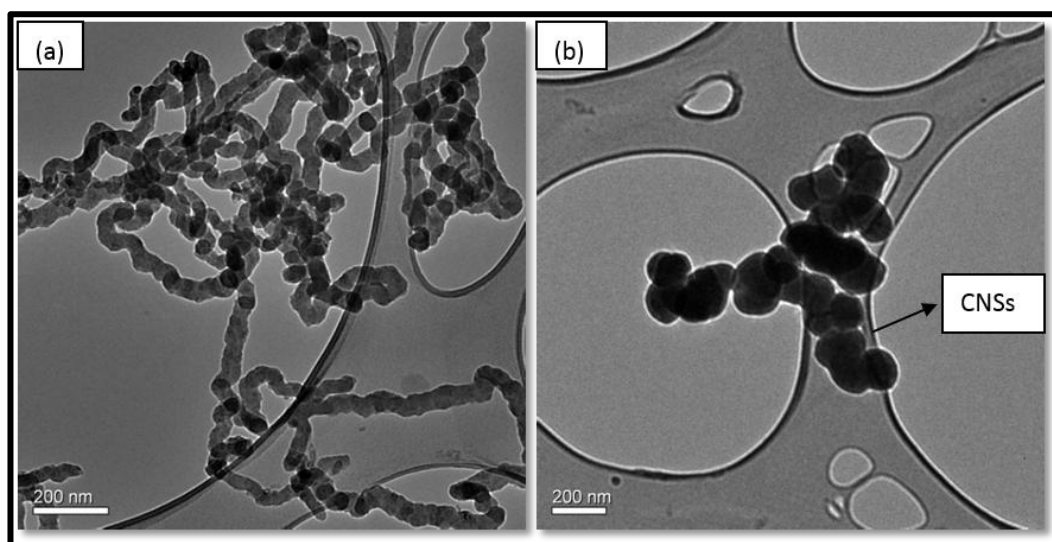


Figure 5.6: TEM micrographs of CNFs produced from H_2 , C_2H_2 / N_2 CNFs synthesis at (a) 550 °C and (b) 650 °C.

Increasing the temperature to 650 °C, carbon nanospheres CNSs with an average particle diameter of 144 nm (Fig. 5.7b) were formed. The formation of these CNSs could be due to pyrolysis as it was shown by Cele *et al.* that at high temperatures CNSs can form with or without a catalyst³¹. In this study though, we suspect that it could be the order in the introduction of these gases at these temperatures that could cause the formation of these CNSs in the presence of the fly ash catalyst. The diameter distributions of both these carbonaceous material that were formed are shown in Figs. 5.7a and 5.7b.

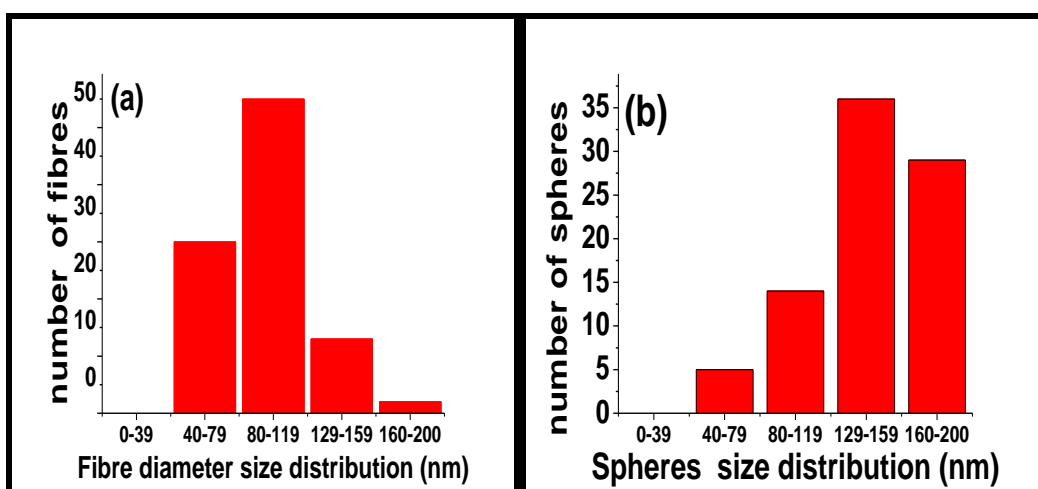


Figure 5.7: Fibre size distributions of CNMs produced from N₂, C₂H₂_H₂ synthesized at (a) 550 °C and (b) 650 °C.

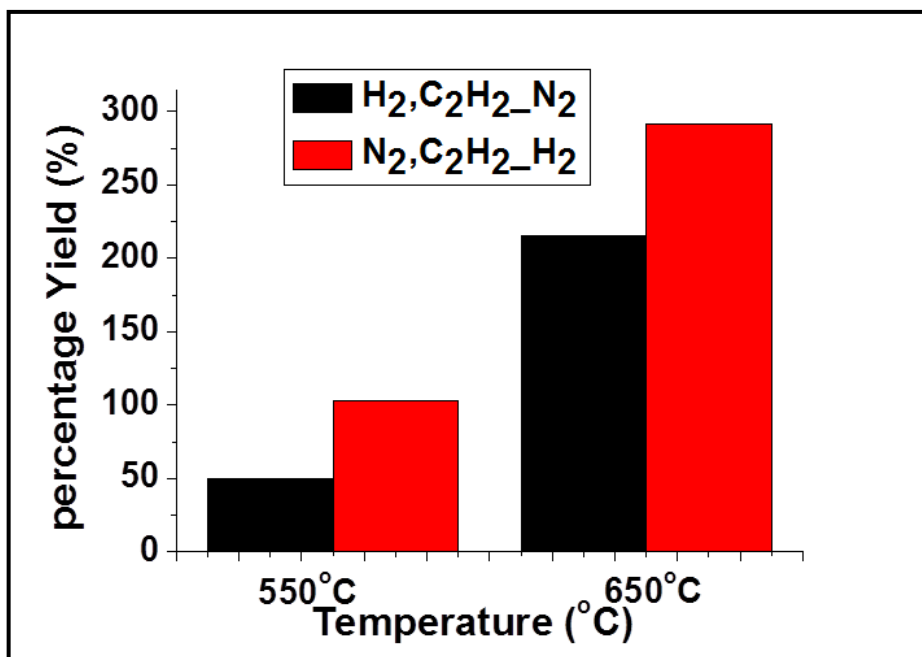


Figure 5.8: A plot of the percentage yield of CNMs grown from 550 °C–650 °C using H₂, C₂H₂-N₂ or N₂, C₂H₂-H₂ as carrier gases in the reaction of fly ash with C₂H₂.

5.3.2.4 Synthesis of CNMs by reaction of fly ash and C₂H₂ using N₂ as a pre-treatment and H₂ as a carrier gas (N₂,C₂H₂-H₂)

When N₂ gas was used during the pre-reaction stage and H₂ was used as a carrier gas during the reaction, it was noted that, more uniform CNFs were formed at 550 °C (Fig. 5.6a) vs (Fig. 5.3b) with approximately twice the yield as before and a narrow diameter. However, increasing the temperature to 650 °C, resulted in slight decrease in the percentage yield as compared to when H₂ was used without any pre-treatments from 370% (Fig. 5.8) to 291% (Fig. 5.1). Though there was a slight decrease in the yield, a bimodal distribution with large diameter CNFs and mostly thin diameter CNFs were formed (Fig. 5.10b).

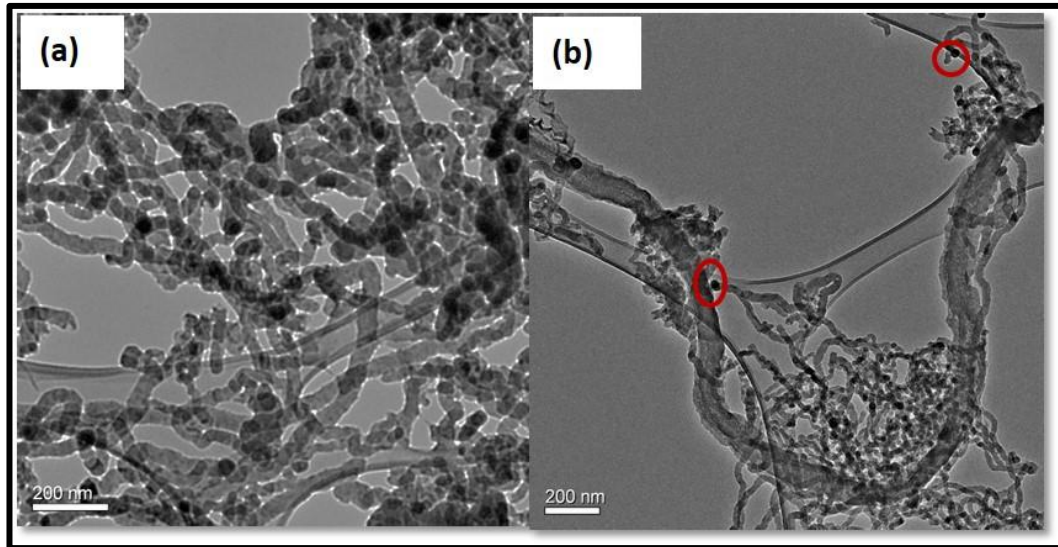


Figure 5.9: TEM micrographs of CNFs produced from (N₂, C₂H₂_H₂) synthesized at (a) 550°C and (b) 650°C.

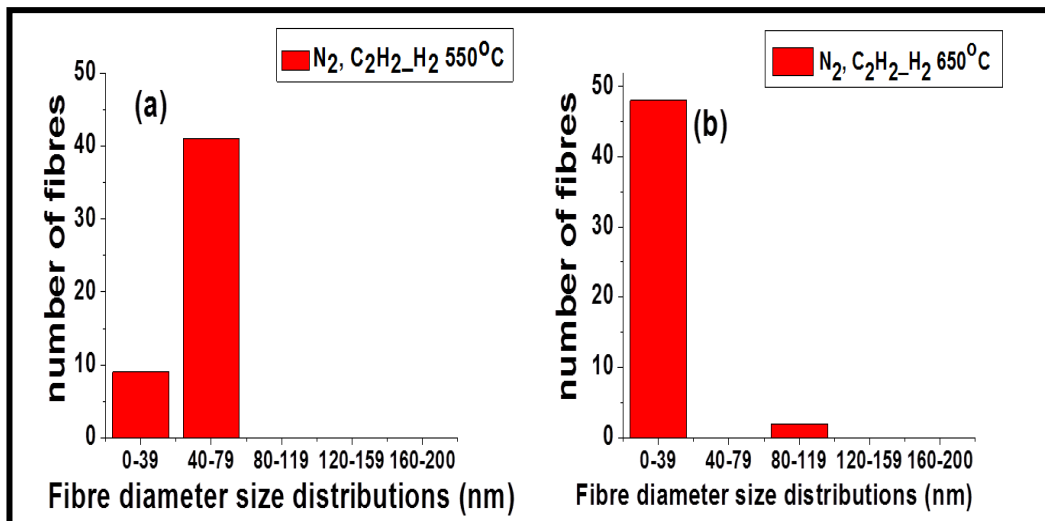


Figure 5.10: Fibre size distributions of CNMs produced from N₂, C₂H₂_H₂ synthesized at (a) 550 °C and (b) 650 °C.

From these results it is clear that tip growth is favoured at high temperatures. As the temperature increased the yield also increased (Fig.5.8). The majority of the fibre diameters sizes decreased and only 4% increased to a size range of 80-119 nm. This phenomenon can be best explained and discussed using a combination of the catalyst and gas chemistry. According to the Arrhenius equation, chemical reactions are enhanced exponentially when the temperature increases, for

example, when the growth temperature was above 650 °C, the inside of the furnace was covered with brownish liquid and black soot. Upon increasing the temperature, pyrolytic decomposition of C₂H₂ was enhanced and occurred not only on the substrates but on the surface of the furnace tube. We can assume that increments of the concentration of active carbon species from the decomposed C₂H₂ with the temperature resulted in a correspondingly increased yield of CNFs. However, though a further increase in temperature was not feasible due to the excess carbon deposits on the surface of the catalyst particles. Excess carbon deposition can lead to the deactivation of the catalyst particles, thus preventing diffusion of the carbon species, thus resulting in the lower growth rate and amorphous like structures as was seen at 750 °C.

5.3.2.5 Synthesis of CNMs by reaction of fly ash and C₂H₂ using H₂ as a carrier gas at varying flow rates of (C₂H₂/N₂)

In an attempt to form CNMs of different morphologies, H₂ was used as a carrier gas and varying flow rates of C₂H₂/N₂ (25, 50, and 75 ml) were studied. At a low flow rates of C₂H₂ (25 ml/min), poor carbon deposition yields were achieved, with minimal amount of carbon growth. In Figure **S5.1 (a-b)**, TEM images demonstrate that large short fibres are formed with a lot of amorphous carbon at 550 °C, while at an increased temperature, nanofibres changed to thin long fibres and tip growth was observed in both these materials. Increasing the C₂H₂ flow rate to 50 ml/min and reducing the N₂ flow rate to 50 ml/min at 550°C, resulted in an increase in the yield. Carbonaceous materials with the formation of straight fibres and spirals were formed (Fig. **S5.1 (c-d)**). At this flow rate and temperatures of 650 °C, a further increase in the yield formation with large fibres was observed with a lot of small tubes. The increase in the yield was expected as more C₂H₂ flowed into the system (Fig. **S5.2**).

5.3.3.1 Laser Raman spectroscopy analyses (Graphicity Studies)

To further assess the quality of the CNFs and confirm their formation, laser Raman spectroscopy was used. Raman spectroscopy is an effective technique that gives information about the graphitic and defective nature of the carbon structures

that are formed. Figures. 5.11a and 5.11b show C₂H₂ treated fly ash under N₂ and H₂ gases, respectively.

5.3.3.2 Raman spectroscopy analyses of CNMs formed by reaction of fly ash and C₂H₂ in N₂ and H₂ respectively

As shown in Fig. 5.11a and 5.11b, laser Raman spectroscopy confirmed the presence of CNFs with D and G bands observed at 1350 cm⁻¹ and 1590 cm⁻¹, respectively¹. The D-band was observed due to the disordered features present in the CNFs while the G band was due to the ordered stretching mode of the C-C bond in the graphite plane. An increase in the degree of disorder CNFs formed in N₂ was observed as the reaction temperature was increased. This behaviour could be explained in terms of the longer exposure to N₂, which upon saturation of the growing edge caused the growth rate to also slow down (as shown in Fig. 5.1)²⁶. In these cases N₂ can either be substituted by carbon or form defects in the CNF.

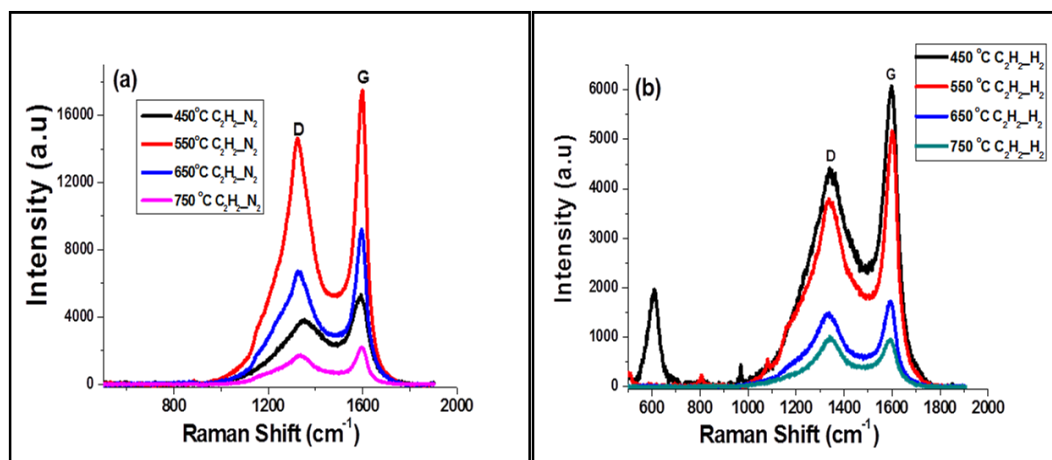


Figure 5.11: Laser Raman spectroscopy spectra of CNFs synthesized at various temperatures in the presence of carrier gases under (a) N₂ and (b) H₂, respectively.

In the presence of H₂ (Fig. 5.11b), the same trend as with N₂ was also observed, leading to CNFs having an I_D/I_G ratio of >1 at 750 °C. These results are similar to those reported in previous studies where Fe supported catalysts were used, resulting in the formation of a large amount of defected carbon beyond optimal

temperatures¹⁷. In the case with N₂ only, here side reactions with H₂ seem to be the reason for this trend.

5.3.3.3 Laser Raman spectroscopy analyses of CNMs formed by reaction of fly ash and C₂H₂ using H₂ as a pre-treatment and N₂ as a carrier gas

The lowest degree of disorder ($I_G/I_D=1.14$.) was evident at 550 °C Fig. (5.12a). These results were expected because more uniform CNFs were observed under TEM, with a narrower and a more controlled diameter distribution. Under these conditions at increased temperatures (650 °C), defective carbon was more prevalent ($I_G/I_D=0.85$) as shown in Fig. 5.12.

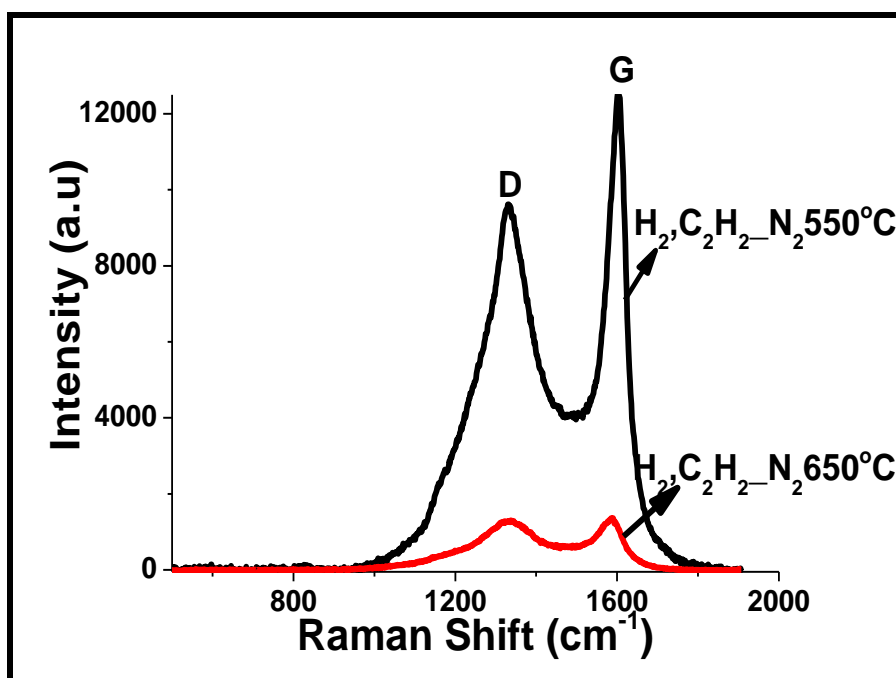


Figure 5.12: Laser Raman spectroscopy spectra of CNFs synthesized from C₂H₂ when H₂ was used during pre-reaction and N₂ as a carrier gas at (a) 550°C and (b) 650°C

5.3.3.4 Laser Raman spectroscopy analyses of CNMs formed by reaction of fly ash and C₂H₂ using N₂ as a pre-treatment and H₂ as a carrier gas

By interchanging the two gases, a clear distinction was observed; more graphitic CNFs were formed by using N₂ during the pre-reaction prior to using H₂ as a carrier gas in the presence of C₂H₂. Likewise, at higher temperatures 650 °C, the I_D/I_G ratios were even higher as shown in Fig. 5.13.

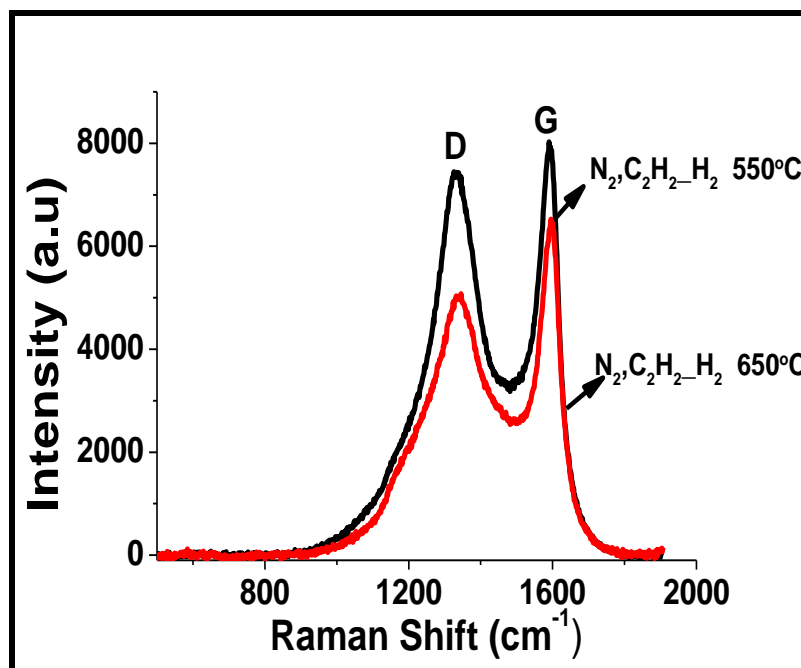


Figure 5.13: Laser Raman spectroscopy spectra of CNFs synthesized from C_2H_2 when N_2 was used during pre-reaction and H_2 as a carrier gas at: (a) $550^\circ C$ and (b) $650^\circ C$

These results concur with the TEM images where at lower temperatures ($550^\circ C$) more linear fibres were observed and after increasing the temperature to $650^\circ C$, a combination of thick and thin fibres was observed. To understand the thermal stability of these materials that had been formed, thermogravimetric analyses were conducted.

5.3.5 Thermal stability analyses

Thermogravimetric analyses (TGA) can be used to determine both the purity of materials and give information on the thermal stability of CNTs/CNFs. Thermogravimetric analysis was carried out to investigate the thermal degradation behaviour of the carbon nanomaterials.

5.3.5.1 Thermal stability of CNMs formed by reaction of fly ash and C_2H_2 in N_2 and H_2 respectively

According to literature, amorphous carbon typically oxidises in air at temperatures below $400^\circ C$, whereas CNTs oxidise at higher temperatures at $800^\circ C$ ²⁸. The

TGA data showed that between 300-400 °C, there was slight mass loss for CNFs formed at 450 °C. This indicated that there was still some amorphous carbon which was confirmed by SEM (Fig. 5.2a) that showed the material contained large amounts of fly ash. Previous studies have shown that fly ash contains a lot of amorphous carbon. The weight derivative (Fig. 5.14b), showed that an increase in the temperature resulted in a higher decomposition temperature. The peaks also shifted from broad to a narrower shape, and only one type of peak was observed, which indicates there was mostly one type of carbon formed.

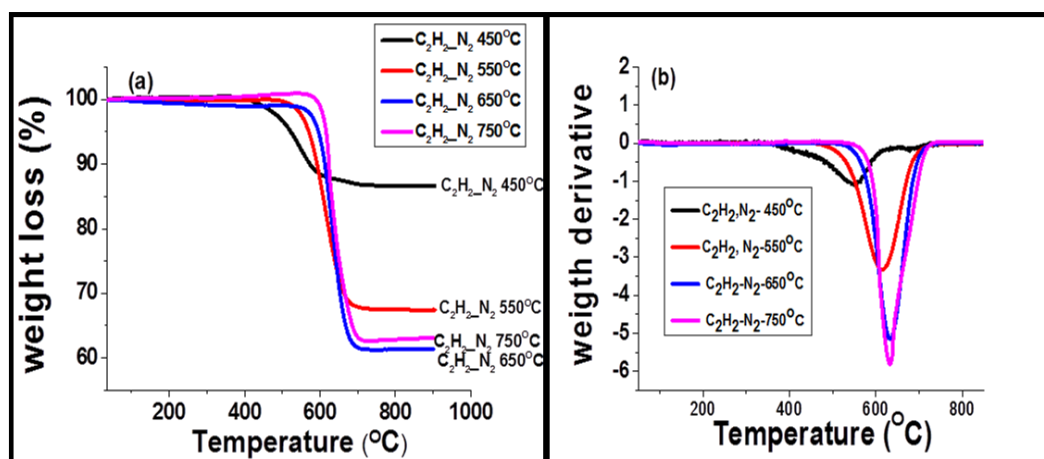


Figure 5.14: Thermal stability of CNFs formed at varying temperatures (450-750 °C) in the presence of N₂ gas (a) percentage weight loss (b) weight derivative

In the presence of H₂ no mass loss was experienced below 400°C. There was a rapid and incomplete weight loss experienced at 400 °C, 480 °C, 540 °C and 630 °C, in these samples, showing that the fly ash did not decompose completely. There were other impurities or possibly different forms of carbon as shown by the two peaks at 450 °C (Fig. 5.15b). The CNFs that formed at 750 °C (Fig. 5.15b) were more thermally stable as shown by the higher decomposition temperatures.

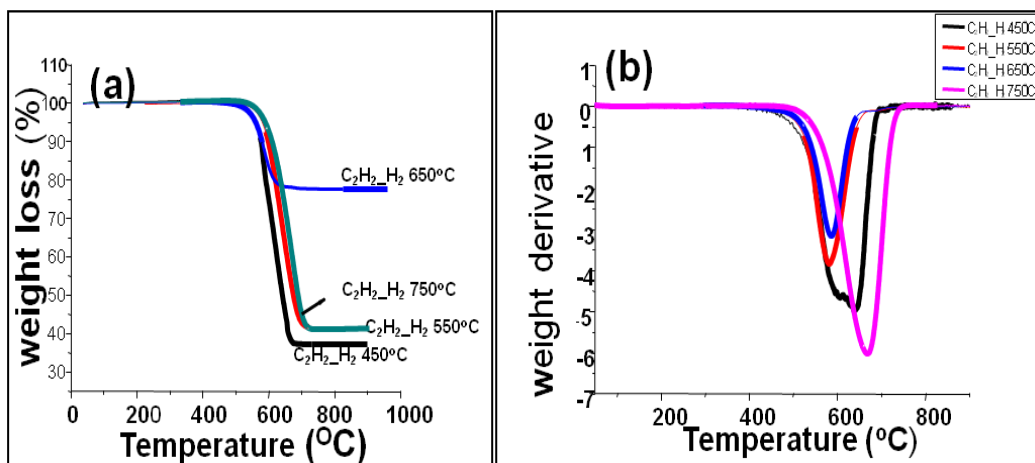


Figure 5.15: Thermal stability of CNFs formed at varying temperatures (450-750°C) in the presence of H₂ gas (a) percentage weight loss (b) weight derivative

5.3.5.2 Thermal stability of CNMs formed by reaction of fly ash and C₂H₂ using H₂ as a pre-treatment and N₂ as a carrier gas

In Fig. 5.16, TGA results showed that the CSs formed were more stable than the uniform CNFs. The CNFs and CSs were stable up to 560 °C and 630 °C, respectively. Different forms of carbon or impurities were also observed in (Fig. 5.16b), as shown by the three peaks. This though does not corroborate with the TEM results (Fig. 5.6a), shown earlier implying that other forms of carbon shown, are from the 35% unreacted fly ash.

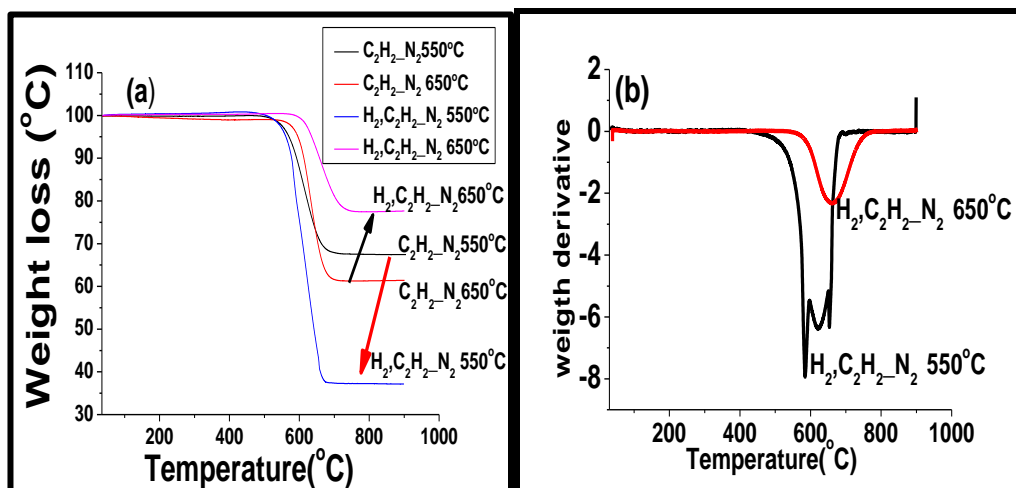


Figure 5.16: (a) Thermal stability and (b) derivative of CNFs synthesized materials at 550°C and 650°C temperatures using H₂ as a pre-reduction gas and N₂ as a carrier gas

5.3.5.3 Thermal stability of CNMs formed by reaction of fly ash and C₂H₂ using N₂ as a pre-treatment and H₂ as a carrier gas

By interchanging the gases in H₂, C₂H₂_N₂, the CNFs produced were highly stable and started decomposing at temperatures beyond 550 °C. These CNFs also showed a lower amount of impurities as shown by the sharp derivative curves (Fig. 5.17b). Comparing the fibres formed at 650 °C, with the ones that were pre reacted with N₂ reveals more unburnt fly ash residue than the one where no pre-treatment was experienced.

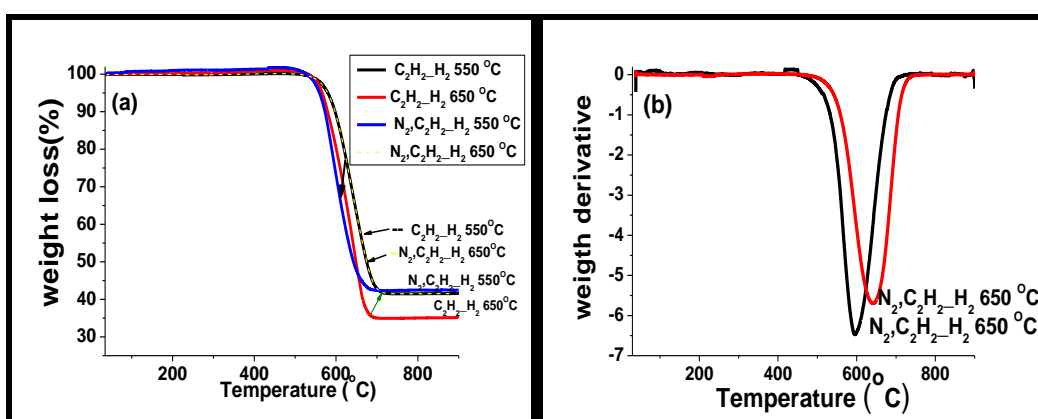


Figure 5.17: (a) Thermal stability and (b) derivative of CNFs synthesized materials at 550 °C and 650 °C

5.3.6 Composition, mineral phase and oxidation state studies

To confirm the elements responsible for CNF formation, XRD and Mössbauer spectroscopies were employed on samples synthesized at 650 °C where maximum yield was achieved.

5.3.6.1 Mineral phase identification analyses (PXRD)

In Fig. 5.18, it is clear that materials where CNFs had formed, sharp peaks and mineral phases (quartz, mullite and hematite) were identified. In the formation of spheres (N_2 , $C_2H_2-H_2$) a broad peak was evident, which could represent amorphous carbon and iron silicates present in the sample.

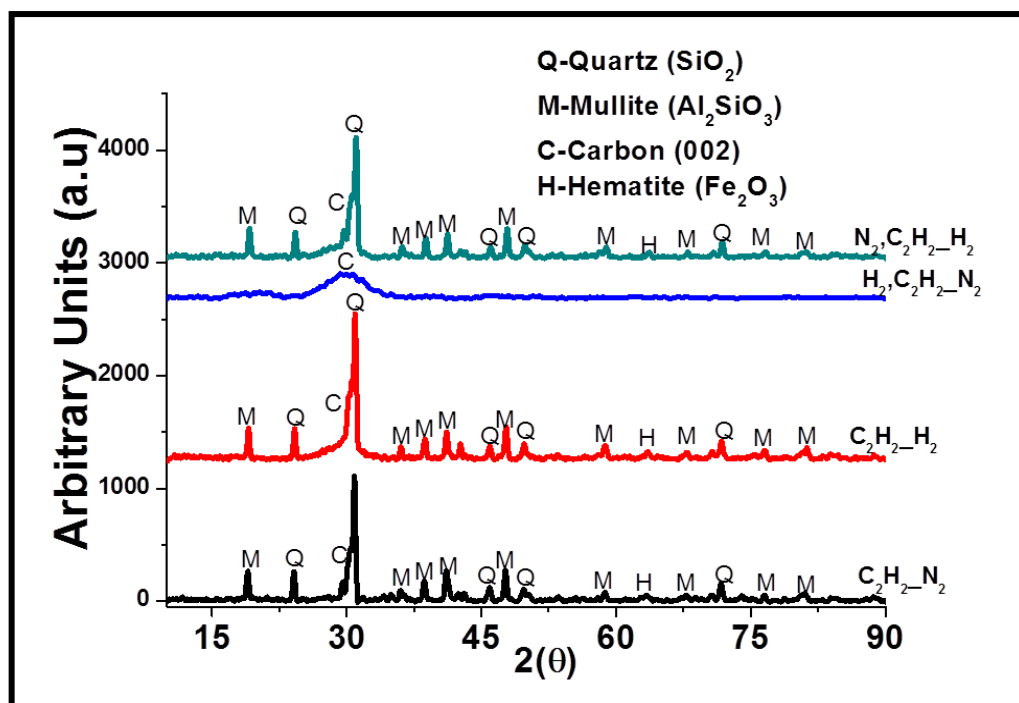


Figure 5.18: PXRD patterns of C_2H_2 treated sample in the presence of (a) $C_2H_2-H_2$, (b) $C_2H_2-H_2$, (c) H_2 , $C_2H_2-N_2$ and (d) N_2 , $C_2H_2-H_2$, for samples synthesized at 650 °C

5.3.6.2 Mössbauer spectroscopy

From previous studies it has been shown that ^{57}Fe Mössbauer spectroscopy is a technique that is able to identify all forms of iron²⁹. This was shown in our previous study, where Fe_3C was identified as the element responsible for CNF formation while using PXRD, this phase could not be identified. In order to obtain the chemical and structural information of iron containing materials, three main

hyperfine parameters, namely the isomer shift, quadrupole splitting and magnetic splitting needed to be investigated.

Mössbauer spectroscopy was conducted on the samples and the resulting fitted Mössbauer spectra obtained for all the CNMs synthesized at 650°C are shown in Fig. 5.19. For $C_2H_2_N_2$, the spectra are characterized by broadened six-line patterns and the central region was dominated by a distribution of quadrupole split doublets. The magnetic feature for $C_2H_2_N_2$ was fitted with three sextets (SX1, SX2 and SX3), while the spectra for CNMs synthesized by $C_2H_2_H_2$ and N_2 , $C_2H_2_H_2$ were each fitted with one sextet (SX1). For the different reaction conditions, either one or two doublets were required in the central region to give good fits.

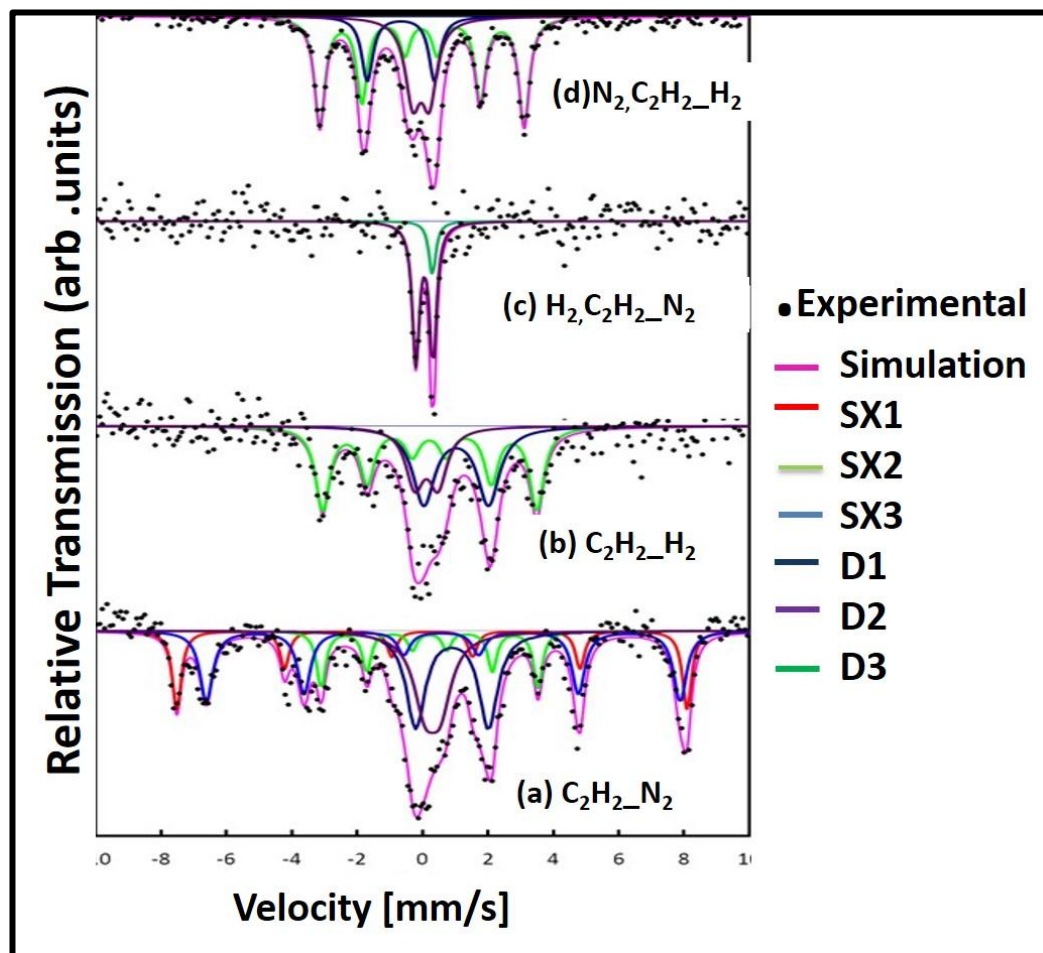


Figure 5.19: Room temperature Mössbauer parameters for: the acetylene treated sample in the presence of (a) $C_2H_2_N_2$, (b) $C_2H_2_H_2$, (c) H_2 , $C_2H_2_N_2$, and (d) N_2 , $C_2H_2_H_2$, for samples synthesized at 650 °C

Table5. 1: Summary of the hyperfine parameters obtained from the fits to the data for all the samples

		SX1	SX2	SX3	D1	D2	S1
	B_{hf} (T)	48.34	20.55	44.89	-	-	
C₂H₂_N₂	δ (mm/s)	0.29	0.22	0.60	0.90	0.31	-
	ΔE_Q (mm/s)	-0.01	0.00	0.06	2.22	0.47	-
	Area (%)	17	14	26	23	20	-
	B_{hf} (T)	-	20.29	-	-	-	-
C₂H₂_H₂	δ (mm/s)	-	0.21	-	1.03	0.12	-
	ΔE_Q (mm/s)	-	0.01	-	1.98	0.71	-
	Area (%)	-	47	-	33	20	-
	B_{hf} (T)	-	-	-	-	-	-
H₂, C₂H₂_N₂	δ (mm/s)	-	-	-		0.07	0.18
	ΔE_Q (mm/s)	-	-	-		0.56	0
	Area (%)	-	-	-		84	16
	B_{hf} (T)	-	20.84	-	-	-	-
N₂, C₂H₂_H₂	δ (mm/s)	-	0.17	-	0.85	0.19	-
	ΔE_Q (mm/s)	-	-0.03	-	2.22	0.54	-
	Area (%)	-	56	-	17	27	-

For C₂H₂_N₂, the hyperfine parameters extracted for SX1 and SX3 were: $B_{\text{hf}} = 48.34$ T, $\delta = 0.29$ mm/s; $E_Q = -0.01$ mm/s and $B_{\text{hf}} = 44.99$ T, $\delta = 0.60$ mm/s; $\Delta E_Q = 0.06$ mm/s, respectively. These values corresponded to Fe³⁺ ions on tetrahedral A-sites, and Fe^{2.5+}-like average signals from octahedral B-sites, respectively and were identified as magnetite (Fe₃O₄). The SX2 spectral component with hyperfine parameters of $B_{\text{hf}} = 20.55$ T, $\delta = 0.22$ mm/s; $\Delta E_Q = 0.00$ mm/s was identified as an iron carbide (Fe₃C). For this sample, the hyperfine parameters determined for D1 and D2 are $\delta = 0.90$ mm/s; $\Delta E_Q = 2.22$ mm/s and $\delta = 0.31$ mm/s; $\Delta E_Q = 0.47$ mm/s characteristic of ferric and ferrous ions, respectively. The quadrupole split doublets were attributed to iron silicates.

In the presence of hydrogen, C₂H₂_H₂, only one sextet, SX2 with a reduced magnetic field was observed in the spectrum with hyperfine parameters of $B_{\text{hf}} = 20.29$ T, $\delta = 0.21$ mm/s; $\Delta E_Q = 0.01$ mm/s which has been identified as nanocrystalline iron carbide (Fe₃C). The hyperfine parameters of $\delta = 1.03$ mm/s; $\Delta E_Q = 1.98$ mm/s and $\delta = 0.12$ mm/s; $\Delta E_Q = 0.71$ mm/s obtained for D1 and D2, respectively are very similar to those obtained for the nitrogen sample except for the quadrupole splitting of D2 which is lower for the nitrogen sample indicating some structural relaxation.

For the nitrogen sample (C₂H₂_N₂), the total population of the oxides is ~43% compared to 14% area fraction of Fe₃C with the remaining fraction of ~43% attributed to iron silicates. In the presence of hydrogen (C₂H₂_H₂), no oxides were observed resulting in the area fraction of Fe₃C increasing to 47 % with a corresponding increase of 10% in the population of iron silicates.

By interchanging the gases, using H₂ as a pre-reductant in H₂, C₂H₂_N₂ sample, a doublet with hyperfine parameters of $\delta = -0.07$ mm/s; $\Delta E_Q = 0.56$ mm/s and a single line component, $\delta = 0.18$ mm/s was extracted from the fits to the data. This change in structure was expected since under TEM, carbon spheres were formed unlike fibres with all the other series. The iron carbide phase disappeared completely and Fe in the 2+ state (silicate form) dominated the spectrum.

In N₂, C₂H₂_H₂, the Fe₃C phase reappeared with two quadrupole split doublets, when hydrogen was used as a carrier gas, in the presence of N₂ as a pre reaction gas reductant. These results are similar to those reported for C₂H₂_H₂, where the same formation was observed. For this sample, the Fe₃C population increased by 9%, with a corresponding decrease in the silicates fraction, similar to findings also reported elsewhere²⁹. In trying to understand why the Fe₃C phase appears and then disappears during these reactions, Schaper *et al.* showed that the iron carbide acts as an intermediate during the formation of well-ordered graphene layers on its surface³⁰. Therefore when carbon spheres were formed, no Fe₃C was identified.

This phenomenon was also proven by laser Raman spectroscopy and TGA where the I_D/I_G ratio was very much >1 showing a broad peak under the derivative curve.

The identification of Fe_3C as the carbide responsible for well-ordered CNF formation, present in all the phases where well-ordered CNFs were formed and yet in terms of yield, hydrogen as a carrier gas produced much higher yields than nitrogen. Pattison *et al.* found that at high nitrogen concentration, there was a build-up of nitrogen at the catalyst surface where it is exposed to the reactants²⁰. This therefore, leads to reduction in the carbon deposition efficiency on the catalyst leading to the slow growth rate. In a high nitrogen environment, their Environmental Transmission Electron Microscopy (ETEM) studies showed both the nucleation and CNF growth were affected. Nitrogen tends to reduce the surface energy at the CNF/catalyst interface and reduces the carbon extrusion from the catalyst and the growth rate of CNFs.

5.4. Conclusions

This study has shown that it was possible to form CNMs using fly ash as a catalyst without pre-treatment or impregnation of further metals. By varying the CVD experimental conditions, it was shown that CNMs with different structures could be formed. The results revealed that under TEM, CNMs of various morphologies such as CNFs and CNSs were formed in high yields at 650 °C. The high yield formation of CNFs and amorphous carbon compared to CNTs in other studies may have been due to the higher supply rate of carbon than what is required for CNT growth. The use of H_2 as a carrier gas ($C_2H_2-H_2$) at 650 °C produced thin and thick CNFs recorded the highest yield. These fibres were the most graphitic and were shown to be the most thermally stable, with only 35 % fly ash as the remaining material. The use of H_2 as a pre-reaction gas and N_2 as a carrier gas produced, uniform nanofibres with more than 50% of the CNFs found within a very narrow diameter size distributions of 80-119 nm. By increasing the temperature to 650 °C, spheres were formed. From TEM and SEM it was shown that root growth is favoured at low temperature and upon increasing the temperature, tip growth was more prevalent. Laser Raman spectroscopy and

Mössbauer spectroscopic techniques also revealed that three types of carbons were formed, namely: amorphous, graphitic and iron carbide (Fe_3C) or cementite.

5.0 References

1. O. M. Dunens, K. J. MacKenzie and A. T. Harris, *Environmental science & technology*, 2009, **43**, 7889-7894.
2. D. Cordell, J-O Drangert, S. White, *Global Environmental Change.*, 2009, **19**, 292-296 .
3. O. Kayali, *Construction and Building. Material*, 2008, **22**, 2393.
4. I. Yunusa, D. Eamus and D. DeSilva, *Fuel*,2006, **85**, 2337-2342.
5. H. Cho, D. Oh and K. Kim, *Journal of Hazardous Materials*, 2005, **127**, 187-196.
6. R. Iyer and J. Scott, *Resources, Conservation and Recycling.*, 2001, **31**, 217-225.
7. S. Wang and G. Lu. Natural Gas Conversion VIII: Proceedings of the 8th Natural Gas Conversion Symposium, 2011.
8. W. Chen, F. Sheu and R. Savage, *Fuel Processing Technology.*,1987, **16**, 279-286.
9. N. Hintsho, A. Shaikjee, P.K. Tripathi, P. Franklyn and S. Durbach, *RSC. Advances*, 2015,**5**, 53776-53783.
10. A. Yasui, Y. Kamiya, S. Sugiyama, S. Ono, H. Noda and Y Ichikawa, *IEEJ Transaction on. Electrical and. Electonic Engineering* 2009,**4**, 787-794.
11. N. Salah, S.S Habib, Z.H. Khan, A. Memic and M.N. Nahas . *Digest Journal of. Nanomaterial and Biostructures*, 2012,**7**, 1279-1283.
12. A-C Dupuis, *Progress in Materials Science*, 2005, **50**, 929-936.
13. P. Ajayan ,*Chemical. Reviews*, 1999, **99**, 1787-1793.
14. S. Adhikari and S. Fernando, *Journal of Inustrial .Engineering* ,2006, **45**, 875-881.
15. P. Ajayan, B. Wei, D. Wu, C. Xu and H. Zhu. Google Patents, 2003.
16. P. K. Tripathi, L. Gan, M. Liu and N. N. Rao, *Journal of Nanoscience. and Nanotechnology*, 2014,**14**, 1823-1830.
17. N. Hintsho, A. Shaikjee, H. Masenda, D.Naidoo, D. Billing, P.J. Franklyn and S.Durbach, *Nanoscale Research. letters*, 2014,**9**, 1-11.

18. N. Hintsho, L. Petrik, A. Naechev, S. Titinchi and P. Ndungu, *Applied Catalysis. B*, 2014, **156**, 273-281.
19. C. A. Scheider, W.S. Rasband and K.W. Eliceiri, *Nature Methods*, 2012, **9**, 671-677.
20. S.W. Pattinson, R.E Diaz, NA Stelmashenko, *Chemistry of. Materials*, 2013, **25**, 2921-2928.
21. H. Dai, *Surface. Science.*, 2002, **500**, 218-222.
22. K. Kuwana and K. Saito, *Carbon.*, 2005, **43**, 2088-2095.
23. A. Shaikjee, Phd Thesis, University of the Witwatersrand, Thesis, 2012.
24. A. Shaikjee and N.J Coville, *Carbon.*, 2012, **50**, 3376-3384.
25. M. Jung and K. Eun, *Diamond and Related. Materials*, 2001, **10**, 3-9.
26. C-M Seah, S-P Chai and A. R. Mohamed, *Carbon.*, 2014, **70**, 1-8.
27. Q. M. Gong, Z. Li, Y. Wang, B. Wu, Z. Zhang and J. Liang, *Materials Research Bulletin.*, 2007, **42**, 474-480.
28. Z. N. Tetana . PhD Thesis, University of the Witwatersrand, Thesis, 2013.
29. M. Pérez-Cabero, J. Taboada, A. Guerrero-Ruiz, A Overweg and I Rodríguez-Ramos, *Physical Chemistry Chemical Physics*, 2006, **8**, 1230-1236.
30. A. K. Schaper, H. Hou, A. Greiner and F Phillip, *Journal of .Catalysis*. 2004, **222**, 250-258.
31. L. Cele, PhD Thesis, University of the Witwatersrand, Thesis, 2007.

Chapter 6: The effect of CO₂ on the CVD synthesis of carbon nanomaterials using fly ash as a catalyst

6.1 Introduction

Since the rediscovery of carbon nanomaterials (CNMs) in 1991, their production has been found to be a costly exercise. This is mainly due to the catalysts used and the carbon sources¹. In order to remediate this, researchers across the world have tried to find more efficient and cheaper ways of synthesizing CNMs (e.g. carbon nanotubes (CNTs) and carbon nanofibres (CNFs))²⁻⁵

CO₂ is a low energy molecule that is found in abundance on the earth. Due to its relative cheapness and availability, the search for uses of CO₂ has attracted a lot of attention⁶⁻¹³. The need to do this has been increased by the current struggles of global warming that face society and the impending shortage of fossil fuels. Recently researchers have used CO₂ as an alternative carbon source for CNT production. Results showed that parameters such as high pressures, specific temperature ranges, high flow rates and the choice of catalyst support played a crucial role¹⁵⁻¹⁸. In one study, when FeO was used on a support of CaO, CNTs were formed¹⁴. Unfortunately, when Al₂O₃, SiO₂ and MgO were used as supports, no CNTs were produced¹³. However this method still suffers from low CNT yields and high energy consumption because of the very high carbonization temperatures that are required. These conditions tend to be unsuitable for such approaches to be scaled up.

Recent studies have shown that an addition of a small amount of an oxygen containing species to the carbon source (e.g. C₂H₂) improves the yield of CNMs¹⁹. For example, the addition of oxygen which has been shown to act as a scavenger of hydrogen radicals has provided conditions that were suitable for CNM synthesis. On the other hand the addition of water, which acts as an etching agent

that prevents the encapsulation of catalyst particles by amorphous carbon, increased the CNT yield, extended lifetime of the catalyst and an enhanced initial growth rate as compared to those of classical C₂H₂ decomposition reactions²⁸.

This chapter reports on the use of two waste products, namely: fly ash and CO₂ to produce CNMs. It further demonstrates the use of fly ash as a catalyst and CO₂ as an additive or as a carbon source prior to the reaction with C₂H₂ improved the yields of CNMs, in the CVD synthesis method.

6.2 Experimental

6.2.1 Synthesis of CNFs

CNFs were synthesised using coal fly ash produced from the Roscheville power station. For these syntheses, carbon deposition was achieved through chemical vapour deposition of acetylene (C₂H₂) or carbon dioxide (CO₂) over waste fly ash. Carbon depositions were achieved by CVD reactions of: 1) Only CO₂, 2) CO₂ together with C₂H₂ (i.e. CO₂/C₂H₂) or 3) CO₂ followed by C₂H₂ (i.e. CO₂_C₂H₂) over the waste coal fly ash. The synthesis procedure followed was described in Section 3.3.1, except the flow rate was kept constant at 100 ml/min, reaction time to 45 min and the temperature used ranged from 500-900 °C for these reactions.

6.2.2 Characterisation of CNFs

The synthesized CNFs samples were characterized using scanning electron microscopy (SEM), thermogravimetric analysis (TGA), laser Raman spectroscopy and X-ray diffraction (XRD). For each characterisation, procedures described in Section 3.4.1, 3.4.5 and 3.4.6 and 3.4.7 respectively were followed. Brunner-Emmet Teller (BET) were employed as described in Sections 3.4.3.

6.3 Results and Discussion

A summary of the different approaches of using CO₂ as well as the various outcomes (to be discussed in further detail later on) is shown in Fig.6.1.

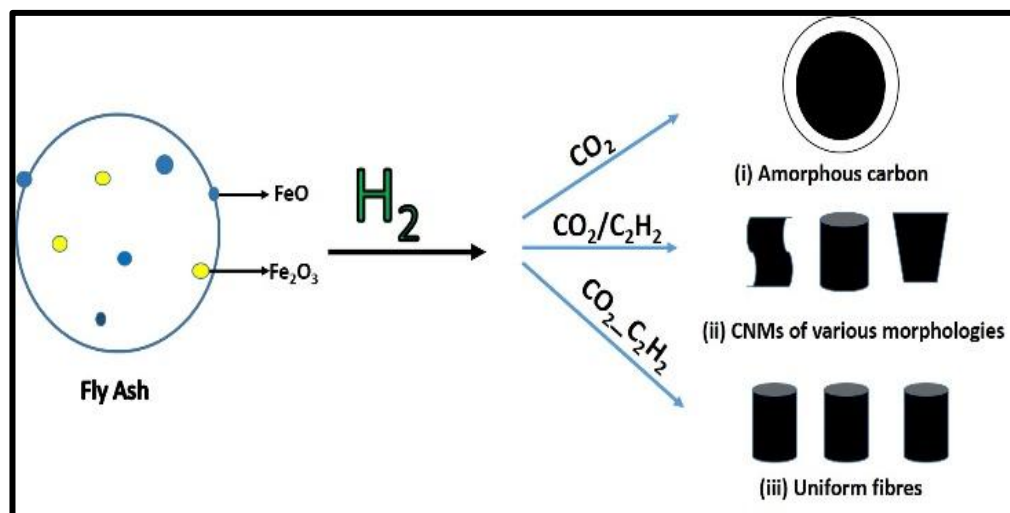


Figure 6.1: Synthesis of CNMs using CO₂ as a sole carbon source, as an additive and as a carbon source prior to the reaction with C₂H₂ (CO₂_C₂H₂)

6.3.1 CO₂ as a carbon source

The morphologies of the products from the CO₂ treated fly ash are shown in Figs. 6.2a-d. These images show that various kinds of amorphous carbon had been formed. In some cases coal ash particles exhibited spherical shapes Fig.6.2c and in others irregularly shaped ones (Fig. 6.2d). These differences in the amorphous carbon could possibly be due to the various mechanisms of fly ash formation or due to the incomplete oxidation of the precursor coal²⁴.

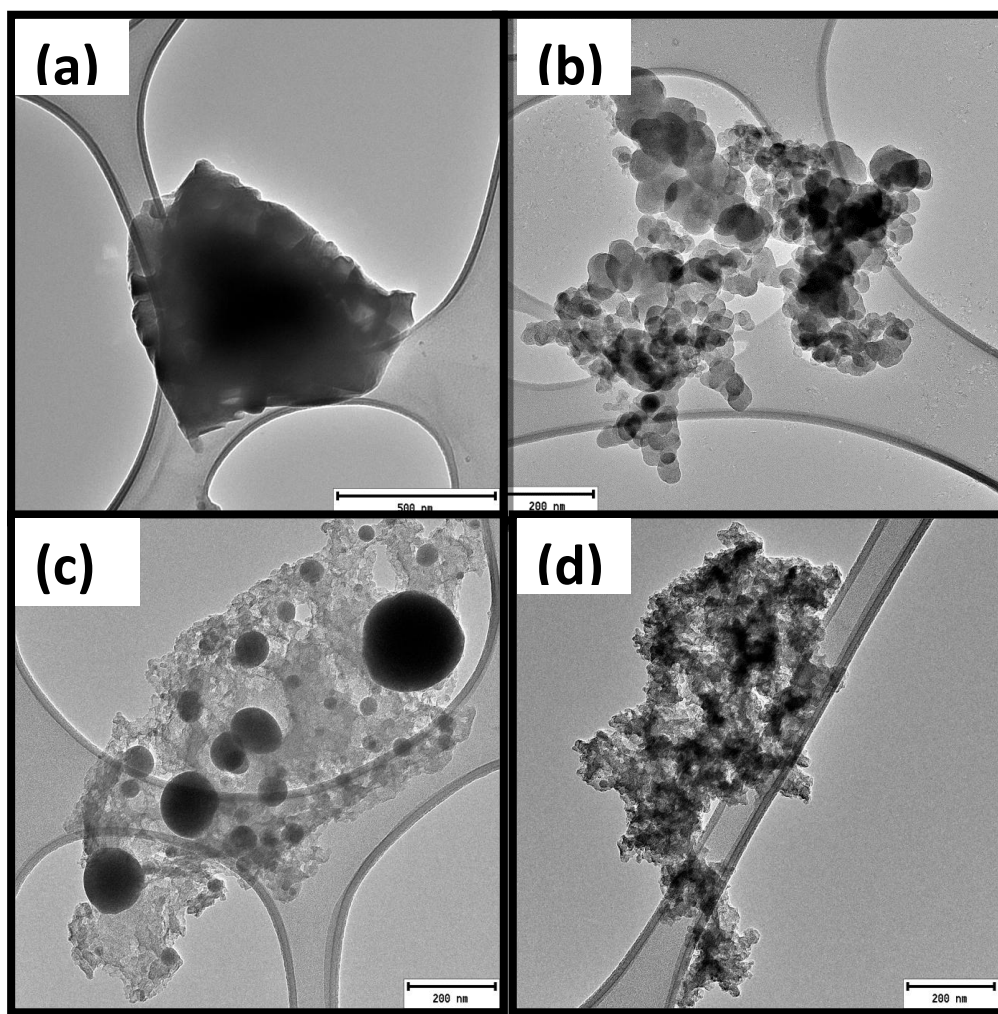


Figure 6.2: TEM images of various amorphous carbon materials grown at 900 °C showing (a) Sheet-like material, (b) Sphere-like materials, (c) Carbon with metal particles and (d) Amorphous carbon with what appears to be unreacted fly ash

The as-received fly ash and CO₂ reacted fly ash were analysed by SEM, (Fig. 6.3a-b). Fig. 6.3a shows the spherical shape of the as-received fly ash, while Fig. 6.3b shows the CO₂ reacted fly ash. Laser Raman spectroscopy confirmed the presence of both amorphous and graphitic carbon, as shown by a high D (disordered) peak and a low G (graphitic) peak Fig. 6.3c²⁵. The presence of the high D peak indicated that the carbon products that formed were poorly graphitised¹⁶.

When as-received fly ash was used as a catalyst it was found that the very low yields of nanocarbon materials were formed at 900 °C, while at temperatures between 500-800 °C and above 1000 °C, only irregularly shaped amorphous carbon materials were formed. This is in contrast to other studies where CO₂ was used as a sole carbon source and CNTs were formed¹⁵⁻¹⁸. In those studies iron and cobalt were used as catalysts. The lack of CNT formation in this study could have been caused by the large quantities of Al₂O₃, SiO₂ and MgO found in the fly ash^{19,20}. On the other hand, it is possible that the rate of carbon supply exceeded the growth rate of CNTs, since this has been shown to result in the formation of amorphous carbon and fibres as compared to tubes¹³. Our results, in a similar manner to Xu *et al.*, have revealed that the reduction of CO₂ to graphitic CNMs is sensitive to both the catalyst and the temperature used¹⁸. This work, together with other studies, has shown that more research is still required to understand the growth of CNMs from CO₂ as a sole source of carbon.

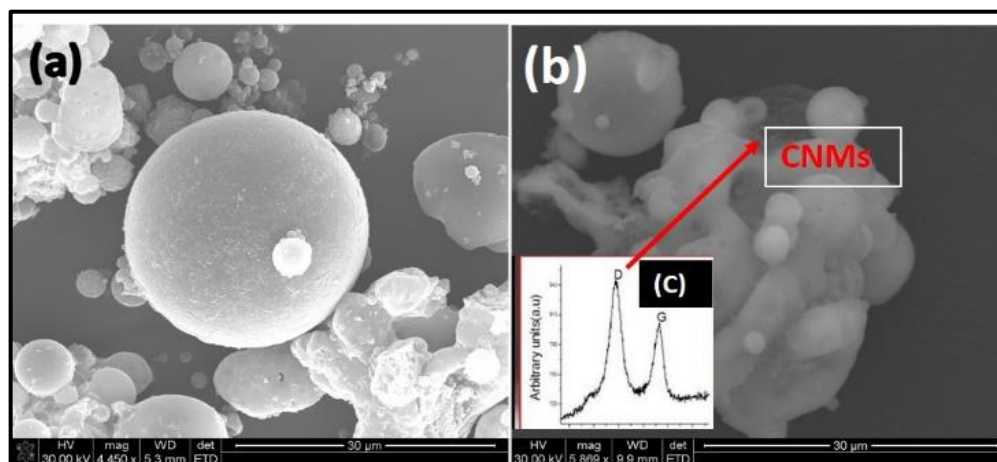


Figure 6.3: SEM images of (a) As-received fly ash, (b) Carbon materials grown at 900°C (c) Laser Raman spectroscopy of CNMs formed at 900°C

Based on the difficulties experienced in using CO₂ as a sole carbon source for CNT formation, Magrez *et al.* attempted a triple point junction reaction, where CO₂, C₂H₂ and the FeO metal catalyst were all used in one reaction¹⁹. This was done in an effort to increase the yield and favour the production of more CNTs at lower temperatures. While their study found a dramatic increase in the yield of CNTs, it was also found that this decreased at higher temperatures. In another study using Fe/MgO as a catalyst, ethanol as a carbon source and acetonitrile as a nitrogen source, a similar trend was reported²⁶. Here this effect was attributed to the O₂ containing species which were believed to oxidise the carbon at higher temperatures. Similarly it is known that the etching effect of OH radicals disrupts the initiation stage of CNT growth²⁹. In this present study the reaction temperatures employed were from 500 °C to 700 °C, using as-received fly ash as a catalyst and CO₂ as an additive to C₂H₂, which was the main carbon source.

6.3.2 CO₂ as an additive to C₂H₂

When CO₂ was employed as an additive to C₂H₂, the results obtained indicated that there was a three-fold increase in the yield in carbonaceous materials formed from 500 °C to 600 °C, which then remained constant at 700 °C. Laser Raman spectroscopy conducted on these products (Fig. 6.4c) showed that the I_G/I_D ratio increased as the reaction temperature was increased. This suggested that the degree of ordered carbon increased as the reaction temperature was increased.

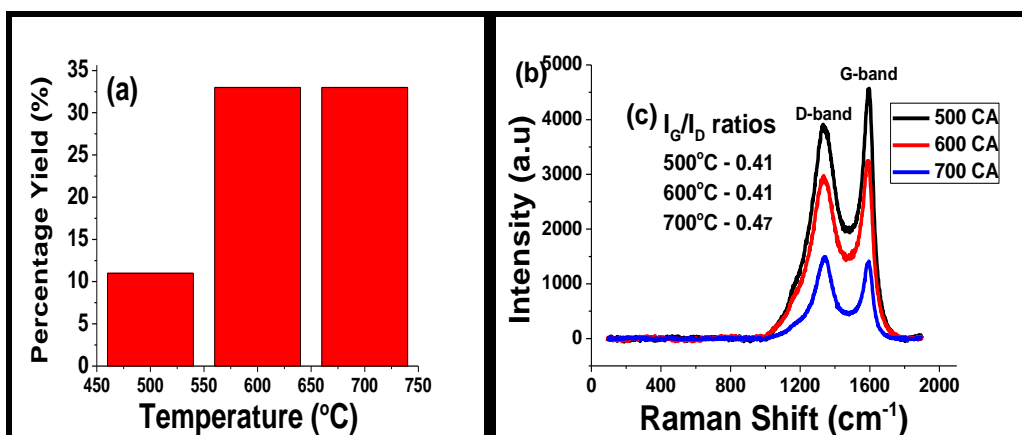


Figure 6.4:(a) Percentage yields of CNMs produced (b) Raman spectroscopy spectra of CNMs grown between 500-700°C and (c) I_D/I_G ratios of CNMs

TGA was conducted on all of these products to test their thermal stability. As shown in Fig. 6.5a, the percentage of carbonaceous products formed from the fly ash increased from 500 °C to 600 °C and then remained relatively constant at 700°C. This trend was consistent with that of the percentage yields, as noted in Fig. 6.4a.

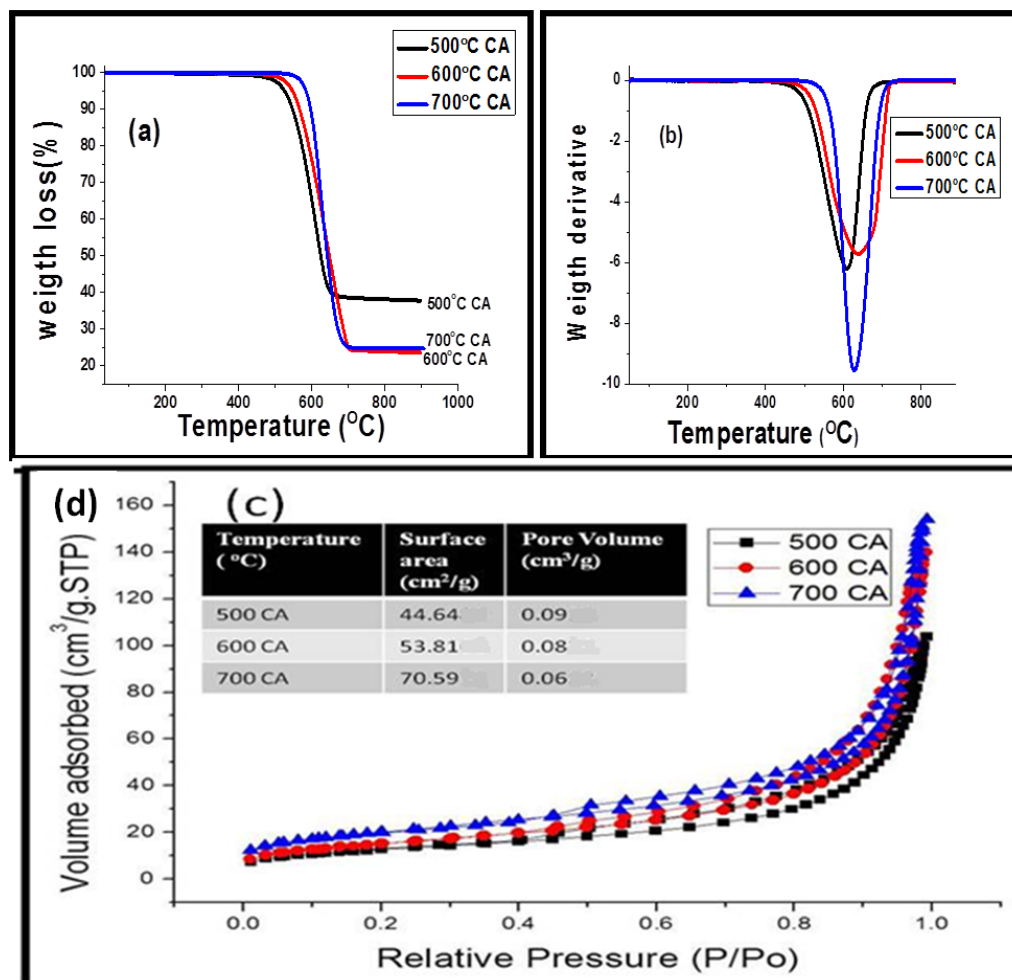


Figure 6.5: (a) TGA profile, (b) Weight loss derivative, (c) Adsorption isotherms and (d) BET surface area and pore volumes of CNMs grown between 500-700°C.

Likewise the increase of the first weight derivative Fig. 6.5b to higher temperatures as the reaction temperature was increased (i.e. from c.a. 600 °C to 640 °C), suggested an increase in the amounts of graphitic materials. This coincided with a corresponding decrease in the I_G/I_D ratio (Fig. 6.4c) and a shift from straight fibres of various diameters at 500 °C and 600 °C (Figs. 6.6a-d) to

straight and coiled fibres at 700 °C (Figs. 6.6e-f). Similarly, as the graphitic nature of these materials increased it was observed that their surface areas also increased (Fig 6.5c). Based upon the adsorption/desorption data, a type III hysteresis loop was observed, which corresponded to a material with non-porous structures.

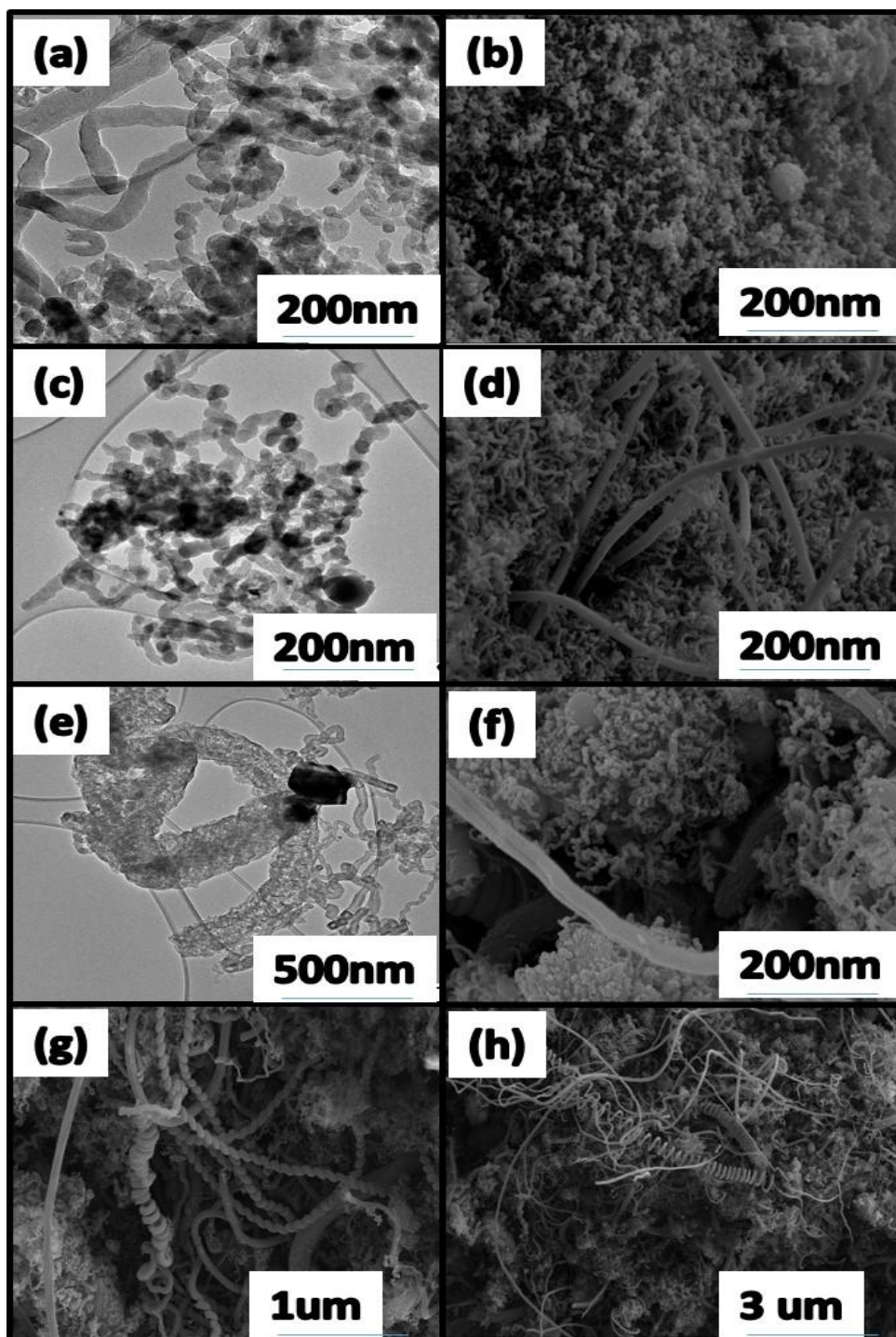
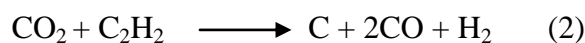
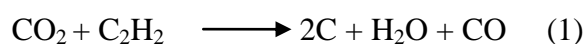


Figure 6.6:TEM and SEM images of CNF/Ts formed (a-b) 500 °C,(c-d) 600 °C and (e-h) 700 °C.The block gives the size of the scale bar

Unlike in the previous case where CO₂ was used as the sole carbon source, it was noted that upon reaction between the two gases a popping noise was heard which became increasingly louder as the reaction temperature was increased. This was most likely due to the presence of the oxygen containing species (i.e. CO₂) reacting with the hydrocarbon in the presence of the fly ash catalyst²⁷. A previous study has shown that at least two types of reactions (equations (1) and (2)) occurred when CO₂ and C₂H₂ were co-reacted for CNT synthesis¹⁹:



Here it was found that the type of catalyst with support, as well as the reaction temperature used played a huge role in terms of the materials that were produced. Undoubtedly, the formation of carbon from the side reactions between CO₂ and C₂H₂ (equations (1) and (2)) must have played a role in the dramatic increase in the percentage yield that was observed from 500 °C to 600 °C.

6.3.3 CO₂ as a carbon source prior to C₂H₂

To avoid these potentially dangerous reactions from occurring, a further study was conducted where CO₂ was introduced into the reaction zone on its own first. CO₂ was then flushed out with H₂ for 15 min. This was then followed by the introduction of C₂H₂. These reactions (as described previously) were also carried out in the temperature range between 500 °C to 700 °C.

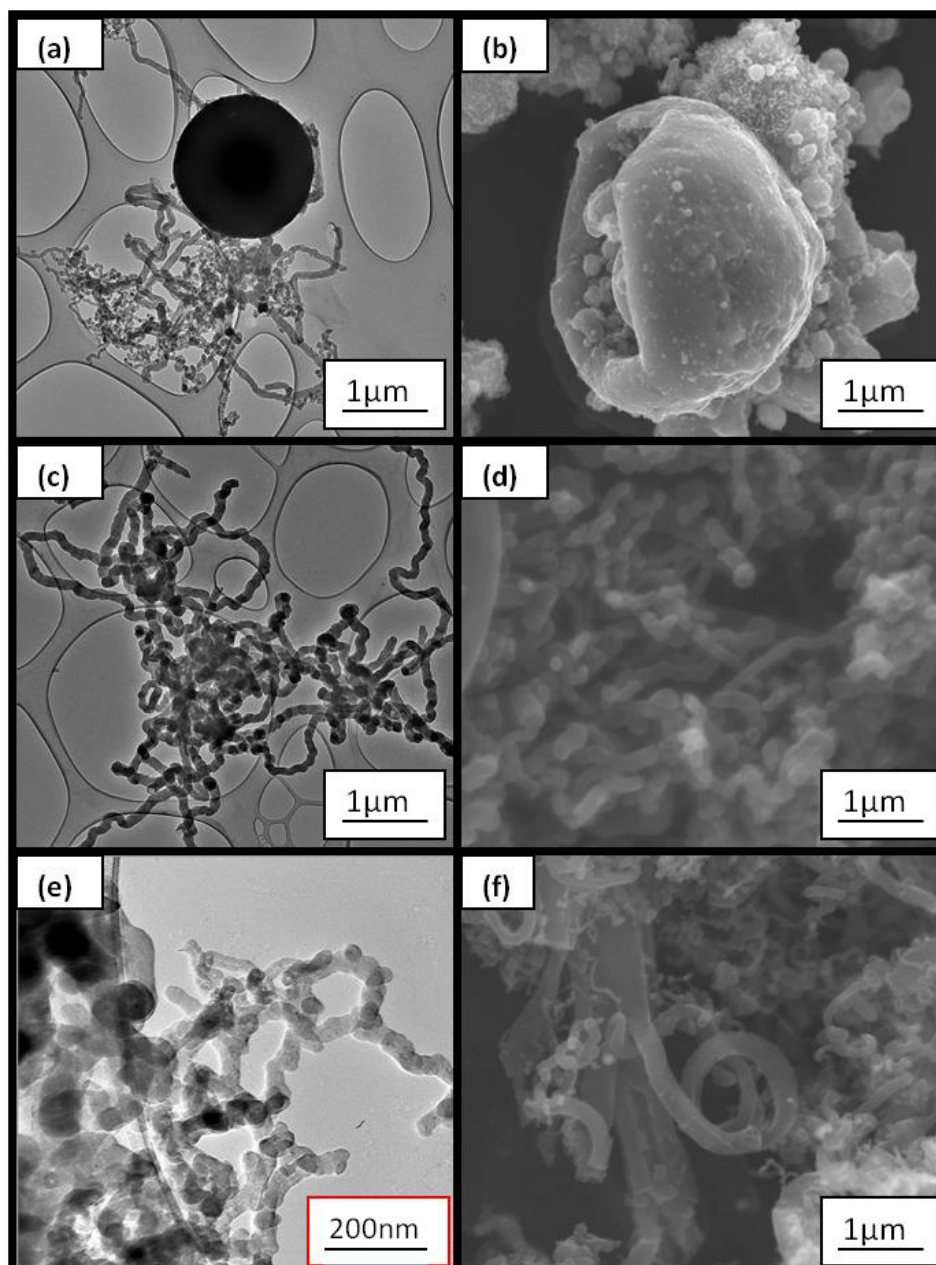


Figure 6.7: TEM and SEM images of CNF/Ts formed (a-b) 500 °C, (c-d) 600 °C and (e-f) 700 °C

In Fig. 6.7a-b, it can be observed that regularly and irregularly shaped carbon nanofibres were formed when subjected to CO_2 and then C_2H_2 . Small amounts of CNTs were also observed among the products. In Fig. 6.7c-d well-defined uniform CNFs, with a narrow particle size range, were observed. In Fig. 6.7e-f, carbon nanofibres of various diameters were observed together with

agglomerations of materials, which may have been caused by the sintering of the fly ash catalyst during the reaction.

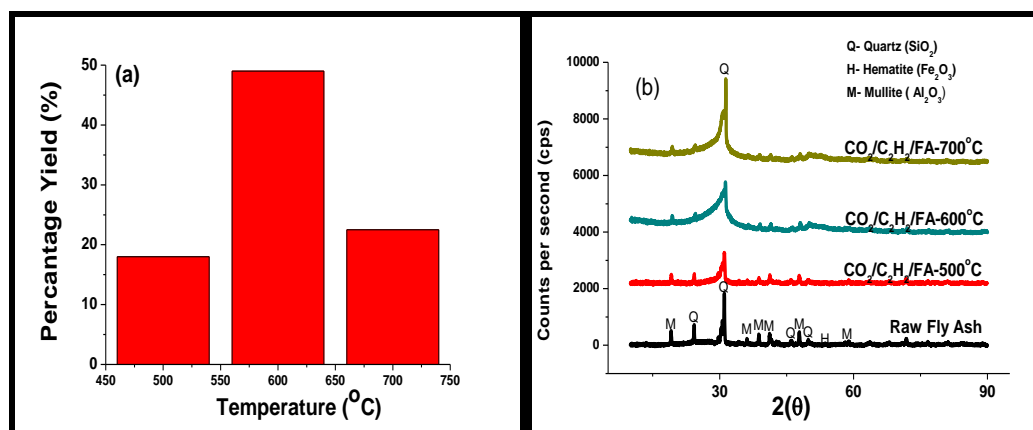


Figure 6.8: (a) Percentage yields of CNMs produced and (b) PXRD diffractograms of the raw fly ash and the CNMs that were formed from 500-700°C

As before the yields of CNMs formed revealed a slight increase at 500 °C with the use of CO₂ as a carbon source prior to the reaction with C₂H₂ as compared to when CO₂ was used as an additive. On the other hand, at 600 °C the yield increased to 49%, which was an increase of about 17% by comparison when CO₂ was used as an additive with C₂H₂. Unlike when CO₂ was used as an additive, in this case when the temperature was increased to 700 °C the percentage yield of the CNMs decreased (Fig. 6.8a). This also corresponded with an increase in the crystallinity of the fly ash from 500 °C to 700 °C as observed in Fig. 6.8b. The reduction in the percentage yield may either have been caused by sintering at 700 °C or by the presence of an oxygen species (i.e. CO₂) which has previously been shown to limit the growth of CNMs at higher temperatures¹⁹.

The thermal stabilities of the CNMs formed at the various temperatures are displayed in Fig 6.9a. As was the trend with the percentage yields (Fig 6.8a), the percentage of carbonaceous products formed from the fly ash increased from 500 °C to 600 °C and then decreased at 700 °C. However, the first weight derivative (Fig. 6.9b) increased as the reaction temperature was increased, which suggested an increase in the amounts of graphitic materials. As might have been expected from the uniformity of the CNMs formed using CO₂ in this way at 600°C (Fig 6.7

b), these materials had the highest I_G/I_D ratio of all the materials formed in all three cases and under all three temperatures (Figs. 6.9c).

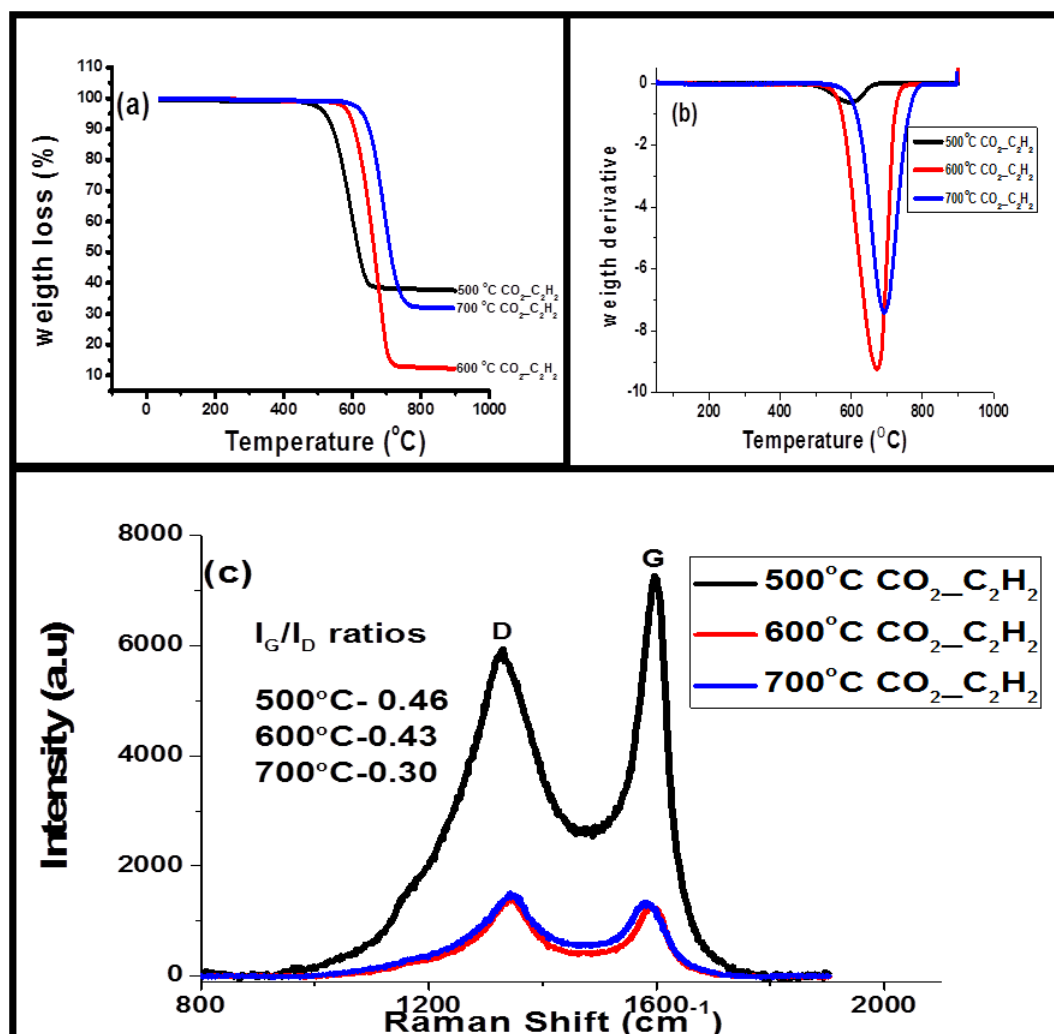


Figure 6.9:(a) Thermal decomposition (b) Weight loss derivative, (c) laser Raman spectroscopy spectra and I_G/I_D ratio of CNF products from fly ash exposed to CO_2 and then C_2H_2 at 500-700°C

6.4 Conclusions

In this study a CVD method of producing CNMs over fly ash as a catalyst by using CO_2 as a sole carbon source, an additive and a carbon source prior to the reaction with C_2H_2 was presented. Here it was shown that using CO_2 as a sole carbon source gave low yields and poorly formed materials, which was consistent with similar studies. When CO_2 was used as either an additive or a carbon source prior to the reaction with C_2H_2 the yield of CNMs formed increased drastically

between 500 °C and 600 °C. However, only in the case where the fly ash catalyst was pre-reacted with CO₂ and then C₂H₂, were the highest yields of carbon nanofibres formed which were more uniformly sized and more graphitic at 600 °C. Finally, this study has shown that the use of two waste materials, fly ash and CO₂ (together with C₂H₂) can be used to cost effectively synthesise CNMs.

6.5 References

1. S. Iijima and T. Ichihashi, *Japanese. Journal of Applied Physics*, 1993, **32**, L107–L109.
2. P. J. Harris and P. J. Harris, *Cambridge University Press*, 2009.
3. M. Terrones, W. K. Hsu, H. W. Kroto and D. R. Walt, *Springer*, 1999, pp. 189–234.
4. H.-S. P. Wong and D. Akinwande, *Cambridge University Press*, 2011.
5. S. Bhaviripudi, E. Mile, S. A. Steiner, A. T. Zare, M. S. Dresselhaus, A. M. Belcher and J. Kong, *Journal of American. Chemical Society*, 2007, **129**, 1516–1517.
6. A. M. Cassell, J. A. Raymakers, J. Kong and H. Dai, *Journal of Physical Chemistry. B*, 1999, **103**, 6484–6492.
7. A. Peigney, P. Coquay, E. Flahaut, R. E. Vandenberghe, E. DeGrave and C. Laurent, *Journal Physical. Chemistry. B*, 2001, **105**, 9699–9710.
8. E. Couteau, K. Hernadi, J. W. Seo, L. Thien-Nga, C. Mik'ó, R. Gaal and L. Forro, *Chemical Physics. Letters*, 2003, **378**, 9–17.
9. A.-C. Dupuis, *Progress in Material. Science*, 2005, **50**, 929–961.
10. S. Sharma and S. Lakkad, *Surface Coat Technology*, 2009, **203**, 1329–1335.
11. M. H. Rummeli, F. Schaffel, A. Bachmatiuk, D. Adebimpe, G. Trotter, F. Bornert, A. Scott, E. Coric, M. Sparing and B. Rellinghaus, *ACS Nano*, 2010, **4**, 1146–1152.
12. N. Salah, S. S. Habib, Z. H. Khan, A. Memic and M. N. Nahas, *Digest Journal of. Nanomaterials Biostructures*, 2012, **7**, 1279–1288.
13. O. M. Dunens, K. J. McKenzie and A. T. Harris, *Environmental Science. and Technology*, 2009, **43**, 7889–7894.

14. G. Ordorica-Garcia, M. Nikoo, M. Carbo and I. Bolea, *Journal of Petroleum. Technology*, 2012, **51**, 362–375.
15. M. Motiei, Y. R. Hacohen, J. Calderon-Moreno and A. Gedanken, *Journal of American Chemical Society.*, 2001, **123**, 8624–8625.
16. Z. Lou, Q. Chen, W. Wang and Y. Zhang, *Carbon*, 2003, **41**, 3063–3067.
17. Z. Lou, C. Chen, H. Huang and D. Zhao, *Diamond and Related. Materials*, 2006, **15**, 1540–1543.
18. X.-J. Xu and S.-M. Huang, *Materials. Letters*, 2007, **61**, 4235–4237.
19. A. Magrez, J. W. Seo, V. L. Kuznetsov and L. Forró, *Angewandte Chemie., International Edition.*, 2007, **119**, 445–448.
20. N. Hintsho, A. Shaikjee, H. Masenda, D. Naidoo, D. Billing, P. Franklyn and S. Durbach, *Nanoscale Research. Letters*, 2014, **9**, 1–11.
21. Z. Yu, D. Chen, B. Tøtdal and A. Holmen, *Materials Chemistry Physics.*, 2005, **92**, 71–81.
22. A. V. Melechko, V. I. Merkulov, T. E. McKnight, M. Guillorn, K. L. Klein, D. H. Lowndes and M. L. Simpson, *Journal of Applied Physics*. 2005, **97**, 041301–041339.
23. D. L. Plata, E. R. Meshot, C. M. Reddy, A. J. Hart and P. M. Gschwend, *ACS Nano*, 2010, **4**, 7185–7192.
24. S. Ikeda, K. Tachi, Y. H. Ng, Y. Ikoma, T. Sakata, H. Mori, T. Harada and M. Matsumura, *Chemistry of Materials.*, 2007, **19**, 4335–4340.
25. S. K. Yadav, S. S. Mahapatra, H. J. Yoo and J. W. Cho, *Nanoscale Research Letters.*, 2011, **6**, 122.
26. P. Ayala, A. Grüneis, C. Kramberger, M. Rummeli, I. Solorzano, F. Freire Jr and T. Pichler, *Journal of Chemical Physics*, 2007, **127**, 184709.
27. G. Bepete, Z. N. Tetana, S. Lindner, M. H. Rummeli, Z. Chiguvare and N. J. Coville, *Carbon*, 2013, **52**, 316–325.
28. K. Hata, T. Yamada, K. Mizuno, M. Yumura and S. Ijima, *Science*, 2004, **306**, 1362.
29. K. Mackenzie, O. Dunens and A. Harris, *Industrial Engineering Chemistry Research*, 2010, **49**, 5323–5338.

Chapter 7: Comparison of Grootvlei and Duvha coal fly ash and testing their tensile strength.

7.1 Introduction

The CVD method has been extensively used in the synthesis of carbon nanofibres (CNFs). Other methods, such as laser ablation, arc discharge and more recently, electrospinning have also been used. When CNFs are grown in a fluidised bed reactor, CNMs have been shown to be low cost¹. Thus far there has been one study that has reported on the use of fly ash as a catalyst to make CNFs¹¹. Three other studies, reported on the synthesis of CNTs from treated or impregnated coal fly ash^{2,3,14}. This difference could be due to the fly ash composition as South African coal fly ashes are mostly produced from bituminous coals (Table S7.1).

CNFs derived from pure catalysts have been used in many applications, such as catalysis, biomedical and more recently, composite materials. In this study, we have focused on their use in composites, where they were used as reinforcing fillers since they have been shown to have a high potential to improve the mechanical properties of polymers¹². Compared to other fibres, carbon nanofibres have many superior properties such as low weight, high elastic moduli and a high fracture strain. Work presented by Bikiaris *et al*, showed that the strength of carbon fibres increased as the diameter of the fibres decreased⁴.

Carbon nanotubes (CNTs) have generally been used as ideal fillers for polymers. This is due to them possessing excellent mechanical strength as high as 1TPa tensile modulus⁵. Typical mechanical properties of CNTs are given in Table 7.1. However, their high cost and difficulty in dispersing in the polymer matrix have reduced their widespread use as reinforcement fillers⁶. However, CNFs that are grown from waste material and used as received, present a more economical option than CNTs derived from expensive catalyst.

Table 7. 1: Mechanical properties of CNTs ⁸

Property	SWNT	DWNT	MWNT
Typical Diameters (nm)	1	4-6	20-25
Density (g/cm ³)	1.2-1.5	1.5	1.6-2.0
Elastic modulus (TPa)	0.9-1	0.6-1	0.3-1
Tensile strength (GPa)	100-600	25-65	15-75
Elongation at break (%)	5.5	30	

CNFs promise to transform many fields in material science, and have been shown to be a major component in nanotechnology due to their high tensile strength, modulus and relatively low cost⁶. CNFs are therefore, attracting major attention for potential applications in a variety of applications such as aerospace, chemical, medicinal and automobile industries⁶.

There has been a lot of interest in the composite industry and these can be found in a recent review by Mitall *et al.* where they discussed the role of CNTs and graphene as fillers in reinforced polymer nanocomposites⁶. Though there has been extensive research in the field, there are limited studies on CNT/polyester composites in literature. To mention a few, Muthu *et al.* used reinforced polyester nanocomposites to improve the dispersion and mechanical properties of polyester⁸. Different functionalised CNT loadings were added to the polymer and to obtain an optimal loading and improve the dispersion of the filler within the polymer matrix. Their results showed that the highest tensile strength was achieved at 1% loading. Shokrieh *et al.* also tested the mechanical properties of polyester nanocomposites reinforced with MWCNTs⁹. Their results showed an improvement of the tensile and flexural strength. A low loading of CNFs (0.05%) was enough to give a 20% ultimate tensile strength improvement.

Of the above studies, none have reported on the use of CNFs to improve the strength of a polyester. Here, we report the comparison of two different fly ashes

as catalysts for CNF synthesis. Based on the products formed, the one with better mechanical properties was used as a filler to improve the strength of polyester composites. It was then used to examine a loading (0.125, 0.25 and 0.5 %) at which the highest tensile strength be obtained.

7.2. Experimental

7.2.1 Materials

The gases used (hydrogen and acetylene) in the synthesis of CNFs were purchased from Afrox, South Africa. Synthesized CNFs were used as fillers for the polymer composites. Luperox curing agent and polyester resin (GP-LAM 40) matrix were bought from AMT composites, RSA. The density of the polymer at room temperature was 1.155 g/cm^3 as supplied by the manufacture. NCS Waxol (NCS, RSA) was used to polish the mold surface to ensure a clean surface before lamination. AMR8 release agent (AMT, RSA) was applied on the steel mould for easy removal of the finished components. All the reagents used were of analytical grade.

7.2.2 Synthesis of CNFs

CNFs were synthesised from fly ash produced from two different power stations, namely, Duvha and Grootvlei. For the CNF synthesis, carbon deposition was achieved through CVD of acetylene over the fly ash. The synthesis was done as described in Section 3.3.1, except that the flow rate was kept constant at 100 ml/min, with the reaction time adjusted to 45 min and the temperature used was changed to $650 \text{ }^\circ\text{C}$ for both reactions.

7.2.3 Characterisation of CNFs

To identify the metals and the quantities contained in a Duvha and Grootvlei coal fly ashes, X-ray fluorescence (XRF) spectroscopy was employed using a method described in Section 3.4.8. The as-received fly ash and synthesized CNF samples were characterized using scanning electron microscopy (SEM), thermogravimetric analysis (TGA) and Laser Raman spectroscopy. For each characterisation,

procedures described in Section 3.4.1, 3.4.5 and 3.4.6 respectively were followed. Nanofibre diameter distributions were measured using Image J¹³.

7.2.4 Fibre composite fabrication procedure

CNF/polyester composites were manufactured using the Vacuum Resin Transfer Moulding (VRTM) method as described in Section 3.5. Briefly, the fibre composites (FCs) specimens were fabricated with different fibre mass fractions of 0.125, 0.25 and 0.5% for all the untreated CNFs.

7.2.5 Mechanical Characterisation of CNFs

The CNF/polyester nanocomposites were tested to determine the mechanical properties of these materials. The tensile specimens were fabricated based on ASTM D638- 08: 2010. The tensile testing procedure was performed as described in Sections 3.6.1.1.

7.3 Results and discussion

7.3.1. XRF analyses

XRF analysis identified the elements contained in the Grootvlei and Duvha coal fly ashes and their quantities. Figure 7.1 shows that Al_2O_3 and SiO_2 are the most dominant phases and account for more than 80% of the materials. FeO and CaO could also be identified and combined; they constitute more than > 15% of the ash. The rest of the compounds, namely, Fe_2O_3 , MgO, MnO, TiO, NiO, Na_2O , P_2O_5 , Cr_2O_3 , account for < 5% of the two fly ashes. Based on these compositions, both these ashes can thus be classified as class F fly ashes, as they contain less than 10% of lime (CaO)⁹. This type of ash comes generally from the burning of harder, older anthracite and bituminous coal¹⁷. The compounds of interest in our study were the FeO and Fe_2O_3 species that had been previously identified as the elements responsible for CNF synthesis in our previous study¹¹. Therefore, the question arises: will the morphology and 5 % difference in the iron contents of these ashes affect the yield, morphology and properties of the CNFs formed from the ash?

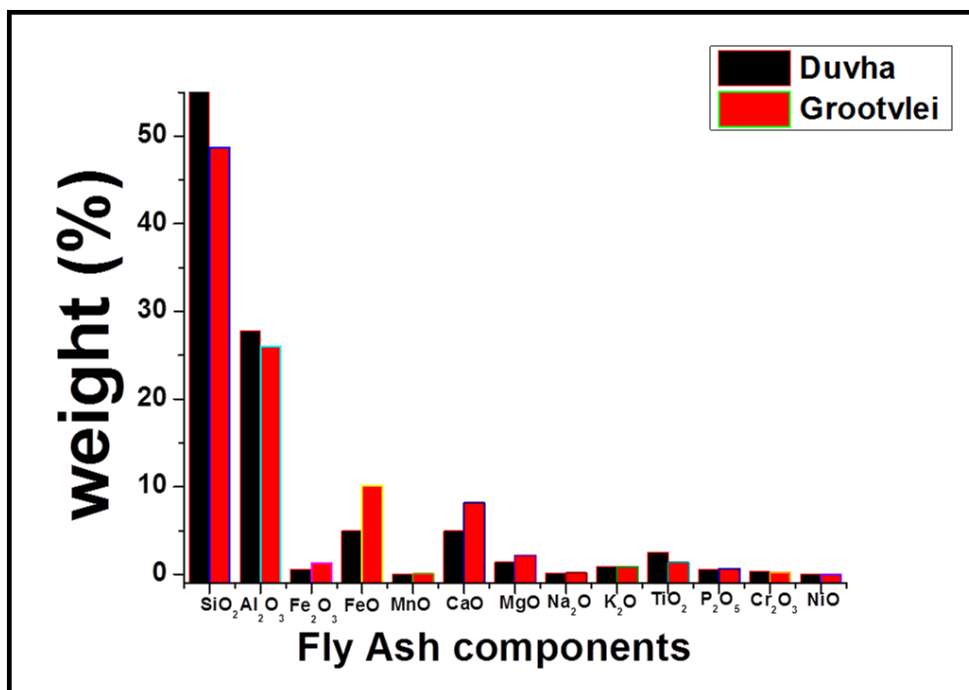


Figure 7.1: XRF analyses of Duvha and Grootvlei coal fly ash components

7.3.2 Morphological and Product yield Studies

Under SEM observation, the as-received fly ash materials (Fig. 7.3a-b) appeared to be spherically shaped which may be due to inter-particulate fusion during the cooling of the fly ash¹¹. In Fig. 7.3a, Duvha ash was observed to have a smooth surface with a mixture of mostly spherically shaped particles. Grootvlei ash (Fig.7.3b), had a rough surface and the fused material had the appearance of amorphous carbon. The smooth surface could be due to the glassy phase covering the surface¹⁷. As demonstrated by Fig 7.3c, CNFs synthesized from Duvha fly ash showed long isolated fibres with the structure remaining uniform and unchanged as can be seen under SEM. On the other hand, CNFs synthesized from Grootvlei fly ash formed a mixture of short, long, thick and thin fibres.

The product yield of these CNFs was very high compared to the previously reported yield (Chapter 5, Fig 5.1) of other ashes obtained from Roscheville fly ash at the same temperatures. CNFs synthesized from Grootvlei ash gave close to a 400% yield (Fig.7.2) while those from Duvha fly ash showed more than 300% yield. Size diameters of as-received fly ashes from Duvha and Grootvlei were found to be between 2-100 μm and $> 100 \mu\text{m}$ respectively. According to Shao *et.*

al., these CNF can be described as hollow cenosphere or non-crystalline glass beads since these microspheres are between 30 and 100 μm^{18} . Using Image J, CNFs from Duvha and Grootvlei ashes were found to have an average diameter distribution of 50-70 nm and 30-465 nm, respectively.

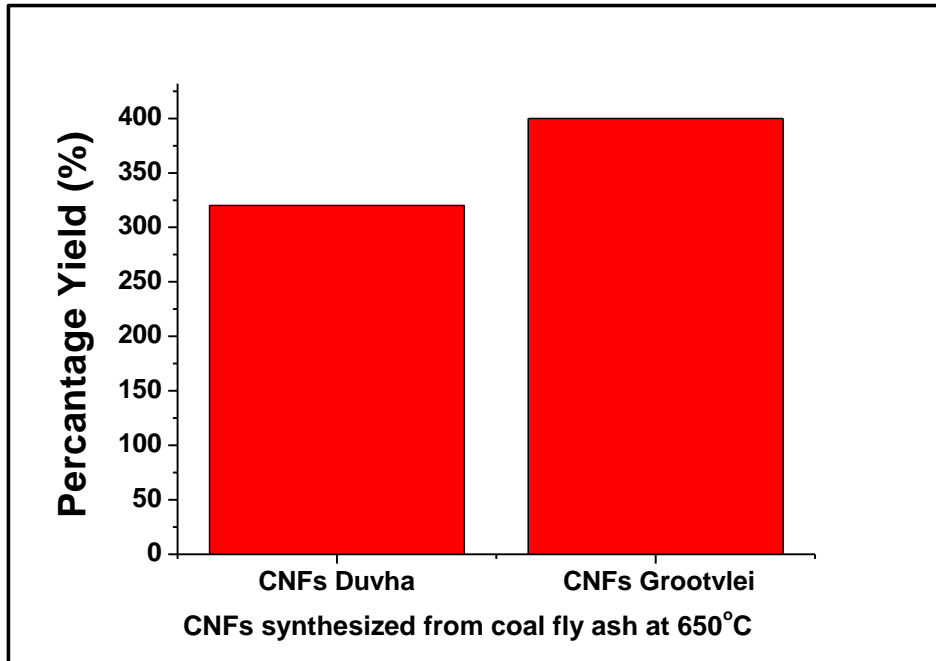


Figure 7.2: Percentage yield of CNFs formed from coal fly ashes from Duvha and Grootvlei

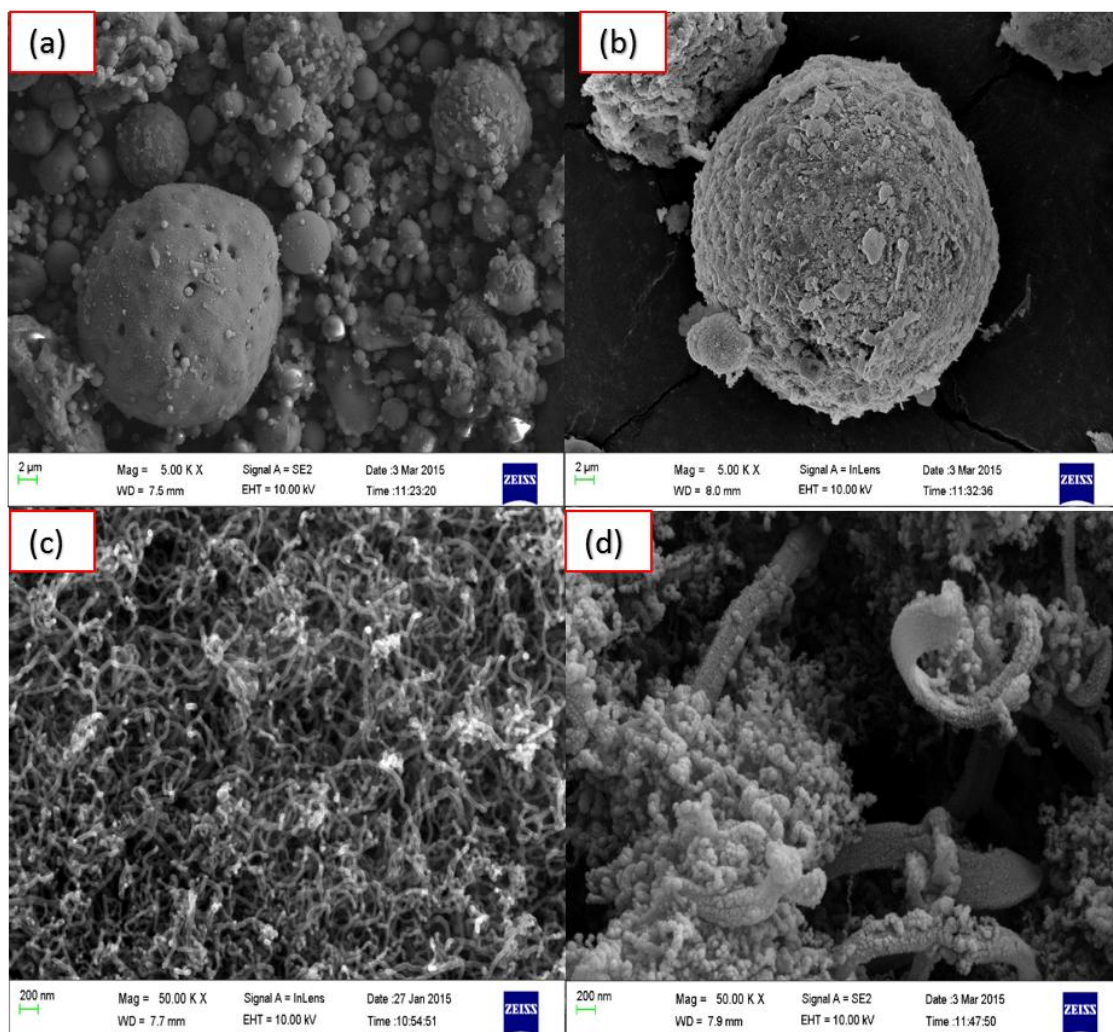


Figure 7.3: (a) SEM micrographs of CNFs produced from fly ash (a) Duvha fly ash (b) Grootvlei ash, (c) CNFs from Duvha ash and (d) CNFs from Grootvlei ash.

7.3.3. Graphiticity and thermal stability studies

To further assess the quality of the CNFs formed and their thermal stability, laser Raman spectroscopy and thermogravimetric analysis was used, respectively. For both sets of CNFs, peaks at 1350 cm^{-1} and 1590 cm^{-1} were observed and the intensity ratio of these peaks, known as the D-band (due to disordered carbon features) and G-band (due to the ordered graphitic carbon features) respectively, represents the degree of graphitization of carbon in the reaction products⁵. As Fig. 7.4a shows, the disordered carbonaceous nature of the CNFs was very high with a more prevalent D band. As Fig. 7.4b shows, CNF from Duvha were the most

graphitic as was shown by the low I_D/I_G ratio of 1.18 compared to CNFs from Grootvlei. The difference in the thermal stability between these CNFs was minimal, with the CNFs from Duvha slightly more stable as shown by the higher decomposition temperature. This result fully agrees with the previously reported studies where it was shown that the more graphitic the material, the higher the decomposition temperature. There was also an 8% difference in the amount of unburnt fly ash, as CNFs from Duvha ash had a 30% residual catalyst while CNFs from Grootvlei ash had a 22% residual catalyst. This could be attributed to the 8% ($\text{SiO}_2 + \text{Al}_2\text{O}_3$) difference from the original fly ash catalysts as was shown by XRF (Fig. 7.1).

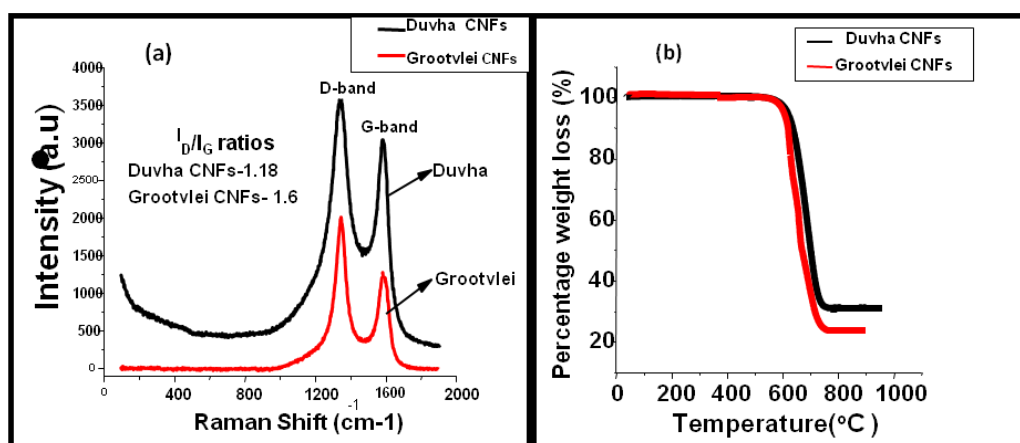


Figure 7.4: (a) Laser Raman spectroscopy spectra and (b) thermogravimetric analysis of spectra of CNFs produced from fly ash synthesized at 650 °C

Comparing the two fly ashes (Duvha versus Grootvlei), Grootvlei produced the highest yield of fibres of various shapes and sizes. This high yield could be due to the higher iron content as was seen from XRF analyses (Fig.7.1). Even though CNFs produced from Duvha ash had a lower yield, they had better properties. They formed uniform diameters (50-70 nm), were more graphitic and more stable fibres. Also from TGA, the clean burning of the fibres from Duvha ash between 600-650 °C, is highly indicative of the uniform type of carbon deposits. Due to these observations, the succeeding studies were conducted using CNFs from Duvha ash.

7.3.8 Evaluation of Tensile Strength

Using CNFs synthesized from Duvha fly ash, a number of nanocomposite (CNFs/polyester) specimens of various weight fractions (0.125, 0.25, and 0.5%) were tested to obtain the tensile mechanical properties. Fig. 7.5a-b shows the ultimate tensile strength and Young's modulus of the different samples tested. The figure shows that the tensile strength increased as the CNF loading increased (from 0.125 to 0.25%). At higher loadings (0.5%), there was a decrease in the tensile strength. The results show that increasing the amount of filler content increased the tensile strength, which reached a peak at 0.25% and subsequently decreased thereafter. This ultimate tensile strength is attributed to a good dispersion of the CNFs (Fig 7.6c) within the polyester matrix. Fig. 7.7a-d shows the fracture surface of samples at 0.0, 0.125, 0.25 and 0.5% CNF contents. As can be seen in Fig. 7.6a, the fracture of neat polyester is much smoother than the fracture surfaces of composites indicating a typical brittle nature of the polyester. Fig. 7.6b, c and d show rougher surfaces which are caused by the addition of CNFs particles which enhance the defects and if not properly distributed, result in the material becoming more brittle. This decrease in the tensile strength at 0.5% loading may have been caused by the agglomeration (Fig 7.6d). This agglomeration of CNFs causes stress concentration, resulting in the sample to fail at lower stresses and this decreases the mechanical properties of the nanocomposites. These results concur with the previously reported results by Muthu and Paskaramoorthy and Shrokieh *et al.* where they used CNFs from pure catalysts and found that where there is agglomeration, the samples quickly fail^{8,9}. Their optimum loadings though, were 0.1% and 0.5% respectively, which was different from the optimum loading (0.25%) in this study. That may be due to the type of filler that were used in their studies, as there were MWCNT, DWCNTs and CNFs in the Muthu study.

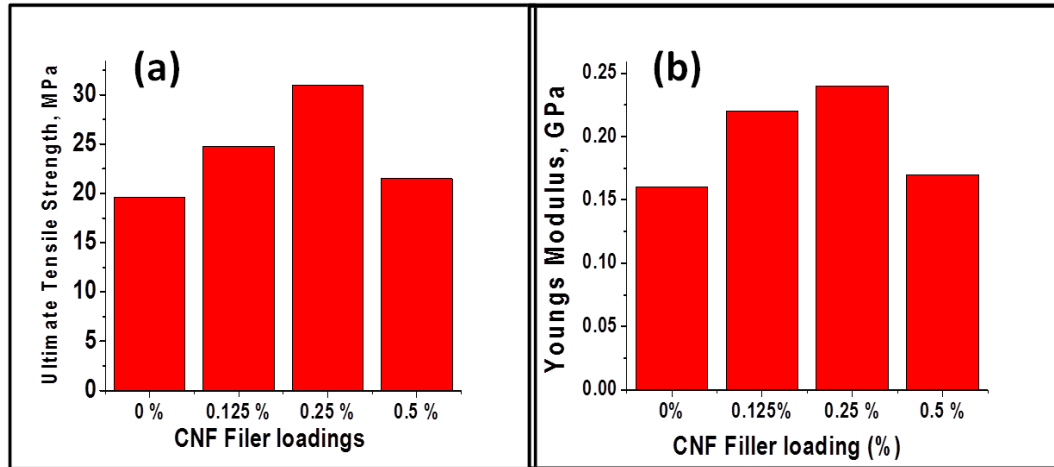


Figure 7.5: (a) Tensile strength and (b) Young's Modulus of untreated and acid treated polyester composites

Shokrieh *et al.* suggested that increasing the sonication time or output may assist with the better dispersion of the CNM filler at high loadings within the polyester matrix⁸. Although this may be the case, other studies have shown that even though sonication might lead to better dispersion, agglomerates might still be there⁵. Also, there is a high possibility of reducing the CNF length of which if it is too long, might result in poor mechanical properties such as tensile strength. We suggest the use of oxidative treatments to assist with the bonding between the filler and matrix. Several authors have shown that if you change the CNM surface from hydrophobic to a hydrophilic state, the interaction of the CNMs and polymer matrix becomes easier¹⁸. Additionally, because HCl/HNO₃ has been shown to have a cleaning effect on the removal of impurities from carbon nanomaterials, this might have an enhanced effect, thus increasing the mechanical properties even more.

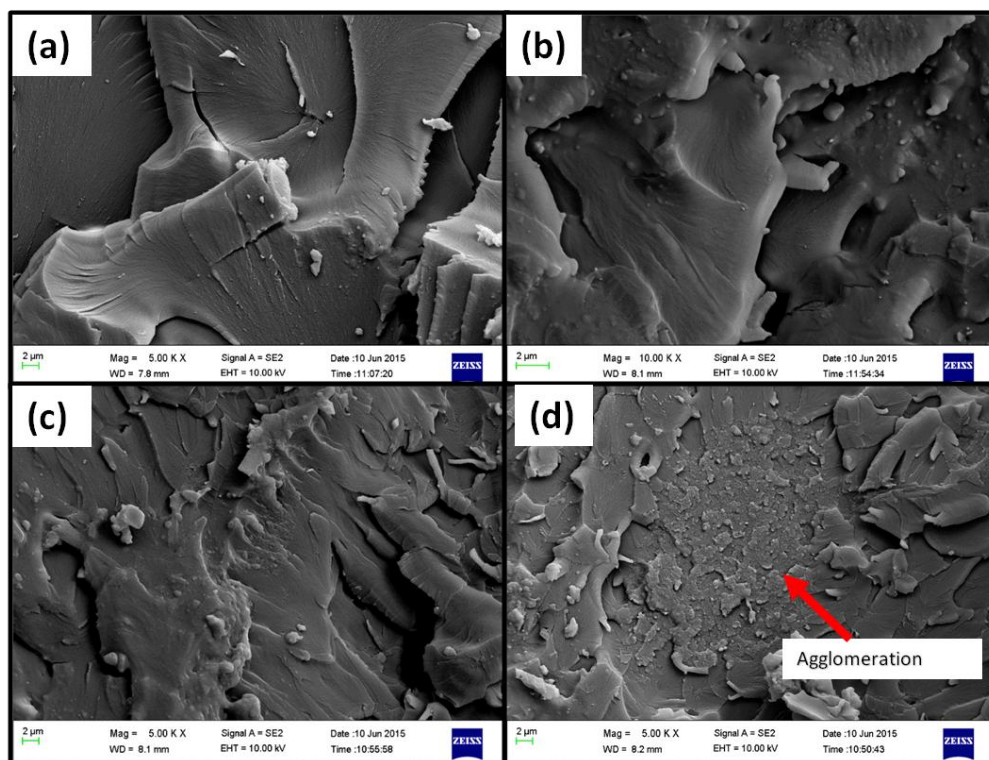


Figure 7.6: SEM images of fractured specimens (a) Neat polyester, (b) 0.125% CNFs, (c) 0.25% CNF and (d) 0.5% CNF loading

7.4. Conclusions

A comparison between Duvha fly ash and Grootvlei fly ash for the synthesis of CNFs was done to see if the morphology of these ashes will have an effect on the CNMs formed. CNFs from Grootvlei produced the highest yield and purity but compared to CNFs from Duvha they were not uniform in terms of their diameter sizes. The Grootvlei CNFs were found to be highly disordered and had a decreased thermal stability. Based on these findings, mechanical tensile strength tests were done using CNFs synthesized from Duvha fly ash. Different loadings of CNFs synthesized from Duvha fly ash were added to the polyester matrix and a 0.25% loading was found to give the highest tensile strength. At higher loadings, agglomeration was observed. This may be avoided through the use of sonication when mixing the filler and the matrix. Oxidative treatment of CNFs was also suggested to assist with the interaction between the CNFs and polymer matrix, which in turn will assist in enhancing the mechanical properties of these composites.

7.5 References

1. J. Kong, A. Cassel and A. Dai, *Chemica. Physics Letters*, 1998, **292**, 567-574.
2. A. Yasui, Y. Kamiya, S. Sugiyama, S. Ono, H. Noda and Y. Ichikawa, *IEEJ Transactions on Electrical and Electronic Engineering*, 2009, **4**, 787-789
3. N. Salah, S.S Habib, Z.H. Khan, A. Memic and M.N. Nahas . *Digest. Journal. Nanomaterial. Biostructures*. 2012, **7**, 1279-1285.
4. D. Bikiaris, A. Vassiliou, K. Chrissafis, K. Paraskevopoulos, A. Jannakoudakis and A. Docoslis, *Polymer. Degradation. and Stability* 2008, **93**, 952-967.
5. P. M. Ajayan, L. S. Schadler, C. Giannaris and A. Rubio, *Advanced. Materials*. 2000, **12**, 750-753.
6. G. Mittal, V. Dhand, K. Y. Rhee, S.-J. Park and W. R. Lee, *Journal. of Industrial. and Engineering Chemistry*. 2015, **21**, 11-25.
7. A. T. Seyhan, M. Tanoğlu and K. Schulte, *Material. Science. and Engineering: A*. 2009, **523**, 85-92.
8. S. J. Muthu and R. Paskaramoorthy, *Polymer Composites*.2012, **33** 866-871.
9. M. M. Shokrieh, A. Saeedi and M. Chitsazzadeh, *Journal of Nanostructures. in Chemistry*. 2013, **3**, 1-5.
10. M. Murarescu, D. Dima, G. Andrei and A. Circiumaru, *Digest. Journal. of Nanomaterials. and Biostructures*. 2014, **9**, 653-665.
11. N. Hintsho, A. Shaikjee, H. Masenda, D. Naidoo, D. Billing, P. Franklyn and S. Durbach, *Nanoscale Ressearch letters*.2014, **9**,1-11.
12. N. Hintsho, A. Shaikjee, P. K. Tripathi, P. Franklyn and S. Durbach, *RSC Advances*. 2015, **5**, 53776-53781.
13. W. Rasband, *National Institutes of Health: Bethesda, MD, USA*, 1997, 2012.

14. O. M. Dunens, K. J. MacKenzie and A. T. Harris, *Environmental Science & Technology*. 2009, **43**, 7889-7894.
15. F. H. Gojny, J. Nastalczyk, Z. Roslaniec and K. Schulte, *Chemical Physics letters*. 2003, **370**, 820-824.
16. M. J. Palmeri, K. W. Putz and L. C. Brinson, *ACS Nano* 2010, **4**, 4256-4264.
17. N. M. Musyoka, MSc Thesis, *University of the Western Cape*; 2009.
18. J. Shao, Z. Wang, H. Li, X. Shao, *Proceedings of the 14th International Pittsburgh Coal Conference*, 1997.

Chapter 8: Mechanical Testing of polyester nanocomposites using treated CNMs produced from Duvha fly ash

8.1 Introduction

Carbon nanoparticles have recently gained recognition in science and industry due to their unique properties they possess. In recent years carbon nanomaterials (CNMs) have been used in various applications due to their excellent physical, chemical and mechanical properties¹. Particular interest has been given to composite materials where CNMs are added as a reinforcement to improve the mechanical properties of polymer materials². One of the benefits of using these CNMs, when used as a filler, is their high aspect ratio which can be as high as 1000, which can induce better adhesion with the polymer matrix. Adhesion is an important factor for effective enhancement of the nanocomposites properties³. A high aspect ratio results in the percolation of the fillers at very low concentration and makes them attractive for use in a broad spectrum of applications, especially as reinforcing fibres in nanocomposites⁴.

To achieve maximum enhancement of most of the nanocomposites properties, the interfacial adhesion and the dispersion of the CNMs should be homogeneous in the polymer matrix, which means that the surface interaction between the filler and matrix needs to be optimised⁵. As CNMs can be made quite long with significant accumulated van de Waals forces, these CNMs tend to entangle, resulting in agglomerates in the polymer matrices⁶. To increase the interfacial bond between the polymer and CNMs, surface modification of the CNMs has to be considered. One method of doing this is by covalent modification, which involves the use of attaching reactive groups by treating the CNMs with acids^{7,8}. This treatment normally leads to the shortening of the CNM's length and formation of surface reactive groups such as hydroxyl, carbonyl and carboxylic groups^{6,9}.

Ajayan and collaborators were the first to report on a CNT/polymer composite¹⁰. Thereafter there was extensive research in the field and these results can be found in a recent review¹¹. In this review the focus was on the use of CNTs and graphene as carbon nanofillers to improve the strength of different kinds of polymers. Factors such as CNT shape, dispersion, size and alignment were shown to be of high importance as they played a major role in enhancing the mechanical properties of polymer nanocomposites. Although many polymers have been tried, there are only a few reported studies on CNM/polyester composites in literature¹²⁻¹⁵.

Seyhan *et al.* tested the tensile mechanical behaviour of MWCNT and DWCNT modified vinyl ester polyester hybrid composite¹². Muthu *et al.* used reinforced polyester nanocomposites to improve dispersion and mechanical properties¹³. They found that functionalisation drastically improved the mechanical properties of the nanocomposites. Shokrieh *et al.* tested the mechanical properties of polyester nanocomposites reinforced with MWCNT¹⁶. Their mechanical test results showed an improvement of the tensile and flexural strengths. In a recent study Murasescu *et al.* investigated the synthesis of polyester composites functionalised with carbon nanotubes by oxidative reactions and chemical deposition¹⁴. A three point bending test was performed which assisted in identifying the suitable method for functionalisation in order to obtain a good dispersion of CNTs into a saturated polyester matrix.

Of the above studies none have reported on the use of CNFs to improve the strength of polyester. This chapter highlights the effects of treating CNFs using various treatments to improve the interfacial adhesion between the filler and matrix. Tensile, flexural and impact tests were conducted to obtain the mechanical properties of the polyester nanocomposites.

8.2 Experimental

8.2.1 Materials

The gases used (hydrogen and acetylene) in the synthesis of CNFs were purchased from Afrox. Synthesized CNFs were used as fillers for the polymer composite. Luperox curing agent and polyester resin (GP-LAM 40) matrix were purchased from AMT composites. The density of the polymer at room temperature was 1.155 g/cm^3 as indicated by the supplier. NCS Waxol was used to polish the surface to ensure a clean surface before lamination. AMR8 release agent was applied on the vacuum resin assisted mould (VRTM) for easy removal of the finished components. All the reagents used were of analytical grade.

8.2.2 Synthesis of CNFs

CNFs were synthesised using coal fly ash produced from Duvha power station. For these syntheses, carbon deposition was achieved through chemical vapour deposition of acetylene over waste fly ash. The synthesis procedure followed was described in Section 3.3.1, except the flow rate was kept constant at 100 ml/min, reaction time to 45 min and the temperature used was $650 \text{ }^\circ\text{C}$ this reaction.

8.2.3 Functionalisation of CNFs

The CNFs formed were functionalized using KMnO_4 and HCl/HNO_3 respectively. For each treatment, 4 g of the CNFs was used. The CNFs were functionalised before blending with the polyester. For the KMnO_4 and HCl/HNO_3 , treatment, the procedures that were followed were described in Section 3.3.2.1 and 3.3.2.2 respectively.

8.2.4 Characterisation of CNFs

The synthesized CNFs samples were characterized using scanning electron microscopy (SEM), Thermogravimetric analysis (TGA), laser Raman spectroscopy and X-ray diffraction (XRD). For each characterisation, procedures described in Section 3.4.1, 3.4.5 and 3.4.6 respectively were followed. Nanofibre diameter distributions were measured using Image J⁵. To identify the added oxygen groups and their effect on the surface area, Fourier transform infrared (FTIR) spectroscopy and Brunner-Emmet Teller (BET) method were employed as described in Sections 3.4.4 and 3.4.3 respectively.

8.2.5 Fibre composite fabrication and testing procedure

CNF/polyester composites were manufactured using the Vacuum Resin Transfer Moulding (VRTM) method. The fibre composite (FCs) specimens were fabricated with the same fibre mass fractions of 0.25% for all the different treated CNFs.

The CNF/polyester nanocomposites were tested to determine the mechanical properties of these materials. The tensile, flexural and impact test specimens were fabricated based on ASTM D638- 08: 2010, ASTM D790- 07: 2010 and ASTM D256- 06a: 2010 respectively. The testing procedures followed were described in Section 3.6.1.1., 3.6.1.2 and 3.6.1.3 correspondingly. The tensile, flexural and impact specimens are shown in Figure 3:S1, S2 and S3.

8.3 Results and discussion

8.3.1 N₂ Physisorption

The N₂ physisorption data for untreated and oxidised carbon nanofibres are presented in Table 8.1. Untreated CNFs were found to have a surface area of 22.5 m²g⁻¹ and a pore volume of 0.20 cm³g. The average pore diameter was about 21.3 nm and no micropores were present.

Table8. 1: N₂ Physisorption data of untreated and acid oxidized CNFs

Materials	Surface Area (m²g⁻¹)	Pore Volume (cm³/g)	Pore diameter (nm)
CNFs	37.35	0.20	21.31
KMnO₄	42.36	0.22	22.48
HCl/HNO₃	22.93	0.13	22.77

Upon oxidation in KMnO₄, there was a change in the pore diameter and no micropores were formed. However a slight increase in the surface area and pore volume was observed. This could be due to the microstructure rough surface, thus resulting in a high pore volume. In contrast, with the HCl/HNO₃ treatment, there was a decrease in the surface area, pore volume and average pore diameter. Oxidation in these strong acids probably resulted in changes in the

macrostructure, the fibres probably broke or some were completely removed. To confirm these findings, morphological studies were carried out.

8.3.2 Morphological Studies

Untreated CNFs from Duvha showed long isolated fibres with the structure remaining uniform and unchanged as can be seen under SEM. After acid treatment with both HCl/HNO₃ and KMnO₄, the length of the CNFs became slightly shorter and less ordered. CNFs treated with KMnO₄ further went on to show some surface roughness as well, and this explains why there was an increase in the surface area (Table 8.1). CNFs treated with HCl/HNO₃ looked clean and the structure was still intact. CNF diameters of untreated CNFs were found to have an average distribution of 50-70 nm. Upon oxidation the fibre sizes became thicker, in KMnO₄ and HCl/HNO₃ average size diameters distribution of 40-240 nm and 40-200 nm were measured respectively.

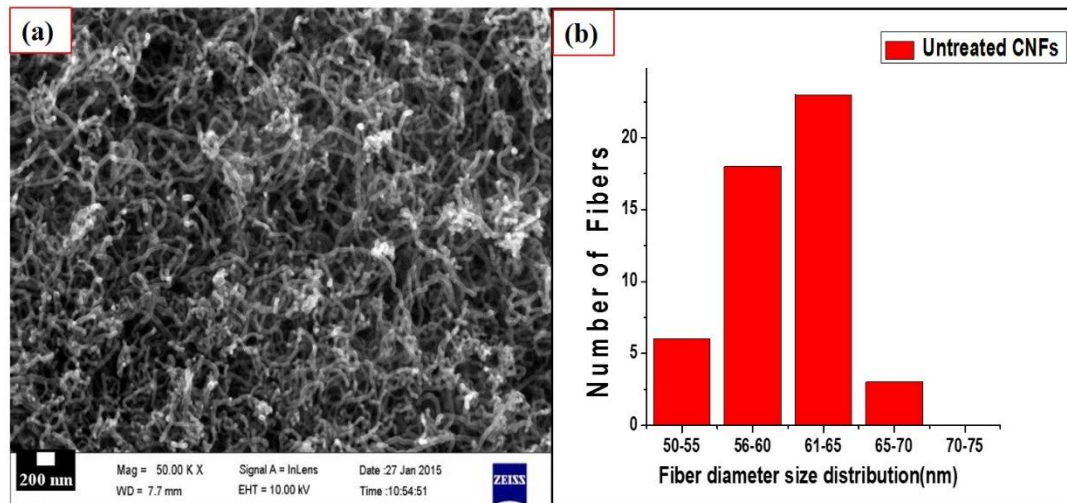


Figure 8.1: (a) SEM micrographs of CNFs produced from fly ash and (b) Fibre diameter size distribution of CNFs at 650 °C respectively

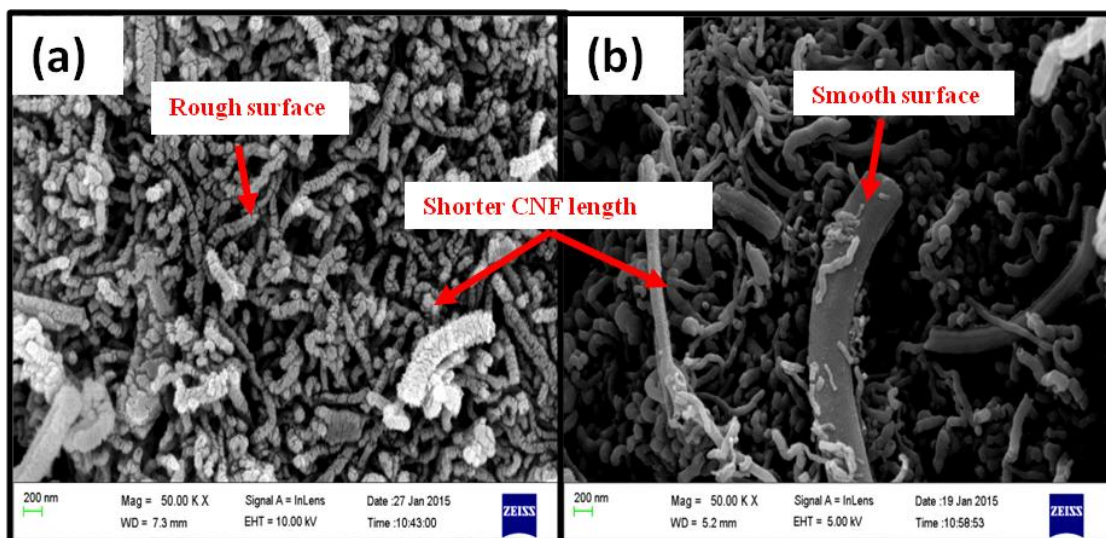


Figure 8.2: a) SEM micrographs of CNFs produced from fly ash treated with (a) KMnO_4 and (b) HCl/HNO_3

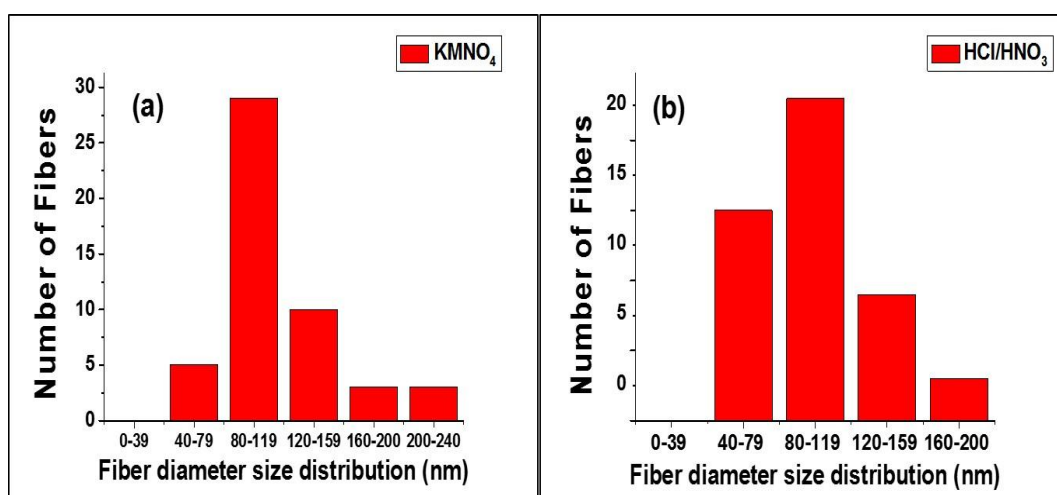


Figure 8.3: Fibre size distributions of CNFs produced from fly ash synthesized at 650 °C, treated with (a) KMnO_4 and (b) HCl/HNO_3

8.3.3 Graphicity studies

To further assess the quality of the CNFs and confirm their formation, laser Raman spectroscopy was used. Raman spectroscopy is an effective technique that gives information about the graphitic and defective nature of CNFs that are formed. Fig. 8.4a-b shows CNFs formed from fly ash and treated with KMnO_4 and HCl/HNO_3 respectively.

As expected, the spectrum of the CNFs from Duvha fly ash, peaks at 1350 cm^{-1} and 1590 cm^{-1} were observed. The intensity ratio of these peaks, known as the D-band (due to disordered carbon features) and G-band (due to the ordered graphitic carbon features) respectively, represents the degree of graphitization of carbon in the reaction products⁵. As can be seen, the intensity of the untreated CNFs was very high with the D band more prevalent. In the presence of KMnO_4 , the CNF structure looked completely destroyed (Fig 8.4a). Upon increasing the magnification (Fig. 8.4b) could one notice there was a peak at the D region (1320cm^{-1}). A peak at around 600 cm^{-1} was also identified, which could be attributed to residual KMnO_4 . Upon treatment with HCl/HNO_3 , the intensity decreased and there was shift in the graphitic nature of the CNFs. The CNFs became more graphitic and this was shown by the higher I_G/I_D ratio of >1 .

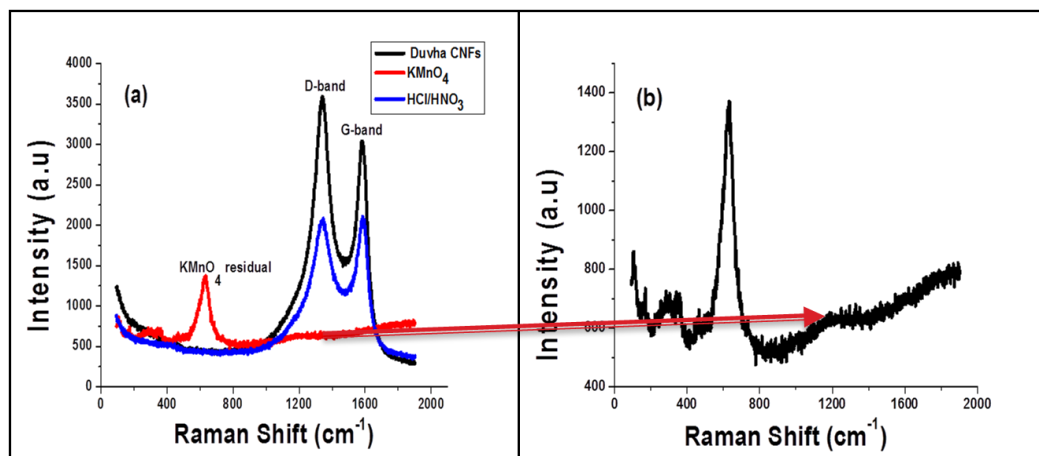


Figure 8.4: Laser Raman spectroscopy spectra of CNFs produced from fly ash, synthesized at $650\text{ }^{\circ}\text{C}$ and treated with (a) KMnO_4 and HCl/HNO_3 (b) enlarged view of the CNFs treated with KMnO_4

8.3.4 Powder X-ray diffraction studies

The PXRD patterns of untreated CNFs and fibres that were treated with HCl/HNO_3 and KMnO_4 respectively are presented in Fig. 8.5. In the structure of untreated fibres, several graphite peaks can be distinguished, the strongest of which is the d (002) reflection at $2\Theta=30^{\circ}$. Further peaks can be assigned to mullite, quartz and hematite, which originate from the original growth catalyst (fly ash). In the presence of KMnO_4 , the strongest graphite peak exhibited at $2\Theta=30^{\circ}$, the width became narrow and the other peaks disappeared meaning that

the crystallinity had been destroyed and these CNFs were mostly amorphous carbon. These results are in agreement with results shown earlier with Raman spectroscopy. The acid treated CNFs with HCl/HNO₃, still exhibited all the graphite reflections, but there was a shift, slightly to the left. In addition some quartz and mullite peaks had disappeared. The absence of some of the peaks shows that acid treatment successfully removed some of the residual catalyst.

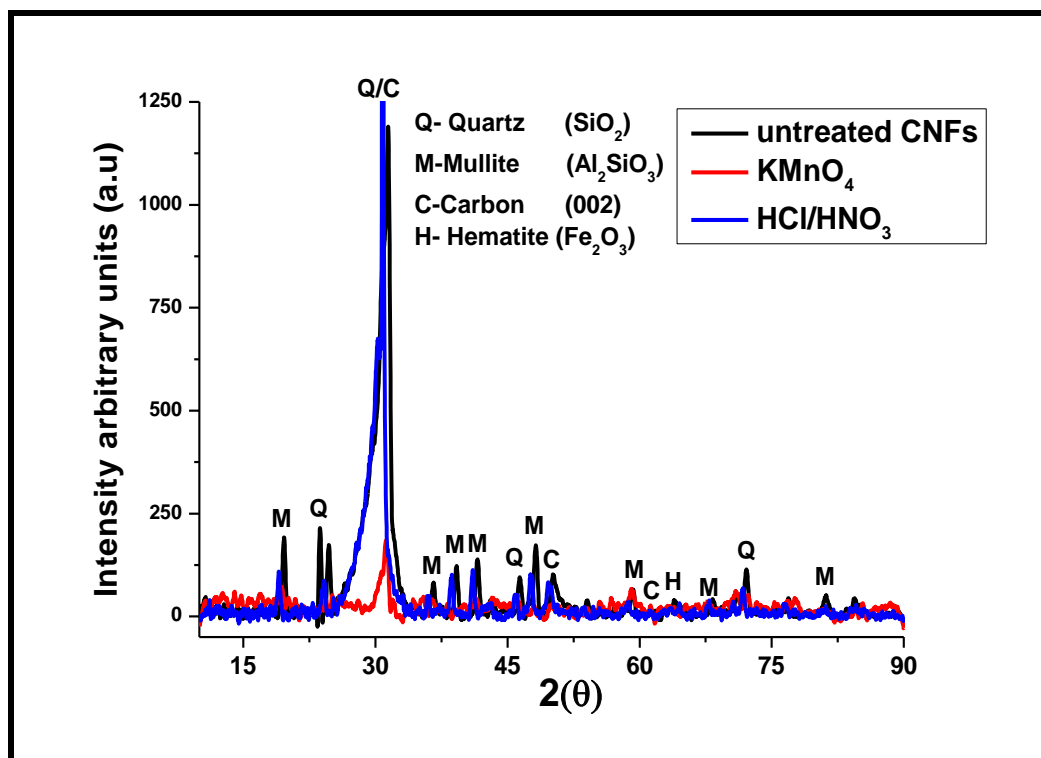


Figure 8. 5:PXRD diffractograms of CNFs produced from fly ash at 650°C and treated with KMnO₄ and HCl/HNO₃ respectively

8.3.5 Infrared spectroscopy studies

The presence of oxygen containing surface groups on the CNF was established by IR spectroscopy. For comparison purposes, the transmission levels of all spectra were kept approximately the same. Figure 8.6, shows the 2100 - 3500 cm⁻¹ region of the IR spectra of untreated and treated CNFs. All band assignments are summarized in Table 8.2 and all the changes observed in the IR spectra after the oxidative treatments. Untreated CNFs had several peaks that were observed, between 2375-2650 cm⁻¹, there was a peak exhibiting C-C bonding. CH₂/CH₃ bands were also identified at 2875 and 2916 cm⁻¹ respectively. At 3425 cm⁻¹ a

weak carboxylic band was observed. Upon oxidation in KMnO_4 a strong carboxylic band at 2375 cm^{-1} was identified and the CH_2/CH_3 bands disappeared

In the presence of HCl/HNO_3 , weaker carboxylic bands appeared, CH_2/CH_3 peaks shifted to the right and their intensities become weaker.

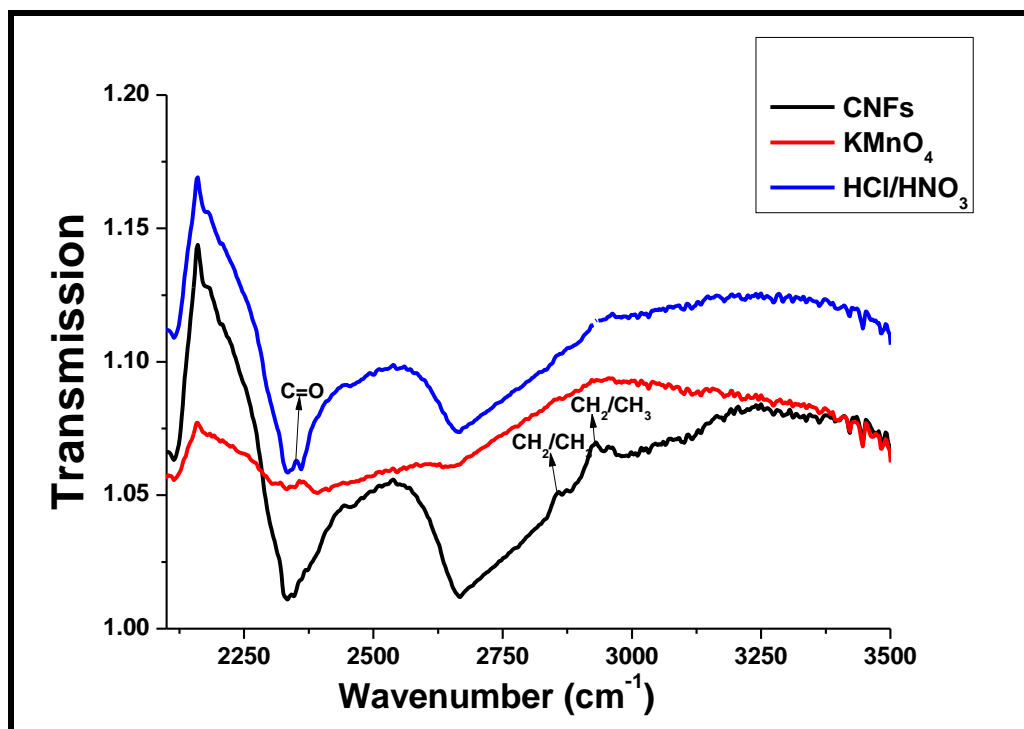


Figure8. 6: FTIR spectra of CNFs produced from fly ash synthesized at 650 °C and treated with KMnO_4 and HCl/HNO_3

Table 8.2: FTIR spectroscopy band assignment table of CNFs produced from fly ash synthesized at 650°C and treated with KMnO₄ and HCl/HNO₃

Wavenumber (cm ⁻¹)	Band assignments	CNF	KMnO ₄	HCl/HNO ₃
2350	Carboxylic (C=O)		+	+
2375-2650	C-C peak	X	-	i
2875	CH ₂ /CH ₃	X	-	s
2916	CH ₂ /CH ₃	X	-	s

Band representations: x band present, + band appears, - band disappears, i band intensity increased, d band intensity decreases, s band shift

These results have shown that functionalisation of these CNFs with KMnO₄ and HCl/HNO₃, was successful. Acid treatment was shown to be the most effective as the insertion of the carboxylic groups occurred and the structure was still maintained. This data corroborates with the SEM, Raman spectroscopy, XRD and BET data presented initially.

8.3.6 Thermal stability

To obtain additional information and confirm the thermal stability of these materials, thermogravimetric analysis was carried out to investigate the thermal degradation behaviour of untreated CNFs and acid treated CNFs. Figure 8.7a shows a typical TGA percentage weight loss profile and Fig.8.7b shows the weight derivative.

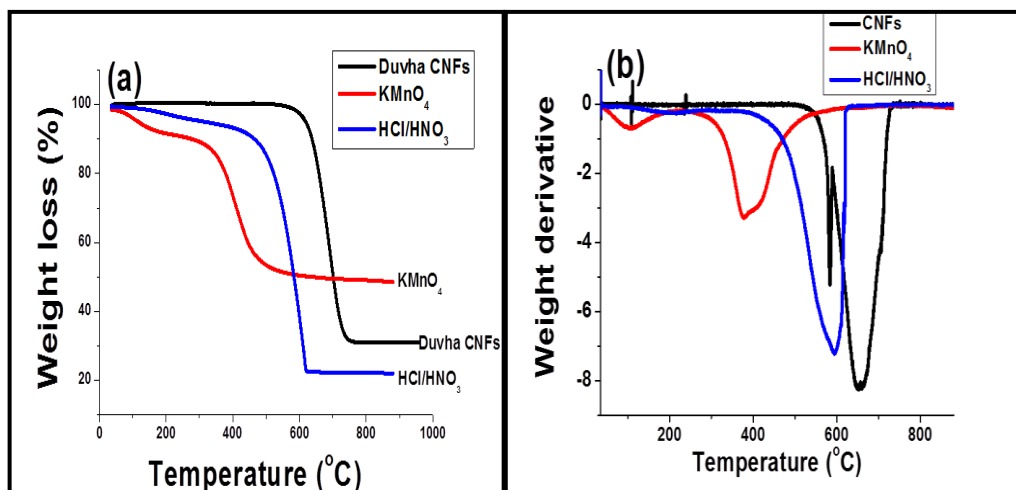


Figure 8.7:(a) Percentage Weight loss and (b) Weight derivative of CNFs produced from CNFs synthesized at 650 °C and treated with KMnO₄ and HCl/HNO₃

From the above figures it can be seen that untreated CNFs had the highest decomposition temperature, where the CNFs started decomposing at >550 °C, with a weight loss of more than 70%. There were also different forms of carbon, these could be assigned to the carbon nanofibres and amorphous carbon found in the fly ash. As can be seen in the weight loss graph, there was still a lot of fly ash catalyst (30%) that was unreacted of which amorphous carbon could come from it. Oxidising these CNFs in KMnO₄ the decomposition temperature of the CNFs was greatly reduced. Two decomposition phases were shown, the first one between 100 °C- 250 °C and the second one between 300-450 °C, these could be ascribed to the H₂O adsorbed and CO₂. In Fig 8.7b the water peak at 150 °C, could be ascribed to the loss of physisorbed water and the CO₂ peak at 375 °C may be attributed to the loss of carboxylic acid groups.

Comparing with the untreated CNFs it means that there was an increase in the oxide content in the material. This could be due to oxidative cleavage, where the carbon hydrogen bonds were broken to form a carbon oxygen bond and from the mass weight that remains of approximately 44%, one can confirm the product to be CO₂. Acid treatment of these CNFs in HCl/HNO₃ also resulted in a lower decomposition temperature as compared to untreated CNFs. One type of carbon

was formed as there were no impurities observed under the derivative weight curve as shown by one sharp peak. There was also a loss of CO₂ band as shown by the decomposition that occurred between 280-300°C. This could have been caused by the reduced oxide content on the acid treated CNFs. This can also be proven by the 20% unreacted ash that is left behind, as this shows that most of the oxides and impurities were removed from acid treatment.

8.3.7 Evaluation of Tensile Strength

A number of nanocomposite specimens were tested to obtain their mechanical properties. Figure. 8.8 shows respectively, the stress strain curve, Young's Modulus and the tensile strength of the different samples tested. As observed by the increased stress, both the Young's Modulus and tensile strength increased with the addition of untreated/raw CNFs to the neat polyester. Oxidising CNFs in KMnO₄ resulted in the decrease in the strength. This could be due to the structure collapsing as was seen in Fig.8.6 (Raman spectroscopy) and Fig.8.8 (TGA), where the G peak had completely disappeared and decomposition temperatures had decreased to lower temperatures, respectively.

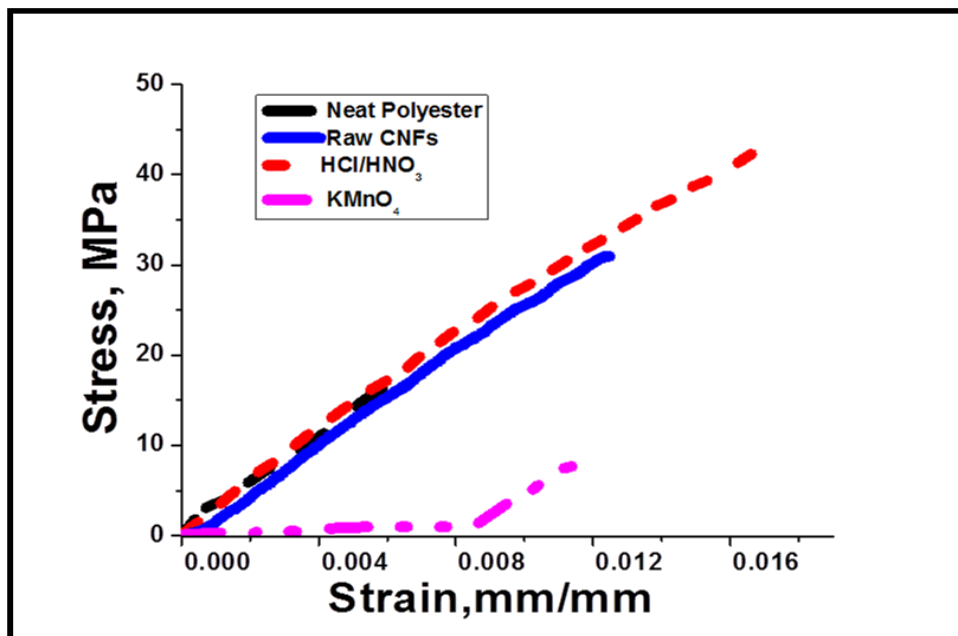


Figure 8.8: Stress vs strain graph of untreated and acid treated polyester composites

In contrast, functionalising these CNFs in acid, the tensile strength was greatly improved. These results show that acid functionalised CNFs have a greater influence on the mechanical properties than the untreated CNFs. The reason for the significant increase could be attributed to the improved dispersion of these CNFs within the matrix. In addition the functionalized groups on the surface of the CNTs may have promoted a strong chemical interaction between the CNFs and the matrix.

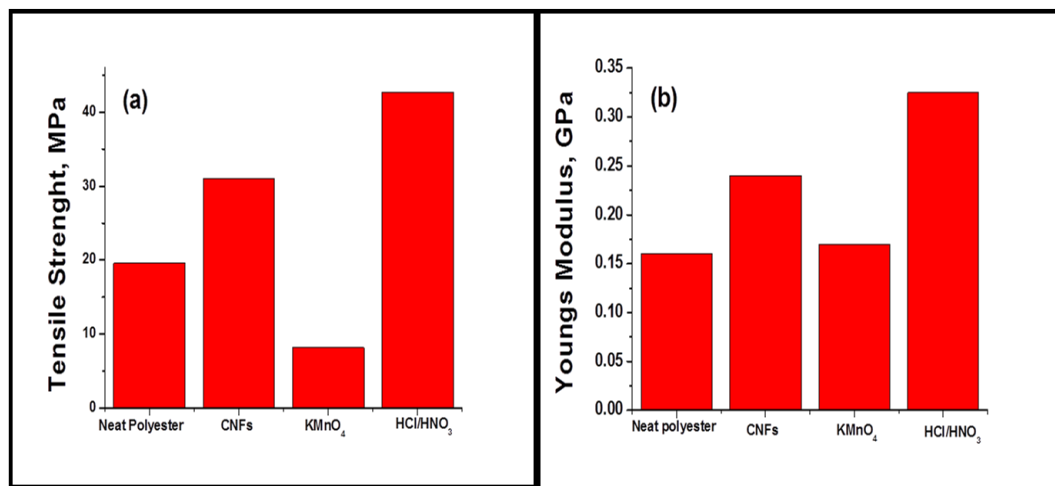


Figure 8.9: (a) Tensile strength and (b) Young's Modulus of untreated and acid treated polyester composites

8.3.8 Evaluation of Flexural Toughness

The three point bending tests were performed on the CNF polyester composites. Figure 8.10 shows the flexural stress of the composites for the untreated and treated CNFs. Adding untreated and treated CNFs to the CNM/polyester composites had a more significant effect on the flexural properties compared with the tensile properties. The result of the flexural tests followed the same pattern as the tensile tests. The CNFs treated with HCl/HNO₃ showed the greatest flexural enhancement by 25%. Similar to the tensile modulus, the flexural modulus was also enhanced with the acid treated CNFs (Fig. 8.11).

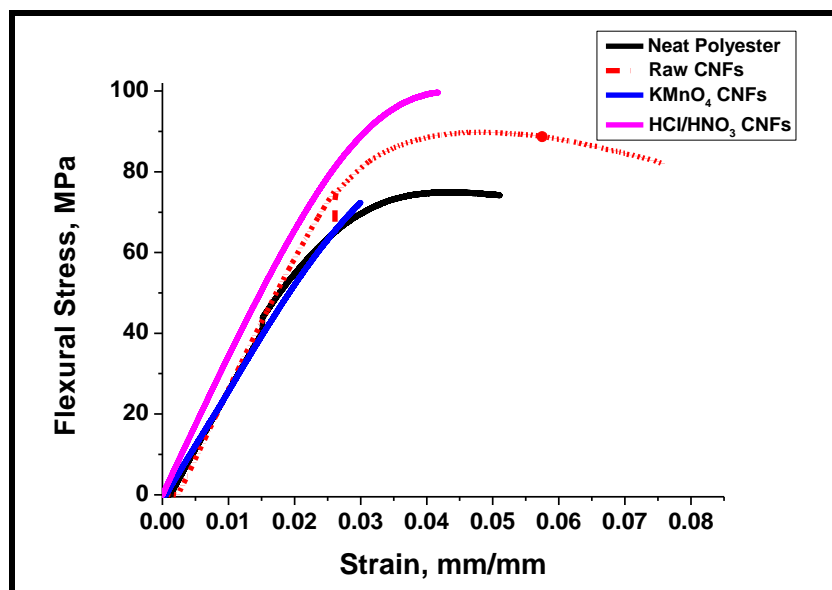


Figure 8. 10: Flexural stress vs strain graph of untreated and acid treated polyester composites

The higher flexural strength compared to the tensile could be caused by the nature of the flexural test in which the area above the neutral axis is subjected to the compression²¹. A similar trend in the flexural strength was reported by Shokrieh *et al.*²¹. The ultimate flexural strength was achieved at 0.3% loading with a 31% improvement²¹. In studies by Sanchez *et al.* and Hosain *et al.* the ultimate flexural strengths (UFS) were achieved at lower loadings of 0.1%^{22,23}. At higher weight fractions the strength decreased. Muthu *et al.* also achieved the UFS with acid treated CNTs but at a 1% loading¹³. These different loadings required to achieve the UFS are mostly dependent on the type of filler used. Though that is the case, UFS was achieved at loading less than 1% and with functionalized fillers.

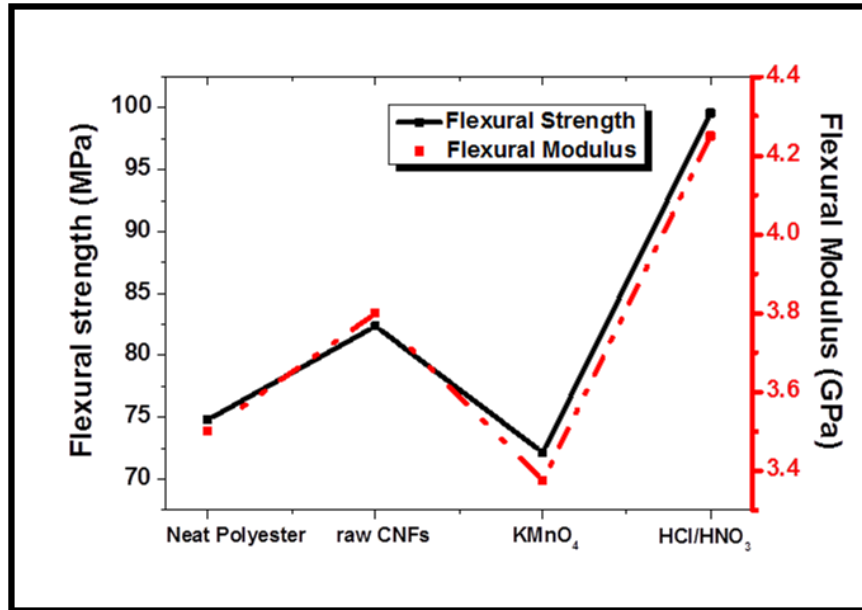


Figure 8. 11: Flexural properties of untreated and acid treated polyester nanocomposites

8.3.9 Evaluation of Fracture Toughness

Experimental determination of the fracture toughness was performed on the unnotched nanocomposite specimens. Figure 8.12, shows the fracture toughness values of the nanocomposites for untreated and acid treated polyester composites. The results show that the fracture toughness values of untreated nanocomposites was significantly higher than those of plain polyester. Treating the CNFs with KMnO₄ the fracture toughness of these nanocomposites was reduced. As stated before, this could be due to the CNF structure changing as was shown in the previous results.

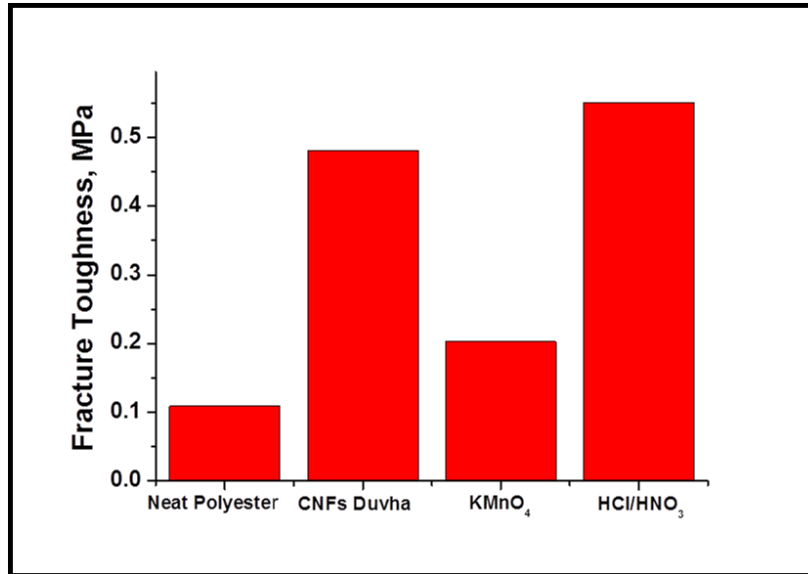


Figure 8. 12: Fracture toughness of Modulus of untreated and acid treated polyester composites

Some studies have pointed out that the use of CNTs with a high surface area leads to an improved tensile strength and fracture toughness^{2,3,24}. However the same effect is not expected to occur in resins polymerised via free radicals such as polyester. This is due to the fact that free radicals generated by the decomposition of the initiator (MEKP) catalyst, could be easily entrapped within the galleries of the CNT/Fs. Treatment in HCl/HNO₃ resulted in the highest improvement on the toughness value as compared to the neat polyester. To understand the reasons for the improvement of fracture toughness on the untreated CNFs and HCl/HNO₃ treated CNFs, an investigation on the failed samples by SEM was conducted. Figure 8.13, shows SEM images from the nanocomposites specimens that failed in the impact test. In the figure below, in both instances, it can be seen that the CNFs are protruding on the fracture surface and are evenly distributed. There was also no agglomeration observed. For the greater improvement to have occurred in HCl/HNO₃ nanocomposites, load transfer must have taken place. This is caused by the sufficient adhesion between the CNF and the matrix formed from the strong chemical interaction that must have taken place between the functionalised groups on the CNFs surface and the matrix²⁵.

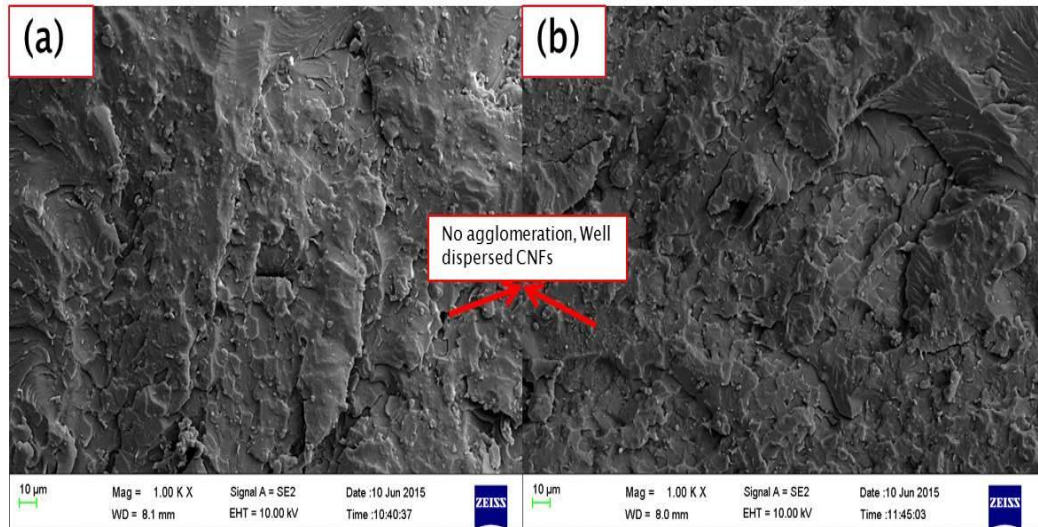


Figure 8. 13: SEM micrographs of CNFs produced from fly ash (a) untreated and (b) HCl/HNO₃

8.4 Conclusions

In this chapter we report the use of CNFs derived from a waste coal fly ash in any application. The tensile mechanical behaviour and fracture toughness of polyester nanocomposites was investigated. The CNFs were functionalized by oxidation. The mechanical properties of nanocomposites reinforced by HCl/HNO₃ functionalized CNFs were substantially better than those of non-functionalized CNFs. In both cases, the CNFs were well dispersed and evenly distributed in the polyester matrix. Treatment of CNFs with KMnO₄ resulted in the carbon structure changing form, thus leading to poor mechanical strength. Acid treatment in HCl/HNO₃ resulted in fibres that were more graphitic, due to the cleaning effect of acids in removing mostly alumina and silica. Carboxylic groups were introduced in the CNFs and that led to an improved bonding between the CNFs and the polyester matrix. This bonding resulted in an enhanced mechanical strength of the polyester. In closing, this study has shown that it is possible to use a waste material, which is fly ash to make a filler that will be responsible for improving polymer materials.

8.5 References

1. Z. Spitalsky, D. Tasis, K. Papagelis and C. Galiotis, *Progress in polymer science*, 2010, **35**, 357-401.
2. F. H. Gojny, M. Wichmann, U. Köpke, B. Fiedler and K. Schulte, *Composites Science and Technology*, 2004, **64**, 2363-2371.
3. F. H. Gojny, M. H. Wichmann, B. Fiedler and K. Schulte, *Composites Science and Technology*, 2005, **65**, 2300-2313.
4. D. Bikiaris, A. Vassiliou, K. Chrissafis, K. Paraskevopoulos, A. Jannakoudakis and A. Docoslis, *Polymer Degradation and Stability*, 2008, **93**, 952-967.
5. M. Ayatollahi, S. Shadlou, M. Shokrieh and M. Chitsazzadeh, *Polymer Testing*, 2011, **30**, 548-556.
6. F. Avilés, J. Cauich-Rodríguez, L. Moo-Tah, A. May-Pat and R. Vargas-Coronado, *Carbon*, 2009, **47**, 2970-2975.
7. N. Karousis, N. Tagmatarchis and D. Tasis, *Chemical Reviews*, 2010, **110**, 5366-5397.
8. M. M. Stylianakis, J. A. Mikroyannidis and E. Kymakis, *Solar Energy Materials and Solar Cells*, 2010, **94**, 267-274.
9. V. Datsyuk, M. Kalyva, K. Papagelis, J. Parthenios, D. Tasis, A. Siokou, I. Kallitsis and C. Galiotis, *Carbon*, 2008, **46**, 833-840.
10. P. M. Ajayan, L. S. Schadler, C. Giannaris and A. Rubio, *Advanced Materials*, 2000, **12**, 750-753.
11. G. Mittal, V. Dhand, K. Y. Rhee, S.-J. Park and W. R. Lee, *Journal of Industrial and Engineering Chemistry*, 2015, **21**, 11-25.
12. A. T. Seyhan, M. Tanoğlu and K. Schulte, *Materials Science and Engineering: A*, 2009, **523**, 85-92.
13. S. J. Muthu and R. Paskaramoorthy, *Polymer Composites*, 2012, **33**, 866-871.
14. M. Murarescu, D. Dima, G. Andrei and A. Circiumaru, *Digest Journal of Nanomaterials and Biostructures*, 2014, **9**, 653-665.
15. A. Battisti, A. A. Skordos and I. K. Partridge, *Composites Science and Technology*, 2010, **70**, 633-637.

16. M. M. Shokrieh, A. Saeedi and M. Chitsazzadeh, *Journal of Nanostructure in Chemistry*, 2013, **3**, 1-5.
17. N. Hintsho, A. Shaikjee, H. Masenda, D. Naidoo, D. Billing, P. Franklyn and S. Durbach, *Nanoscale Research Letters*, 2014, **9**, 1-11.
18. N. Hintsho, A. Shaikjee, P. K. Tripathi, P. Franklyn and S. Durbach, *RSC Advances*, 2015, **5**, 53776-53781.
19. W. Rasband, *National Institutes of Health: Bethesda, MD, USA*, 1997, **2012**.
20. O. M. Dunens, K. J. MacKenzie and A. T. Harris, *Environmental science & technology*, 2009, **43**, 7889-7894.
21. M. Shokrieh, A. Saeedi and M. Chitsazzadeh, *Materials & Design*, 2014, **56**, 274-279.
22. M. Sánchez, M. Campo, A. Jiménez-Suárez and A. Ureña, *Composites Part B: Engineering*, 2013, **45**, 1613-1619.
23. M. Hossain, M. Hossain, M. Hosur and S. Jeelani, *Journal of Engineering Materials and Technology*, 2015, **137**, 031005.
24. F. H. Gojny, J. Nastalczyk, Z. Roslaniec and K. Schulte, *Chemical Physics Letters*, 2003, **370**, 820-824.
25. M. J. Palmeri, K. W. Putz and L. C. Brinson, *ACS nano*, 2010, **4**, 4256-4264.

Chapter 9: Conclusion and recommendations

This chapter highlights the major findings of this thesis. A summary of the contributions that this dissertation has made and the recommendations for future research are presented here.

9.1 Introduction

Studies have shown that carbon nanomaterials such as carbon nanotubes, carbon nanofibres and carbon nanospheres can be produced using several methods but the chemical vapour deposition method has been shown to be the most reliable. A lot of focus across the globe has been on the use of different catalysts and carbon sources that will lead to the desired CNF morphology at a cost effective price. Also these CNMs because of their exceptional properties have been vastly used in the polymer applications.

The aims of this study were to explore ways of overcoming some of the current drawbacks associated with the synthesis of CNMs such as, the use of expensive catalysts, low product yields and non-uniform morphology. Another challenging factor for the application of CNMs in composite materials, is their interaction with the polymer matrix which is limited because of their hydrophobic nature.

In this study these disadvantages were overcome by producing CNMs from a waste material viz. coal fly ash as a catalyst. Fly ash is known to contain metals responsible for CNT/CNF formation, without pre-treatment or impregnation. Additionally the effect of an oxygen containing carbon source such as CO₂ either as sole source or an additive, as studies from literature had shown that a small addition of an oxygen species to a known carbon source can greatly enhance the product yield of the CNMs formed. Acid treatment of the synthesized CNMs, by adding O₂ groups on the surface alter the CNF chemical nature from hydrophobic to hydrophilic. This treatment also assisted in removing some of the impurities as shown by TGA, thus making the interaction between the filler and matrix more favourable.

9.2 Conclusions

9.2.1 Synthesis of CNFs from coal fly ash

CNFs were successfully synthesized using fly ash as a catalyst. The TEM images of the resulting CNFs (synthesized using H_2/C_2H_2 mixture) showed that the samples contained more than 95% of CNFs with linear morphology. Mössbauer spectroscopy showed that cementite (Fe_3C) was the element responsible for CNM (CNF/Ts) formation from fly ash. This study has shown that it is possible to synthesize CNMs from South African coal fly ash without pre-treatment or impregnation of the ash with other metals.

9.2.2 Effect of gas environment, flow rate and temperature of CNM morphology

From the initial investigation, a parametric study was necessary in order to obtain the best conditions to form CNMs, in-terms of yield and morphology. Reaction parameters such as reaction temperature, carrier and pre-reaction gases and flow rate studies were conducted. The results showed that all the parameters had an influence in the formation of these CNMs. The highest yields were obtained at 650 °C with a flow rate of 100 ml/min. When H_2 was used as a pre-reaction gas rather than N_2 as a carrier gas, using C_2H_2 as a carbon source, a more uniform morphology was achieved at 550 °C. Increasing the temperature to 650 °C, resulted in carbon nanospheres (CNSs) being formed. Mössbauer spectroscopy showed that 3 types of carbon were formed: amorphous, graphitic and cementite. From this study we were able to find the best conditions to form CNMs of a good standard.

9.2.3 Effect of CO_2 on the CVD synthesis of CNMs from coal fly ash

Using a waste material, CO_2 as the carbon source, CNMs could only be formed at 900°C. Pre-reacting CO_2 and switching to C_2H_2 resulted in the highest yield and formation of various helical CNFs. This study showed that CO_2 on its own is not a good carbon source. When used in conjunction with a known carbon source (C_2H_2) gave better results in terms of yield and CNM formation than C_2H_2 on its own. This is due to the amount of oxygen contained in CO_2 as only a small

amount is required to increase the yield when used in conjunction with a known carbon source.

9.2.4 Comparison of two different ashes for CNM synthesis and testing their tensile strength

Comparing two different ashes (Grootvlei and Duvha), showed that the physical and chemical properties of different ashes does play a role in the CNM product formed even if the synthesis conditions are the same. CNFs from Duvha ash were the more uniform, graphitic and thermally stable. The proceeding mechanical strength studies were explored using these. Low optimum loadings of 0.25% were required to obtain the best tensile strength for polyesters.

9.2.5 Effect of various treatments on CNFs and testing their tensile and impact tests

In an attempt to further increase the mechanical strength of polyester nanocomposites, CNFs at 0.25% loading were acid treated using KMnO_4 and HCl/HNO_3 . TEM micrographs showed that there was a change in morphology as their length became shorter. For KMnO_4 treated CNFs, the surface morphology became rougher and for HCl/HNO_3 became cleaner and smooth. The mechanical strength of the acid treated CNFs was vastly improved. This effect was expected as it is known from literature that HCl/HNO_3 has a cleaning effect. Also because of their retained structure, the carboxylic groups added from the treatment assisted with the interaction between the filler and polymer matrix, thus improving the mechanical properties of these polyesters.

In the course of addressing the hypothesis and research questions, the physical and chemical properties of the CNMs were prepared by the CVD method. The CVD method was demonstrated as a powerful, cost effective method for producing CNMs without the multiple processing stages. The study has also assisted in understanding the influence of treated or untreated CNFs, optimum loading to be used for improvement of the mechanical properties of polyesters. Therefore, the scientific goals of producing CNMs from a waste material and

improving the mechanical properties of polyester nanocomposites was achieved. The knowledge gained from this project can be used to better understand the CNMs properties for various other applications in the future as well.

9.3 Recommendations

Based on the analysis and conclusions of the study, a number of recommendations regarding future research are as follows:

- Though the CVD synthesis method produced CNMs with a uniform and controlled morphology under the right conditions, it would be interesting to explore a different method such as wet impregnation for comparison and see if there will be further improvement. All literature studies to date, where fly ash was used as a catalyst for CNM synthesis, was produced via the CVD method.
- In order to form CNFs of high quality, as was observed under TGA, there was still a lot of unreacted fly ash and impurities. In the formed CNFs the unburnt coal ash could be cleaned through etching out unburnt Al, Si, etc using acids such as HF. These purer CNMs will have better mechanical properties, thus leading to an improvement in the polymer composites
- In the treatment of CNFs with KMnO_4 a study on various lower concentrations needs to be conducted so as to avoid the destruction of the CNF structure at high 1M concentrations. A destruction in CNF structure resulted in poor mechanical properties when these CNFs were used as filler.

APPENDICES: Supplementary Material

Chapter 3: Supplementary



Figure S3.1: Dog bone shape of specimen for tensile testing

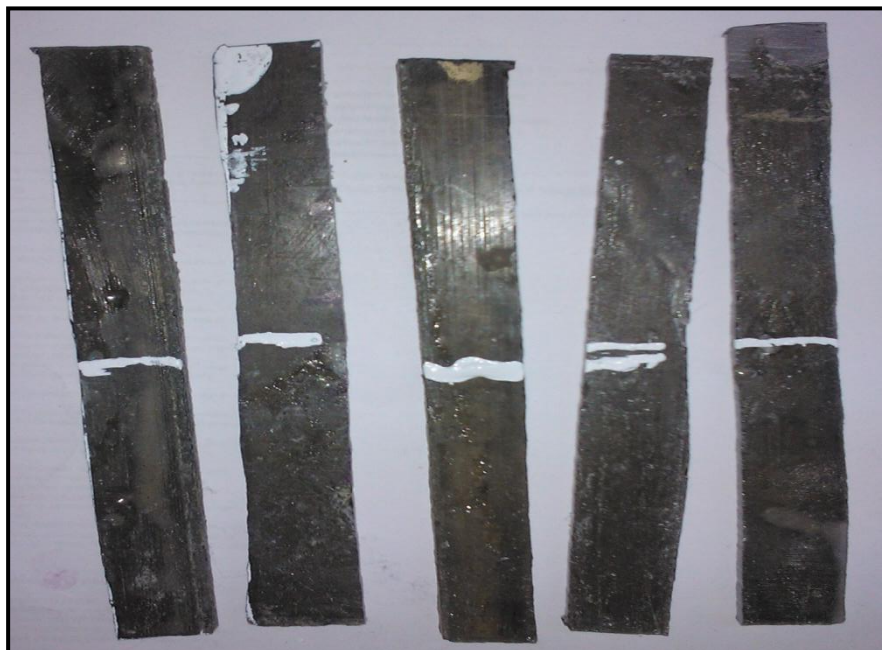


Figure S3.2: Specimens for flexural testing



Figure S3.3: Specimen for Impact testing

Chapter 5: *Supplementary*

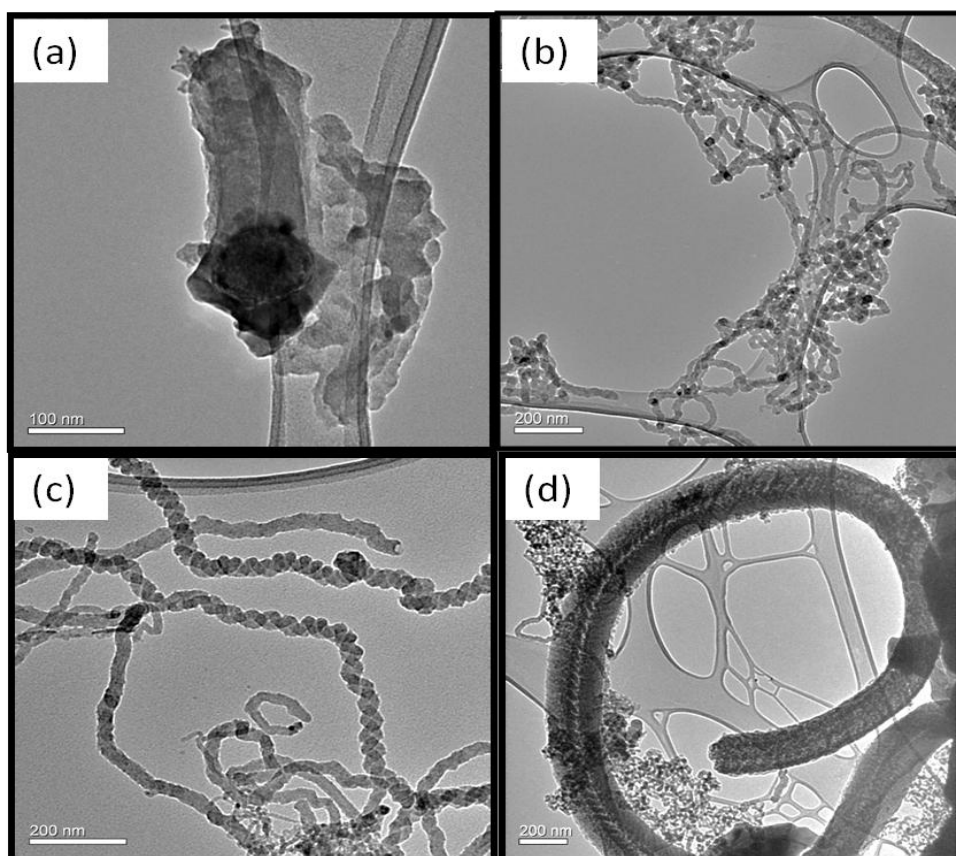


Figure S5.1: TEM images showing carbon nanofibres produced from H₂ used during all phases, (a-b) C₂H₂ at 25/ml during reaction time and N₂ at 75ml/min (c-d) C₂H₂ at 50/ml and N₂ at 50ml/min

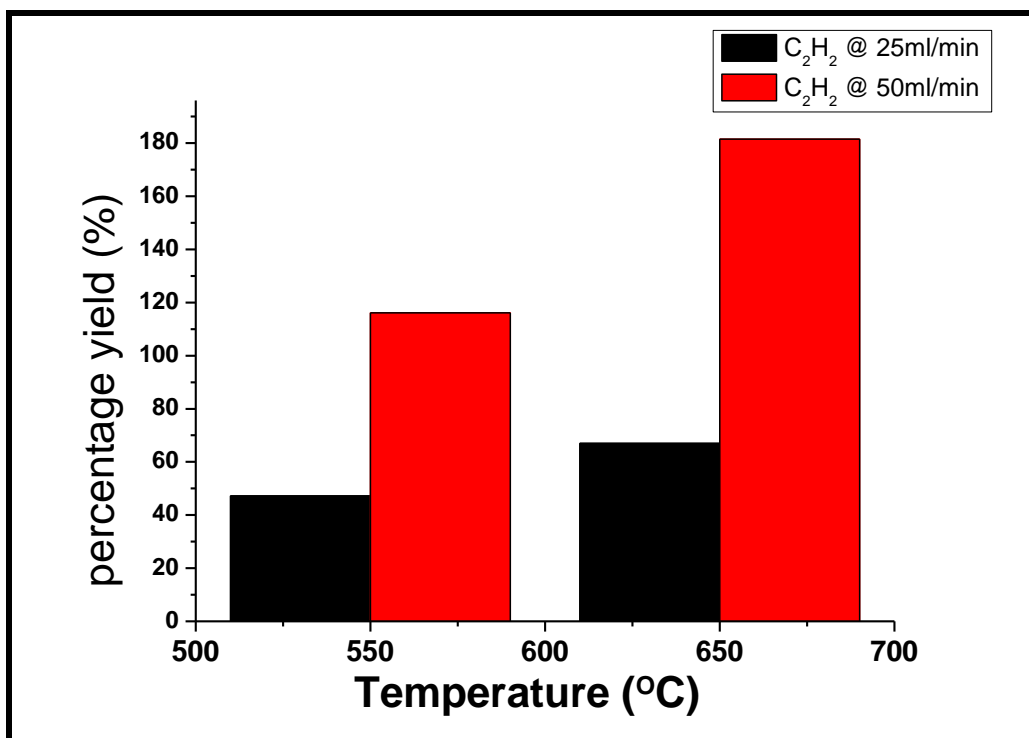


Figure S5.2: Percentage yield of carbon nanofibres at varying flow rates of 25/ml C₂H₂ during reaction time and at 50/ml C₂H₂ and N₂ at 50ml/min

Chapter 7: *Supplementary*

Table S7.1 Fly ash components

Fly ash Components (%)	Duvha	Grootvlei
SiO ₂	55.03	48.64
Al ₂ O ₃	27.76	26.02
Fe ₂ O ₃	0.81	1.26
FeO	5.03	10.2
MnO	0.08	0.07
CaO	5	8.17
MgO	1.43	2.18
Na ₂ O	0.14	0.17
K ₂ O	0.90	0.90
TiO ₂	2.52	-
P ₂ O ₅	0.53	0.66
Cr ₂ O ₃	0.33	0.66
NiO	0.07	0.01

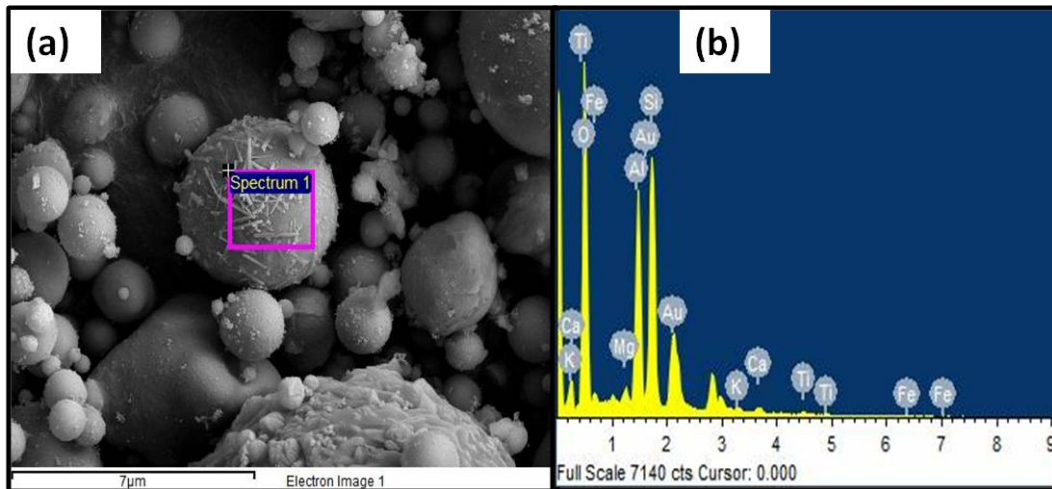


Figure S7.1(a) Raw Duvha fly ash and (b) EDS of Duvha ash

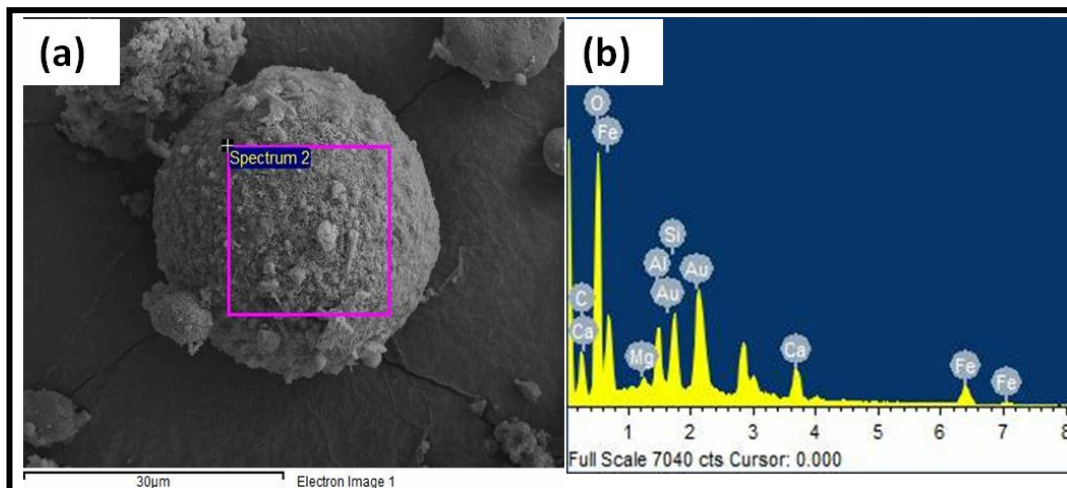


Figure S7.2: Raw Grootvlei fly ash and (b) EDS of Grootvlei ash

Table S7.2 Comparison of Fly ash properties

Fly ash Properties	Roscheville	Duvha	Grootvlei
Fe%	5.61	5.84	11.46
I_D/I_G ratios	1.3	1.18	1.6
% Yield	375%	325%	400%
T^o Decomposition	550°C	598°C	605°C

Chapter 8: *Supplementary*

Table S8.1: XRD phases that had peak shifting to the left

Phases	Raw CNFs	Acid treated CNFs
Mullite	17.5 ^o	17.0 ^o
	36	35.5
	38.5	38.00
	40.5	40.0
Quartz	47.5 ^o	47.2
	73	72.5